DISSERTATION

INFLUENCE AND REGULATION OF PCBP2 AND YTHDF2 RNA-BINDING PROTEINS DURING SELF-RENEWAL AND DIFFERENTIATION OF HUMAN INDUCED PLURIPOTENT STEM CELLS

Submitted by

Adam M. Heck

Graduate Degree Program in Cell and Molecular Biology

In partial fulfillment of the requirements

For the Degree of Doctor of Philosophy

Colorado State University

Fort Collins, Colorado

Fall 2019

Doctoral Committee:

Advisor: Carol J Wilusz
Co-Advisor: Jeffrey Wilusz

Erin Osborne Nishimura
Tai Montgomery
Wen Zhou

ABSTRACT

INFLUENCE AND REGULATION OF PCBP2 AND YTHDF2 RNA-BINDING PROTEINS DURING SELF-RENEWAL AND DIFFERENTIATION OF HUMAN INDUCED PLURIPOTENT STEM CELLS

Embryonic stem cells (ESCs) are able to self-renew or differentiate into any cell type in the body, a property known as pluripotency that enables them to initiate early growth and development. However, the ethical implications of harvesting and manipulating ESCs hinders their use in basic research and the clinical applications. Thus, the discovery that somatic cells can be exogenously reprogrammed into induced pluripotent stem cells (iPSCs) offers new and exciting possibilities for gene therapy, personalized medicine and basic research. However, more research is needed into the mechanisms involved in regulating pluripotency in order for iPSCs to reach their full potential in the research lab and clinic.

To maintain a state of self-renewal, yet also be able to rapidly differentiate in response to external signals, pluripotent stem cells need to exert tight control over gene expression through transcriptional and post-transcriptional mechanisms. There are several notable transcriptional networks that regulate pluripotency, but the post-transcriptional mechanisms remain poorly characterized. mRNA decay is one form of post-transcriptional regulation that can help to both maintain the steady-state of a transcriptome or facilitate its rapid remodeling. To this end, degradation rates are influenced by the elements contained in an mRNA and the RNA-binding proteins (RBPs) they associate with. Previous reports have indicated the RNA modification N^6-methyladenosine (m^6A) and C-rich sequence elements (CREs) can affect mRNA decay in pluripotent stem cells. Therefore, we sought to further understand the roles of m^6A and CREs in

mRNA decay in stem cells by characterizing the expression and mRNA targets of two RBPs that recognize these elements, YTHDF2 and PCBP2, respectively.

In this thesis, I report YTHDF2 is differentially regulated in pluripotent and differentiated cells and that YTHDF2 contributes to pluripotency by targeting a group of mRNAs encoding factors important for neural development. The down-regulation of YTHDF2 during neural differentiation is consistent with increased expression of neural factors during this time. Moreover, YTHDF2 expression is regulated at the level of translation via elements located in the first 300 nucleotides of the 3' untranslated region of *YTHDF2* mRNA. Based on these results, I propose that stem cells are primed for rapid differentiation by transcribing low levels of mRNAs encoding neural factors that are subsequently targeted for degradation, in part by YTHDF2, until differentiation is induced.

On the other hand, PCBP2 is up-regulated upon differentiation of pluripotent stem cells and regulates several mRNAs associated with pluripotency and development, including LIN28B. Notably, expression of long non-coding RNAs (lncRNAs) that contain human endogenous retrovirus element H (HERV-H) is influenced by PCBP2. HERV-H lncRNAs are almost exclusively expressed in stem cells and play a role in maintaining a pluripotent state, although their functions are not fully understood. Intriguingly, some HERV-lncRNAs can also regulate PCBP2 expression, as altering the expression of LINC01356 or LINC00458 effects PCBP2 protein levels. Based on these results, I propose the reciprocal regulation of PCBP2 and HERV-H lncRNAs influences whether stem cells maintain a state of self-renewal or differentiate.

Taken together, these findings demonstrate that YTHDF2 and PCBP2 post-transcriptionally regulate gene expression in stem cells and influence pluripotency.

ACKNOWLEDGEMENTS

The saying ‘it takes a village’ is not far off when it comes to the number of people who have helped and supported me on this journey. To those whom I do not mention by name, and there will be many, know that I still greatly appreciate what you did for me during my graduate career.

I would like to start off by thanking my advisor Dr. Carol Wilusz whose guidance and support have been instrumental to my success as a researcher. In addition, our back and forth during the writing process of my thesis and other published works, painful as it was at times for both us, helped to vastly improve my written communication skills. I would also like to thank my co-advisor Jeff Wilusz for his advice regarding my projects, scientific research and life in general. These discussions often occurred over beers and/or bowling, which I always appreciated. I want to thank my graduate committee members Drs. Erin Osborne Nishimura, Tai Montgomery and Wen Zhou for their active involvement in my dissertation project and contributions to my scientific progress. A special thanks to Dr. Osborne Nishimura who was my go-to for any and all computational questions I had during my sequencing analysis.

I am thankful for research training support from the GAUSSI computational training program at CSU and the Graduate Research Fellowship Program both through the National Science Foundation. I would like to than Drs. Thomas Chen, Carol Wilusz and Asa Ben-Hur for giving me the opportunity to participate in the GAUSSI computational training program. I would also like to thank Dr. Stu Tobet and my fellow members of his Fall 2015 grant writing course who helped me hone my application for the Graduate Research Fellowship Program. These programs provided research funding and educational experiences, which greatly enhanced my graduate student experience.

Throughout my graduate school journey, members of the Wilusz Lab have provided me with advice, protocols, reagents, laughs and, most importantly, friendship. I will also be thankful for their help and support. Dr. Aimee Jalkanen helped show me the ropes when I first began and

also taught me how to culture iPS and HFF cells. Dr. Annie Zhang Bargsten shared many a laugh with me and provided me with numerous reagents and protocols. John Anderson taught me several techniques, helped me track down supplies, reagents and protocols and answered countless questions. Dr. Donnie Evans was my co-pilot for the latter portion of the PCBP2 project and provided expertise and reagents. Dr. Phillida Charley helped me setup and run several experiments. Dr. Dan Michalski provided valuable insights, particularly in the design of the RNA pulldown experiment. John Brown, Erica Reith, Cary Mundell and Lyv Quillen all provided valuable assistance during their summer or semester research sessions and I was proud to mentor all of them. Saving the best for last, I want to give a shout out to Dr. Joe Russo who is my science 'big brother'. He provided me with invaluable advice and support as well as reagents shared labor and good times in lab, for all of which I am truly thankful.

I am also extremely grateful for the amazing and supportive community of graduate students and post docs in the CMB program, particularly the 2014 cohort I came in with, as well as the BMS department. A special thanks to Dr. Mark Stenglein and Dr. Justin Lee and the Next Generation Sequencing Core at CSU, who not only helped me navigate the sequencing process, but also generously provided a critical enzyme for my library preparation. I would also like to thank Dr. Brian Geiss who provided me with training and access to a luciferase plate reader and fluorescence microscope As well as Dr. Alan Schenkel for allowing me to use his fluorescence microscope. Thanks to Dr. Dan Sloan for providing access to his TapeStation2200 machine and insightful advice during the design and analysis of my RNA sequencing data.

Finally, I appreciate all the love and support I have received from family, friends, the Small Council, roommates and colleagues throughout this time. I would especially like to thank my parents Kim and Jon Heck as well as my sister Kari and brother Andy for their love and always being there for me all of these years. Most of all, I want to thank my wife, Ashley, who is my biggest supporter. She has been with me step for step during this journey; from late night study

sessions during our first year, to writing our prelim proposals at the same desk in our third year, to defending within a week of each other. I am forever grateful that she came into my life.

TABLE OF CONTENTS

Chapter 1: Introduction

This project addresses two important aspects of the contribution of RNA-binding proteins that contribute to post-transcriptional control mechanisms to human stem cell biology. First, we explored the role of the N^6-methyladenosine (m^6A) reader protein YTHDF2 on the targeted regulation of gene expression during pluripotency and beyond. Next, we investigated the role of poly(C)-binding protein 2 (PCBP2), a C-rich element (CRE) RNA-binding protein, on stem cell biology due to the fact that messenger RNAs (mRNAs) containing CREs are dramatically regulated during development. Collectively, this project provides a variety of insights into the post-transcriptional control of early development. This introduction will begin with an overview of stem cell biology followed by a discussion of mechanisms of mRNA decay since this post-transcriptional process is the major cytoplasmic contributor to changes in gene expression patterns. Finally, I will provide the detailed scientific premise for studying both m^6A RNA methylation as well as PCBP proteins in the context of stem cell biology.

1.1 Stem cells

1.1.1 Embryonic stem cells

Embryonic stem cells (ESCs) possess the unique characteristics of self-renewal and pluripotency, granting them the ability to replicate indefinitely or differentiate into other cell types. These exclusive traits allow them to play a critical role during development of an organism (Odorico et al. 2001). During embryogenesis, ESCs differentiate in order to form the three primary germ layers: endoderm, mesoderm and ectoderm (Itskovitz-Eldor et al. 2000). In adult tissue, multipotent stem cells can act as reservoirs, replenishing cells which are rapidly turned over or damaged. For example, the hematopoietic stem cells (HSCs) in bone marrow function to continually replace red and white blood cells (Crane et al. 2017).

1.1.2 Induced pluripotent stem cells

The field of stem cell biology was revolutionized in the mid-2000s when Yamanaka and colleagues demonstrated that both mouse and human adult fibroblasts, aka somatic cells, can be reprogrammed into induced pluripotent stem cells (iPSCs) simply by transfecting in a group of transcription factors (Takahashi and Yamanaka 2006; Takahashi et al. 2007). These genes OCT4, SOX2, KLF4 and MYC, along with NANOG (Boyer et al. 2005; Pan and Thomson 2007), became known as the major pluripotency factors. Since then, various combinations of transcription factors, RNA-binding proteins (RBPs) and microRNAs (miRNAs) have been shown to yield iPSCs from somatic cells (Takahashi and Yamanaka 2016; Zviran et al. 2018).

1.1.3 Naïve and primed pluripotent states

Pluripotency is dynamic over the course of development. Typically, pluripotent stem cells can be classified as either naïve or primed based on their ability to maintain self-renewal following inhibition of mitogen-activated protein kinase kinase (MEK) signaling (Nichols and Smith 2009; Weinberger et al. 2016). MEK is a member of the MAPK/ERK signaling pathway and thus contributes to the regulation of various cellular processes including cell cycle entry and proliferation, differentiation, survival and apoptosis (Sun et al. 2015). Naïve stem cells exhibit higher expression of pluripotency factors, coupled with lower expression of lineage-specific factors, which enables them to maintain a state of self-renewal following abrogation of MEK signaling and/or other epigenetic regulators (Nichols and Smith 2009; Weinberger et al. 2016). Conversely, the reciprocal expression profile is observed in primed stem cells, lower pluripotency and higher lineage-specific expression, which results in differentiation and/or apoptosis following MEK inhibition. The current model in the field suggests naïve stem cells transition into primed stem cells over the course of development to enable a more rapid response when differentiation is induced (Weinberger et al. 2016; Collier et al. 2017; Kalkan et al. 2017; Ware et al. 2014). iPSCs, particularly human iPSCs, are typically reprogrammed into a

primed state. However, there are ways to coax iPSCs into a naïve state and maintain them there (Gafni et al. 2013; Weinberger et al. 2016). It is important to highlight these aspects of pluripotency, as this study works with human iPSCs reprogrammed from foreskin fibroblasts (HFFs). Thus, our results reflect the response of stem cells in a primed state.

1.1.4 Clinical applications of iPSCs

The ability to reprogram easily obtainable cell types, such as skin fibroblasts, into pluripotent stem cells and subsequently induce differentiation into less accessible cell types (such as neurons) provides new avenues for gene therapy, personalized medicine and basic research (Cubillo et al. 2018; Avior et al. 2016; Karagiannis 2019). In fact, some of these avenues are already being explored. In 2017, one of the first peer-reviewed papers using iPSC transplantation as a treatment described its success in treating age-related macular degeneration (Mandai et al. 2017). Currently, clinical trials are underway investigating an iPSC-derived neuron replacement therapy for Parkinson's disease (Loring 2018). In regards to basic research, differentiation of patient iPSCs into neural cell types has been utilized to study Alzheimer's disease for several years (Penney et al. 2019). Furthermore, reprogramming grants researchers the opportunity to study gene expression in different cell types that are genetically identical.

Despite the plethora of clinical applications, the precise mechanisms by which stem cells control gene expression to maintain pluripotency and self-renewal or drive differentiation remain poorly characterized. Moreover, implantation of iPSCs into primary tissue has shown high potential for tumor formation (Yoshihara et al. 2017). Therefore, additional insight into the mechanisms governing pluripotency will help to improve the efficiency and accuracy of reprogramming and allow the full clinical potential of iPSCs to be met.

1.2 Regulation of the transcriptome in stem cells

Stem cell differentiation events are prevalent throughout the lifetime of an organism. From the formation of the germ layers in early development (Rossant and Tam 2017; Stirparo et al. 2018), to differentiation of HSCs to replenish lost blood cells in adults (Crane et al. 2017); these events play a critical role in development, regeneration and maintenance of tissues and organs. The ability of stem cells to self-renew, while remaining poised to rapidly differentiate in response to an external cue, requires complex, properly executed maneuvers to modulate the transcriptome and ensure the desired outcome is achieved.

1.2.1 Transcriptional regulation

At the level of transcription, factors like OCT4, SOX2, KLF4, NANOG and others promote expression of genes that favor a pluripotent state (Cacchiarelli et al. 2015; Hainer et al. 2019). For example, OCT4 promotes the expression of several members of the TGFβ/ACTIVIN/NODAL signaling pathway, including NODAL itself, which is crucial for maintaining pluripotency in ESCs (Babaie et al. 2007; James et al. 2005). Likewise, NANOG drives transcription of ESSRB in stem cells which facilitates self-renewal independent of cytokines like Leukemia Inhibitory Factor (LIF) (Festuccia et al. 2012; Latos et al. 2015). Alternatively, up-regulation of lineage-specific transcription factors like PAX6 for the ectoderm or FOXA2 for the endoderm during differentiation (Kuang et al. 2019), promotes acquisition of gene expression programs for specific germ layers (Tsankov et al. 2015; Godoy et al. 2018; Stirparo et al. 2018). Concomitantly, substantial chromatin remodeling occurs during differentiation which influences the transcription rates of pluripotent and lineage-specific genes (Alajem et al. 2015; Kurimoto et al. 2015). Notably, the promoters of many lineage-specific genes exhibit bivalent modifications (i.e. both activating (H3K4me3) and repressive (H3K27me3) marks are present). This bivalent modification keeps them in a transcriptionally

silent state, but poised for immediate action (Fisher and Fisher 2011; Harikumar and Meshorer 2015). Together, these events provide a foundation for the dynamic transcriptome of stem cells.

1.2.2 Post-transcriptional regulation

Transcription is an energy-expensive and time-consuming process that relies on multiple downstream events (processing, export, translation, decay etc.) to impact cell function. The rapid and highly coordinated transcriptome remodeling that occurs during differentiation requires extensive post-transcriptional regulation (Zhao et al. 2017a; Serrano-Gomez et al. 2016; Eckersley-Maslin et al. 2018). Stem cells utilize a variety of regulatory elements and factors including RBPs (Emani et al. 2015; Ju Lee et al. 2017), RNA modifications (Heck and Wilusz 2019; Geula et al. 2015), miRNAs (Xu et al. 2009; Zeng et al. 2018; Worringer et al. 2014) and lncRNAs (Santoni et al. 2012; Wang et al. 2013b; Guttman et al. 2011) to facilitate rapid remodeling of the transcriptome when the time is right; but also to act as a preventative measure against precocious differentiation. These factors can achieve the desired regulation through multiple mechanisms. In this study, we chose to focus on mRNA decay because it is integral to remodeling the transcriptome during differentiation (Oh et al. 2018; Zhao et al. 2017b; Zhang et al. 2017a) and to restraining expression of lineage-specific genes in pluripotent cells (Lloret-Llinares et al. 2018; Lou et al. 2014). Moreover, mRNA decay plays a role in the reprogramming of somatic cells into iPSCs (Kami et al. 2018). Despite these findings, relatively little is known about the mechanisms and factors that facilitate mRNA decay in pluripotent stem cells. Thus, understanding the interplay or networking between the RNA decay machinery and other aspects of gene expression in stem cells is needed to further elucidate the depth of regulation that occurs.

1.3 mRNA decay as a regulatory mechanism[1]

Degradation plays a major role in regulating both the quantity and quality of RNA in the cell. The abundance of an RNA transcript is a reflection of both its rate of synthesis and degradation. Beyond the examples specific to pluripotency and differentiation mentioned above, there are numerous reports regarding the regulation of gene expression associated with major cellular responses occurring at the level of differential RNA stability (Chen and Shyu 2017; Yamada and Akimitsu 2019). There is also a growing body of evidence to suggest cross-communication or buffering occurs between transcription and RNA decay that contributes to the homeostasis of gene expression (Chavèz et al. 2016). Below, we provide an overview of the mRNA decay pathway including the major steps and players involved. See Figure 1.1 for a diagram of the mRNA decay pathway.

1.4 The major steps and mechanisms of mRNA decay in eukaryotes[1]

1.4.1 Step one: deadenylation/removal of the poly(A) tail

Deadenylation is the initial, and often rate-limiting step of the traditional exonucleolytic decay pathways (Fig. 1.1). Deadenylases are recruited to RNA substrates by a variety of RBPs and complexes (Du et al. 2016a; Stowell et al. 2016; Yamaji et al. 2017). There are two enzymatic complexes which carry out the majority of cytoplasmic deadenylation in eukaryotes (Wahle and Winkler 2013). The Poly(A) Nuclease (PAN) PAN2/PAN3 complex is thought to be responsible for preliminary poly(A) trimming (Wolf and Passmore 2014). PAN2 functions as the catalytically active subunit, while PAN3 is critical in recruitment of PAN2 to the poly(A) tail and efficient poly(A) tail shortening (Jonas et al. 2014; Schäfer et al. 2014; Wolf et al. 2014).

[1] Section 1.3, 1.4 and the associated figure are modified from: The Interplay between the RNA Decay and Translation Machinery in Eukaryotes. Cold Spring Harbor Perspectives Biology. Vol. 10, No. 5, May 1, 2018.

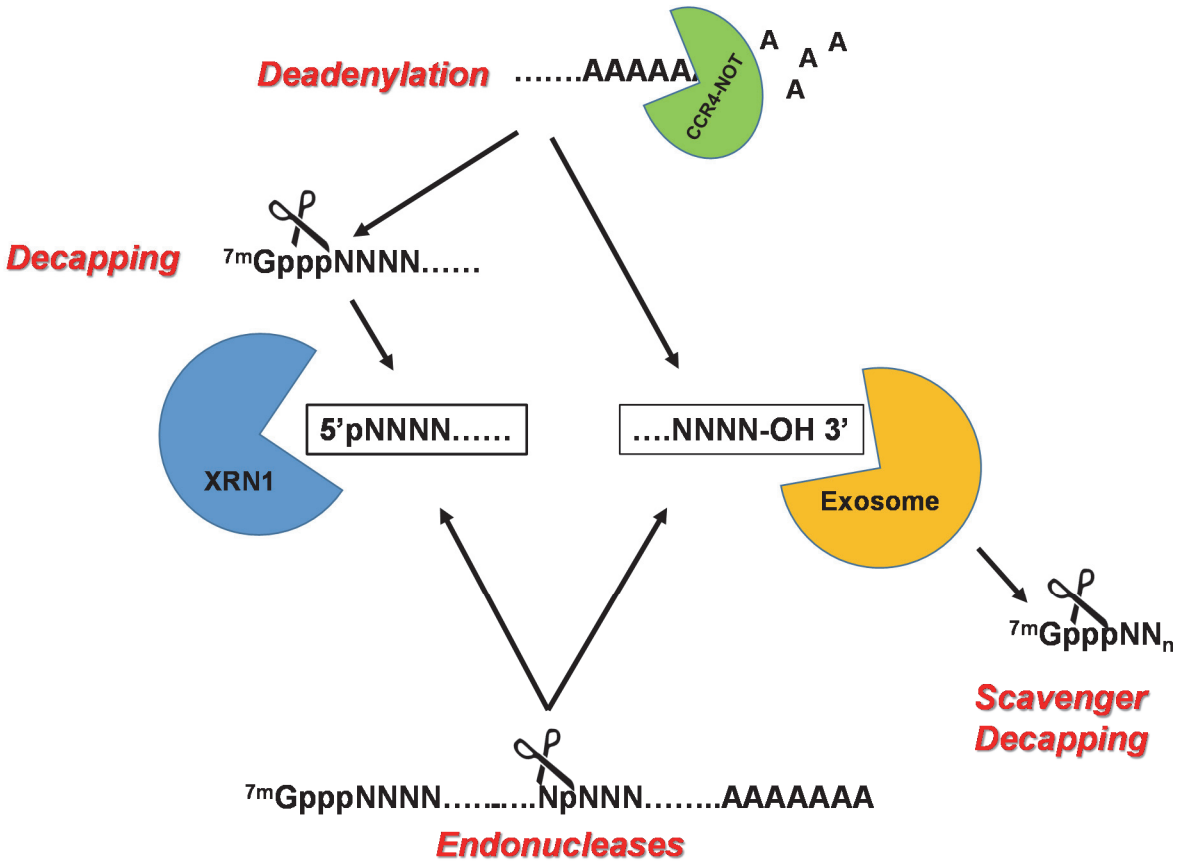

Figure 1.1: The multiple pathways for exonucleases to gain access to RNAs targeted for degradation. 5'-3' exoribonucleases (XRN1) require a 5' monophosphate while 3'-5' exoribonucleases (the exosome) require an accessible 3' hydroxyl. A 5' monophosphate can be generated in a regulated fashion by the process of decapping, which can be deadenylation [poly(A) tail shortening]-dependent or deadenylation-independent. Deadenylation itself generates an accessible 3' hydroxyl for exoribonucleases. In the 3'-5' exonuclease pathway, the scavenger decapping enzyme DCPS acts on short capped oligonucleotides to promote full degradation. Finally, rather than remodeling the natural 5' and 3' ends of the target mRNA, endoribonucleases, including the RISC complex of the RNAi pathway, can cleave a transcript internally and generate fragments with 5' monophosphate and 3' hydroxyl ends for exonucleolytic decay.

Subsequently, the bulk of deadenylation is carried out by the CCR4-NOT complex (Collart and Panasenko 2017; Tang et al. 2019). While several proteins comprise this complex, the three key proteins appear to be NOT1, CCR4 (CNOT6) and CAF1/POP2 (CNOT7). NOT1 serves as the structural backbone of the complex (Basquin et al. 2012), whereas CCR4 and CAF1/POP2 are the catalytically active deadenylases (Maryati et al. 2015). Recent evidence suggests that CCR4 and CAF1/POP2 deadenylases can also remove terminal non-adenosine residues, if the complex is anchored to the RNA substrate by upstream adenosine tracts (Niinuma et al. 2016). Finally, in addition to PAN2/PAN3 and CCR4-NOT, eukaryotic cells also contain a number of additional deadenylases which can influence poly(A) tail length (Skeparnias et al. 2017) and play roles in small RNA biogenesis. Of these, PARN, the most extensively studied, can interact with the 5' cap of mRNA substrate to enhance enzymatic activity/processivity (Virtanen et al. 2013; Niedzwiecka et al. 2016). Several studies have reported that polyadenylation, specifically alternative polyadenylation (aka APA), is important for pluripotency and reprogramming (Brumbaugh et al. 2018; Lackford et al. 2014; Ji and Tian 2009).

1.4.2 Step two: decapping/removal of the 5' cap to generate a 5' monophosphate

In addition to a key role in promoting translation initiation, the 7-methyl-guanosine (m^7G) cap on mRNAs also serves to protect transcripts from highly active 5' to 3' exoribonucleases that are present in both the nucleus and cytoplasm of eukaryotic cells (Fig. 1.1) (Jones et al. 2012). Thus, the process of decapping is a crucial step in the decay of many mRNAs, and can be either deadenylation-dependent or deadenylation-independent. The majority of decapping activity is thought to be provided by DCP2, but recent work has identified seven additional NUDIX proteins (e.g. NUDT3 and NUDT16) as well as DXO proteins that act on distinct RNA subsets (Grudzien-Nogalska and Kiledjian 2017) and alternative cap structures (Jiao et al. 2017). Typically, at least a portion of these decapping enzymes can be found in membraneless compartments of ribonucleoprotein (RNP) complexes known as Processing bodies (P-bodies)

(Luo et al. 2018). The well-characterized DCP2 enzyme requires several additional co-factors *in vivo* to effectively access mRNA substrates, as well as attain an optimally active enzymatic conformation (Wurm et al. 2017). Decapping cofactors include DCP1, the Lsm1-7 complex, PATL1 (Pat1), DDX6 (Dhh1), LSM14 (Scd6) and a set of EDC proteins.

1.4.3 Step three (Option 1): 5' to 3' exoribonucleolytic decay in the cytoplasm

XRN1 is the primary 5' to 3' cytoplasmic exonuclease and is well-conserved throughout eukaryotes (Fig. 1.1) (Jones et al. 2012). XRN1 preferentially degrades RNAs with a 5' monophosphate end – precisely corresponding to the 5' termini left following mRNA decapping or most endonucleolytic RNA cleavages. XRN1 is a highly processive enzyme that generally can only be stalled by rather elaborate RNA structures – for example, three helix junction knot-like structures found in flavivirus RNAs (Chapman et al. 2014). Interestingly, there is growing evidence that XRN1 plays a key role in overall RNA decay and homeostasis of gene expression (Chavèz et al. 2016). Repression of XRN1 by stalling on flavivirus structures results in a concomitant repression of decapping and deadenylation in the infected cell (Moon et al. 2012, 2015). This could be due to interactions between XRN1 and other proteins involved in RNA decay (Chang et al. 2019). In addition, buffering effects between mRNA transcription and degradation rates appear to be mediated by XRN1 in some fashion (Timmers and Tora 2018; Singh et al. 2019).

1.4.4 Step three (Option 2): 3' to 5' exonucleolytic decay in the cytoplasm

Deadenylation generates an unprotected 3' end of an mRNA, which is vulnerable 3' to 5' decay. This form of decay is performed primarily by a multi-subunit complex called the exosome (Fig. 1.1) (Zinder and Lima 2017). The core of the exosome (Exo9) consists of nine protein subunits that are highly conserved throughout eukaryotes, but nucleolytically inactive. Exo9 binds to the catalytically active subunit RRP44 to form the active exosome (Exo10) (Kowalinski

et al. 2016; Zinder et al. 2016). Following 3' to 5' decay, the m^7G cap is removed from the remaining short oligonucleotide by the scavenger decapping enzyme DCPS (Liu et al. 2008) along with FHIT/Aph1 (Taverniti and Seraphin 2015). The exosome is capable of performing specific functions based on association with different co-factors. In the case of stem cell differentiation, depletion of either the exosome or its cofactor RBM7 leads to the stabilization of lowly expressed transcripts in different cell types (Lloret-Llinares et al. 2018). This suggests RBM7 may guide the exosome to these transcripts. However, the precise mechanism remains uncharacterized.

1.4.5 An alternative way to induce mRNA decay: endonucleolytic decay

The generation of an accessible 5' monophosphate or 3' hydroxyl for an exoribonuclease is the key step in turnover of the body of the mRNA (Fig. 1.1). In addition to deadenylation and decapping, an appreciation of the extent that endoribonucleases contribute to general mRNA decay has significantly increased over the years. In addition to the well-characterized cleavage events that occur during miRNA and siRNA-mediated RNA interference (RNAi) (Park and Shin 2014), there are numerous other endoribonucleases that target and cleave mRNAs in a regulated fashion for subsequent exonucleolytic decay. Because endoribonuclease activity significantly modulates the fate of an mRNA, these enzymes are tightly regulated. In fact, cells contain a cysteine-rich ribonuclease inhibitor (RNH1) to protect them from the plethora of unwanted 'RNase A' type ribonucleases secreted by cells in their environment (Thomas et al. 2016). There are several endoribonucleases that play significant roles in the regulation of mRNA stability, and subsequent gene expression, in mammalian cells (Uehata and Takeuchi 2017; Rath et al. 2015; Tavernier et al. 2017; Shan et al. 2017). Of note for this study is the RNase P/MRP complex because of its recent association with cleavage of m^6A modified RNAs (Park et al. 2019).

1.5 Elements and factors that facilitate mRNA decay

mRNA degradation is typically not initiated spontaneously. As touched on above, deadenylases, decapping enzymes or endoribonucleases, must be recruited to target transcripts by proteins or miRNAs (trans-acting factors) that recognize specific sequence elements or post-transcriptional modifications (cis-acting elements). Below we discuss the influence several cis-acting elements and the trans-acting factors which recognize them have on mRNA decay.

1.5.1 Cis-acting elements

Cis-acting elements can influence mRNA decay and impact the transcriptome to varying degrees based on their prevalence. Ubiquitous modifications like the 5' cap and poly(A) tail can be directly acted upon by mRNA decay pathway enzymes (see section 1.4). Alternatively, the specific, and sometimes lengthy, sequence elements recognized by miRNAs and some RBPs allow for shared mRNA targets and the co-regulation of several functionally related transcripts (~10-500 transcripts may be impacted per miRNA or RBP). Between the 5' cap/poly(A) tail and miRNA/RBP binding sites, reside several other cis-acting elements which are present in thousands of transcripts and thus able to regulate a significant portion of the transcriptome in response to external signals, such as developmental cues. Several of these cis-acting elements, including RNA modifications (Geula et al. 2015), AU-rich elements (AREs) (Yamaji et al. 2017), C-rich elements (CREs) (Neff et al. 2012) and pyrimidine tracts (Shibayama et al. 2009) modulate pluripotency and differentiation in stem cells by regulating gene expression via mRNA decay. Oftentimes, these types of cis-acting elements are located in the 5' or 3' untranslated regions (UTRs) of transcripts; but some, like RNA modifications, can also be found in the open reading frame (ORF) (Meyer et al. 2012; Dominissini et al. 2012). The mechanism and to what degree these cis-acting elements can promote or repress mRNA degradation often depends on the associated trans-acting factor, some of which are described below.

1.5.2 Trans-acting factors

1.5.2.1 miRNAs mediating mRNA decay

There are numerous examples of miRNAs modulating gene expression in stem cells to promote a pluripotent state or to drive differentiation. The Let-7 family of miRNAs and miR-145 down-regulate several key pluripotency factors including OCT4, LIN28, MYC, SOX2 and KLF4 (Xu et al. 2009; Melton et al. 2010). In contrast, expression of miR-138, miR-294 and miR-302 promotes self-renewal and inhibits differentiation of ESCs (Ye et al. 2012; Wang et al. 2013a).

To silence and specifically degrade mRNA targets, miRNAs form an RNP complex with Argonaute (AGO) proteins and other co-factors called the RNA-induced silencing complex (RISC) (O'Brien et al. 2018). Once the RISC is formed, it targets specific mRNAs based on their complementarity to the seed sequence of the loaded miRNA (Lewis et al. 2005). Upon binding to an mRNA, the RISC represses translation of the target mRNA, but also promotes the eventual decay of the mRNA via recruitment of mRNA decay enzymes. For example, the RISC co-factor TNRC6A (also known as GW182) serves as a hub for both deadenylase complexes, CCR4-NOT and PAN2/3, as well as the exosome to promote 3' to 5' degradation (Bartel 2018; Huntzinger et al. 2013; Jonas and Izaurralde 2015). Moreover, the RISC can also recruit DCP2 and its co-factors to enable 5' to 3' degradation via XRN1 (Rehwinkel et al. 2005; Behm-Ansmant et al. 2006; Nishihara et al. 2013). A perfect or near perfect match between a miRNA and mRNA target triggers endonucleolytic cleavage via AGO proteins (Song et al. 2004) and renders the cleaved mRNA vulnerable to exonucleolytic degradation in both directions. Although this can occur in mammals, these events are rare and more commonly occur in plants (Sieburth and Vincent 2018). Thus, miRNAs can facilitate all major pathways of mRNA degradation.

1.5.2.2 RBPs mediating mRNA decay

To date, there are more than 1,500 known RBPs, and varying portions of this population play a role in almost every major cellular pathway and function (Hentze et al. 2018; Gerstberger

et al. 2014). In terms of mediating degradation, RBPs can influence every facet of the mRNA decay pathway (Fenger-Grøn et al. 2005; Webster et al. 2019; Park et al. 2019; Thoms et al. 2015; Kretschmer et al. 2018). Intriguingly, RBPs can even monitor mRNA decay rates and influence transcription accordingly (Gilbertson et al. 2018). When an mRNA is degraded, most notably by XRN1, RBPs that were bound to the mRNA, like Cytoplasmic Poly(A) Binding Protein 1 (PABPC1) and LA-related protein 4 (LARP4), translocate to the nucleus and interact with RNA Polymerase II (RNAP II) to influence transcription of the degraded mRNA (Küspert et al. 2015). However, the full mechanistic pathway for how this occurs remains uncharacterized. For brevity, we focus on a few key examples of RBP-mediated mRNA decay that pertain to some of the cis-acting elements mentioned above.

Numerous RBPs interact with AREs. Of these, Hu antigen R (HuR or ELAV1) and Tristetraprolin (TTP aka ZFP36) are two well-characterized examples. Intriguingly, there are several reports that indicate HuR-mediated stabilization plays a crucial role in stem cell maintenance and differentiation (McDermott et al. 2018; Wang et al. 2014c; Carelli et al. 2019). Moreover, quiescence of muscle stem cells is modulated by TTP-mediated mRNA decay (Hausburg et al. 2015). TTP binds to the sequence UUAUUUAUU, which is considered to be the canonical destabilizing element of AREs (Lai et al. 2005; Brewer et al. 2004). Upon binding, TTP promotes deadenylation, and subsequent 3’ to 5’ degradation, through direct recruitment of the CCR4-NOT complex and the exosome (Lykke-Andersen and Wagner 2005; Hau et al. 2007). Additionally, TTP can deliver ARE-containing mRNAs to P-bodies for decapping (Franks and Lykke-Andersen 2007) and facilitate miRNA-dependent mRNA decay (Jing et al. 2005). Conversely, HuR stabilizes ARE-containing mRNAs (Peng et al. 1998) by impeding and even replacing TTP interactions (Tiedje et al. 2012), as well as blocking miRNA binding (Wang et al. 2014c).

Like AREs, pyrimidine tracts and their associated trans-acting factors polypyrimidine tract-binding proteins (PTBPs) have several reported roles in stem cell maintenance and

differentiation (Li et al. 2014b; Shibayama et al. 2009; Yeom et al. 2018; Vuong et al. 2016). One of the more notable examples involves a change in PTBP1 and PTBP2 expression and activity during neural differentiation (Li et al. 2014b; Vuong et al. 2016; Suckale et al. 2011; Makeyev et al. 2007). PTPB1 expression in pluripotent stem cells helps to repress neural-specific splicing programs and promote self-renewal. Upon induction of neural differentiation, PTBP1 expression is reduced, allowing PTBP2 to take over and initiate a splicing program that is critical for neuronal maturation and survival. However, the activities of PTBP1/2 are not entirely antagonistic, as they do serve redundant functions in other aspects of regulating gene expression (Zheng et al. 2012; Vuong et al. 2016).

The connection between PTBP functions and mRNA decay is not always as direct compared to AREs. Like the above example, many of these mechanisms indirectly mediate mRNA decay, primarily through changes in splicing. For example, PTBP1-mediated splicing regulates maturation of miR-124, which subsequently influences the expression of neuronal-specific factors (Yeom et al. 2018; Makeyev et al. 2007). On the other hand, PTBP1 can modulate alternative polyadenylation (APA) which directly impacts a transcripts vulnerability to the exosome and/or potential binding sites for other decay-associated factors (Domingues et al. 2016; Castelo-Branco et al. 2004; Le Sommer et al. 2005). In one of the more direct examples, interactions between PTBP3 and *ZEB1* mRNA result in stabilization of the transcript and help to promote the epithelial-mesenchymal transition (EMT) (Hou et al. 2018). Although the exact mechanism remains uncharacterized, it is believed the presence of PTBP3 may inhibit binding of miRNAs or other RBPs that promote degradation.

In this thesis, we chose to further explore two groups of RBPs; those which recognize the RNA modification m^6A, termed m^6A readers, and those that bind to CREs, specifically the PCBP family. In recent years, there has been mounting evidence that both of these factors are utilized by stem cells to regulate gene expression (Geula et al. 2015; Ghanem et al. 2018, 2015). In terms of RNA decay, the YTH N^6-methyladenosine RNA-binding protein YTHDF2 facilitates the

clearance of unwanted mRNAs during certain periods of development (Li et al. 2018b; Ivanova et al. 2017; Zhao et al. 2017b). Moreover, our lab and others has previously shown that mRNAs containing CREs exhibit differentially stability in pluripotent stem cells compared to differentiated fibroblasts (Neff et al. 2012; Huang et al. 2015b); likely due in part to differential expression of some of the PCBP proteins. Below, we provide a more detailed look at the current state of m^6A methylation and the PCBPs.

1.6 The m^6A methylation pathway[2]

Virtually all RNA species including mRNAs, transfer RNAs (tRNAs), ribosomal RNAs (rRNA), miRNAs and lncRNAs can experience methylation at various positions (m^1A, m^5C, 2'-O-methyl etc.). Of these modifications, m^6A has the best characterized effects on gene expression and was the first shown to modulate mRNA abundance (Dominissini et al. 2012; Meyer et al. 2012). m^6A modification can modulate the fate of an mRNA at the level of splicing (Xiao et al. 2016), cleavage/polyadenylation (Kasowitz et al. 2018), subcellular localization (Roundtree et al. 2017; Edens et al. 2019), decay (Wang et al. 2014b) and translation (Wang et al. 2015b). Moreover, m^6A is the most prevalent internal mRNA modification in many eukaryotic species (Bodi et al. 2010; Luo et al. 2014; Lence et al. 2017; Meyer et al. 2012; Dominissini et al. 2012). Although m^6A was discovered over 40 years ago (Perry and Kelley 1974; Wei et al. 1976; Desrosiers et al. 1974), its cellular function was only characterized through recent advancements in antibody-based precipitation and high-throughput sequencing. Since 2012, ~10,000 m^6A sites have been documented in over a quarter of human transcripts (Meyer et al. 2012; Dominissini et al. 2012; Chen et al. 2015a). The precise impact m^6A marks have on RNA metabolism and gene expression is dictated by the actions of methyltransferases ('writers'),

[2] Section 1.6 and the associated figures are modified from: Small changes, big implications: The impact of m^6A RNA methylation on gene expression in pluripotency and development. Biochimica et Biophysica Acta (BBA) - Gene Regulatory Mechanisms. Vol. 1862, No. 9, September, 2019.

demethylases (‘erasers’) and m^{6}A binding-proteins (‘readers’), many of which are now known to play roles in pluripotency and development.

1.6.1 The How, Where, When and Why of m^{6}A Writing

The N^6-position of adenosine in RNAs can be methylated by four separate methyltransferase activities: CAPAM (also known as PCIF1) targets 2’-O-methyladenosine found adjacent to the 5’ cap to produce m^{6}A$_m$ (Akichika et al. 2019; Cowling 2019), DIMT1L catalyzes dimethylation of two adjacent adenosines in18S rRNA (Zorbas et al. 2015; Lafontaine et al. 1995), whereas METTL16 (Warda et al. 2017; Brown et al. 2016; Pendleton et al. 2017; Shima et al. 2017; Doxtader et al. 2018; Ruszkowska et al. 2018) and the METTL3/METTL14 (Liu et al. 2014) heterodimer are responsible for internal m^{6}A modifications. For brevity, we will be focusing on the METTL3/METTL14 methyltransferase which installs the vast majority of internal m^{6}A marks on mRNAs and lncRNAs. The remaining methyltransferase activities are described in more detail in Heck and Wilusz, 2019. METTL3/METTL14 is part of the surprisingly large m^{6}A writer complex which can be divided into two sub-complexes: the m^{6}A-METTL complex (MAC), which comprises METTL3 and METTL14 (Liu et al. 2014), and the m^{6}A-METTL-associated complex (MACOM), comprising WTAP, ZC3H13, RBM15/15B, VIRMA and HAKAI (Ping et al. 2014; Guo et al. 2018; Yue et al. 2018; Knuckles et al. 2018; Růžička et al. 2017) (Fig. 1.2). In order to perform catalysis, the m^{6}A writer must be localized appropriately within the cell and directed to appropriate sites on each RNA. Furthermore, activity must be regulated such that methylation is restricted to the appropriate developmental stage and/or RNA region. We discuss how these functions are achieved below.

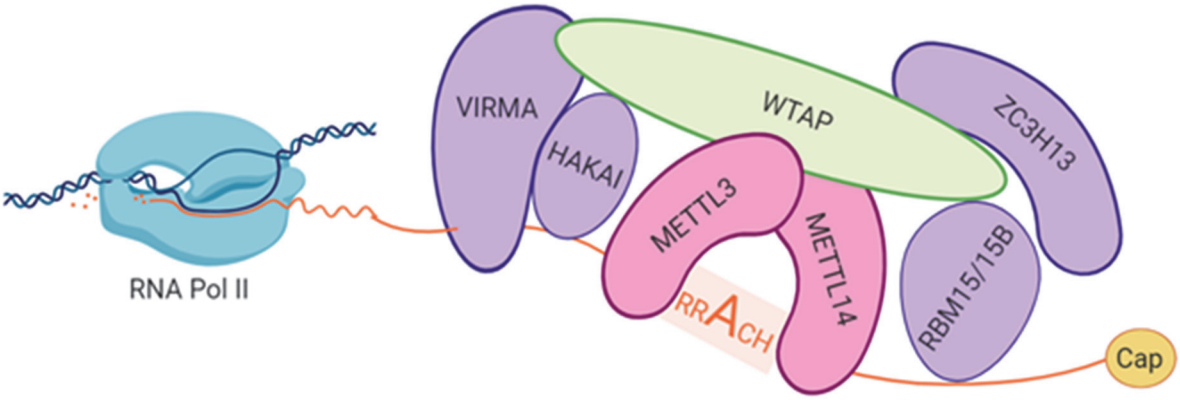

Figure 1.2: The m^{6}A writer complex. The m^{6}A writer complex targets RNAs as they are transcribed. The m^{6}A-METTL complex (MAC; shown in pink), consisting of the METTL3/14 heterodimer, is the catalytically active subcomplex which methylates adenosine at sites matching the RRACH consensus. WTAP is the major scaffolding protein that connects the MAC and m^{6}A-METTL-associated complex (MACOM). The composition and/or activity of MACOM subunits can influence the distribution of m^{6}A across a transcript. VIRMA and HAKAI favor 3' methylation, while RBM15/15B facilitates 5' methylation.

1.6.1.1 Methyltransferase Activity (How is m^{6}A added?)

The MAC is responsible for the methyltransferase activity of the writer complex (Liu et al. 2014; Schöller et al. 2018). Briefly, this reaction entails the transfer of a methyl group, from an S-Adenosyl Methionine (SAM) molecule, onto the sixth nitrogen of the adenosine base. METTL3 is the sole catalytic subunit and the only one able to bind the SAM methyl donor (Wang et al. 2016b, 2016a; Śledź and Jinek 2016; Huang et al. 2018b). While METTL3 possesses weak methyltransferase activity *in vitro*, the METTL3/METTL14 heterodimer exhibits substantially higher catalytic activity (Liu et al. 2014). Although METTL14 does not perform catalysis, it is essential for methyltransferase activity, providing structural stability, and allosterically enhancing the methyltransferase activity of METTL3 (Schöller et al. 2018; Wang et al. 2016b, 2016a). Interactions between METTL3 and METTL14 form a cavity where the RNA substrate is bound (Śledź and Jinek 2016; Wang et al. 2016a, 2016b).

The methyltransferase domains of METTL3 and METTL14 are highly conserved among eukaryotes, with functional homologs in *Drosophila* (Ime4 and Cg7818, respectively) (Hongay and Orr-Weaver 2011; Lence et al. 2017), *Arabidopsis* (Mta and Mtb, respectively) (Zhong et al. 2008; Růžička et al. 2017) and *S. cerevisiae* (IME4 and KAR4; although the role of KAR4 remains uncharacterized) (Clancy et al. 2002; Lence et al. 2018). Consistent with their high level of conservation, these proteins are essential for viability in mammals and plants, and play vital roles in embryonic development, sex determination and gametogenesis (Bodi et al. 2012; Kan et al. 2017; Schwartz et al. 2013; Aguilo et al. 2015; Geula et al. 2015; Wang et al. 2018c; Lin et al. 2017; Xu et al. 2017; Haussmann et al. 2016). Depletion of either protein in human cell lines results in a marked global decrease in m^{6}A levels (Ping et al. 2014; Liu et al. 2014).

1.6.1.2 Methyltransferase Specificity (Where on the mRNA?)

When it comes to methylation, not all adenosines are created equal. The context of the adenosine is critical in determining where and whether a transcript is modified. MAC target sites

are enriched for the short and low complexity consensus m^{6}A motif, RRACH (Rottman et al. 1994; Liu et al. 2014; Ping et al. 2014). However, the expected occurrence of the RRACH motif in RNAs (~1 modification per 85 nucleotides) is much higher than the observed one m^{6}A modification per ~1000 nucleotides (Dominissini et al. 2012; Linder et al. 2015; Chen et al. 2015a; Meyer et al. 2012). Only a fraction of adenosines found within this motif are actually modified, supporting the existence of additional layers of regulation. Such regulation likely includes selective recruitment of the MAC to specific RNA substrates and is influenced by the surrounding sequence context (such as structure, and availability of binding sites for competing factors).

Recent studies are starting to reveal how MAC is recruited to specific RNAs. There is evidence for interactions between MAC and chromatin/transcription factors including CEBPZ (Barbieri et al. 2017), SMAD2/3 (Bertero et al. 2018) and ZFP217 (Aguilo et al. 2015). These interactions facilitate (CEBPZ, SMAD2/3) or repress (ZFP217) m^{6}A modification of transcripts derived from promoters dependent on these transcription factors. For example, in stem cells SMAD2/3 is activated by TGFβ signaling and binds promoters of genes involved in early cell fate, including NANOG. It then recruits WTAP and MAC to allow RNA methylation. Marking these transcripts with m^{6}A helps prime stem cells for a timely exit from pluripotency (Bertero et al. 2018). More broadly, an interaction between METTL14 and trimethylated histone H3 (H3K36me3) may help recruit MAC to nascent RNAs/RNAP II (Huang et al. 2019) and thereby promote m^{6}A deposition. These observations suggest that transcripts can be selected for modification as they are transcribed and also supports that the epigenome can directly influence the epitranscriptome.

Once MAC is recruited to an mRNA, there is further regulation to determine which sites within that transcript will be modified. Specificity is conferred by METTL3 via its two CCCH-type zinc finger domains (Huang et al. 2018b) and METTL14 through a C-terminal domain containing RGG repeats (Schöller et al. 2018). Recent observations imply that the sequence context, and

its match to the preferred consensus, may be a driving factor determining the distribution and extent of m^{6}A modification (i.e. the m^{6}A signal is 'hard-coded' into the mRNA sequence). In further support of this hypothesis, a remarkable number of m^{6}A sites, and the flanking sequences, are conserved across vertebrates (Zhang et al. 2019c; Dominissini et al. 2012), and in some cases even in organisms as distant as yeast (Garcia-Campos et al. 2019b).

It is important to note that m^{6}A is not uniformly distributed across the length of the transcript (Figure 1.3). There are distinct preferences for the 5' and 3' UTRs (Dominissini et al. 2012; Meyer et al. 2012; Patil et al. 2016; Liu et al. 2017). Interestingly, the consensus RRACH motif is also enriched in these areas, particularly near the stop codon (Zhang et al. 2019c), and H3K36me3 chromatin marks also show a skewed enrichment around stop codons (Huang et al. 2019), which may contribute to enhanced MAC recruitment. In addition, the FTO demethylase may prune the methyl group from sites at the 5' end (Zhao et al. 2014, 2018; Zhou et al. 2015a) resulting in an overall enrichment of m^{6}A at the 3' end of RNAs. In exons, the vast majority of m^{6}A marks are located internally, residing at least 50 nucleotides away from splice junctions (Ke et al. 2017). Moreover, there is an enrichment of m^{6}A in long (>200 nucleotides) internal exons (Ke et al. 2017; Dominissini et al. 2012; Schwartz et al. 2014; Zhang et al. 2019c). The purpose and mechanism by which this is achieved is unclear. Interestingly, introns are rarely methylated when compared to exons, despite containing nearly three times the amount of sequence in chromatin-associated nascent pre-mRNA (Ke et al. 2017; Chen et al. 2015a). One explanation for this observation could be that the splicing machinery outcompetes or has priority over the m^{6}A writer complex for access to nascent RNA. As well as being concentrated in specific regions of the RNA, m^{6}A sites are often found in clusters, similar to DNA methylation sites in CpG islands (Meyer et al. 2012; Chen et al. 2015a; Ke et al. 2017; Linder et al. 2015; Zhang et al. 2019c). Clustering may be achieved in part through an association between the METTL3 and RNAP II that facilitates methylation when transcription slows (Slobodin et al. 2017), but also inherently requires that the available consensus sites be clustered.

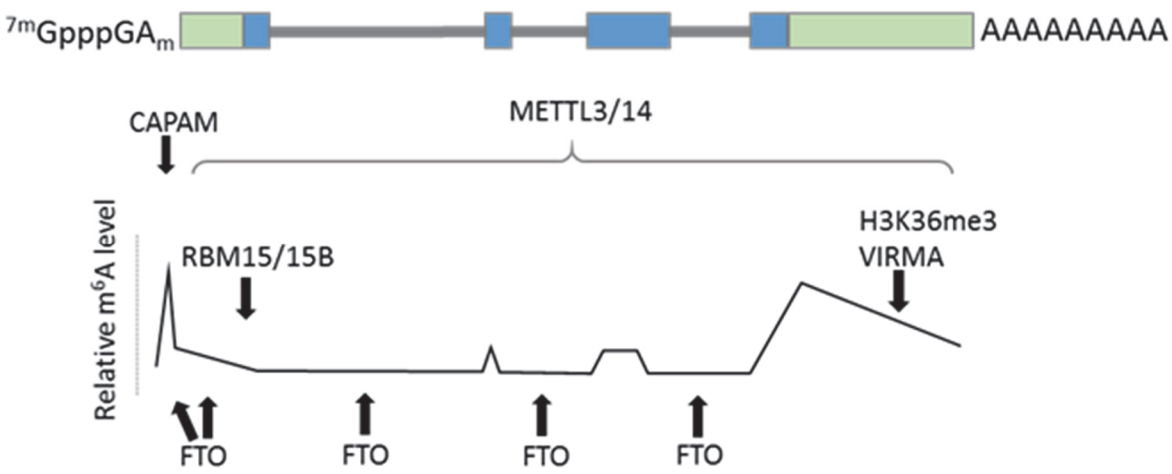

Figure 1.3: Factors influencing the distribution of m^6A and m^6A_m on mammalian mRNAs. The overall m^6A landscape in physiological conditions is determined primarily by the distribution of consensus motifs recognized by the methyltransferases (CAPAM, METTL3/14). However, it can be influenced by demethylases such as FTO, which prunes m^6A from introns and across the transcript. Moreover, certain components of the MACOM, namely RBM15/15B and VIRMA, can favor methylation at the 5' and 3' ends respectively. Finally, there is evidence that histone modifications can influence m^6A deposition.

Finally, the MAC can be directed to a specific location on an RNA through interaction with components of the MACOM, some of which are RBPs. Specifically, VIRMA recruits the m^{6}A writer complex to sites near the stop codon and within the 3' UTR (Yue et al. 2018), while RBM15 and RBM15B binding sites are enriched in the 5' UTR of transcripts (Patil et al. 2016). RBM15/15B both bind U-rich sequences through canonical RRMs, whereas VIRMA lacks a characterized RNA binding domain, but may be recruited to mRNAs through interaction with the cleavage and polyadenylation machinery (Yue et al. 2018). Interestingly, depletion of VIRMA in human cells resulted not only in a decrease in m^{6}A marks near the stop codon and within the 3' UTR, but also a significant increase in methylation at 5' UTRs (Yue et al. 2018). This suggests that RBM15/15B and VIRMA may compete for recruitment of the writer complex to the 5' and 3' UTR regions of a transcript, respectively. HAKAI, an E3 ubiquitin ligase, may also guide MACOM to specific sites or modulate activity of the complex, but more work is needed to uncover its exact role (Růžička et al. 2017). Changes in expression or activity of proteins like these may facilitate developmental changes in the distribution of m^{6}A, such as the switch from 3' UTR to 5' UTR m^{6}A seen during cerebellum development in mice (Ma et al. 2018).

To sum up, the MAC is recruited to specific RNAs/RNAP II through interactions with histones and transcription factors. m^{6}A is then deposited on RNAP II transcripts in positions that are selected in large part on the basis of how close they match the preferred motif for METTL3/METTL14. However, the final distribution of m^{6}A is also influenced through recruitment and repression of the methyltransferase by RBPs, and histone marks, as well as through removal of the modification at the 5' end by the demethylase, FTO (Zhao et al. 2014; Jia et al. 2011). As a result, m^{6}A is concentrated towards the 3' end of RNAs.

1.6.1.3 Methyltransferase Localization

It is clear that m^{6}A modification occurs early in the life of an mRNA (Ke et al. 2017; Knuckles et al. 2017) and this is consistent with the observation that the writer complex accumulates in

nuclear speckles. These membraneless organelles congregate near sites of active transcription and serve as a reservoir for factors that participate in transcription and pre-mRNA processing (Galganski et al. 2017). WTAP, the third subunit of the core methyltransferase, plays no characterized role in catalysis or substrate selection but is essential for proper MAC localization to nuclear speckles (Liu et al. 2014), as is ZC3H13 (Wen et al. 2018). Importantly, if the MAC is not appropriately localized, it does not function: depletion of WTAP or ZC3H13 results in a profound global reduction in m^{6}A methylation (Wen et al. 2018; Ping et al. 2014; Liu et al. 2014).

1.6.1.4 Regulating the Writer

Cells modulate m^{6}A profiles in response to differentiation cues and external signals such as heat shock, DNA damage or stress (Batista et al. 2014; Zhou et al. 2015a; Yu et al. 2018; Engel et al. 2018; Xiang et al. 2017). The complexity of the m^{6}A writer allows for many levels of regulation; changes in abundance of individual subunits, and post-translational modifications (PTMs) likely influence activity at different stages of development and differentiation. However, to date we have only scratched the surface in identifying how such regulation is achieved. METTL3, being the catalytically active subunit, is an obvious target for regulation, and is targeted by miRNAs (Du et al. 2017) and SUMOylation (Du et al. 2018). Other subunits appear to be dependent on METTL3 for their stability or expression (Sorci et al. 2018) and can also be impacted by PTMs (Schöller et al. 2018). However, there are still many knowledge gaps with respect to how these events regulate methyltransferase activity and the m^{6}A landscape overall.

1.6.2 m^{6}A erasure

Modifications of nucleic acids, including the 5’ cap and poly(A) tail on RNA and methylation of cytosine in DNA, are generally reversible; their removal is catalyzed by dedicated enzymes (decapping enzymes, deadenylases, and T5-methylcytosine hydroxylases, respectively) with well-characterized consequences such as decay/inactivation of RNAs and de-repression of

gene expression. The m^{6}A modification is also reversible, through the action of two enzymes in the α-ketoglutarate-dependent dioxygenase (AlkB) family (ALKBH5 and FTO/ALKBH9). Both ALKBH5 and FTO remove internal m^{6}A modifications, and thus can directly oppose the action of METTL3. However, as discussed below, ALKBH5 activity is restricted both temporally and spatially, suggesting that it is not a global regulator of all methylated mRNAs. A major impact of FTO may arise from its ability to target m^{6}A$_m$ adjacent to the 5' cap structure, especially in snRNAs (Mauer et al. 2017, 2019).

Like other AlkB proteins, ALKBH5 and FTO utilize an α-ketoglutarate (αKG) domain to recognize the m^{6}A-modified RNA, and also bind Fe(II) and αKG cofactors (Fedeles et al. 2015; Jia et al. 2011; Zheng et al. 2013). In addition, they possess a nucleotide recognition domain that interacts with the RNA substrate. Upon substrate recognition the demethylases catalyze oxidative dealkylation of m^{6}A to regenerate an unmodified adenosine (Zheng et al. 2013; Baltz et al. 2012; Feng et al. 2014a; Xu et al. 2014a; Shen et al. 2014). Interestingly, intermediates of this reaction have been detected in mRNAs isolated from human cells and mouse tissue. Moreover, *in vitro* assays have indicated the presence of these intermediates attenuates the binding affinity of m^{6}A readers (Fu et al. 2013). However, more work is needed to discern if there are any major biological effects. The ALKBH5 protein is localized to nuclear speckles and is thought to act upon nascent mRNAs (Zheng et al. 2013), whereas FTO shuttles between nucleus and cytoplasm (Wei et al. 2018; Zhou et al. 2015a) and can affect both nascent and mature transcripts (Jia et al. 2011; Su et al. 2018; Wei et al. 2018; Zhao et al. 2014; Mauer et al. 2017; Ke et al. 2017). Importantly, although the AlkB protein family is conserved across eukaryotic and bacterial domains, ALKBH5 and FTO are found only in vertebrates (Robbens et al. 2008; Zheng et al. 2013), although *Arabidopsis* has two alternative demethylases, ALKBH9B (Martínez-Pérez et al. 2017) and ALKBH10B (Duan et al. 2017). The fact that eraser proteins are absent from lower eukaryotic organisms, which have both writers and readers of m^{6}A,

suggests that demethylation is unlikely to play a general role in reversing all m^6A modifications but rather may have evolved to act on specific substrates and/or in response to external signals.

In support of this idea, knockout of ALKBH5 has no discernable effect on overall health in mice but results in profound defects in spermatogenesis, leading to male infertility (Zheng et al. 2013). Although ALKBH5 has the potential to broadly counteract the action of METTL3, it appears this is not its primary role in most cell types. Outside of the testes, the impact of ALKBH5-mediated demethylation on overall levels of m^6A is modest (Zheng et al. 2013) and m^6A status of mRNAs does not vary greatly as they mature and enter the cytoplasm (Ke et al. 2017). These two observations again support that only a subset of m^6A modifications are targeted for removal by ALKBH5. However, it is not clear how selectivity may be achieved as the evidence for any sequence preference is weak (Zheng et al. 2013; Zou et al. 2016). Although the overall influence of demethylation by ALKBH5 in most normal cells is modest based on the robust health of knockout mice (Zheng et al. 2013; Tang et al. 2018), the protein is upregulated in hypoxia (Thalhammer et al. 2011) and in certain cancer cells (Zhang et al. 2017b) and modulates expression of number of transcripts such as TFEB, FOXM1, and NANOG (Song et al. 2019; Zhang et al. 2017b, 2016a). Thus, for some transcripts and responses ALKBH5 may be important.

In contrast to ALKBH5, FTO knockout has quite dramatic effects in mice with links to obesity and neurogenesis (Robbens et al. 2008; Church et al. 2010; Wu et al. 2018b; Ma et al. 2018) although some phenotypes may be due to indirect effects on neighboring genes (Fawcett and Barroso 2010; Tung et al. 2014). Since the recent discovery that FTO specifically targets m^6A_m to reverse methylation adjacent to the cap (Mauer et al. 2017), it is not so clear what proportion of FTO's impact on gene expression is due to removal of m^6A_m versus m^6A or even m^1A (Wei et al. 2018). It should also be noted that MeRIP-seq experiments are, at least in part, at the mercy of m^6A antibody specificity which currently have difficulties distinguishing between m^6A and m^6A_m (McIntyre et al. 2019; Mauer et al. 2017). There is evidence to suggest FTO may prune

m^{6}A from the 5’ UTR of specific mRNAs in the nucleus and that this activity is blocked during stress (Zhao et al. 2014, 2018; Zhou et al. 2015a; Yu et al. 2018)(see below). This is consistent with m^{6}A being more abundant at the 3’ end and around the stop codon in mammals, while being prevalent around both the start and stop codons in *Arabidopsis* (Luo et al. 2014), which lack FTO (Robbens et al. 2008; Luo et al. 2014). Conversely, there is also evidence that FTO acts on m^{6}A sites outside of the 5’ UTR (Hess et al. 2013; Zhou et al. 2018), suggesting that the demethylase activity of FTO is not confined to any one region of transcripts. In addition, FTO associates with intronic sequences which may partially explain why introns exhibit significantly lower levels of modification than exons (Bartosovic et al. 2017) (Fig. 1.3). However, it is hard to distinguish whether effects of FTO on splicing are due to altered function of snRNAs (which have m^{6}A$_m$ cap structures and are essential components of the splicing machinery) versus changes in binding of RBPs that are recruited or repressed by m^{6}A (see Heck and Wilusz, 2019 for more details).

Overall, demethylation may have a significant effect on expression and/or processing of specific transcripts, or during certain cellular responses, but more research is required to tease out when in the RNA life cycle demethylation occurs and how widespread its influence really is. This topic has been debated recently (Zhao et al. 2018; Darnell et al. 2018; Mauer and Jaffrey 2018; Ke et al. 2017; Mauer et al. 2017; Wei et al. 2018). Many of the points and observations made in this debate are discussed above; but to summarize, the debate focuses on how dynamic m^{6}A truly is and the activity of FTO. One side argues that the vast majority of methylation/demethylation events occur on nascent pre-mRNA (Ke et al. 2017; Darnell et al. 2018). Thus, once an mRNA disassociates with the transcriptional machinery, its m^{6}A profile is fairly well determined. Moreover, they propose the primary target of FTO is m^{6}A$_m$, present only at the 5’ cap, and not m^{6}A (Mauer et al. 2017; Mauer and Jaffrey 2018), implying there is no known demethylase that primarily erases m^{6}A modifications. The opposing side presents evidence of FTO activity specifically in the cytoplasm, indicating that demethylation can occur

post-transcription (Zhao et al. 2018; Wei et al. 2018). Moreover, FTO targets both m^6A_m and m^6A equally in the cytoplasm, but is preferentially to m^6A in the nucleus. They also highlight an independent study which observed an enrichment of FTO binding sites near the stop codon and throughout the 3' UTR (not m^6A_m sites) as well as at the transcription start site (like to be m^6A_m sites) (Bartosovic et al. 2017). Ultimately, this debate underscores the fact that more research is required to fully understand the nature of m^6A dynamics.

1.6.3 How m^6A affects RNA fate: Functions of the m^6A readers

Deposition of m^6A does not immediately trigger degradation or activate translation. Rather, m^6A influences RNA secondary structure and association with proteins and other RNAs to direct altered processing (Kasowitz et al. 2018; Xiao et al. 2016), export (Roundtree et al. 2017; Edens et al. 2019), translation (Wang et al. 2015b; Shi et al. 2017; Li et al. 2017) or decay (Wang et al. 2014b; Du et al. 2016a; Shi et al. 2017; Wojtas et al. 2017) (Fig. 1.4). The presence of m^6A favors a single stranded conformation and can therefore disrupt stem-loop structures (Roost et al. 2015) in a process termed 'm^6A switching' (Liu et al. 2015b). In some cases, this can allow enhanced binding of proteins like HNRNPC, which, in turn, alters abundance and alternative splicing of target mRNAs (Liu et al. 2015a; Zhou et al. 2015b). Alternatively, m^6A can block proteins from binding (Liu et al. 2017; Wu et al. 2018a; Arguello et al. 2017). For example, inhibition of HuR binding, due to the presence of m^6A, leaves mRNAs susceptible to miRNA-mediated degradation (Wang et al. 2014c). Although indirect influences on protein and miRNA binding have a significant impact, for brevity, this section will focus on the recruitment of proteins that directly recognize m^6A (a.k.a. m^6A readers) and their effects on RNA metabolism.

1.6.3.1 Reader Recognition of m^6A

The best characterized m^6A readers are members of the YTH domain-containing family of proteins, namely YTHDF1-3, YTHDC1 and 2 in mammals. The YTH domain was originally

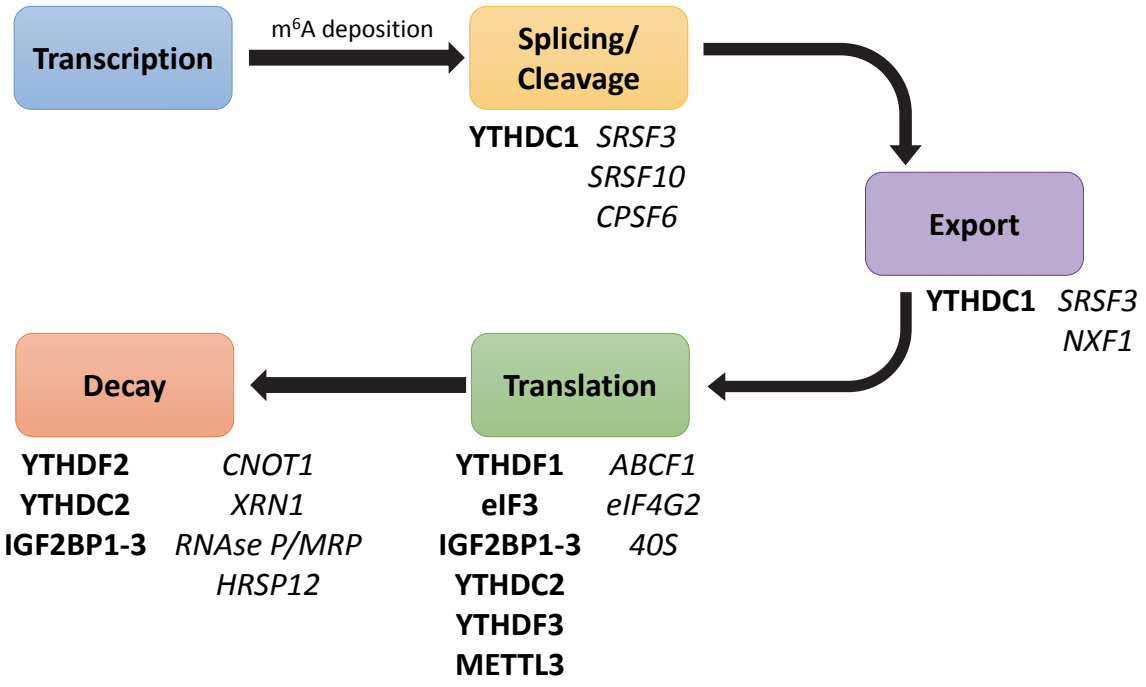

Figure 1.4: m^{6}A influences mRNA function from cradle to grave. Recognition of m^{6}A by methyl-reader proteins, bolded, can influence various RNA processes including splicing/cleavage, nuclear export, translation and decay. Often, reader proteins interact with or recruit effector proteins, italicized, to carry out a given function. They can also compete with miRNAs and RBPs.

identified in the splicing factor YT521-B/YTHDC1 (Zhang et al. 2010a; Imai et al. 1998), and is now known to confer m^6A-dependent RNA-binding activity (Stoilov et al. 2002; Zhang et al. 2010c). In all cases, the preference for m^6A-modified RNA is specified by an aromatic cage that forms a hydrophobic pocket around the modified nucleotide (Xu et al. 2014b, 2015; Li et al. 2014a; Zhu et al. 2014).

Beyond this, it is not clear whether each YTH protein recognizes a distinct motif that allows it to act on a unique population of mRNAs, or if binding is dictated primarily by relative availability and affinity of each family member. Furthermore, whether YTH domains can accommodate m^6A_m adjacent to the 5' cap has not been explored. Although there is some evidence for sequence preference outside of the clear requirement for m^6A, this must be evaluated critically, as experiments involving capture and sequencing of RNAs bound by YTH proteins inevitably give a motif that overlaps with that of the MAC (i.e. RRACH) (Hsu et al. 2017; Xiao et al. 2016; Wang et al. 2015b, 2014b; Li et al. 2017). For YTHDC1, *in vitro* and structural analyses support that there is a specific interaction with the G at the -1 position, relative to the methylated A, that does not occur in other YTH proteins (Xu et al. 2015, 2014b). Intriguingly, another *in vitro* selection assay, using SELEX-based approach, indicated YTHDC1 is highly preferential towards the canonical RRACH motif, whereas YTHDF1/2 more readily bind to non-canonical m^6A-modified motifs (i.e. CUAGA or CUAGU) (Arguello et al. 2019).

Other interactions between the RNA and YTH domain (Li et al. 2014a; Zhu et al. 2014; Wojtas et al. 2017), and possibly regions outside of the YTH domain (Lao and Barron 2019; Wang et al. 2014b; Xu et al. 2015), could confer additional sequence specificity. Such interactions must be important at some level, as RNAs less than 5 nucleotides long bind poorly to YTH proteins compared to longer transcripts (Xu et al. 2015). Additional specificity may also be derived from interactions of the YTH proteins with factors associating elsewhere on the RNA. For example, YTHDC1 interacts with 3' end formation factors which could favor binding towards the 3' end of mRNAs (Kasowitz et al. 2018).

The subcellular location of the RNA also influences its accessibility to different YTH proteins. In the nucleus, YTHDC1 has a much higher concentration (Xiao et al. 2016) whereas the other YTH proteins are more abundant in the cytoplasm (Wang et al. 2014b; Shi et al. 2017; Wang et al. 2015b; Hsu et al. 2017). At this point, the extent to which the sequence context of an m^6A site dictates reader binding potential and the subsequent fate of a modified RNA is an area in need of further investigation. Moreover, while the YTH domain accommodates m^6A, there is evidence that these proteins also associate with N^1-methyladenosine modified substrates (Dai et al. 2018) and that binding can occur independent of METTL3-mediated methylation (Zhang et al. 2019b).

It is also worth considering that multiple YTH proteins are programmed to recognize the same or adjacent methylated residues, as YTHDF1-3 have numerous shared targets (Li et al. 2017; Shi et al. 2017; Patil et al. 2016). These proteins appear to cooperate to modulate translation and decay, but it is not clear whether multiple YTH proteins bind simultaneously to the RNA substrate at adjacent m^6A residues, or if the first YTH protein to bind engages the others through protein-protein interactions (Fig. 1.5).

Although the majority of research on m^6A readers and their biological functions focuses on YTH proteins, other proteins with different RNA binding domains have been implicated as m^6A readers. The best supported of these are the insulin-like growth factor 2 mRNA-binding proteins (IGF2BP1-3) (Müller et al. 2018; Huang et al. 2018a), the eIF3 complex (Meyer et al. 2015) and PRRC2A (Wu et al. 2019). In these cases, there is compelling evidence for preferential binding of each factor to m^6A modified RNAs, but the structural basis of these interactions is unknown as all available crystal structures were derived using unmodified substrates. FMR1, or FMRP, has also been implicated as a potential m^6A reader (Arguello et al. 2017; Edupuganti et al. 2017), but binding of FMR1 to m^6A sites may be influenced more by the sequence context rather than the modification itself (Zhang et al. 2018a).

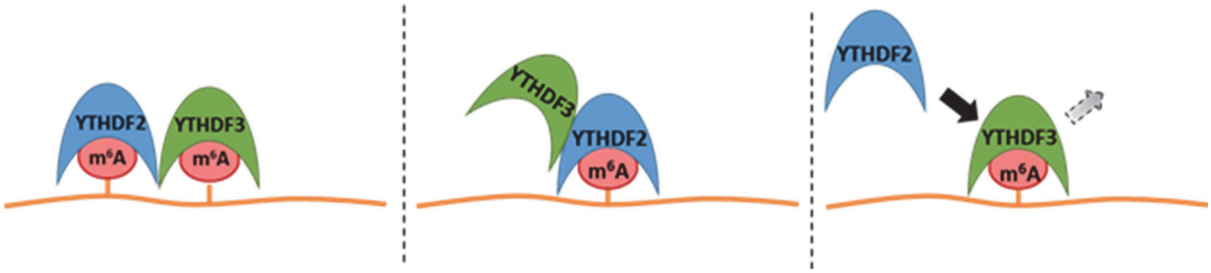

Figure 1.5: Competition and Collaboration between Reader Proteins. There are multiple possible mechanisms by which reader proteins interact with each other when binding to m^6A including: i). Reader proteins bind adjacent m^6A and recruit effectors to simultaneously influence multiple aspects of metabolism, ii). Reader protein binds m^6A and recruits other readers along with effectors, again allowing simultaneous impact on multiple pathways, iii). Reader proteins compete for single m^6A and shuttle mRNA down different pathways.

1.6.1.2 m^{6}A effects on decay

As mentioned above, m^{6}A readers have been shown to influence numerous aspects of the RNA life cycle including processing (Kasowitz et al. 2018; Xiao et al. 2016), export (Roundtree et al. 2017) and translation (Wang et al. 2015b; Shi et al. 2017; Li et al. 2017). For brevity, we have chosen to only highlight the effects on decay here, as they pertain directly to this study. For more detailed information about how m^{6}A impacts other aspects of the RNA life cycle please see Heck and Wilusz, 2019.

Multiple studies have shown that m^{6}A methylated transcripts are less stable than their unmodified counterparts (Du et al. 2016a; Wang et al. 2014b; Chen et al. 2015a; Batista et al. 2014; Geula et al. 2015; Shi et al. 2017), and YTHDF2 is the primary culprit causing this destabilization(Wang et al. 2014b). Under physiological conditions, a majority of YTHDF2 binding sites are found near the stop codon and within the 3' UTR (Wang et al. 2014b), which likely reflects the natural distribution of m^{6}A (Meyer et al. 2012; Dominissini et al. 2012). Upon substrate binding, YTHDF2 accelerates the degradation of target transcripts through direct recruitment of the CCR4-NOT deadenylase complex (Du et al. 2016a) via an interaction between YTHDF2 and the CNOT1 subunit of the deadenylase. As deadenylation is the first and rate-limiting step in decay of most mRNAs, modulating this step has a significant effect on overall mRNA decay rates (Łabno et al. 2016). At the same time, YTHDF2 can also work with the HRSP12 RBP to recruit RNAse P/MRP endonuclease (Park et al. 2019). YTHDF2-mediated decay represses transcripts encoding cell cycle regulators such as Cyclin A2 (CCNA2) and CDK2 (Wu et al. 2018b), and also clears populations of unwanted mRNAs such as maternal transcripts during oocyte maturation (Ivanova et al. 2017) and transcripts favoring self-renewal in differentiating hematopoietic stem cells (HSCs) (Li et al. 2018c). YTHDF2 plays an important role in clearing RNAs during cell state transitions such as the maternal-to-zygotic (Zhao et al. 2017b) and the epithelial-mesenchymal transitions (Chen et al. 2017).

While YTHDF2 makes the most obvious contribution to m^{6}A dependent mRNA decay, there is evidence that other YTH proteins also interface with the mRNA decay machinery. YTHDF2 and YTHDF3 both enhance deadenylation somewhat when tethered to a reporter mRNA (Du et al. 2016a), but this might perhaps be explained by observations that YTH proteins, and particularly YTHDF3, can augment the binding of other family members (such as YTHDF2) to their substrates (Shi et al. 2017). YTHDC2 is also able to down-regulate its targets, presumably by destabilizing them (Hsu et al. 2017), and has been implicated as an RNA stability factor in the germline, where it interacts with a meiosis-specific protein known as MEIOC (Abby et al. 2016; Soh et al. 2017). The interaction of MEIOC and YTHDC2 with mitosis-promoting transcripts, including CCNA2, enhances their decay and facilitates a sharp transition into meiosis (Bailey et al. 2017; Soh et al. 2017). These experiments indicate a primitive role for m^{6}A in meiosis that may be conserved from yeast to humans, as m^{6}A deposition only occurs during meiosis in *S. cerevisiae* (Bodi et al. 2015; Chia and van Werven 2016; Agarwala et al. 2012). The exact mechanism by which YTHDC2 influences decay in meiotic cells needs more study. While there is strong evidence for direct interaction between YTHDC2 and the 5'-3' exoribonuclease XRN1 (Kretschmer et al. 2018), XRN1 can only act on mRNAs that have already been committed to destruction by endonucleolytic cleavage or decapping (Braun et al. 2012). Furthermore, XRN1 is required for meiosis in *S. cerevisiae,* but its catalytic activity is dispensable (Solinger et al. 1999), suggesting that the interaction with XRN1 may not be directly responsible for the ability of YTHDC2 to enhance mRNA turnover.

The IGF2BP family of proteins also modulate the decay of m^{6}A-modified transcripts but unlike YTHDF2 and YTHDC2, IGF2BPs stabilize methylated transcripts (Huang et al. 2018a). In some cases, this is achieved through sequestration of methylated mRNAs into stress granules (Degrauwe et al. 2016), but stabilization can also be caused by impeding binding of destabilizing factors such as miRNAs (Müller et al. 2018). It is also worth noting that m^{6}A on its own can also modulate mRNA stability by perturbing binding of factors with overlapping target

sites. For example, the presence of m^{6}A impedes HuR binding and thereby favors association miRNAs at neighboring sites to enhance decay of developmental transcripts such as *IGF2BP3* and *FGF5* (Wang et al. 2014c).

Regulation of reader activity can be achieved through standard mechanisms including gene expression, subcellular localization and PTMs. In terms of gene expression, YTHDF2 is repressed by two miRNAs (Yang et al. 2017; Li et al. 2018a), while YTHDC2 is inducible by TNFα (Tanabe et al. 2014). Previously mentioned observations of YTHDF2 re-localizing to the nucleus during heat shock (Yu et al. 2018; Zhou et al. 2015a) and PTMs on YTHDC1 (Rafalska et al. 2004) infer there may be other instances of regulation awaiting discovery. Future studies regarding the mechanisms and situations by which reader activity is regulated will provide useful insight about the impact m^{6}A has on global gene expression.

1.6.4 How does m^{6}A-mediated mRNA decay influence pluripotency and development?

To summarize, m^{6}A is added to a large proportion of mRNAs and non-coding RNAs (ncRNAs) in many different tissues and cell types and can influence most, if not all, aspects of RNA metabolism. It is not surprising then that m^{6}A methylation has a great influence on both cell and organism function. However, despite the almost ubiquitous nature of m^{6}A modification, its power is observed most clearly in stem cells and during development (Geula et al. 2015; Batista et al. 2014; Wang et al. 2018c; Zhang et al. 2017a; Wang et al. 2014c), when large-scale coordinated changes in gene expression occur to determine cell fate. The effects of reducing m^{6}A methylation are highly cell-type dependent, suggesting that methyltransferase activity, the RNA targets it modifies, and/or the activity/abundance of methyl-readers are regulated in a cell-specific manner. Ultimately though, a common theme is that cell fate decisions are skewed following loss of methylation (Geula et al. 2015; Chen et al. 2019; Zhang et al. 2017a; Li et al. 2018b; Lin et al. 2017; Xu et al. 2017; Wu et al. 2018c; Wang et al. 2018a), suggesting that m^{6}A helps maintain stem cells in a balanced state where they are able to self-renew but also primed

to rapidly and efficiently differentiate down one or more pathways. When either methylation itself, or the activity of methyl-readers, is perturbed, the balance tips and cells are committed to a specific fate or permanently detained in the self-renewal program. The effects of m^{6}A-mediated mRNA decay on developmental decisions appear to occur through at least three mechanisms, which are discussed below.

1.6.4.1 Tipping the balance of dosage-sensitive master regulators

In many cases, methylation of mRNAs encoding one or two dosage sensitive master regulators (generally signaling or transcription factors) is pivotal. If expression of these key targets rises above, or falls below a threshold, it pushes the cell to differentiate, or alternatively into a permanent state of self-renewal or quiescence. A good example of this occurs during myeloid differentiation. Loss of METTL3 results in activation of quiescent HSCs to a proliferative state (Yao et al. 2018), while METTL14 (Weng et al. 2018a) and YTHDF2 (Li et al. 2018c; Wang et al. 2018b) are required for self-renewal of active HSCs – as silencing either gene favors myeloid differentiation. Two key targets of METTL14 in this process are the MYB and MYC transcription factor mRNAs whose expression is down-regulated following METTL14 depletion (Weng et al. 2018a). Moreover, upstream of this, m^{6}A deposition on the *NOTCH1* mRNA can promote its destabilization via YTHDF2 and repress Notch signaling. This favors the endothelial-hematopoietic transition (Lv et al. 2018; Zhang et al. 2017a).

1.6.4.2 Clearing unwanted mRNAs from the transcriptome

During differentiation and development, massive changes in gene expression occur which require that existing transcripts are cleared to make way for those being induced to specify the new cell type. Recent studies have found that m^{6}A methylation, through recruitment of the decay promoting factor YTHDF2, plays vital roles in clearing unwanted transcripts. During the maternal-zygotic transition in zebrafish, YTHDF2 associates with over one third of maternally

loaded mRNAs and induces their decay (Zhao et al. 2017b). Similarly, maternal mRNA clearance during mouse oocyte maturation is disrupted following loss of YTHDF2 (Ivanova et al. 2017). Interestingly, newly transcribed zygotic mRNAs are m^{6}A methylated, but their abundance is not generally affected by removal of YTHDF2 (Zhao et al. 2017b). Further investigation will be needed to determine what distinguishes the maternally supplied methylated mRNAs from those derived from the zygotic genome. Evidence suggests that there are multiple redundant mechanisms for maternal mRNA clearance which ensures robustness and reduces the influence of random variation (Sha et al. 2019).

YTHDF2 also clears mRNAs during differentiation events in downstream development. For example, timely differentiation of neural progenitor cells (NPCs) is dependent on YTHDF2-mediated clearance of several m^{6}A-modified transcripts that encode factors involved in negative regulation of neural development including NRP2, NRXN3, FLRT2, PTPRD and DRD2 (Li et al. 2018b). Because of this, loss of YTHDF2 in mice results in delayed neurogenesis and reduced neurite outgrowth.

1.6.4.3 Potentiating transcriptional changes for sharp transitions

It is clear that m^{6}A is deposited on many mRNAs, and thus has a widespread impact on overall gene expression. In this respect, m^{6}A modification is reminiscent of miRNA-mediated regulation. miRNAs fine tune gene expression, buffer against noise and confer robustness on biological systems (Ebert and Sharp 2012); all roles that can also be attributed to methylation. Specifically, while transcriptional changes are central to initiating cell fate transitions during development, methylation and its downstream effects are key to ensuring these transitions are carried through in a sharp and coordinated fashion. To this end, methylation is used to facilitate neuroectoderm differentiation through a mechanism activated by TGFβ signaling (Bertero et al. 2018). TGFβ signaling is required to maintain a pluripotent state and functions by activating

SMAD2/3 transcription factors. The MAC is recruited by activated SMAD2/3 to its target genes, resulting in enhanced methylation and destabilization of several mRNAs whose transcription is induced by TGFβ signaling, including that encoding the pluripotency factor NANOG (Bertero et al. 2018). It is well known that unstable transcripts respond more rapidly to external cues (Crisp et al. 2017; Eichelbaum and Krijgsveld 2014), thus by destabilizing its target mRNAs, methylation facilitates sharper down-regulation of pluripotency factors when TGFβ signaling is inhibited. This in turn allows timely exit from pluripotency and efficient entry into the neuroectoderm differentiation program.

1.7 Poly(C)-binding Proteins

The second pair of cis-acting element and associated trans-acting factors investigated in this thesis is CREs and the PCBP family (Makeyev and Liebhaber 2002; Leidgens et al. 2013). As mentioned above, our lab and others have reported that mRNAs containing CREs exhibit differential stability in pluripotent stem cells and differentiated fibroblasts (Neff et al. 2012; Huang et al. 2015b). Below, we provide more detailed information about the PCBPs and their known roles in self-renewal and differentiation.

The four members of the protein family, PCBP1-4 (aka αCP1-4 or HNRNPE1-4), are evolutionarily related and expressed rather broadly in both human and mouse tissues (Makeyev et al. 1999; Makeyev and Liebhaber 2000; Leffers et al. 1995). PCBPs can influence gene expression at various levels including transcription (Choi et al. 2008; Thakur et al. 2003), splicing (Ji et al. 2018), translational silencing (Wang et al. 2010; Ostareck et al. 2001) or enhancement (Bedard et al. 2004; Thomson et al. 2005) and mRNA decay (Chen et al. 2018; Hwang et al. 2017; Ho et al. 2013; Han et al. 2013b). In terms of biological outcomes, PCBPs have roles in regulation of iron levels within the cell (Yanatori et al. 2016; Leidgens et al. 2013; Li et al. 2012), immune response (Zhou et al. 2012; You et al. 2009) and, most importantly for

this study, proliferation and differentiation (Ghanem et al. 2015; Zhang et al. 2015b; Ye et al. 2016; Pio et al. 2004; Li et al. 2016).

1.7.1 Structure and binding capabilities of PCBPs

1.7.1.1 Domain and sequence conservation

PCBP1 and PCBP2 are closely related with nearly a 90% amino acid sequence similarity (Tommerup and Leffers 1996). This is largely due to the fact PCBP1 is an intronless, retrotransposed derivative of PCBP2 (Makeyev et al. 1999). In contrast, PCBP3 is more divergent and PCBP4 is the most distantly related to PCBP2 with only 48% amino acid sequence similarity (Makeyev and Liebhaber 2000; Chkheidze and Liebhaber 2003). The common thread which ties these proteins together is the presence of three HNRNPK homology (KH) domains (Makeyev and Liebhaber 2000). To this end, the general structure of the PCBPs is fairly similar with the first two KH domains occurring consecutively near the N-terminus followed by a variable length of intervening amino acid sequence and the third KH domain located at near the C-terminus (Sidiqi et al. 2005; Du et al. 2007, 2005; Fenn et al. 2007; Du et al. 2008).

1.7.1.2 Subcellular localization

In addition to the KH domains, all of the PCBPs contain at least one nuclear localization signal (NLS) present within the third KH domain, dubbed NLS II (Chkheidze and Liebhaber 2003). PCBP1 and 2 also possess a second NLS, NLS I, that is located within the variable sequence between KH domains two and three. As a result, PCBP1 and 2 localize to both the nucleus and the cytoplasm, whereas PCBP3 and 4 are primarily cytoplasmic (Chkheidze and Liebhaber 2003; Berry et al. 2006).

1.7.1.3 Nucleotide binding and other interactions

As would be expected, the KH domains are critical for recognition and binding of CREs. Structural analyses characterizing the interactions between different PCBP KH domains and the human C-rich telomeric DNA (5'-AACCCTA-3') have indicated the PCBPs are capable of binding to sequence motifs with as few as three cytosine residues (Du et al. 2005; Fenn et al. 2007; Du et al. 2007). I.e. the ACCC or CCCT element of the C-rich strand. Moreover, this interaction can occur with RNA or single stranded DNA as the target. Several stabilizing forces including hydrogen bonding, electrostatic interactions and van der Waals contacts act in concert to modulate the interaction. Intriguingly, there is also evidence that PCBP-RNA/DNA interactions may alter protein conformation, thereby revealing protein-protein interaction surfaces for PCBP-binding partners (Du et al. 2007, 2008). In an unbound state, the first two KH domains exist in a pseudodimer. However, the two KH domains must disassociate from each other to bind a DNA/RNA target. This disassociation results in the conformational changes necessary to reveal interaction surfaces for PCBP-binding partners.

1.7.2 PCBP-mediated mRNA decay

To date, multiple mechanisms have been reported for how PCBPs both promote and repress mRNA decay.

1.7.2.1 Stabilization of PCBP targets

PCBP1 has been shown to stabilize mu opioid receptor (MOR) mRNA by binding to CREs in the 3' UTR (Hwang et al. 2017). Phosphorylation of PCBP1 via protein kinase A (PKA) enables PCBP1 to recruit poly(A)-binding protein (PABP) and AU-rich element RNA-binding protein 1 (AUF1, also known as HNRNPD), both of which have previously been shown to enhance mRNA stability (Al-Khalaf and Aboussekhra 2019; Yi et al. 2018), to *MOR* mRNA. Likewise, PCBP1 interacts with CREs in the 3' UTR of endothelial nitric oxide synthase (eNOS) mRNA and

enhances stability by blocking potential binding sites for miR-765 (Ho et al. 2013). Other examples of PCBP1 (Shi et al. 2018a), PCBP2 (Xin et al. 2011; Chen et al. 2018) and PCBP4 (Scoumanne et al. 2011) promoting the stabilization of target transcripts have also been reported. However, the mechanisms by which stabilization occurs are not fully characterized.

1.7.2.2 Destabilization of PCBP targets

Conversely, there are several reports that describe how interactions with PCBP2 destabilizes target transcripts (Zhang et al. 2015a; Han et al. 2013b; Ren et al. 2016). In two of these instances, PCBP2 interacts with CREs in the 3' UTRs of transcripts to facilitate degradation (Han et al. 2013b; Zhang et al. 2015a). However, the precise mechanism(s) by which this occurs remain(s) elusive. Despite this, there are characterized mechanisms for how PCBP2 activity is regulated. Phosphorylation of PCBP2 by the MAP kinase, ERK1/2, increases protein stability and subsequent abundance (Chang et al. 2007), thus allowing for increased PCBP2 activity. On the other hand, miR-328, which is itself C-rich, can be used as a decoy to soak up PCBP2 and decrease its activity (Eiring et al. 2010; Saul et al. 2016). These same regulatory mechanisms can also influence the other members of the PCBP family (Hong 2017; Choi et al. 2009).

1.7.3 How do CREs and PCBPs influence pluripotency and development?

When considering the roles of PCBPs in pluripotency and development, it is important to note there are numerous links between aberrant expression of PCBPs and cancer growth/progression (Ye et al. 2016; Pio et al. 2004; Chen et al. 2015b, 2018; Zhang et al. 2015b). Although these are not direct ties to pluripotency or development, they could be indicative of a larger role for the PCBPs. With that being said, there are several reported instances of PCBPs playing a direct role in pluripotency and development. For instance, our lab has previously observed that mRNAs containing CREs are differentially expressed in iPSCs

compared to HFFs (Neff et al. 2012). Moreover, this differential expression is likely due to the destabilization of CRE-containing mRNAs in iPSCs. This observation has been reported by other labs as well when comparing murine ESCs and differentiated fibroblasts (Huang et al. 2015b), indicating this mechanism is conserved in mammals.

Beyond the influence on mRNA stability, it has been observed that knockout of PCBP1 in mice is lethal by day E8.5, but death can occur as early as E3.5 (Ghanem et al. 2015). Intriguingly, this lethality is believed to arise due to a problem during the transition from a naïve to primed pluripotent state (Nazarov et al. 2019). However, the precise mechanism remains uncharacterized. Similarly, PCBP2 knockout also results in embryonic lethality, due to cardiovascular and hematopoietic abnormalities (Ghanem et al. 2015). However, PCBP2 null embryos survive until day E13.5. These differences in timing and manifestation of embryonic death suggest that, despite being evolutionary conserved and containing a high percentage of amino acid similarity, these two proteins play distinct roles in development (Ghanem et al. 2015). Indeed, there is additional evidence for this hypothesis as PCBP1 plays an important role in myoblast maintenance/differentiation (Espinoza-Lewis et al. 2017) whereas PCBP2 promotes erythropoiesis (Ghanem et al. 2018). Depletion of PCBP1 leads to muscle defects (Espinoza-Lewis et al. 2017). Mechanistically, PCBP1 directly interacts with AGO2 to modulate miRNA maturation and that inhibition of PCBP1 led to a reduction in muscle miRNA production and ultimately muscle defects (Espinoza-Lewis et al. 2017). Alternatively, PCBP2 promotes definitive erythropoiesis by modulating splicing of the hematopoietic master regulator, RUNX1 (Ghanem et al. 2018). The examples above illustrate the diverse nature in which PCBPs can influence pluripotency and development. However, these findings represent only bits and pieces of complete function of PCBPs during development and underscore the fact that more research is necessary to understand the full picture.

1.8 Rationale and Hypotheses

1.8.1 m^{6}A-mediated mRNA decay in stem cells

Multiple studies have indicated that m^{6}A methylation is crucial in early development and the maintenance of pluripotent stem cells (Geula et al. 2015; Aguilo et al. 2015; Batista et al. 2014; Wen et al. 2018; Bertero et al. 2018). Global m^{6}A levels are relatively high in pluripotent stem cells and their reduction impairs both self-renewal and differentiation capabilities. To this end, mRNAs encoding several of the major pluripotency factors are methylated in pluripotent stem cells (Wang et al. 2014c; Batista et al. 2014; Aguilo et al. 2015; Bertero et al. 2018). Despite this, relatively little is known regarding the expression and activity of individual readers in pluripotent stem cells. Each m^{6}A reader influences different aspects of the RNA life cycle, thus characterizing the expression and activity of individual readers in stem cells is critical to our understanding of how m^{6}A modulates pluripotency and differentiation. Previous studies have indicated YTHDF2, which is primarily associated with facilitating mRNA decay (Wang et al. 2014b; Du et al. 2016a), plays an important role in the clearance of unwanted mRNAs in other cell-state transitions that occur during development (Chen et al. 2017; Zhao et al. 2017b; Ivanova et al. 2017; Li et al. 2018b). Based on this information, *we hypothesized that YTHDF2 has a prominent role in mediating the influence of m^{6}A methylation on pluripotency and differentiation in stem cells*. One major goal of this dissertation was to test this hypothesis at a molecular/mechanistic level.

1.8.2 The influence of CREs on mRNA decay in stem cells

Previous work from our lab and others demonstrated that mRNAs containing CREs are differentially regulated in pluripotent stem cells compared to differentiated fibroblast cells (Neff et al. 2012; Huang et al. 2015b). Several RBPs recognize and bind to CREs including the PCBP family of proteins (Makeyev and Liebhaber 2002; Leidgens et al. 2013). Of note, PCBP2 is essential for early development and hematopoiesis (Ghanem et al. 2015, 2018) as well as

myeloid cell differentiation (Eiring et al. 2010). Given that self-renewal is a common characteristic shared between pluripotent stem cells and cancer cells, it is also relevant that PCBP2 expression is altered in several forms of cancer (Chang et al. 2007; Chen et al. 2018; Perron et al. 2018; Han et al. 2013b). Thus, PCBP2 is of particular interest in regards to the regulation of gene expression in stem cells. In terms of function, PCBP2 regulates several steps of RNA metabolism (Xia et al. 2015; Yanatori et al. 2016; Ji et al. 2013, 2018; Smirnova et al. 2019) including decay (Han et al. 2013b; Zhang et al. 2015a). Based on the evidence outlined here, *we hypothesized that PCBP2 helps to regulate differentiation and self-renewal of pluripotent stem cells by modulating the stability of mRNAs containing CREs.* Therefore a second goal of this dissertation was to test this hypothesis at a molecular/mechanistic level.

Chapter 2: Materials and Methods

2.1 Cell culture and transfection

2.1.1 Induced pluripotent stem cells

A matched set of male HFFs and reprogrammed iPSCs were purchased from System Biosciences. iPSCs were grown on MatriGel coated plates (Corning). In accordance with manufacturer protocols, MatriGel was diluted in DMEM/F12 (+ L-glutamine, + 15 mM HEPES, - phenol red; Gibco) for application onto plates. iPSCs were cultured in either exclusively mTesR1 media (STEMCELL Technologies) or a combination of mTesR1 and StemFlex (Thermo Fisher Scientific) media with no antibiotics at 37°C in 5% CO_2. Briefly, the combination culture consisted of passaging iPSCs in StemFlex for the first 1-2 days (to increase yield), then switch back to mTesR1 and changed daily for the remainder of the culturing period. Cells were passaged every 7 days using either ReLeSR (STEMCELL Technologies) or manual passage by visual selection. iPSCs were cryopreserved in mTeSR1 or StemFlex media with 10% dimethyl sulfoxide (DMSO), cooled overnight to -80°C and stored long-term in liquid nitrogen.

2.1.1.1 Differentiation/induction of iPSCs

Differentiation/induction of iPSCs was performed using an assortment of media from STEMCELL Technologies (see Table 2.1 for details). iPSCs were passaged onto new MatriGel coated plates in StemFlex and left to attach overnight. Approximately 24 hours after passaging, media was removed and replaced with a lineage-specific media. Cells were cultured in lineage-specific media for up to 7 days, depending on manufacturer and experimental protocols, with media changed daily.

2.1.2 Human foreskin fibroblasts

HFFs were cultured in DMEM (4.5g/L glucose) supplemented with 2 mM L-glutamine, 0.1 mM non-essential amino acids, 10% Fetal Bovine Serum (FBS; Atlas Biologicals) and 0.37% sodium bicarbonate with penicillin (50 units/mL) and streptomycin (50 µg/mL; Hyclone) antibiotics at 37°C in 5% CO_2. Media was changed every 2 to 4 days and cells were passaged at a 1:2 or 1:3 ratio every 5 to 7 days. To passage cells, media was removed, cells were washed with 1X sterile phosphate buffer saline (PBS, Corning) and incubated with a 1:1 ratio of sterile PBS to 0.25% trypsin/EDTA (Thermo Fisher Scientific-Hyclone) at 37°C until cells detached. Media was then added to quench the trypsin reaction. Cells were collected via centrifugation at 300 x g for 5 minutes before being resuspended in media for plating. HFFs were cryopreserved in 50% media, 40% FBS, and 10% DMSO, cooled overnight to -80°C, and stored long-term in liquid nitrogen.

2.1.3 HeLa cells

HeLa cells were cultured in DMEM (4.5g/L glucose) supplemented with 2 mM L-glutamine, 10% NewBorn Calf Serum (NBCS; Peak Serum) and 0.37% sodium bicarbonate with penicillin (50 units/mL) and streptomycin (50 µg/mL) antibiotics at 37°C in 5% CO_2. Media was changed daily or every 2 days and cells were passaged at a 1:3 to 1:10 ratio every 2-4 days, depending on cell confluency and experimental planning. To passage cells, media was removed, cells were washed with 1X PBS and incubated with a 1:1 ratio of sterile PBS to 0.25% trypsin/EDTA at 37°C until cells detached. Media was then added to quench the trypsin reaction. Cells were collected via centrifugation at 500 x g for 5 minutes before being resuspended in media for plating. HeLa cells were cryopreserved in 50% media, 40% FBS, and 10% DMSO, cooled overnight to -80°C and stored long-term in liquid nitrogen.

2.1.4 Transfections

2.1.4.1 Transfection of siRNAs

Transient knockdown (KD) was achieved by transfecting cells with siRNAs supplied by Millipore Sigma (see Table 2.2 for detailed information about the siRNAs used). Transfections of iPSCs were carried out using Stemfect transfection reagent (Stemgent) in accordance with manufacturer's recommendations. Alternatively, jetPRIME transfection reagent (Polyplus) was used to transfect HeLa cells. Cells were transfected at a 50 μM concentration of siRNAs daily for 2-6 days, depending on the experiment, and harvested approximately 24 hours after the final transfection.

2.1.4.2 Transfection of plasmids

Reporter plasmids were transfected into iPSCs, HFFs and HeLa cells using different transfection reagents optimized for each cell type. iPSCs were transfected with *Trans*IT®-LT1 transfection reagent (Mirus) and Opti-MEM™ I (Thermo Fisher Scientific) in accordance with the 'Reverse Transfection of Human Induced Pluripotent Stem (iPS) Cells' protocol (https://www.mirusbio.com/assets/misc_technical_documents/reverse-transfection-of-human-ips-cells-with-transit-lt1-transfection-reagent.pdf) with the following exceptions: i. no ROCK inhibitor was used, ii. the protocol was scaled down from a 6- to 96-well plate format, iii. ReLeSR (STEMCELL Technologies) was used instead of Accutase™. HFFs were transfected with a combination of Lipofectamine LTX (Thermo Fisher Scientific) and FuGene HD (Promega) in Opti-MEM™ I in accordance with a previously published protocol (Ishiguro et al. 2017). Briefly, a ratio of 1 μL LTX reagent to 1 μL FuGene HD reagent to 1 μg of plasmid was used during complex formation. HeLa cells were transfected via jetPRIME transfection reagent (Polyplus) in accordance with the manufacturer's recommendation. A 3 μL reagent/μg of plasmid ratio was used during transfection. DNA and siRNA co-transfection HeLa cells was

performed using jetPRIME in accordance with manufacturer's protocols. In all cases, cells were assayed or harvested approximately 24 hours after the final transfection.

2.2 Plasmids and cloning

2.2.1 YTHDF2 3' UTR luciferase reporter plasmids

Luciferase reporter plasmids used the *Renilla* Luciferase psiCHECK™-1 (Promega) as a backbone with *XhoI* and *NotI* as the upstream and downstream restriction sites, respectively. Fragments of the YTHDF2 (NM_016258.3) 3' UTR were amplified from cDNA using *PfuUltra II* Fusion High-fidelity DNA Polymerase (Agilent). Primers (see Table 2.3) for each insert were designed with a 4 base pair overhang to allow for maximum restriction enzyme (RE) digestion. Following PCR amplification, inserts were size-selected and gel purified using the Wizard® SV Gel and PCPR Clean-Up kit (Promega) in accordance with manufacturer's protocols. The backbone and inserts were then subjected to digestion via *XhoI* and *NotI* FastDigest REs (Thermo Fisher Scientific) at 37°C for approximately 25 minutes. Samples were then cleaned via phenol/chloroform extraction, ethanol (EtOH) precipitated and resupsended in nuclease free water. Backbone and insert DNA concentrations were quantified via spectrophotometry using a Nanodrop2000 (Thermo Fisher Scientific). Inserts were then ligated into the backbone via a T4 DNA Ligase reaction (New England Biolabs) at 16°C overnight. A 1:3 backbone to insert ratio was used for the ligation reaction. DH5α *E. coli* competent cells were transformed with the ligation reactions via heat shock, plated on Luria broth agar plates, with ampicillin as a selective marker, allowed to grow overnight at 37°C. Selected colonies were screened by PCR using the same primers from the cDNA amplification step. Positive colonies were selected and plasmid DNA was purified using the ZymoPURE II Plasmid Maxiprep kit (Zymo Research) and verified by Sanger sequencing (Genewiz).

2.2.2 HERV-H long non-coding RNA over-expression plasmids

For over-expression constructs, p3XFLAG-CMV™-10 (Millipore Sigma) was used as the backbone for LINC01356 and pcDNA™3.1(+) (Thermo Fisher Scientific) was used as the backbone for LINC00458. Both of these vectors use the cytomegalovirus (CMV) promoter, bovine growth hormone (BGH) polyadenylation signal and contain *BamHI* and *EcoRI* restriction sites in the multiple cloning sequence. In the case of LINC01356 and p3XFLAG-CMV™-10, *BamHI* was used as the upstream RE and *EcoRI* the downstream. For LINC00458 and pcDNA™3.1(+), it was vice versa. Full length LINC01356 and LINC00458 transcripts were amplified from cDNA using *PfuUltra II* Fusion High-fidelity DNA Polymerase. The primers used can be found in Table 2.3. The remainder of the cloning process was as described above in section 2.2.1.

2.3 RNA Isolation

RNA isolation was performed using TRIzol Reagent (Thermo Fisher Scientific) in accordance with manufacturer's protocols. Total RNA was treated with DNase I (Thermo Fisher Scientific) for 30 minutes as 37°C. When necessary, removal of plasmid DNA was achieved by treating RNA samples with TURBO DNase (2 units/µg of RNA; Ambion) in 50 µL reactions for 45 minutes at 37°C. Removal of DNase enzymes was achieved by phenol/chloroform/isoamyl alcohol (25:24:1) extraction and EtOH precipitation. RNA purity and quantity was assessed via a NanoDrop 2000 spectrophotometer (Thermo Fisher Scientific) and RNA was stored at -80°C.

2.4 Reverse transcription

Reverse transcription (RT) was performed in 20 µL reactions using Improm-II Reverse Transcriptase (Promega) with slight modifications to the manufacturer's protocol. Specifically,

the reaction was primed with 0.5 µg of a 3:1 mixture of random hexamers:oligo $(dT)_{20}$ and RiboLock (Thermo Fisher Scientific) was included as an RNase inhibitor.

2.5 Reverse transcription digital PCR

For reverse transcription digital PCR (RT-dPCR), cDNA was diluted such that the template copy number was between 10 and 100,000 and used in dPCR reactions with QX200 ddPCR™ EvaGreen Supermix (Bio-Rad) and transcript-specific primers. Detailed information about the primers used for each transcript can be found in Table 2.4. Droplet generation was performed using a QX200 Droplet Generator (Bio-Rad) in accordance with manufacturer's protocols. Droplets were transferred to a 96-well plate and heat sealed with pierceable foil using the PX1 PCR Plate Sealer (Bio-Rad). A 2-step amplification was performed in a C1000 Touch Thermal Cycler with 96-Deep Well Reaction Module (Bio-Rad) with annealing/extension at 60°C for 60 seconds and denaturation at 95°C for 30 seconds and a 2.5°C/second ramp rate. Fluorescence of each droplet was interrogated using the QX200 Droplet Reader (Bio-Rad) and transcript copy numbers were determined using the QuantaSoft™ Software (Bio-Rad). Transcript copy numbers were normalized to GAPDH across compared samples and expression changes were reported as relative mRNA abundance or fold-change.

2.6 Protein preparation

Protein from cell lysates was prepped in one of two ways. In both cases, cell lysates were quantified via Pierce™ Rapid Gold BCA kit (Thermo Fisher Scientific) in accordance with manufacturer's protocols and stored at -20°C.

2.6.1 Protein isolation using RIPA buffer

Cells were collected and pelleted by centrifugation at 1000x g and 4°C for 5 minutes and washed twice in 10 mL of cold PBS. After the second wash, cells were re-suspended in 100-500 μL of RIPA buffer (50 mM Tris-Cl pH 7.5, 1% NP40, 0.5% Sodium Deoxycholate, 0.05% SDS, 1 mM EDTA, 150 mM NaCl, 1 mM PMSF and 1mM DTT), with Protease Inhibitor Cocktail (Millipore Sigma) and incubated for 10 minutes at 4°C with gentle rotation. Cells were then lysed via sonication with 5x10 second pulses at 6-7W output with 1 minute of rest on ice in between. After lysis, cell debris was pelleted via centrifugation at ~15,000 *g* for 10 minutes at 4°C and supernatant was transferred to a new tube.

2.6.2 Protein isolation using TRIzol

Protein was prepared from TRIzol samples in accordance with manufacturer's protocols. Briefly, any residual nucleic acids were precipitated out of the organic phase via EtOH and centrifugation and the supernatant was transferred to a new tube. Protein was precipitated using isopropanol and pelleted via centrifugation. The protein pellet was washed 3x with 0.3M guanidine hydrochloride in 95% EtOH before a final wash with EtOH. The pellet was then left to air dry to remove any residual EtOH before being resuspended in 3:1 8M urea to 1% SDS solution.

2.7 Western blotting

20-40 μg of whole cell lysate was mixed with 6X Laemmli buffer (0.5 M Tris-HCl pH 6.8, 50% glycerol, 12% SDS, 9% DTT and 0.06% bromophenol blue), denatured at 95°C for 5 minutes and cooled on ice for approximately 5 minutes. Proteins were then resolved on an 8% polyacrylamide gel containing SDS, transferred to an Immobilon® PVDF membrane (EMD Millipore) and probed with primary antibodies at room temperature for 2 hours (see Table 2.5 for

details). Membranes were washed, then incubated for 1 hour at room temperature with HRP-conjugated anti-rabbit (1/5000; Bio-Rad) or anti-mouse (1/5000; Santa Cruz Biotechnology) antibodies. After washing, membranes were treated with SuperSignal® West Dura Extended ECL reagent (Thermo Fisher Scientific) and luminescence was assessed on the ChemiDoc XRS+ system (Bio-Rad) or the Azure Sapphire Biomolecular Imager (Azure Biosystems). Band intensities were assessed using ImageLab software (Bio-Rad) and normalized to GAPDH.

2.8 4-Thiouridine (4sU) labeling and half-life analysis

4sU labeling and subsequent half-life analysis was performed as described in (Russo et al. 2017). Briefly, cells were labeled with 4sU at concentration of 400 μM for 4 hours. RNA was collected and isolated using TRIzol reagent. Prior to fractionation, a 4sU-labeled synthetic transcript (Dharmacon) with the following sequence: 5′-AUUUAGGUGACACUAUAGGAUCCUCUAGAGUCGACCUUCUCCCUAUAGUGAGUCGUAUUAGCA[4-S-U]CAG-3′, was spiked into samples to assess fractionation efficiency. 20-40 μg of total RNA and was labeled with MTSEA-biotin-XX (Biotium) and fractionated using μMACS streptavidin magnetic beads (Miltenyi Biotec). Transcript abundance was measured using RT-dPCR, and half-life was calculated based on the ratio of labeled to unlabeled RNA (Rädle et al. 2013).

2.9 RNA immunoprecipitation (RIP)

iPSCs were detached from 10-cm plates using ReLeSR (STEM CELL Technologies), pelleted by centrifugation at 1000x g at 4°C for 5 minutes and washed twice in 10 mL of cold PBS. After the second wash, cells were re-suspended in 10 mL of cold PBS and RNA-protein crosslinking was performed by adding 0.3% formaldehyde. Cells were incubated in the crosslinking solution for 10 minutes at room temperature with gentle rocking. 1.4 mL of 2M

glycine (pH 7.0) was added to quench the crosslinking reaction. Cells were then pelleted at 1000x g and 4°C for 5 minutes and washed twice in 10 mL of cold PBS. Cell pellets were stored at -80°C until further processing.

Cell pellets were thawed and re-suspended in 1 mL of low stringency (LS) RIPA buffer (50 mM Tris-HCl pH 7.5, 1% NP40, 0.5% Sodium Deoxycholate, 0.05% SDS, 1 mM EDTA, 150 mM NaCl, 1 mM PMSF and 1mM DTT) with Complete Mini EDTA-free Protease Inhibitor Cocktail tablets (Millipore Sigma) and RiboLock RNase inhibitor (Thermo Fisher Scientific). Cells were incubated in LS RIPA buffer for 10 minutes at 4°C with gentle rotation and then lysed by passing through a 25 gauge needle 10-12 times. Samples were spun down at ~15,000 *g* for 10 minutes at 4°C. Cell extracts (supernatant) were transferred to new tubes and were precleared by incubation with 20 µL of magnetic protein G beads (New England BioLabs) for 60 minutes at 4°C with gentle rotation. Beads were removed from the extracts using a magnetic stand. After preclearing, a 100 µL aliquot was set aside to serve as the input. Then, 450 µL samples were incubated with 20 µL of either YTHDF2- or PCBP2-specific or IgG (control; see Table 2.5) antibodies with rotation at 4°C for 60 minutes. After incubation, 20 µL of magnetic protein G beads was added and samples were again incubated with rotation at 4°C for 60 minutes. Beads were then retrieved and resuspended in 500 µL of high stringency (HS) RIPA buffer (50 mM Tris-HCl pH 7.5, 1% NP40, 1% Sodium Deoxycholate, 0.1% SDS, 1 mM EDTA, 1 M NaCl, 1 M Urea, 1 mM PMSF and 1mM DTT), with Complete Mini EDTA-free Protease Inhibitor Cocktail tablets and RiboLock RNase inhibitor included, and incubated with rotation at 4°C for 5 minutes. This was repeated for a total of five washes. To reverse the crosslinking, beads were re-suspended in 100 µL of TEDS buffer (50 mM Tris-Cl pH 7.0, 5 mM EDTA, 1% SDS, 10 mM DTT) and 50 µL of TEDS buffer was added to Input samples. IP and Input samples were then incubated at 70°C for 45 minutes. 300 and 450 µL of TRIzol was added to IP and Input samples, respectively. Samples were stored at -80°C until RNA could be extracted (see Section 2.3 RNA Isolation). Upon completion of RNA isolation, RNA samples were suspended in 4 µL of

water and the full volume was taken into the reverse transcription reaction. RT-dPCR was used to measure RNA abundances in YTHDF2 or PCBP2 IP, IgG IP and Input samples. Percent of Input (PoI) was determined and fold enrichments were calculated as YTHDF2 or PCBP2 PoI/IgG PoI for a specific mRNA. Protein samples were obtained from independent RIPs and protein abundance was assessed via western blot to measure RIP efficiency.

2.10 Immunofluorescence staining

Circular coverslips were placed on 6- or 10-cm dishes and coated with MatriGel prior to seeding. Cells were seeded, cultured and treated in accordance with previously described protocols (See section 2.1 Cell Culture and Transfection). After treatment, coverslips were collected and washed twice in 1 mL of PBS. Cells were fixed in a 3.7% formaldehyde PBS solution for 10 minutes at room temperature with slight agitation. After fixing, cells were washed twice in 1 mL of PBS and permeabilized in 70% EtOH overnight at 4°C. Cells were blocked by incubating in 1 mL of blocking buffer (20 mg/mL Bovine Serum Albumin Fraction V and 0.02% Triton X-100) overnight at 4°C. Following blocking, cells were probed with a 1:100 dilution of primary antibody in blocking buffer and placed in a humidity chamber at 37°C for two hours (See Table 2.5 for details). Cells were washed five times with PBS-T (0.02%) for 1 minute with slight agitation. Cells were then probed with Alexa Fluor®568-conjugated anti-rabbit (Abcam) or anti-mouse (Abcam) at a 1:500 dilution in blocking buffer and placed in a humidity chamber at 37°C for two hours. After incubation, cells were again washed five times with PBS containing 0.1% Tween-20 (PBS-T) for 1 minute with slight agitation. Slides were then mounted using one drop (~100 μL) of ProLong® Diamond Antifade Mountant with DAPI (Life Technologies) and left to cure in the dark at room temperature overnight. Slides were visualized using an Olympus IX71 inverted fluorescent microscope at 100X magnification using the 31000 DAPI/Hoechst filter (EX360, EM460) to visualize DAPI and the 41002 TRITC (Rhodamine)/Cy3 filter (EX535,

EM610) to visualize Alexa568. Images were captured using a Q Imaging Retiga 2000R camera. Background fluorescence was determined by measuring slides probed with secondary antibody only and the minimum threshold of images was adjusted accordingly. Nucleus size was analyzed via ImageJ (Schneider et al. 2012).

2.11 MazF digestion and analysis

MazF digestion and analysis was performed according to a published protocol (Garcia-Campos et al. 2019a) with some modification. Briefly, 100 ng of total RNA was digested by 20 units of MazF enzyme (Takara Bio, Cat# 2415A) supplemented with 4 µL 5X *Maz*F buffer (200 mM sodium phosphate, pH 7.5, 0.05% Tween-20), 0.8 µL DMSO and 0.5 µL RNase inhibitor (Thermo Fisher Scientific) in a 20 µL reaction. Samples were denatured at 70°C for 5 minutes then incubated at 37°C for 30 minutes. Digested RNA was purified by phenol/chloroform/isoamyl alcohol (25:24:1) extraction and EtOH precipitation, then subjected to RT-dPCR as previously described (See sections 2.3 RNA Isolation, 2.4 RT and 2.5 dPCR) with one exception. 100% random hexamer was used to prime the reaction instead of 3:1 mixture of random hexamers:oligo $(dT)_{20}$. Three primer sets were designed to create different products from the same transcript. The ACA product contained two unprotected ACA motifs, the control product contained no ACA motifs and the m^6A product contained the methylated ACA motif of interest. Methylation ratios were generated using the formula: m^6A product abundance/Control product abundance. To compensate for enzymatic efficiency between samples and RT efficiency across different areas of the transcript, a normalization ratio was generated using the same formula, but with samples lacking MazF. The same analysis protocol was employed with the ACA product to generate a background ratio. This background ratio was subtracted from the methylation ratio in order to get a more accurate quantification of methylation status.

2.12 Luciferase assays

For assessment of luciferase activity, cells were seeded equally into 96-well µClear® plates (Greiner Bio-One; 5,000 HeLa cells per well, 3,000 HFFs per well, or an equal volume of resuspended iPSCs). For RNA abundances, cells were seeded into 6-well plates (Greiner Bio-One). Cells were transfected (see Section 2.1.4) with a 4:1 ratio of *Renilla* luciferase experimental construct to *Firefly* luciferase control (pGL4.13; Promega). Approximately 24 hours after transfection, cells were assessed for luciferase activity or collected in TRIzol to measure RNA abundances (see sections 2.3-2.5 for RNA measurement). Luciferase assays were performed using the Dual-Glo® Luciferase Assay System kit (Promega) and activity was quantified on a Victor™ X5 Plate Reader (PerkinElmer). Data analysis of luciferase activity of experimental constructs was performed according to previously published protocols (Van Etten et al. 2013) and compared to an empty vector control. To ensure the observed differences were due to changes in translation efficiency and not influenced by mRNA abundance, luciferase activity for each construct was normalized to the mRNA abundance. Data were reported as relative *Renilla* luciferase activity.

2.13 *In vitro* transcription

To create a template for the *in vitro* transcription reaction, the first 300 nucleotides of the YTHDF2 3' UTR was amplified using *PfuUltra II* Fusion High-fidelity DNA Polymerase and a forward primer with the SP6 promoter sequence (see Table 2.3). A size-matched control was also created by digesting the empty pGEM4 plasmid with *Slm1*. In both cases, the templates were gel purified via the Wizard® SV Gel and PCPR Clean-Up kit (Promega) in accordance with manufacturer's protocols and validated via Sanger sequencing (Genewiz). *In vitro* transcriptions were performed using SP6 RNA Polymerase (Fermentas) in the presence of Biotin-14-CTP (Thermo Fisher Scientific) and incubated for 75 minutes at 37°C to generate biotinylated RNAs.

Reactions then were incubated with DNase I (Thermo Fisher Scientific) to remove template DNA and cleaned up via phenol/chloroform extraction, EtOH precipitated and quantified via spectrophotometry using a Nanodrop 2000c (Thermo Fisher Scientific).

2.14 RNA pulldown and mass spectrometry

The full *in vitro* transcription reactions generated from section 2.13 were incubated with 100 µL of µMACS streptavidin magnetic beads (Miltenyi Biotec) for 10 minutes at room temperature with slight agitation (~300 rpm) to bind the RNAs to the column. Immediately following the 10 minute incubation, 350 µL of pre-cleared HeLa cell extracts (prepared as described in (Ford et al. 1999; Sokoloski et al. 2008)) supplemented with 5 µL of liquid protease inhibitor (Sigma-Millipore) was added to each reaction and incubated at 4°C for 60 minutes with rotation. Shortly before the completed incubation period, magnetic bead columns were equilibrated with 100 µL of 2X Equilibration Buffer provided in the µMACs kit. Incubated samples were added to individual columns and the Flow Through was collected and stored at -80°C. Columns were washed 5X with 1 mL of Binding/Wash buffer (10 mM HEPES pH 7.0, 10% Glycerol, 1 mM EDTA, 0.5% Triton X-100, 20 u/mL RNase, 1 mM DTT and 50-300 mM KCl). A Binding/Wash buffer with a concentration of 250 mM KCl was used for the samples submitted for mass spectrometry analyses. Flow through from the washes was discarded. RBPs were eluted by adding 200 µL of Binding/Wash buffer with 1M NaCl while the column was still on the magnetic stand and collected in a 1.5 mL tube. Eluted RBP samples were quantified via Pierce™ Rapid Gold BCA kit (Thermo Fisher Scientific). To assess the optimal concentration of KCl, equal volumes of each sample were electrophoresed into a 10% SDS PAGE gel, silver stained and visualized on the ChemiDoc XRS+ system (Bio-Rad). For mass spectrometry submission, approximately 50 µg of each sample was briefly electrophoresed into a 10% SDS PAGE gel, excised from the gel and submitted to the Proteomics and Metabolomics Facility at Colorado

State University. Trypsin digestion and LC-MS/MS protein identification were performed in accordance with previously published protocols (Michalski et al. 2019). Scaffold 4 software (Proteome Software) was used to analyze the mass spectrometry data (Searle 2010).

2.15 Nuclear/Cytoplasmic fractionation

Nuclei and cytoplasm were separated as described previously (Weil et al. 2000). Briefly, cells were removed from culture plate and into ice cold PBS via manual scraping, collected via centrifugation (500 x *g* for 5 minutes), resuspended in NP40 lysis buffer (0.5% NP-40, 10 mM Tris-HCl pH 8.5, 1.5 mM MgCl2, 10 mM EDTA, 140 mM NaCl) and incubated on ice for 5-10 minutes. A small amount of each sample was stained with trypan blue and visualized using a microscope to ensure adequate cell lysis. Once lysis was confirmed, nuclei were pelleted via centrifugation at 500 x *g* for 5 minutes at 4°C. The cytoplasm (supernatant) was transferred into a new tube and an equal volume of TRIzol was added. The nuclei pellet was then washed twice with NP40 lysis buffer before being lysed in 500 µL of TRIzol. RNA was isolated as described in section 2.3 (RNA Isolation). The RNA from the nucleus and cytoplasm was resuspended in an equal volume such that an equal number of cells were represented in 1 µl regardless of RNA concentration. The relative abundance of each transcript in the nuclear and cytoplasmic fractions was then determined via RT-dPCR (see Sections 2.4 and 2.5 for details) and reported as percent RNA in the nucleus. tRNA and 45S pre-ribosomal RNA were used as controls to ensure efficient fractionation was achieved.

2.16 Quantification of miRNA abundance

miRNA abundance was measured by RT-dPCR performed in accordance with a previously described protocol (Git et al. 2010; Neff et al. 2012). Briefly, approximately 1 µg of total RNA was polyadenylated via the Poly(A) Tailing Kit (Ambion) according to the manufacturer's

protocol in a 25 µL reaction. RNA was then cleaned via phenol:chloroform extraction and EtOH precipitation and cDNA was synthesized according to previously described protocols (See section 2.4 RT) using 500 ng of oligo (dT) adapter (Integrated DNA Technologies Inc.). cDNA was then treated with RNase H (Fermentas) for 1 hour at 37°C. Approximately 1 ng of cDNA was added to each reaction for RT-dPCR analysis with human 5S rRNA used as a reference transcript. Detailed information about the primers used for each transcript can be found in Table 2.6.

2.17 Transcript alignment and analysis

Sequences used for HERV-H lncRNAs were based on the NCBI Reference Sequences. RefSeq number for each transcript are listed in Table 2.7. The consensus HERV-H sequence used was generated from Vargiu et al., 2016. Sequence analysis was performed via Geneious Prime 2019.1.1 (https://www.geneious.com). HERV-H lncRNAs were aligned to the HERV-H consensus sequence using BLASTN (Altschul et al. 1997) and the Pairwise/Multiple Alignments function of Geneious Prime, both under default parameters.

2.18 RNA sequencing

2.18.1 Library preparation and sequencing runs

Sequencing libraries were prepared from Control, YTHDF2 or PCBP2 siRNA-treated iPSC total RNA samples (See section 2.3 RNA Isolation, above) as follows. First strand cDNA was generated from 500 ng of total RNA using the SMARTer™ PCR cDNA Synthesis Kit (Takara Bio) in a 10 µL reaction per manual instructions. Reactions were incubated at 42°C for 90 minutes to achieve full-length cDNA synthesis. Second strand synthesis was performed using the Advantage 2 PCR kit (Takara Bio) in a 50 µL reaction with the following thermocycler conditions: 95°C for 15 seconds, 65°C for 30 seconds, 68°C for 6 minutes. Extension time was

set at 6 minutes to accommodate the full-length cDNA synthesis performed during first strand synthesis. Amplification of cDNA was performed for 4-6 cycles. PCR products were isolated using 90 µL of Agencourt AMPure XP Beads (Beckman Coulter) and eluted in 40 µL of TE buffer. DNA concentrations were quantified via the Qubit 3.0 fluorometer (Thermo Fisher Scientific) using the dsDNA HS kit (Thermo Fisher Scientific). DNA was tagmented using Tn5 transposase generously provided by Dr. Mark Stenglein. Preparation of the enzyme and reactions conditions were performed in accordance with a previously published protocol (Picelli et al. 2014). 5 ng of dsDNA, 2 µL of Tn5 Tagmentation Enzyme at a 12.5 µM concentration and a 5X TAPS-DMF buffer (see (Picelli et al. 2014) for recipe) were combined in a final volume of 20 µL. Reactions were incubated at 55°C for 10 minutes to achieve dsDNA fragments of approximately 200-300 base pairs in length. Reactions were terminated by adding 2.5 µL of 0.2% SDS and incubating at room temperature for 5 minutes. Tagmented DNA (5.8 µL) was used as a template for addition of full-length adapters in a 4-primer PCR reaction. This reaction was performed using the KAPA HiFi HotStart ReadyMix (KAPA Biosystems). For details on the tagmentation primers and index oligos used see Table 2.8. PCR products were isolated using AMPure XP beads and eluted in 40 µL of TE buffer. A portion of each library was visualized on the Agilent TapeStation 2200 using D1000 ScreenTape (Agilent) and reagents to verify a median product size of 200-300 base pairs, and concentrations were measured fluorometrically via Qubit. Equal masses of DNA, 10 ng, from each sample were pooled, concentrated with AMPure XP beads and eluted in 40 µL of TE buffer. A portion of the pooled library was run on the Agilent TapeStation 2200 using D1000 ScreenTape and to ensure a median product size of 200-300 base pairs. Final library quantification was performed by the Colorado State University NGS Core using the Illumina library quantification kit (KAPA Biosystems) per manufacturer's protocols. Libraries were sequenced on an Illumina NextSeq 500 instrument using single-end 1 x 75 sequencing from a NextSeq 500/550 High Output Kit v2 (75 cycles) (Illumina) on two separate runs. The mean number of reads per sample was 25-50 million. Base calling was done

via RTA v2.0, and files were converted to fastq using bcl2fastq v2.20.0.422, consistent with standard Illumina protocols.

2.18.2 Quality control and alignment of RNA-seq reads

Quality of sequence reads was assessed via FastQC v0.11.5. Reads were trimmed of adapter sequences and filtered for low-complexity or low-quality reads via Trimmomatic v0.32 (Bolger et al. 2014). rRNA reads were filtered out using Bowtie2 v2.3.4.3 (Langmead and Salzberg 2012) and a reference fasta file of mature 5S, 18S and 28S rRNA sequence obtained from NCBI RefSeq (mature_rRNA.fasta.gz). Filtered reads were mapped to the hg19 genome using TopHat2 v2.0.12 (Kim et al. 2013) under default parameters. Read counts from aligned reads were calculated using HTSeq v0.11.1 (Anders et al. 2015) with the parameters --mode = union --stranded=no --minaqual=20, Samtools v1.9 (Li et al. 2009) and the hg19 genome feature file obtained from GENCODE (hg19, Ensembl 74, hg19_gene_annotations.gtf.gz). It is important to note we obtained only eight million raw reads from one of the six day PCBP2 KD replicates. This is below the 10 million raw read threshold we set and approximately half the number of raw reads generated from the other replicates in the run. For these reasons, this replicate was removed from downstream analyses. Raw and processed RNA-seq data generated in this study, as well as the genome feature file and rRNA fasta file used, were uploaded to the NCBI Gene Expression Omnibus (GEO) database under the accession number GSE133898 (https://www.ncbi.nlm.nih.gov/geo/query/acc.cgi?acc=GSE133898) for YTHDF2 KD experiment and GSE139626 (https://www.ncbi.nlm.nih.gov/geo/query/acc.cgi?acc=GSE139626) for PCBP2 KD experiments.

2.18.3 Computational analyses of RNA-seq data

There were minor differences in the computational analyses workflow between the PCBP2 and YTHDF2 datasets. For the PCBP2 dataset, differential expression analysis was performed

followed by functional annotation of the differentially expressed genes. For the YTHDF2 dataset, a source of unwanted variation was detected. To remove the unwanted variation, the raw count data underwent more extensive normalization via the RUVSeq package (Risso et al. 2014). Normalized count data was then subjected to differential expression analysis followed by functional annotation and overlap analysis.

2.18.3.1 Differential expression analysis

Raw read count data was filtered for detectable genes (> 5 counts per sample) and analyzed for differential expression using DESeq2 v1.22.1 (Love et al. 2014) under default parameters. The quality of datasets was assessed via principle component analysis (PCA) and calculation of sample-to-sample Euclidian distances on variance-stabilized, log-transformed count data. Differentially expression thresholds were set at Benjamin-Hochberg corrected p-value < 0.05 for and $\log_2$-fold change > 1.0 for up-regulated genes and $\log_2$-fold change < 1.0 for down-regulated genes. Transcripts that met both thresholds were classified as differentially expressed. Gene symbol, Entrez Gene ID and gene biotype were retrieved using the biomaRt package v2.38.0 (Durinck et al. 2009) and the hsapiens_gene_ensembl dataset. Hierarchical clustering of differentially expressed genes was performed and plotted on Z-scored intensity values using the heatmap.2 function of the gplots package v3.0.1 (Warnes et al. 2016). Distances were calculated based on the Pearson correlation coefficient and clustering was performed using the unweighted pair group method with arithmetic mean.

2.18.3.2 Removal of unwanted variation via RUVSeq

To remove the unwanted variation, filtered count data was normalized via the RUVSeq package using the RUVr option in accordance with the published protocol (Risso et al. 2014). PCA was performed and Euclidian distances were measured on the normalized data to confirm the removal of unwanted variation.

2.18.3.3 Functional annotation analysis

Gene enrichment analysis was performed using the online functional annotation tool DAVID v6.8 (Huang et al. 2009a, 2009b). Separate lists of Ensembl Gene IDs corresponding to differentially expressed transcripts, either up- or down-regulated, were uploaded and mapped to DAVID gene IDs. Functional annotation cluster was performed to determine overrepresented Gene Ontology biological processes, cellular components and molecular functions. Analysis of overrepresented tissue expression profiles was also performed for the up-regulated list. The top four to five non-redundant terms from each analysis, defined by the lowest FDR corrected p-values were reported along with the number of genes associated with each term and the fold enrichment over background.

2.18.3.4 Overlap analysis

Data for transcripts previously reported to be m^6A-modified via m^6A RIP-seq in hESCs (Batista et al. 2014) or bound by YTHDF2 via PAR-CLIP seq in HeLa cells (Wang et al. 2014b) were obtained through publically available datasets. Lists of gene names for transcripts up-regulated, down-regulated, m^6A-modified and YTHDF2-bound along with all genes detected in each experiment were imported into R v3.5.1 (R Core Team 2018). Overlap analysis was performed using the packages plyr v1.8.4 (Wickham 2011), VennDiagram v1.6.20 (Chen 2018) and futile.logger v1.4.3 (Rowe 2016). Background filtering was performed to ensure only genes that were detected in both experiments were included in the overlap analysis. P-values were calculated via hypergeometric test using the phyper function of the stats package.

2.18.4 Data availability

The accession numbers for the RNA-seq datasets reported in this study are as follows: YTHDF2 KD- GEO: GSE133898; PCBP2 KD- GEO: GSE139626.

2.19 General quantification and statistical analysis

Three independent replicates were performed for each experiment unless noted otherwise. Statistical analyses were performed using GraphPad Prism 8 software (GraphPad Software, Inc.) For RIP analyses, a one-tailed t-test was employed. For all other comparisons, a false discovery rate (FDR) or q-value was calculated using the two-stage step-up method of Benjamini, Krieger and Yekutieli (Benjamini et al. 2006) to correct for multiple comparisons, unless noted otherwise. p-values from t-tests and q-values from FDR tests of less than 0.05 were considered significant.

Table 2.1: Stem cell differentiation medias.

Stem Cell Differentiation Media	Lineage	STEMCELL Tech. Catalog Number
STEMdiff™ Neural Induction Medium	Neuroectoderm	Cat# 05839
STEMdiff™ Mesoderm Induction Medium	Mesoderm	Cat# 05221
STEMdiff™ Definitive Endoderm Kit	Endoderm	Cat# 05110
STEMdiff™ Trilineage Differentiation Kit	All 3 germ layers	Cat# 05230

Table 2.2: siRNA sequences used for knockdown experiments. All siRNAs were purchased from Sigma-Millipore.

siRNA target	Sequence (5' to 3')	Previous Validation/Catalog Number
Negative Control	Proprietary	SIC001-10NMOL
YTHDF2	AAGGACGUUCCCAAUAGCCAA	(Wang et al. 2014b)
METTL3	CUGCAAGUAUGUUCACUAUGA	(Liu et al. 2014)
WTAP	GCAACAACAGCAGGAGUCU	SASI_Hs01_00039282
IGF2BP1	CAGUAUGUGGGUGCCAUUA	SASI_Hs01_00074473
IGF2BP3	GUUGUAAAUGUAACCUAUU	SASI_Hs01_00207964
HNRNPQ	CUAUCGUGGUGGAUAUGAAGA	(Ryu et al. 2019)
PCBP2 #1	CCCACUAAUGCCAUCUUCA	SASI_Hs01_00082600
PCBP2 #2	GCAUUAGCCUGGCUCAAUA	SASI_Hs01_00082601
LINC01356	AAGACAGGAAUAUCAGGUCUC	Custom Designed
LIN28B	AUUUAAAAAAUCUUCCAAAG	SASI_Hs01_00042202

Table 2.3: Primers used for cloning.

Target Fragment	Forward Primer Sequence	Reverse Primer Sequence
YTHDF2 3' UTR Full Length	GATCCTCGAGAAGGCAGTTCTACACAGACT	GATAGCGGCCGCGAGAAGTGATTAATGGTAAA
YTHDF2 3' UTR 0-200	GATCCTCGAGAAGGCAGTTCTACACAGACT	GACGGCGGCCGCAGTTTTTTCTTTTTCTTTTTT
YTHDF2 3' UTR 100-300	GATCCTCGAGGACTTCAGAGACGATTGCA	GACGGCGGCCGCAAAAAGACAAAAAAACAT
YTHDF2 3' UTR 200-400	GGTCCTCGAGTAAACAAAAAATCCCTCTAG	GATAGCGGCCGCGTGTTCTCCAAGTGCAAA
YTHDF2 3' UTR 300-500	GGTCCTCGAGTACTATGTTTTTCGGATTTTTAAG	GATCGCGGCCGCTCCTAGACAAAAATTCTTCAT
YTHDF2 3' UTR 400-600	GATCCTCGAGCTTGAGTTGTGAAGGTTTTG	GATCGCGGCCGCAACATTTCTTAGGACTC
YTHDF2 3' UTR 500-700	GATCCTCGAGAGAATATAACAGTGTTACCC	GATCGCGGCCGCTTCTCTTCCAAAATGCAT
YTHDF2 3' UTR 600-795	GATCCTCGAGTCTGTTCTTGTACATTATACTG	GATAGCGGCCGCGAGAAGTGATTAATGGTAAA
YTHDF2 3' UTR 0-300	GATCCTCGAGAAGGCAGTTCTACACAGACT	GACGGCGGCCGCAAAAAGACAAAAAAACAT
YTHDF2 3' UTR 100-200	GATCCTCGAGGACTTCAGAGACGATTGCA	GACGGCGGCCGCAGTTTTTTCTTTTTCTTTTTT

LINC01356	GATCGAATTCACCCGGCTCCCCAG CGCCGGCTCCC	TCGCGGATCCTTACGCGCCCCCGG CCGAGCCTG
LINC00458	GATTGGATCCCCCTTGGCTGACTC TCTTTT	GGTCGAATTCTCTCACAGTACTTGCT GTAG
YTHDF2 *In Vitro* Transcription	ATGTCATATTAGGTGACACTATAG GAAGGCAGTTCTACACAGACT	AAAAAGACAAAAAAACATAGCATTAT GCTCTG

Table 2.4: Primers used for RT-dPCR.

Gene Target	Forward Sequence	Reverse Sequence
GAPDH	AAGGTGAAGGTCGGAGTCAA	AATGAAGGGGTCATTGATGG
YTHDF2	GCTACAAGCACACCACTTCC	ATTTCCCACGACCTTGACGTT
4sU Spike Control	ATTTAGGTGACACTATAGGATCCTCT AG	GCTAATACGACTCACTATAGGGAGAA G
METTL3	AGCCTTCTGAACCAACAGTCC	GGCTTTCATGCACTCCTCCT
WTAP	GCTTCTGCCTGGAGAGGATTC	GATCTGTGTACTTGCCCTCCA
ST6GALNAC4	GAGCGCATGATGGCCTACTG	CTGACCATCCCATAGACCACG
FBLN2	CAGACCCCAACTCTGTCCAT	GCAGCTCTTCTCCTGCAAGT
NGFR	TGTCTATTGCTCCATCCTGGC	CTGTTGGCTCCTTGCTTGTTC
CHAC1	GTGGTGACGCTCCTTGAAGAT	TTACCTGCTCCCCTTGCACT
WDR62	GGGTAGACGTGGCACAGG	TGGAAGAGCTCTGACCACAC
NLGN3	CTGATCTCGGGGATTCGGG	GTAGAGAGCAGGTCGTCCAAG
TSPYL4	ATGAACGCAGATCCTCTGGC	GTGTTCCCTTCCCGGTTTCT
TOR1AIP2	TTTACGATTTAAAACTTCGCCAGAA	GAGTCTGGGAATGCGTCACA
SYNGAP1	CAAAATCGATGGATGAGAGCCG	AGCCGCTCTTTCAGTGAGTG
LINGO1	ACATGCGATTGGTGACCGAG	CGAGCCTGACAGCACTGAG
OPCML	ATGACGAAGGTCCGTACACC	ACAGGTGTCTCCATGTCACAG
EPHA8	CTCACGTATCCGGCTCATGG	TCGCGCAGGGTAAACTTGAT
CREBBP	CTCAGCTGTGACCTCATGGA	AGGTCGTAGTCCTCGCACAC
SCLM2	GATCGGTGGGACAGAATTTCG	CTCCTCCCAGTGGAAATCATCC
PAX6	TCAGAGCCCCATATTCGAGC	CAAAGACACCACCGAGCTGA
FOSB	GACTCCTTCGGCAGTCCAC	TCCTGGCTGGTTGTGATCG
NANOG	CCTATGCCTGTGATTTGTGG	TTCTCTGCAGAAGTGGGTTG
OCT4	GGCAACCTGGAGAATTTGTT	GTGCATAGTCGCTGCTTGAT
KLF4	ACCAGGCACTACCGTAAACACA	GGTCCGACCTGGAAAATGCT
SOX1	AAAATACTGGAGACGAACGCC	AAGAAAACGCTTTCCGCTTCC
NESTIN	CGCACCTCAAGATGTCCCTC	TTGGGGTCCTGAAAGCTGAG
WDR62 m6A Product	AGACCACCTTCCAAGAAGCC	GACCAGCTCAGTCCGTGC
WDR62 Control Product	GCAGTTCCTCTCAAGCCTCC	TCCATGAGCTTGACCTCTGG
WDR62 ACA Product	CCAGCTGCTCTGACAAAAGC	ATGCAGTTGGTGATCTCCGG
YTHDF3	GAGGAGGAAGCCATGCGTAG	AGGCATTTCCAGAGTCTACATCG

Firefly Luciferase	GATCCTCAACGTGCAAAAGAAGC	TCACGAAGGTGTACATGCTTTGG
Renilla Luciferase	CGCAACTACAACGCCTACCTTC	CCCTCGACAATAGCGTTGGAAAA
YES1	TCCTGCTGGTTTAACAGGTGGTG	TGCTTCCCACCAATCTCCTTCC
PODXL	CAGAGTGAGAAGCAGCTCGT	GGAACAGATGCCAGCCGTAT
FSCN1	TCAGAGCTCTTCCTCATGAAGCT	GTCCAGTATTTGCCTGTGGAGTC
GAP43	CCATGCTGTGCTGTATGAGAAG	CCAGGTGATGCTGTGACTCAT
SYT1	GGCAAAACCCTAGTGATGGC	TACGTAGCGAAGGGAGAAGC
PCBP2	GCTGCACCAGTTGGCAATGCAA	AGCCTTTCACCTCTGGAGAGCTGG
RGS5	CCACCTGCCAAAATGTGCAA	CAGCGAGGTTTTCTGGGTCT
CTGF	CTCGCGGCTTACCGACTG	GGCTCTGCTTCTCTAGCCTG
EGR1	ACCTGACCGCAGAGTCTTTTC	GCGGCCAGTATAGGTGATGG
KLK5	CCTGCACCCACATCTTTCTCT	CATGGCCGCTGCACCTTATT
HESX1	CCTGCAGCTCATCAGGGAAA	CCACCACGCTAGGGATGAA
PTBP2	ATTTTCTCGCCGCTTGTGTG	CAGATCCTCTCTTCACGCCA
HMGB2	TCTGAGGAAAAGCTCGCACC	ACATGGTCTTCCATCTCTCCG
LIN28B	GCACATTAGACCATGCGAGC	CTTTGCTAGCCCCGCCTTC
CDH9	TGTAGGCAAGCTTCACACTGA	AGCCTTGGCACGAAGAATGT
SOX21	GTCCCAGAGACAACCTGCTC	AAATCAATGTTGGCTGCCCG
tRNA	CCTTCGATAGCTCAGCTGGTAGAGC GGAGG	CGGAATCGGAACCAGCGACCTAAGGA TGTCC
45S	GAACGGTGGTGTGTCGTT	GCGTCTCGTCTCGTCTCACT
Global HERV-H	TGGTGCCGTGACTCGGAT	GCTGAGTCCGAAAAGAGAGTC
LINC01356	CCCTGTCCTCCTGCTCTTTG	CATCTGTGATGGTCCAGGGG
LINC00458	AGACTGACACTGCCCAATCG	AGTTCAGTCCAGAAGAAAAAGTCCT
LINC678	GGCAATGGTCAGGTGGAGT	GCCCAAGCAGAAATCAGACAC
LNCPRESS2	TGAAGGTGCTGCTAGTTGGAG	CATTGACGACACTCTTGCTGT
ERVH48	TCGGACTCTCACTGCAGTTG	CTCTAGTCGCCTCTCTGTGC
ESRG	TGGTCTCTTCACACAGACGC	CAGGCTGGTTGGAGTTTTGC
LINC-ROR	CCCTGTCCTCCTGCTCTTTG	AGTGGCTGTCAGGTGAGTTG

Table 2.5: Antibodies used for western blots (WB) and immunofluorescence staining (IF).

Antibody Target	Producer	Catalog Number	Type	WB Dilution Factor (if applicable)	IF Dilution Factor (if applicable)
YTHDF2	ProteinTech	24744-1-AP	rabbit polyclonal	1:1000 in TBS-T	1:100
GAPDH	Millipore	MAB374	mouse monoclonal	1:5000 in PBS-T	NA
METTL3	ProteinTech	15073-1-AP	rabbit polyclonal	1:1000 in PBS-T	NA
WTAP	ProteinTech	60188-1-Ig	mouse monoclonal	1:1000 in PBS-T	NA
PAX6	STEMCELL Technologies	60094	rabbit polyclonal	1:500 in PBS-T	NA
OCT4	STEMCELL Technologies	60093	mouse monoclonal	1:500 in PBS-T	1:100
TRA-1-60	Abcam	ab16288	mouse monoclonal	NA	1:100
SSEA4	Thermo Fisher Scientific	MC-813-70	mouse monoclonal	NA	1:100
SOX1	STEMCELL Technologies	60095	rabbit monoclonal	NA	1:100
NESTIN	STEMCELL Technologies	60091	mouse monoclonal	NA	1:100
YTHDF3	Abcam	ab103328	rabbit polyclonal	1:250 PBS-T	NA
IGF2BP1	Cell Signaling Technology	D33A2	rabbit polyclonal	1:1000 PBS-T	NA
IGF2BP3	Bethyl Laboratories	A303-426A	rabbit polyclonal	1:2000 PBS-T	NA
HNRNPQ	Abcam	ab10687	mouse monoclonal	1:1000 in PBS-T	NA
PCBP2	MBL International	RN025	rabbit polyclonal	1:1000 PBS-T	1:100
PCBP1	Abnova	H00005093	mouse polyclonal	1:1000 PBS-T	NA
PCBP3	Sigma	HPA030247	rabbit polyclonal	1:1000 PBS-T	NA

Table 2.6: Oligonucleotides used for quantification of miRNAs.

Oligonucleotide	Sequence (5’ to 3’)
Poly(T) adapter	GCGAGCACAGAATTAATACGACTCACTATAGGTTTTTTTTTTTT(A/G/C)(A/G/C/T)
Universal Reverse	GCGAGCACAGAATTAATACGACTC
Human 5S rRNA	ACCGGGTGCTGTAGGCT
miR-145	CTCACGGTCCAGTTTTCCC

Table 2.7: NCBI Reference Sequence numbers for HERV-H lncRNAs.

lncRNA	RefSeq Number
LINC01356	NR_103746.1
LINC00458	NR_108062.1
LINC00678	NR_102708.1
LNCPRESS2	NR_125920.1
ESRG	NR_027122.1
ERVH48-1	NM_001308491.1
LINC-ROR	NR_152602.1

Table 2.8: Oligonucleotides used in library preparation and RNA-sequencing.

General Oligonucleotides		
Oligonucleotide	*Forward Sequence*	*Reverse Sequence*
Library Amplification Primers	CAAGCAGAAGACGGCATACG	AATGATACGGCGACCACCGA
Adapter Sequence	CAGATGTGTATAAGAGACAG+CTGTCTCTTATACACATCTG+GAGATGT GTATAAGAGACAG+CTGTCTCTTATACACATCTC	
Sequencing Run Indexes		
Sample ID	*Read1 (i5) index*	*Read2 (i7) index*
3/21/2017 Run		
YTHDF2 KD 1	TCACAACG	AAGACCTA
YTHDF2 KD 2	CCTTACAG	GAACGGTA
YTHDF2 KD 3	TCCTCCTG	GTCCAACA
9/14/2017 Run		
Control 1	GTAGTACG	TCGTCTCA
Control 2	GTCTTCTG	ACAGGCTA
Control 3	TGAATCCG	GTGACTGA
YTHDF2 KD 4	TCACAACG	AAGACCTA
8/15/2018 Run		
6 day Control 1	GAATTGCG	ACTGTGGA
6 day Control 2	GTGAGGAG	GGTTAAGA
6 day PCBP2 KD 1	GAGACCAG	TCGTTGGA
6 day PCBP2 KD 2	TACGCTAG	TCCGTATA
6 day PCBP2 KD 3	GACTGGAG	GTGTCCTA
2 day Control 1	CTACCTCG	GTACGTCA
2 day Control 2	GTTAAGCG	TGCAGTTA
2 day PCBP2 KD 1	GAGTGTTG	TACATGCA
2 day PCBP2 KD 2	GAGCTCTG	GATGATGA
2 day PCBP2 KD 3	TAGGATCG	TAGGACCA

Chapter 3: YTHDF2 destabilizes m^{6}A-modified neural-specific mRNAs to restrain differentiation in pluripotent stem cells

3.1 Introduction

The ability of stem cells to maintain a state of self-renewal, yet also rapidly differentiate in response to external signals requires complex and coordinated control of global gene expression. Although transcriptional changes are integral to this control, stem cells also utilize post-transcriptional regulation to achieve rapid remodeling of the transcriptome during differentiation (Zhao et al. 2017b; Ivanova et al. 2017; Oh et al. 2018; Kami et al. 2018; Lloret-Llinares et al. 2018). The RNA modification m^{6}A is one post-transcriptional mechanism used by stem cells utilize to regulate gene expression (Batista et al. 2014; Geula et al. 2015; Heck and Wilusz 2019; Chen et al. 2015c; Zhang et al. 2017a; Li et al. 2015). m^{6}A is by far the prevalent internal modification RNA species can experience with ~10,000 m^{6}A sites documented in over a quarter of human transcripts (Meyer et al. 2012; Dominissini et al. 2012; Chen et al. 2015a). m^{6}A modifications are deposited, or written, onto RNAs by the methyl-writer complex which can be divided into two sub-complexes; the MAC, consisting of METTL3, the catalytically active subunit of the complex, and METTL14 (Liu et al. 2014), and the MACOM, comprising WTAP, ZC3H13, RBM15/15B, VIRMA and HAKAI (Ping et al. 2014; Guo et al. 2018; Yue et al. 2018; Knuckles et al. 2018; Růžička et al. 2017). Conversely, m^{6}A can also be erased by one of two demethylases, ALKBH5 or ALKBH9/FTO (Zheng et al. 2013; Jia et al. 2011). Although the overall impact of demethylation remains open for debate (Ke et al. 2017; Mauer et al. 2017; Darnell et al. 2018; Zhao et al. 2018). Importantly, the ultimate impact of m^{6}A methylation is dependent on which m^{6}A-binding proteins (readers) interact with the modified RNA. The best-characterized of m^{6}A readers are the YTH (YT521-B homology) family of proteins which consists of YTHDF1-3 as well as YTHDC1 and 2 (Patil et al. 2018). Readers influence the fate

of m^{6}A-modified RNAs at the level of cleavage/polyadenylation (Kasowitz et al. 2018), splicing (Xiao et al. 2016), subcellular localization (Roundtree et al. 2017), translation (Wang et al. 2015b) and decay (Wang et al. 2014b).

METTL3 knockout in mice is lethal by embryonic day 8.5 (E8.5) (Geula et al. 2015) demonstrating that methylation is essential for early development. In fact, m^{6}A methylation is important at the very earliest steps as it is needed for pluripotency in both human and mouse ESCs (Batista et al. 2014; Wang et al. 2014c; Geula et al. 2015; Wen et al. 2018; Chen et al. 2015c; Aguilo et al. 2015; Bertero et al. 2018). Moreover, a reduction in global m^{6}A levels alters the self-renewal and differentiation capabilities of ESCs (Batista et al. 2014; Wang et al. 2014c; Geula et al. 2015; Wen et al. 2018). This is likely in part because mRNAs encoding core pluripotency factors such as SOX2, KLF4, NANOG and MYC (but not OCT4) are m^{6}A-modified (Wang et al. 2014c; Batista et al. 2014; Aguilo et al. 2015; Bertero et al. 2018) leading to altered mRNA stability, translation, export and/or splicing when m^{6}A modification is reduced. The studies described above largely focused on the influence of m^{6}A and methyltransferase activities and did not address which m^{6}A readers execute the coordinated, global changes in gene expression that are necessary to facilitate rapid remodeling of the transcriptome in response to external cues. Characterizing the impact of reader activity is critical to our understanding of how m^{6}A influences pluripotency and development.

Relatively little is known regarding which m^{6}A readers are active in the early embryo and specifically in embryonic stem cells. Of the YTH domain family of proteins, only YTHDF2 and YTHDC1 are embryonic lethal when knocked out, suggesting they play a prominent role in early development (Li et al. 2018b; Kasowitz et al. 2018). However, it is not clear whether these factors mediate the effects of m^{6}A on pluripotency, as their role in stem cells has not been characterized. In differentiated cells, YTHDC1 modulates splicing and export from the nucleus (Xiao et al. 2016; Kasowitz et al. 2018; Roundtree et al. 2017), whereas YTHDF2 facilitates the degradation of m^{6}A-modified transcripts by recruiting deadenylases and endonucleases (Wang

et al. 2014b; Du et al. 2016a; Park et al. 2019). Previous studies have suggested YTHDF2 plays an important role in developmental transitions such as the maternal-to-zygotic transition (Zhao et al. 2017b; Ivanova et al. 2017), epithelial-mesenchymal transition (Chen et al. 2017) and differentiation of NPCs (Li et al. 2018b), where it facilitates the clearance of “old” RNAs to allow establishment of a new gene expression pattern. Based on the evidence outlined above, we hypothesized that YTHDF2 mediates the influence of m^{6}A methylation on pluripotency and differentiation in pluripotent stem cells.

Here, we report that YTHDF2 helps to maintain a pluripotent state by targeting a group of key m^{6}A-modified transcripts encoding neural-specific factors for degradation. When neural differentiation is induced, expression of YTHDF2 decreases along with the level of m^{6}A modification on neural transcripts. This leads to stabilization and increased abundance of neural transcripts which helps to drive differentiation. Depletion of YTHDF2 in self-renewing iPSCs leads to inappropriate expression of neural markers and loss of pluripotency. However, depletion of YTHDF2 during neural induction disrupts expression of both pluripotency and neural-specific factors. Taken together, our findings reveal pluripotent stem cells rely on YTHDF2 to restrain expression of neural-specific factors in order to maintain a pluripotent state until a signal to differentiate is received.

3.2 Results

3.2.1 YTHDF2 is required for pluripotency in human iPSCs

YTHDF2 protein expression is approximately seven-fold higher in iPSCs than in genetically matched HFFs (Fig. 3.1A, B). This dramatic difference in expression between somatic and pluripotent cell types coupled with previous evidence indicating m^{6}A plays an important role in pluripotency (Batista et al. 2014; Wang et al. 2014c; Geula et al. 2015; Wen et al. 2018; Chen et al. 2015c; Aguilo et al. 2015; Bertero et al. 2018) invited further investigation. Therefore, we depleted YTHDF2 in iPSCs using a previously validated siRNA (Wang et al. 2014b). We treated

cells with siRNA over a period of five days and evaluated the effects on pluripotency. Efficient knockdown (KD) was verified at both protein and mRNA levels (Fig. 3.2A, B). Intriguingly, we observed cell and colony morphological changes. As seen in Figure 3.4.2C, YTHDF2 depletion resulted in a loss of the structural integrity of the colony and the edges of the colony became poorly-defined. Moreover, cells were no longer tightly packed within the colony, and individual cells and cell borders could be more easily visualized. These changes are all consistent with differentiation (Nagasaka et al. 2017; Wakao et al. 2012). Other cellular changes linked to differentiation, like enlargement of the nuclei (Rozwadowska et al. 2013) and reduced expression of pluripotency markers TRA1-60 (Grigor'eva et al. 2019; Vilà-González et al. 2019) and SSEA4 (Zhang et al. 2018b) were also observed (Fig. 3.2D, E and Fig. 3.3). In summary, iPSCs depleted of YTHDF2 exhibit phenotypes consistent with loss of pluripotency.

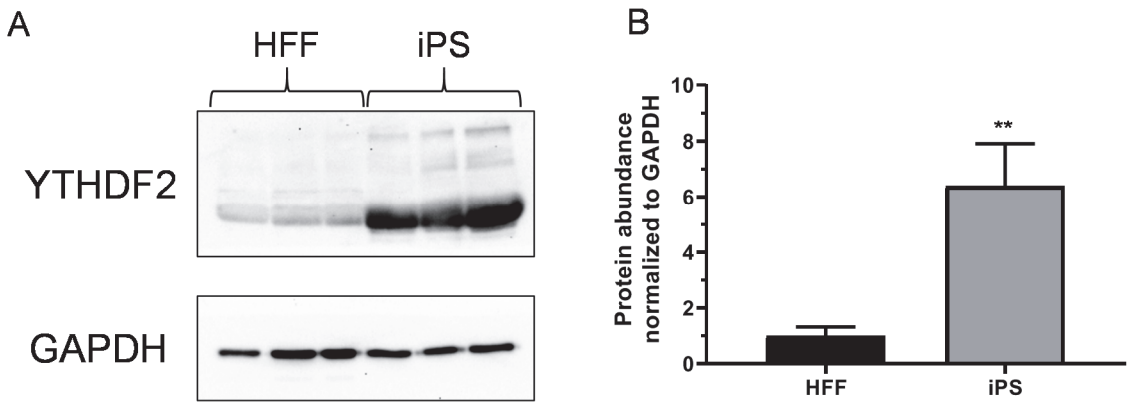

Figure 3.1: YTHDF2 protein is highly expressed in iPSCs. A: Western blot to detect YTHDF2 in three independent iPSC and HFF extracts. GAPDH was used as a loading control. B: Quantification of (A). Asterisks indicate significant difference in the relative mean protein expression between iPSC and HFF samples (**p-value<0.005).

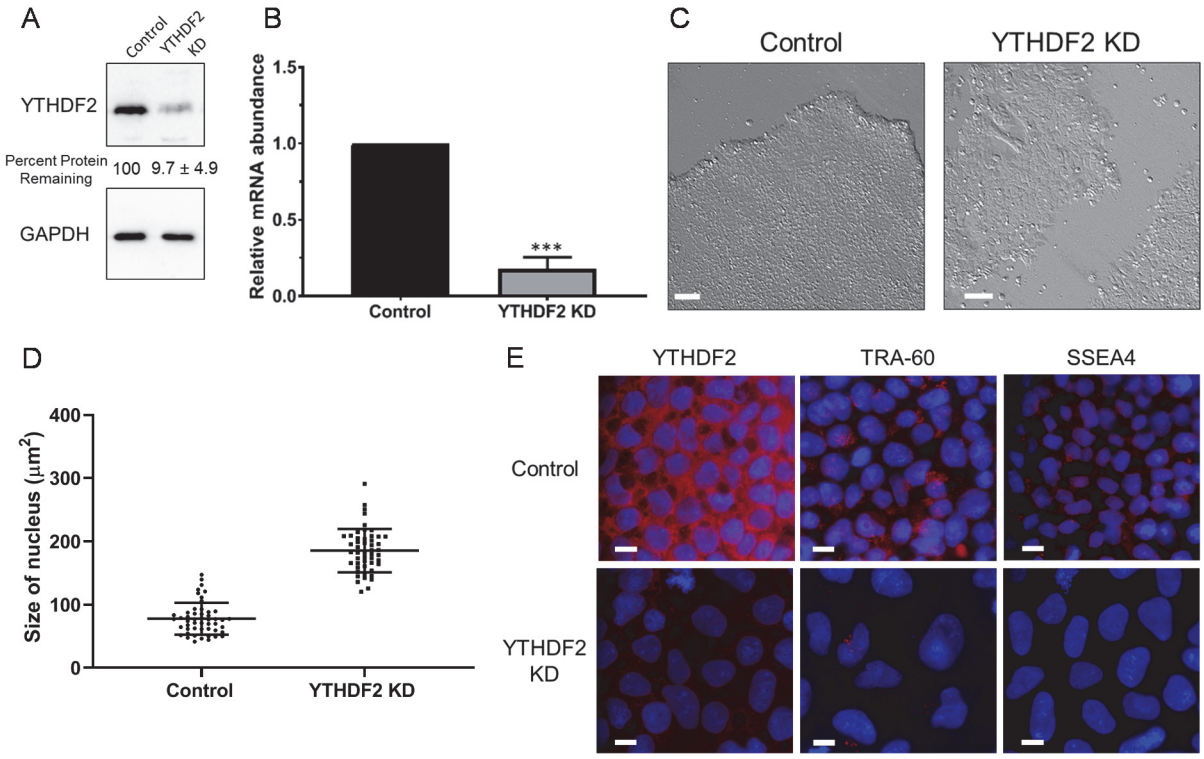

Figure 3.2: Depletion of YTHDF2 in iPSCs results in morphological changes. A: Representative western blot using iPSC extracts to demonstrate effective depletion of YTHDF2. GAPDH was used as a loading control. Percent protein remaining calculated from three independent biological replicates is indicated below the lanes. B: RT-dPCR analysis of YTHDF2 mRNA abundance in siRNA negative control and YTHDF2 depleted samples normalized to GAPDH mRNA. Asterisks indicate significant difference in mean abundance between control and YTHDF2 KD samples (***p-value<0.0005). C: Bright field images of siRNA negative control and YTHDF2-depleted iPSC colonies. Scale bars indicate 100 μm. D, E: iPSCs were subjected to five days of treatment with negative control or YTHDF2 siRNAs. The nucleus was stained with DAPI. (D) Nucleus size of siRNA negative control or YTHDF2 depleted cells (n=50) was quantified via ImageJ. *p-value <0.05. (E) The indicated protein was detected by immunofluorescence (IF) staining. Scale bars indicate 10 μm.

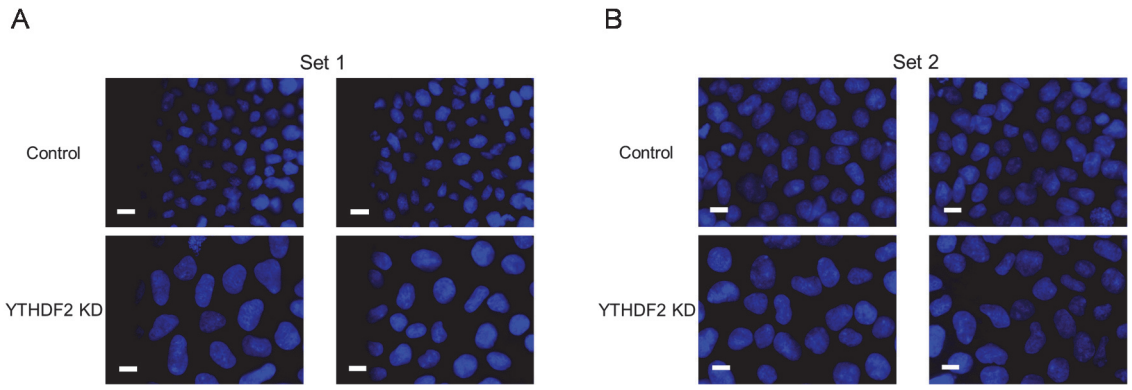

Figure 3.3: Depletion of YTHDF2 in iPSCs results in enlargement of the nucleus. Images used to quantify the nucleus size from 50 cells each in control and YTHDF2 KD samples. Set 1 (A) and set 2 (B) represent two independent replicates. Quantification was performed using ImageJ, results can be seen in Fig. 3.1D.

3.2.2 YTHDF2 depletion affects transcripts required for neural development

To gain insights into the specific transcripts affected by YTHDF2 and learn more about the phenotype adopted following YTHDF2 knockdown, we performed RNA-sequencing on control and YTHDF2-depleted cells. The dataset was normalized using the RUVSeq package (Risso et al. 2014) and differential expression was determined via DESeq2 (Love et al. 2014) (Fig. 3.4). We observed 1689 and 1066 transcripts were up- or down-regulated, respectively (Fig. 3.5A, Table S1). As expected, YTHDF2 itself exhibited a large decrease in expression. To better understand the structure of the dataset, we performed hierarchical clustering of the differentially expressed genes. Our analysis revealed up-regulated transcripts displayed more consistent levels of expression between biological replicates and more robust differences between treatment and control samples when compared to the down-regulated group of transcripts (Fig. 3.4D). This is consistent with YTHDF2 function as a destabilizing RBP, in that depletion is expected to result in increased abundance of target RNAs.

To identify mRNAs that are likely to be direct targets of YTHDF2, we compared our sets of differentially expressed transcripts with transcripts that are m^6A methylated in human embryonic stem cells (Batista et al. 2014). Lists were filtered so only genes were detected in both datasets were used in the analysis (Fig. 3.6). Importantly, almost 70% of the transcripts that were up-regulated following YTHDF2 knockdown were m^6A methylated, far more than expected by chance (Fig. 3.5B). This, and the fact that only 46% of down-regulated RNAs showed evidence of m^6A methylation (Fig. 3.5D) are consistent with previous observations that YTHDF2 recognizes m^6A and recruits RNA decay enzymes (Du et al. 2016a; Park et al. 2019; Wang et al. 2014b). Notably, transcripts with more than 1 m^6A site show a significantly greater change in abundance following YTHDF2 knockdown than those with 0 or 1 sites (Fig. 3.5F). This is consistent with recent evidence that recruitment of multiple YTHDF2 proteins may be required for maximal effect (Ries et al. 2019).

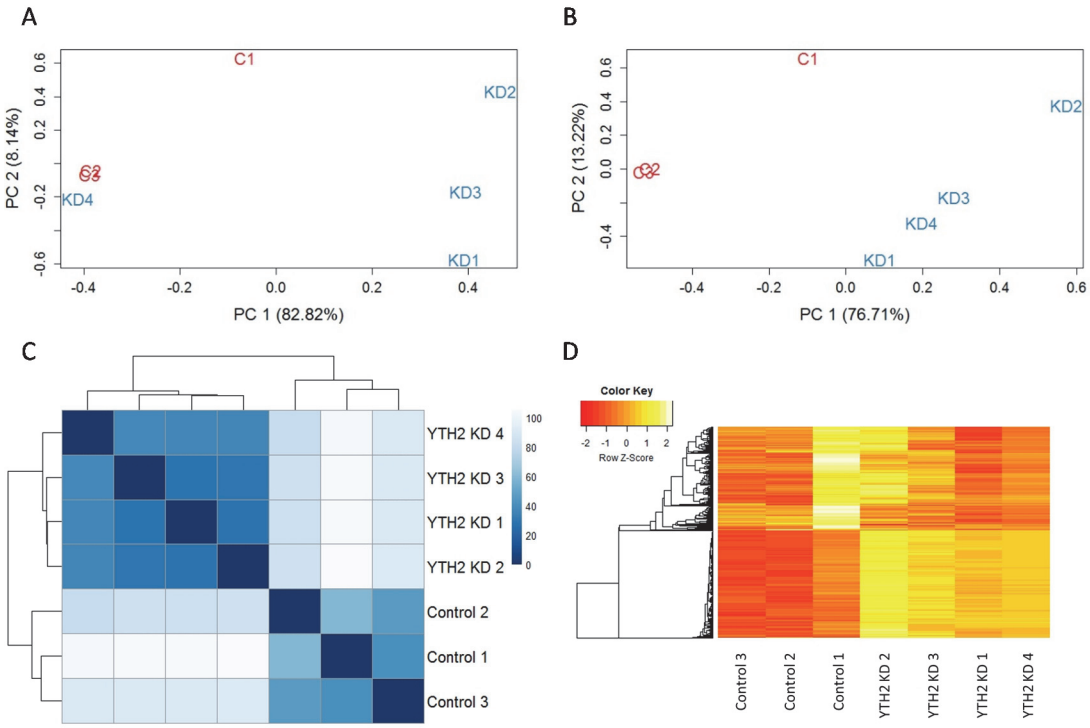

Figure 3.4: Normalization of RNA-seq data by RUVseq package to remove unwanted sources of variation. A: PCA plot of raw read counts generated by the RUVseq package (Risso et al., 2014). Control samples are labeled in red (C) and YTHDF2 depleted samples are labeled in blue (KD). B: RNA-seq samples were normalized using the RUVr function of the RUVseq package (Risso et al., 2014) under default parameters. PCA plot of dataset after normalization shows a distinct separation between control (red) and YTHDF2 KD (blue) replicates as compared to the raw data in A. C: Distance matrix showing the Euclidean distances between RNA-seq replicates. Replicates with a lower distance (darker blue) are more closely correlated in terms of gene expression. Distances were calculated from log-stabilized normalized read counts of all detected transcripts (>5 read counts per replicate). D: Hierarchical clustering of differentially expressed genes was performed on RUVr normalized read counts and plotted according to Z-scored intensity values. Areas of red or yellow to white indicate lower or higher relative expression, respectively.

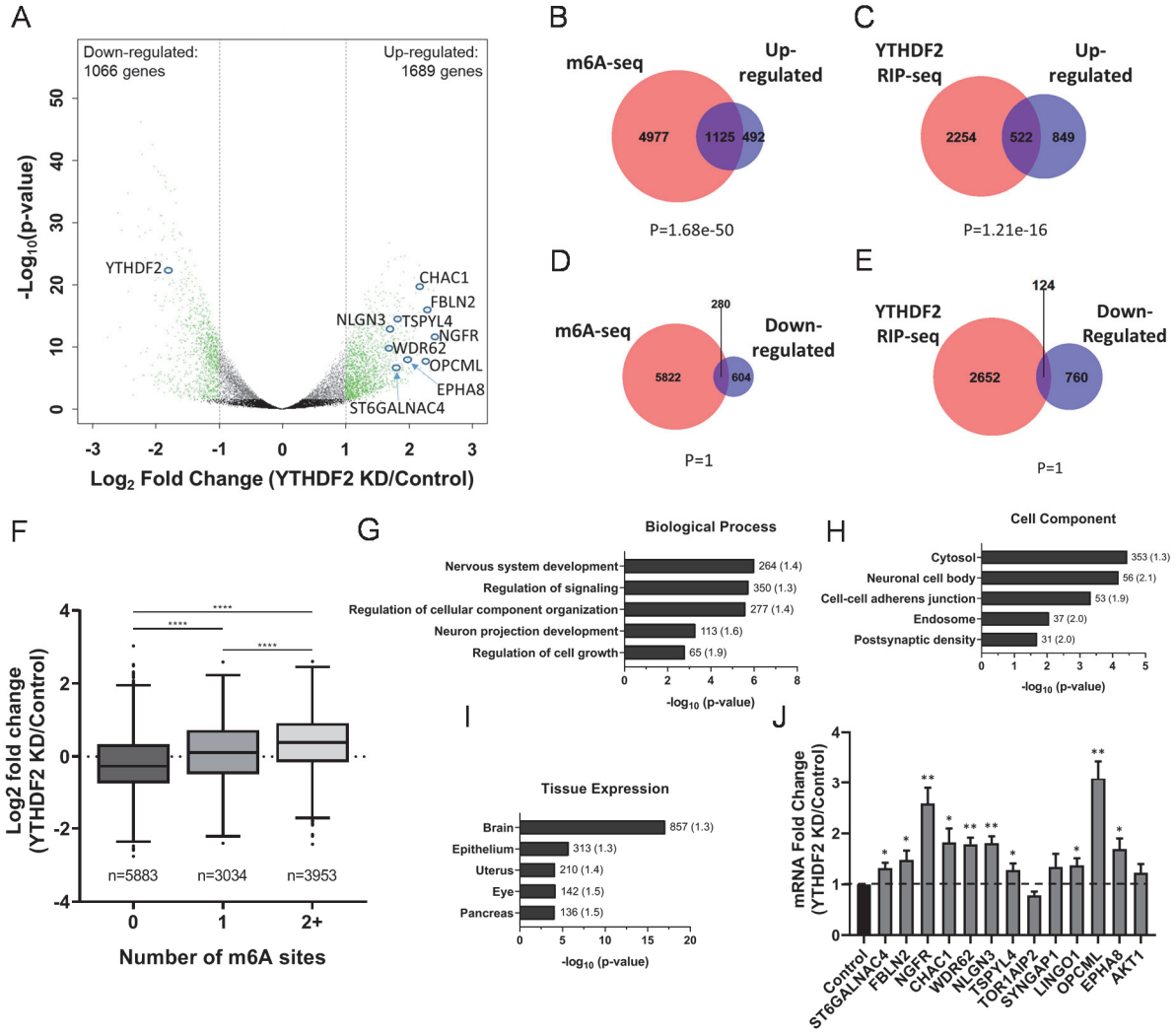

Figure 3.5: YTHDF2 depletion affects transcripts required for neural development. A: Volcano plot generated from sequencing data showing the adjusted p-value (y-axis) plotted against the fold change (x-axis) for individual genes. Differentially expressed genes are shown in green (differential expression: read counts>5, Benjamini-Hochberg adjusted p-value<0.05 and $\log_2$-fold change>1.0, represented by grey dotted lines). B-E: Venn diagrams showing the overlap between transcripts up-regulated (B and C) or down-regulated (D and E) following YTHDF2 depletion and transcripts previously shown to be m^{6}A methylated in hESCs (B and D; Batista et al., 2014) or bound by YTHDF2 (C and E; Wang et al., 2014). P-values were determined using a hypergeometric test. F: Boxplot of the $\log_2$ fold change in expression (YTHDF2 KD/Control), taken from results generated by DESeq2, vs. number of m^{6}A sites. Transcripts were binned based on the number of m^{6}A sites identified in Batista et al., 2014. The central line of the box plot represents the median $\log_2$ fold change expression value. n denotes the number of genes in each bin. Binned groups were compared using an unpaired two-sided Student's t-test (****p-value<0.0001). G-I: Functional annotation clustering of biological process (G), cellular component (H) and tissue expression (I) performed by DAVID on genes up regulated following YTHDF2 depletion. Annotation clusters with the highest enrichment according to FDR p-value are listed. The number of genes in each cluster is shown next to the respective bar and fold enrichment over background is given in parenthesis. J: RT-dPCR analysis of mRNA abundances in control and YTHDF2 depleted samples normalized to GAPDH. Data is reported as fold change (YTHDF2 KD/Control). Asterisks indicate significant difference in mean abundance between control and YTHDF2 KD samples (*p-value<0.05, **p-value<0.005).

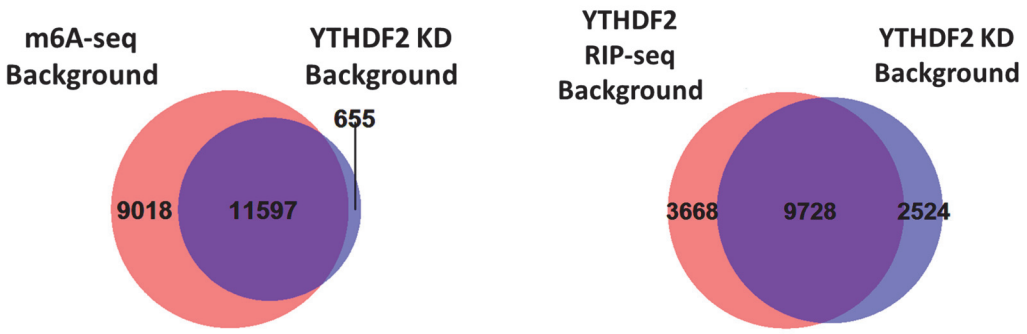

Figure 3.6: Background filtering for overlap analysis. All transcripts detected in the YTHDF2 KD RNA-seq dataset was filtered against all transcripts detected in the m^{6}A-seq dataset (left) or YTHDF2 RIP-seq dataset (right). Only transcripts present in both datasets, 11597 and 9728 for m^{6}A-seq and YTHDF2 RIP-seq, respectively, were used in the downstream analyses.

Overall, these data suggest that a significant proportion of m^{6}A methylated transcripts in iPSCs are targeted by YTHDF2 and that the primary outcome of YTHDF2 binding is reduced RNA abundance, likely through destabilization. We also compared our set of differentially expressed transcripts to those previously shown to be bound by YTHDF2 in HeLa cells (Wang et al. 2014b). Again, only transcripts that were detected in both datasets were used in the analysis (Fig. 3.6). Consistent with the results above, RNAs up-regulated following depletion of YTHDF2 in iPSCs were enriched among the set of transcripts bound by YTHDF2 (Fig. 3.5C). Moreover, there was no significant overlap between the list of down-regulated transcripts and YTHDF2 association (Fig. 3.5E). This is again expected given that YTHDF2 association results in destabilization of mRNAs.

To learn more about the pathways and processes that might be affected by depletion of YTHDF2, we performed Gene Ontology (GO) term analyses via DAVID v8 (Huang et al. 2009a, 2009b). Among the down-regulated genes, which are unlikely to be directly targeted by YTHDF2, we observed some enrichment of transcripts encoding proteins located in the nucleus and/or associated with mitosis but there was no overt connection to pluripotency or development (Fig. 3.7). In contrast, analysis of GO-terms associated with up-regulated transcripts revealed an intriguing link with neural differentiation/development in several categories. Several of the top hits for biological processes (Fig. 3.5G) and cellular component (Fig. 3.5H) have strong associations with neural development. Furthermore, over half of the up-regulated transcripts (857 out of 1689) are commonly expressed in the brain (Fig. 3.5I). These results coincide with previous reports that m^{6}A methylation (Yoon et al. 2017; Wang et al. 2018c; Ma et al. 2018; Zhuang et al. 2019; Chen et al. 2019), and YTHDF2 (Li et al. 2018b), play a role in modulating neural development in mammals. Based on these observations and the fact that up-regulated transcripts are more likely to be directly targeted by YTHDF2, we further characterized several of the most dramatically increased transcripts that encode factors with a role in neural development (Fig. 3.5A).

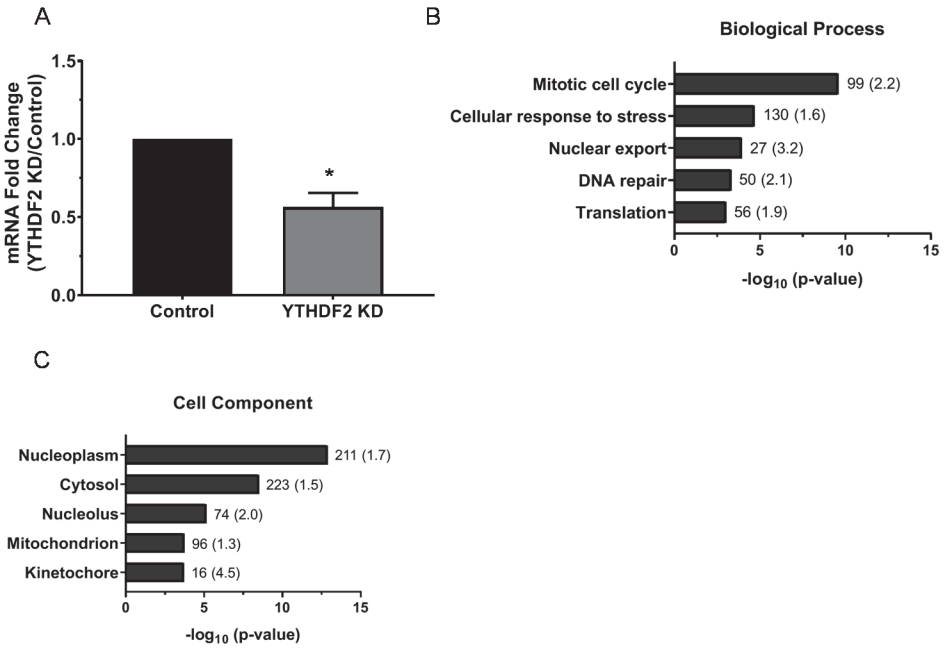

Figure 3.7: Validation and functional annotation clustering of genes down-regulated following YTHDF2 depletion in iPSCs. A: RT-dPCR analysis of SCML2 mRNA abundances in control and YTHDF2 depleted samples normalized to GAPDH. SCML2 was chosen because it exhibited one of the most robust decreases in abundance according to analysis of RNA-seq data. Data is reported as fold change (YTHDF2 KD/Control). Asterisks indicate significant difference in mean abundance between control and YTHDF2 KD samples (*p-value<0.05). B-D: Functional annotation clustering of biological process (B) and cellular component (C) performed by DAVID on genes down-regulated following YTHDF2 depletion. Annotation clusters with the highest enrichment according to FDR p-value are listed. The number of genes in each cluster is shown next to the respective bar and fold enrichment over background is given in parenthesis.

As can be seen in Fig. 3.5J, we were able to independently reproduce our sequencing results, with statistical significance, for a majority of the identified transcripts (10 out of 13). In summary, our results are consistent with the idea that YTHDF2 plays a role neural differentiation by modulating expression of mRNAs encoding factors associated with neural development.

3.2.4 YTHDF2 interacts with neural-associated transcripts

As an m^6A reader, YTHDF2 interacts with target transcripts by binding to m^6A via its YTH domain (Zhu et al. 2014; Li et al. 2014a; Xu et al. 2015). Upon closer examination, all of the neural-associated transcripts we identified possess one or more m^6A site(s) as defined via m^6A-seq experiments performed on human and/or mouse samples (Zheng et al. 2018). We performed RNA immunoprecipitations (RIPs) in iPSCs to assess whether the neural-associated transcripts we identified were selectively bound to YTHDF2. Briefly, YTHDF2-specific and IgG control antibodies were used to retrieve YTHDF2 and associated mRNAs from iPSC extracts following formaldehyde crosslinking. Western blot analysis of Input, IgG immunoprecipitation (IP) and YTHDF2 IP samples revealed YTHDF2 protein was detectable in Input and YTHDF2 IP samples, but not in the IgG IP sample (Fig. 3.8A), demonstrating effective isolation of YTHDF2. RNA was isolated from input, IgG IP and YTHDF2 IP samples and mRNA abundance assessed via RT-dPCR. GAPDH mRNA which has been previously established as a non-methylated transcript that does not bind YTHDF2 (Wang et al. 2014b; Batista et al. 2014) showed no enrichment over IgG, while CREBBP mRNA, which is known to bind YTHDF2, was significantly enriched and served as a positive control (Wang et al. 2014b) (Fig. 3.8B). Interestingly, all of the neural-associated transcripts were highly enriched (>6 fold over IgG) and were significantly enriched when compared to GAPDH (Fig. 3.8B).

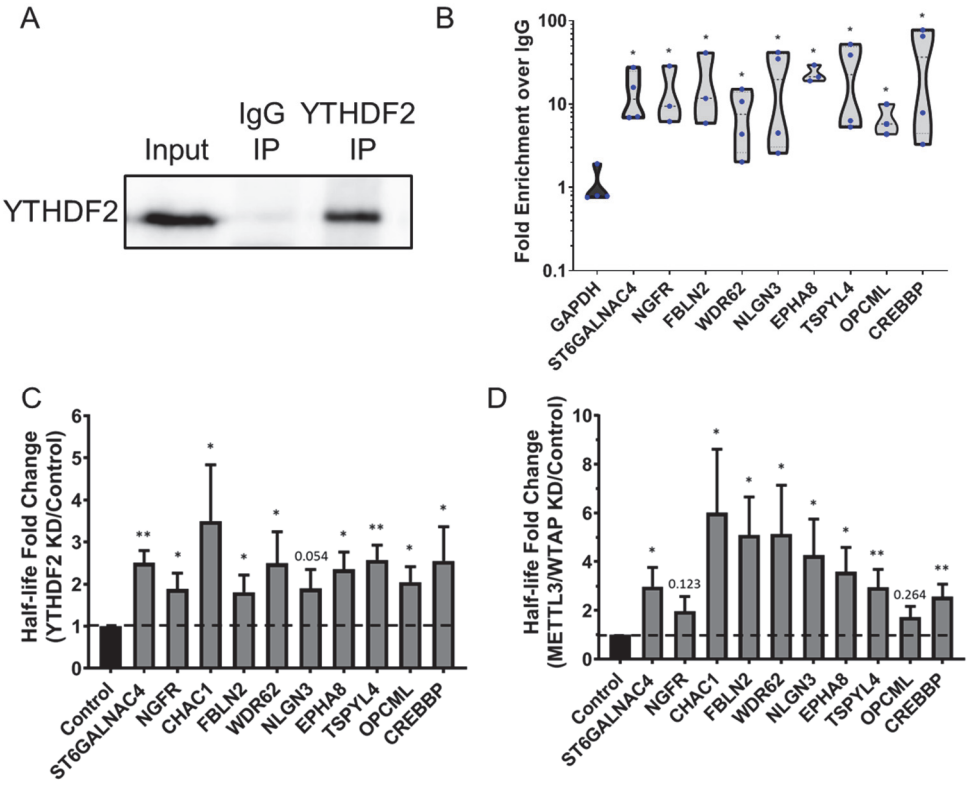

Figure 3.8: YTHDF2 binds to neural-associated transcripts and modulates their half-lives in an m^{6}A-dependent manner. A: Representative western blot showing YTHDF2 protein abundance in Input, IgG IP and YTHDF2 IP samples from RIP experiment. B: RT-dPCR analysis of transcript abundance in IgG and YTHDF2 IP samples. Data is represented in a violin plot as fold enrichment over IgG (YTHDF2 IP/IgG IP). Blue dots indicated individual replicate values (n=3-4). Asterisks indicate significant difference in mean fold enrichment between GAPDH and specified transcripts (*p-value<0.05). C, D: Half-lives from siRNA negative control and YTHDF2 KD (C) or siRNA negative control and METTL3/WTAP KD (D) samples. Data is reported as fold change (YTHDF2 KD/Control). Asterisks indicate significant difference in mean half-life between control and YTHDF2 KD samples (*p-value<0.05, **p-value<0.005). Non-significant p-values are given above bars.

Overall, these results further validate the findings from our RNA-seq experiment and indicate that YTHDF2 directly binds to several neural-associated transcripts in pluripotent stem cells.

3.2.5 YTHDF2 modulates the half-lives of neural-associated transcripts in m^{6}A dependent manner

As previously stated, YTHDF2 facilitates the degradation of target transcripts upon binding (Wang et al. 2014b; Du et al. 2016b). Therefore, we predicted the set of neural-associated transcripts we identified should be stabilized following YTHDF2 depletion. We assessed changes in half-life using 4-thiouridine (4sU) to label and eventually isolate nascent RNAs (Russo et al. 2017). Half-lives were inferred based on the ratio of total to nascent RNA for each transcript (see Materials and Methods for details). As predicted, depletion of YTHDF2 resulted in stabilization for almost all of the neural-associated transcripts tested (Fig. 3.8C). This indicates that YTHDF2 targets neural-specific m^{6}A-modified transcripts in order to facilitate their degradation.

If YTHDF2 is specifically targeting these transcripts through m^{6}A, then loss of m^{6}A should mimic the effect of YTHDF2 depletion. To investigate this, we simultaneously depleted the catalytically active subunit of the methyltransferase complex METTL3 and the major scaffolding subunit WTAP (Fig. 3.9A). Previous studies have shown that depletion of either protein reduces global levels of m^{6}A (Ping et al. 2014; Schwartz et al. 2014; Batista et al. 2014; Yoon et al. 2017; Wang et al. 2018a). As predicted, knockdown of METTL3 and WTAP increased the mRNA half-life for the vast majority (eight out of ten) of the transcripts (Fig. 3.8D). Based on these observations, we conclude that when a cell is in a pluripotent state, YTHDF2 targets neural-associated transcripts for decay in an m^{6}A-dependent manner.

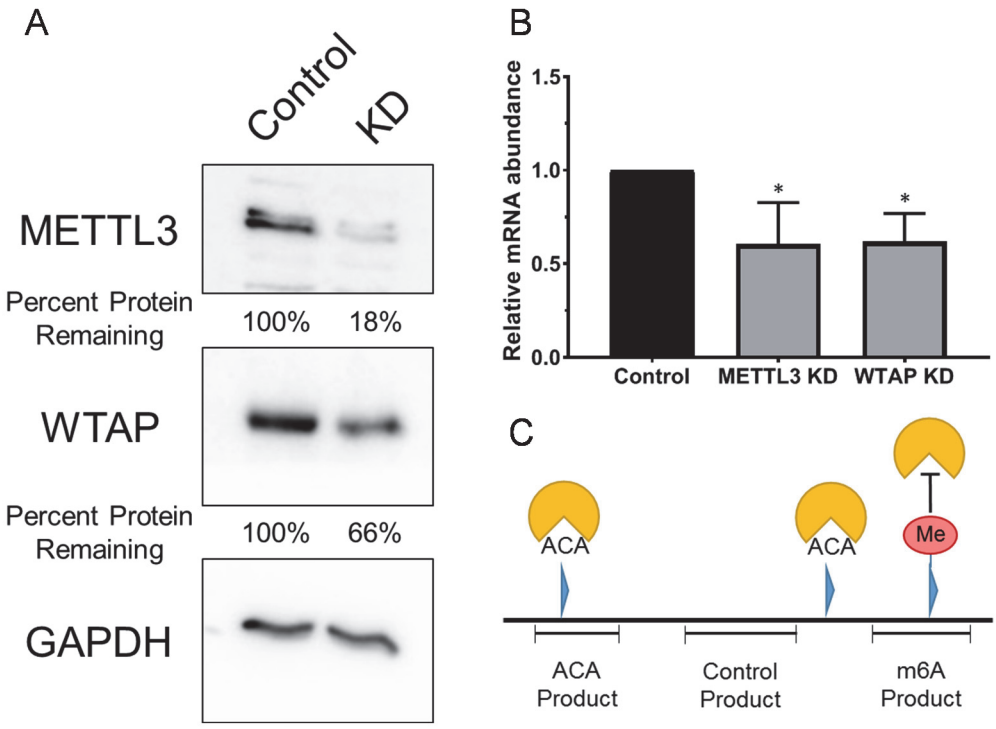

Figure 3.9: Validation of METTL3 and WTAP siRNA-mediated knockdown efficiency and MazF experimental design. A: Representative western blots showing effective depletion of METTL3 or WTAP from iPSC extracts. GAPDH was used as a loading control. Percent protein remaining calculated from three independent biological replicates. In both cases, statistical significance, p-value<0.05, was achieved for the difference in mean protein abundance between control and knockdown samples. B: RT-dPCR analysis of METTL3 or WTAP mRNA abundances in control and knockdown samples normalized to GAPDH. Asterisks indicate significant difference in mean mRNA abundance between control and knockdown samples (*p-value<0.05). C: Cartoon depiction of MazF experimental design. MazF cuts RNA at all ACA motifs but is inhibited by the presence of m^6A. RT-dPCR analysis is performed to quantify the abundance of the specified products. From there, a methylation ratio (i.e. percent methylated) can be determined by calculating the m^6A product abundance/Control product abundance. A background ratio can also be estimated by calculating the ACA product abundance/Control product abundance to account for any inefficiencies of the MazF enzyme.

3.2.6 YTHDF2 expression decreases during neural differentiation

If stem cells are utilizing YTHDF2 to suppress neural-associated transcripts, as suggested by our results above (Fig. 3.5 and 3.8) then YTHDF2 expression or activity may decrease to favor differentiation down the neural pathway into multipotent NPCs. To investigate this idea, we induced differentiation of iPSCs into NPCs and measured the levels of YTHDF2 protein over time. OCT4, a major pluripotency factor, and PAX6, a marker for neural differentiation (Zhang et al. 2010b), were used as controls to demonstrate that differentiation was occurring. As shown in Figures 3.10A, by day six expression of OCT4 protein was almost abolished (Fig. 3.10B) while PAX6 protein expression increased >50-fold (Fig. 3.10C). Notably, YTHDF2 protein expression exhibited a steady decline throughout the time course with a >60% reduction in protein expression by day six (Fig. 3.10A,D). In summary, YTHDF2 protein expression decreases as iPSCs differentiate into NPCs.

3.2.7 Stability of YTHDF2 target transcripts increases during neural differentiation

Based on the changes in mRNA half-life and abundance we observed following YTHDF2 depletion in iPSCs (Fig. 3.5 and 3.8) and the decrease in YTHDF2 expression over the course of neural induction (Fig. 3.10A,D), we predicted the group of neural-associated transcripts we identified as targets of YTHDF2 would exhibit increases in half-life and abundance during neural differentiation. To investigate, we induced neural differentiation for 6 days and then labeled with 4sU for four hours before isolating and processing RNA as before. Neural differentiated samples were compared to non-induced (pluripotent) controls. We observed stabilization for nine out of ten neural-associated transcripts (Fig. 3.10E). Interestingly, stabilization did not uniformly result in elevated mRNA abundance reflecting that other types of regulation are likely also at play (Fig. 3.10F). Overall, these results show that differentiation of iPSCs into NPCs results in stabilization of several neural-associated transcripts, and a decrease in YTHDF2 expression during neural differentiation may facilitate this (Fig. 3.8).

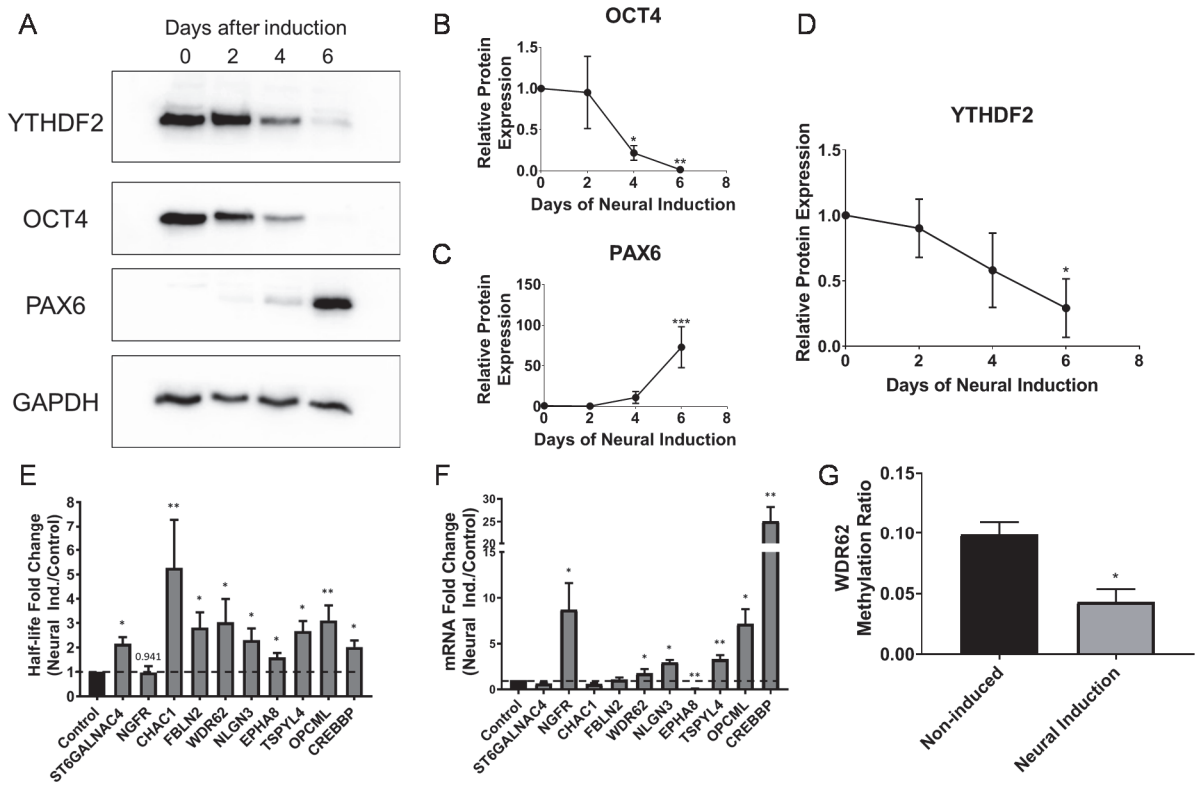

Figure 3.10: Changes in YTHDF2 expression and m^{6}A abundance after neural differentiation increase mRNA half-life and abundance of neural-associated transcripts. A: Representative western blot of YTHDF2, OCT4 and PAX6 protein expression at 0, 2, 4 and 6 days after neural induction. GAPDH was used as a loading control. B-D: Expression OCT4 (B), PAX6 (C) and YTHDF2 (D) over the time course was normalized to GAPDH and the abundance at the 0 day time point was set to 100% for each replicate. Asterisks indicate significant difference between the given time point and 0 days induction (*p-value<0.05, **p-value<0.005, ***p-value<0.0005). E: Half-lives from non-induced (control) and six day neural induced samples. Data is reported as fold change (Neural Induced/Control). Asterisks indicate significant difference in mean half-life between control and neural induced samples (*p-value<0.05, **p-value<0.005). Non-significant p-values are given above bars. F: RT-dPCR analysis of mRNA abundances, normalized to GAPDH, from samples that underwent no induction (control) or six days of neural induction. Data is reported as fold change (Neural Induced/Control). Asterisks indicate significant difference in mean abundance between control and neural induction samples (*p-value<0.05, **p-value<0.005). G: The methylation ratio of WDR62 from samples that underwent no induction (non-induced) and six days of neural induction quantified by MazF-dPCR. Asterisks indicate significant difference in mean methylation ratio between non-induced and neural induced samples (*p-value<0.05).

3.2.8 Neural-specific targets of YTHDF2 also undergo a decrease in m^{6}A deposition upon neural differentiation

Previous studies have shown global m^{6}A abundance and expression of the catalytically active subunit of the m^{6}A writer complex, METTL3, decreases during differentiation (Wang et al. 2018a; Geula et al. 2015; Aguilo et al. 2015). To explore whether this might also influence expression of YTHDF2 substrates, we evaluated methylation during differentiation by modifying a recently published protocol which utilizes the MazF endoribonuclease to quantify m^{6}A abundance at a specific site (MazF-RT-dPCR) (Garcia-Campos et al. 2019a). Briefly, MazF cleaves RNA at ACA motifs and is blocked by N6-adenosine methylation. Thus, following treatment with MazF, RNA regions containing m^{6}A remain intact while unmethylated regions are cleaved and no longer detected by RT-dPCR. The fraction of methylated RNA can be determined by comparing the abundance of a region containing an m^{6}A site with the abundance of a different region lacking ACA (Fig. 3.9C). Unfortunately, many of the neural transcripts associated with YTHDF2 did not contain m^{6}A sites that were amenable to this analysis (i.e. did not have the ACA sequence or had multiple ACA sequences in close proximity) but we identified one m^{6}A site near the stop codon of the WD40 repeat domain 62 (WDR62) transcript which was suitable. Interestingly, we observed an approximate 2-fold drop in m^{6}A deposition at this WDR62 m^{6}A site after 5 days of neural induction when compared to non-induced iPSCs (Fig. 3.10G). In Fig. 3.10E/F above, we observed a 3- and 2-fold increase in mRNA half-life and abundance, respectively, for WDR62 transcripts after neural induction. Thus, upon neural induction, an increase in WDR62 mRNA abundance correlates with both decreased expression of YTHDF2 protein and reduced m^{6}A deposition.

3.2.9 YTHDF2 depletion disrupts neural differentiation of iPSCs

We observed above that extended YTHDF2 depletion in iPSCs increased the size of the nucleus (Fig. 3.2D and Fig. 3.3) and abrogated expression of two pluripotency markers, TRA-1-

60 and SSEA4 (Fig. 3.2E). Both of these observations suggest depletion of YTHDF2 results in loss of pluripotency. Moreover, YTHDF2 binds to and regulates transcripts associated with neural development (Fig. 3.5). We therefore wondered if YTHDF2 depletion influences differentiation down the neural lineage. As an initial test, we again depleted YTHDF2 in iPSCs for 5 days and used immunofluorescence (IF) to examine the protein expression of three neural-specific markers, PAX6, NES (Nestin) and SOX1 (Malchenko et al. 2014; Feng et al. 2014b). Intriguingly, the intensity of staining for the membrane-bound protein Nestin appears to increase, as does the intensity and presence of the transcription factor SOX1 in YTHDF2 depleted cells compared to controls (Fig. 3.11A). However, we were unable to detect expression of PAX6 protein in control or YTHDF2 depleted samples although mRNA was present (Fig. 3.12). These results suggest YTHDF2 depletion in iPSCs can induce some aspects of the neural gene expression program but cannot completely mimic the effects of neural induction.

If YTHDF2 depletion favors neural differentiation, we hypothesized this influence might be potentiated upon neural induction when compared to non-YTHDF2 depleted controls. To evaluate this, we depleted YTHDF2 prior to inducing differentiation and treated with siRNAs again the day neural induction began. We measured the abundances of several pluripotency factor mRNAs (OCT4 and NANOG), and neural-specific factors (PAX6, SOX1 and Nestin). Prior to neural induction, OCT4 and NANOG were unaffected by YTHDF2 depletion, whereas PAX6, SOX1 and Nestin exhibited modest decreases in mRNA abundance (Fig. 3.11B). In contrast, we observed a substantial increase in mRNA abundance for PAX6 at both 2 and 5 days after neural induction in the YTHDF2 depleted samples when compared to controls (Fig. 3.11C).

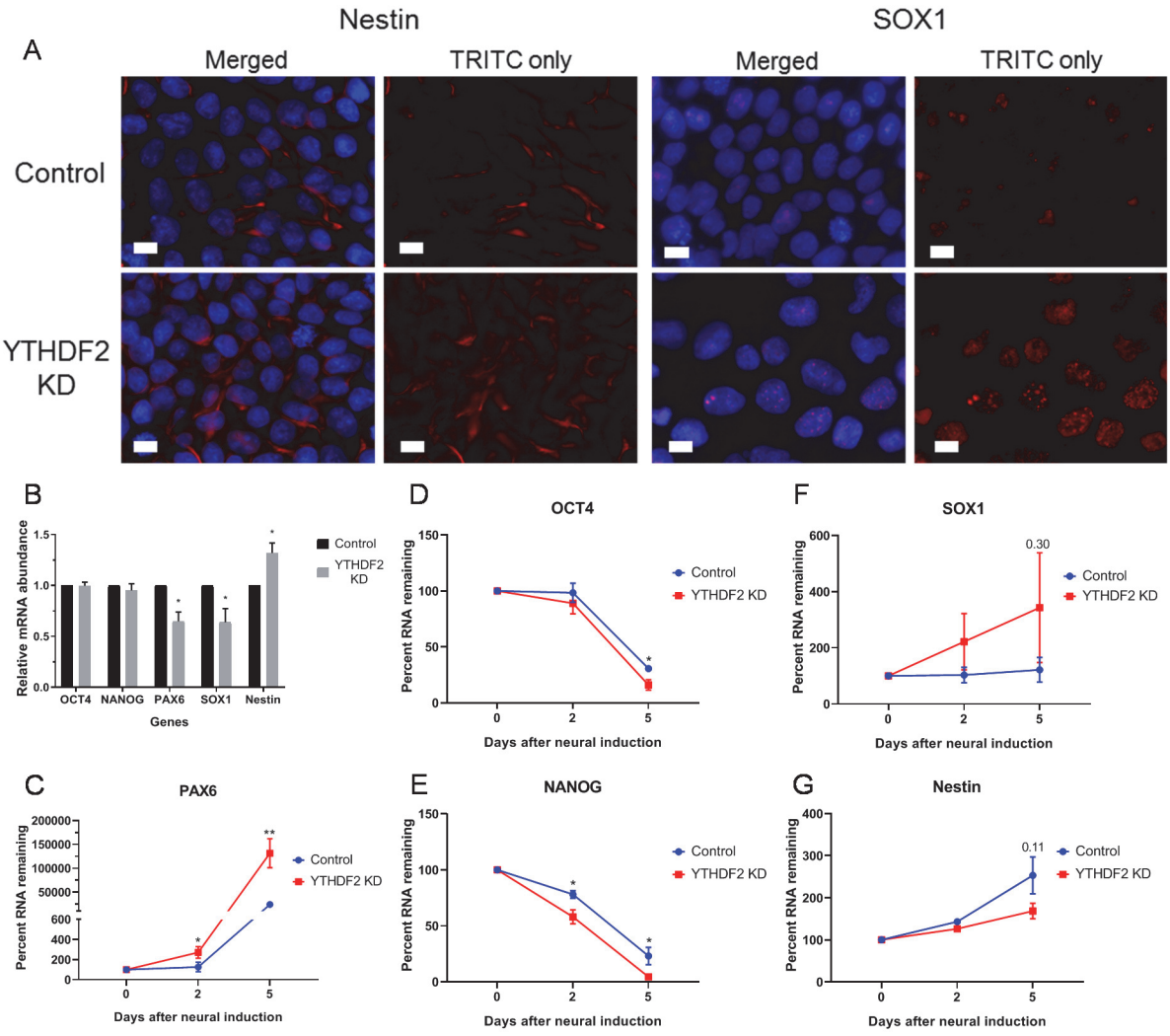

Figure 3.11: YTHDF2 depletion disrupts neural differentiation of iPSCs. A: iPSCs were treated with negative control or YTHDF2-targeting siRNA for five days. The indicated protein was detected by immunofluorescence staining. The nucleus was stained with DAPI. Scale bars indicates 10μm. B: RT-dPCR analysis of mRNA abundances in control and YTHDF2 depleted samples prior to neural induction (0 days). Data is reported as fold change (YTHDF2 KD/Control). Asterisks indicate significant difference in mean abundance between control and YTHDF2 KD samples (*p-value<0.05). C-G: mRNA expression of pluripotency (OCT4 and NANOG) and neural specific (PAX6, SOX1 and Nestin) factors over the course of neural differentiation was quantified via RT-dPCR and normalized to GAPDH. Abundance at the 0 day time point was set to 100%. Asterisks indicate significant difference in the mean percent RNA remaining between control and YTHDF2 KD replicates at that time point (*p-value<0.05, **p-value<0.005).

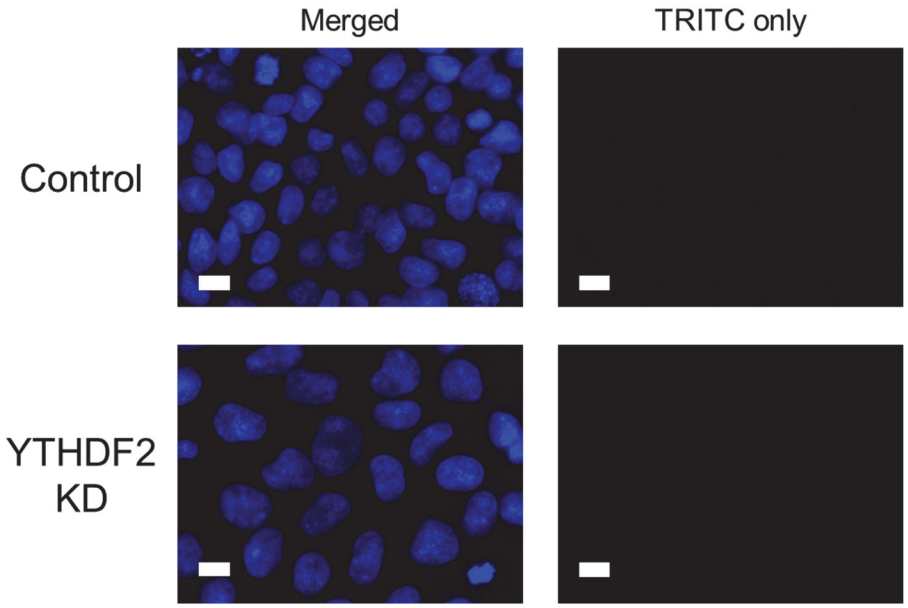

Figure 3.12: PAX6 is undetectable in control or YTHDF2-depleted iSPCs. iPSCs were subjected to five days of treatment with negative control or YTHDF2 siRNAs. PAX6 was detected by immunofluorescence staining using an Alexa Fluor®568-conjugated secondary antibody. The nucleus was visualized by staining with DAPI. Merged (right) and TRITC only (left) images are presented. Scale bar indicates 10 μm.

Moreover, expression of both OCT4 and NANOG were significantly reduced after 5 days of neural induction in YTHDF2 depleted cells compared to controls, with NANOG also being significantly reduced after only 2 days of induction (Fig. 3.11D, E). There was no significant effect on SOX1 or Nestin expression during neural induction (Fig. 3.11F, G). Thus, it appears that depletion of YTHDF2 in iPSCs leads to precocious differentiation with loss of pluripotency and up-regulation of some neural specific factors. Depletion of YTHDF2 prior to and during neural differentiation disrupts the coordination necessary to achieve precise cell state transitions resulting in aberrant expression of pluripotency and neural-specific factors.

3.3 Discussion

In the experiments described above, we have shown that YTHDF2 is important for pluripotency. Through RNA sequencing, we discovered that mRNAs encoding factors associated with neural development are up-regulated following YTHDF2 knockdown. YTHDF2 directly interacts with many of these neural-associated mRNAs, presumably targeting them for degradation in an m^6A-dependent manner. Over the course of neural differentiation, YTHDF2 expression is decreased and at the same time neural-associated mRNAs are stabilized. At least one transcript, WDR62, experiences reduced m^6A methylation during differentiation which could also contribute to stabilization. Reducing expression of YTHDF2 before neural induction disrupts the differentiation process resulting in aberrant expression of both neural and pluripotency factors. Overall, our data support the notion that YTHDF2 is a key m^6A reader in pluripotent cells that specifically restrains neural differentiation.

Previous studies have reported YTHDF2 influences maintenance and differentiation of multipotent stem cells from various lineages (Yao et al. 2019; Wang et al. 2018b; Li et al. 2018c, 2018b; Zhang et al. 2017a; Paris et al. 2019). Here, we show that YTHDF2 plays a role at the earliest stages of development; in pluripotent stem cells. Although mRNAs encoding both pluripotency factors and neural-specific factors can be m^6A-modified (Batista et al. 2014), we

find little evidence that YTHDF2 directly influences expression of pluripotency factors, as only neural-specific mRNAs are enriched in the set of transcripts up-regulated by YTHDF2 knockdown. This is consistent with YTHDF2 being required primarily to clear neural-specific transcripts as they are produced, thereby allowing the pluripotency gene expression program to dominate. Indeed, a similar observation was reported during the endothelial-to-hematopoietic transition in zebrafish where YTHDF2 facilitates the clearance of endothelial-specific genes *notch1a* and *rhoca* to promote hematopoietic stem cell reprogramming (Zhang et al. 2017a). Maintaining neural-specific mRNAs in an unstable state also facilitates their rapid and coordinated upregulation following induction of the neural differentiation program, as unstable mRNAs reach a new steady state more rapidly when transcription changes (Bertero et al. 2018). When YTHDF2 is artificially depleted, iPSCs appear to acquire some features of the neural cell gene expression program while simultaneously being poorly primed for differentiation down the neural pathway upon induction. These outcomes can both be explained by increased stability of neural-specific transcripts seen when either YTHDF2 or m^{6}A itself are reduced. Importantly, once the neural gene expression program has been successfully engaged, long-term stabilization of neural transcripts may occur naturally through down-regulation of both YTHDF2, and methylation.

Interestingly, other studies also indicate that YTHDF2 and m^{6}A are particularly important for neural gene expression programs. Specifically, YTHDF2 depletion in mice compromises neural development, and generates NPCs with reduced abilities to proliferate and differentiate (Li et al. 2018b). These effects correlate with stabilization of neural-specific mRNAs targets. Furthermore, knockout of METTL14 or depletion of METTL3 in embryonic mouse brains alters expression of m^{6}A-modified mRNAs encoding factors important for neurogenesis and neural differentiation (Yoon et al. 2017). Finally, deletion of METTL14 in mouse NPCs reduced proliferation and induced premature differentiation (Wang et al. 2018c). It is unclear how methylated neural-specific transcripts might be selected by YTHDF2 given that a broad

spectrum of transcripts are m^{6}A-modified (Batista et al. 2014). A similar situation exists when m^{6}A-modified maternal mRNAs are cleared from oocytes, while leaving zygotic m^{6}A-modified transcripts intact (Ivanova et al. 2017; Zhao et al. 2017b). It is possible that neural RNAs are somehow marked during transcription or other steps of RNA processing, perhaps by modification of the YTH protein or by recruitment of additional factors. Alternatively, it may be that the sequence context and/or distribution of m^{6}A sites in neural-specific and other affected RNAs is more favorable for YTHDF2 binding.

Recent reports have indicated that m6A modification, and subsequent binding of YTHDF proteins, potentiates the phase separation potential of mRNAs into ribonucleoprotein (RNP) granules (Gao et al. 2019; Fu and Zhuang 2019; Ries et al. 2019). Moreover, the effects are exacerbated by the presence of multiple m6A modifications and YTHDF protein binding events. YTHDF2 specifically was found to shuttle bound mRNAs to Processing bodies (P-bodies) under endogenous conditions (Ries et al. 2019); presumably facilitating their degradation as previously described (Wang et al. 2014b). However, under stress conditions like heat shock, sodium arsenite or endoplasmic reticulum stress, YTHDF2 re-localized, with its bound mRNA, to stress granules (SGs) in a range of cell types (Ries et al. 2019). Once partitioned into these SGs, YTHDF2 does not facilitate mRNA degradation like in P-bodies, but rather transcripts sit in a state of suspended animation. Perhaps a similar phenomenon occurs during differentiation in which YTHDF2 relocalizes to RNP granules formed in response to differentiation being induced? Indeed there is evidence of RNP granules formation that is specific to a cell type or process such as germ granules (Knutson et al. 2017; Dodson and Kennedy 2019) and neuronal RNA granules (Mitsumori et al. 2017; Van Driesche and Martin 2018). Moreover, a handful of studies have previously suggested RNP granules may play a role in differentiation (Gao and Keene 1996; Lin and Tarn 2009). In the context of YTHDF2, it would seem more efficient for the cell to utilize the same protein to regulate transcript expression prior to and localization

immediately following induction. Future studies investigating the localization and PTMs of YTHDF2 prior to and immediately following neural induction may shed some light on this idea.

Among the neural-specific targets of YTHDF2 we identified, WDR62, CHAC1 and NGFR stand out as encoding key factors for neural development. WDR62 regulates neurogenesis via the JNK1 signaling pathway (Xu et al. 2014c) and its depletion disrupts mitotic progression and induces death of NPCs, which ultimately results in primary microcephaly (Nicholas et al. 2010; Bilgüvar et al. 2010; Chen et al. 2014). Moreover, WDR62 has been implicated in the specification of neural and glial progenitor cells during human pluripotent stem cell differentiation (Alshawaf et al. 2017). CHAC1 facilitates neurogenesis by antagonizing the Notch signaling pathway (Chi et al. 2012, 2014), which plays an important role in early neurodevelopment (Zhang et al. 2018c). Finally, the nerve growth factor receptor, NGFR has multiple roles throughout neural development and is a marker for *in vitro* differentiation of hESCs into NPCs (Pruszak et al. 2007; Lee et al. 2007). NGFR targets have been implicated in embryonic stem cell survival (Pyle et al. 2006) and neural lineage definition (Bibel et al. 2004). By targeting these key neural-specific transcripts, YTHDF2 can play a major role in coordinating gene expression changes during neural development.

In conclusion, the ability of m^6A modification to influence self-renewal and neural differentiation of iPSCs is achieved through recruitment of YTHDF2 to neural-specific transcripts. Destabilization of neural-specific mRNAs is important for preventing inappropriate activation of neural gene expression and to permit rapid and coordinated differentiation upon neural induction.

Chapter 4: Elements in the 3'UTR of the *YTHDF2* mRNA promote translation

4.1 Introduction

As described above (see Chapters 1 and 3), m^{6}A influences RNA metabolism in many different tissues, cell types and cellular responses. However, its regulatory potential is most prevalent and well-studied in stem cells and during development (Geula et al. 2015; Batista et al. 2014; Wang et al. 2018c; Zhang et al. 2017a; Wang et al. 2014c; Heck and Wilusz 2019). In addition to the biological impact m^{6}A has on stem cell and developmental biology, it is also important to understand how m^{6}A deposition and the activity of m6A readers change throughout the course of development. Global levels of m^{6}A modification are relatively high in ESCs and decrease as cells differentiate (Batista et al. 2014; Aguilo et al. 2015). Consistent with this observation, the two MAC subunits, METTL3 and METTL14, are highly expressed in pluripotent and multipotent stem cells in comparison to differentiated cell types (Aguilo et al. 2015; Weng et al. 2018a). MAC co-factors like ZFP217 and SMAD2/3 also experience altered expression over the course of differentiation (Aguilo et al. 2015; Bertero et al. 2018), which may influence m^{6}A deposition on certain transcripts.

Examination of m^{6}A distributions and the expression profiles of the writers and erasers is key to understanding how m^{6}A impacts pluripotency and development. However, just as important, if not more so, is the characterization of reader expression profiles and activities during differentiation, as the readers are directly responsible for the fate of modified mRNAs. Beyond our work in Chapter 3 regarding YTHDF2, little is known about the expression profiles of YTH-domain readers in iPSCs or during differentiation. A previous study describing the transcriptomes of hESCs during differentiation into each of the three germ layers indicated there are only subtle changes in abundances of mRNAs encoding the YTH family of readers (Gifford et al. 2013). Likewise, global proteomic profiling during differentiation of human iPSCs (Hurrell

et al. 2019) and ESCs (Rigbolt et al. 2011) has noted modest decreases in expression of YTH family proteins. However, none of these results have been independently verified. In regards to other developmental processes, YTHDC1 and 2 proteins are up-regulated during gametogenesis (Kasowitz et al. 2018; Hsu et al. 2017), whereas YTHDF1 is temporally and spatially regulated during neural development (Shi et al. 2018b; Weng et al. 2018b). In general, these studies demonstrate that regulation of readers can occur, but stop short of characterizing the mechanisms involved.

In contrast to the modest change in mRNA abundance, we reported in Chapter 3 that YTHDF2 protein expression is dramatically increased in iPSCs when compared to HFFs (Fig. 3.1). Non YTH-domain readers, like the IGF2BP family of proteins, are also significantly up-regulated in pluripotent stem cells compared to differentiated cell types (Conway et al. 2016) despite exhibiting little difference in mRNA abundance (Gifford et al. 2013). These observations are consistent with m^6A reader abundance being modulated at the level of translation or protein stability.

The 3' UTR often plays an important role in regulating translation as elements/motifs within this region can provide access points for miRNAs or RBPs (Harvey et al. 2018; Vasudevan et al. 2007; Iwakawa and Tomari 2015). Two miRNAs, miR-145 and miR-493, have previously been implicated in repressing YTHDF2 expression in HeLa cells (Yang et al. 2017; Li et al. 2018a) and several binding sites for RBPs can be predicted or have been observed through CLIP-Seq. . Based on the evidence outlined above, we hypothesized that elements in the 3' UTR of *YTHDF2* mRNA contribute to the observed differences in YTHDF2 protein abundance in iPSCs and HFFs, presumably through recruitment of miRNAs or RBPs.

Here, we report that YTHDF3, which can partner with YTHDF2 to modulate mRNA decay, is only mildly downregulated during differentiation. We verified that changes in YTHDF2 expression are mediated at the protein level in iPSCs, as mRNA levels change little during differentiation. We failed to observe any substantial change in YTHDF2 expression following

over expression of miR-145 suggesting that miR-145 is not responsible for repression of YTHDF2 in HFFs. Using luciferase reporter assays we located sequence elements in the first 300 nucleotides of the YTHDF2 3' UTR that are sufficient to enhance translation of *YTHDF2* mRNA. Through biotinylated RNA pulldowns followed by mass spectrometry (MS), we identified 30 proteins that interact with this region of the YTHDF2 3' UTR. We investigated three of these proteins, IGF2BP1, IGF2BP3 and HNRNPQ (aka SYNCRIP), as well as m^{6}A modifications as putative factors enhancing *YTHDF2* mRNA translation, but were unable to find evidence that any of these factors are involved. Taken together, our findings reveal YTHDF2 protein is highly expressed in pluripotent stem cells and this is achieved through elements in the 3' UTR that facilitate enhanced translation.

4.2 Results

4.2.1 YTHDF2, but not YTHDF3, experiences dramatic changes in protein expression following differentiation of iPSCs

In Chapter 3, we observed that YTHDF2 protein expression was up-regulated approximately 7-fold in iPSCs compared to HFFs (Fig. 3.1). Moreover, YTHDF2 protein expression was reduced approximately 60% during differentiation down the neural lineage (Fig. 3.10). We therefore wondered: i) if other m^{6}A readers experienced a similarly high expression in pluripotent cells, and ii) does YTHDF2 expression change following differentiation down other lineages? To address the first question, we chose to focus on YTHDF3, as there is previous evidence that YTHDF3 also facilitates mRNA decay (Shi et al. 2017). We measured YTHDF3 protein expression in iPSCs and HFFs and observed a nominal increase in expression of YTHDF3 in iPSCs (Fig. 4.1A). However, this increase was neither statistically significant nor as substantial as the change in YTHDF2 expression (Fig. 4.1B). To investigate the second question, we measured expression of YTHDF2 in iPSCs induced to differentiate down the mesoderm lineage. We observed that YTHDF2 expression decreased approximately 50%

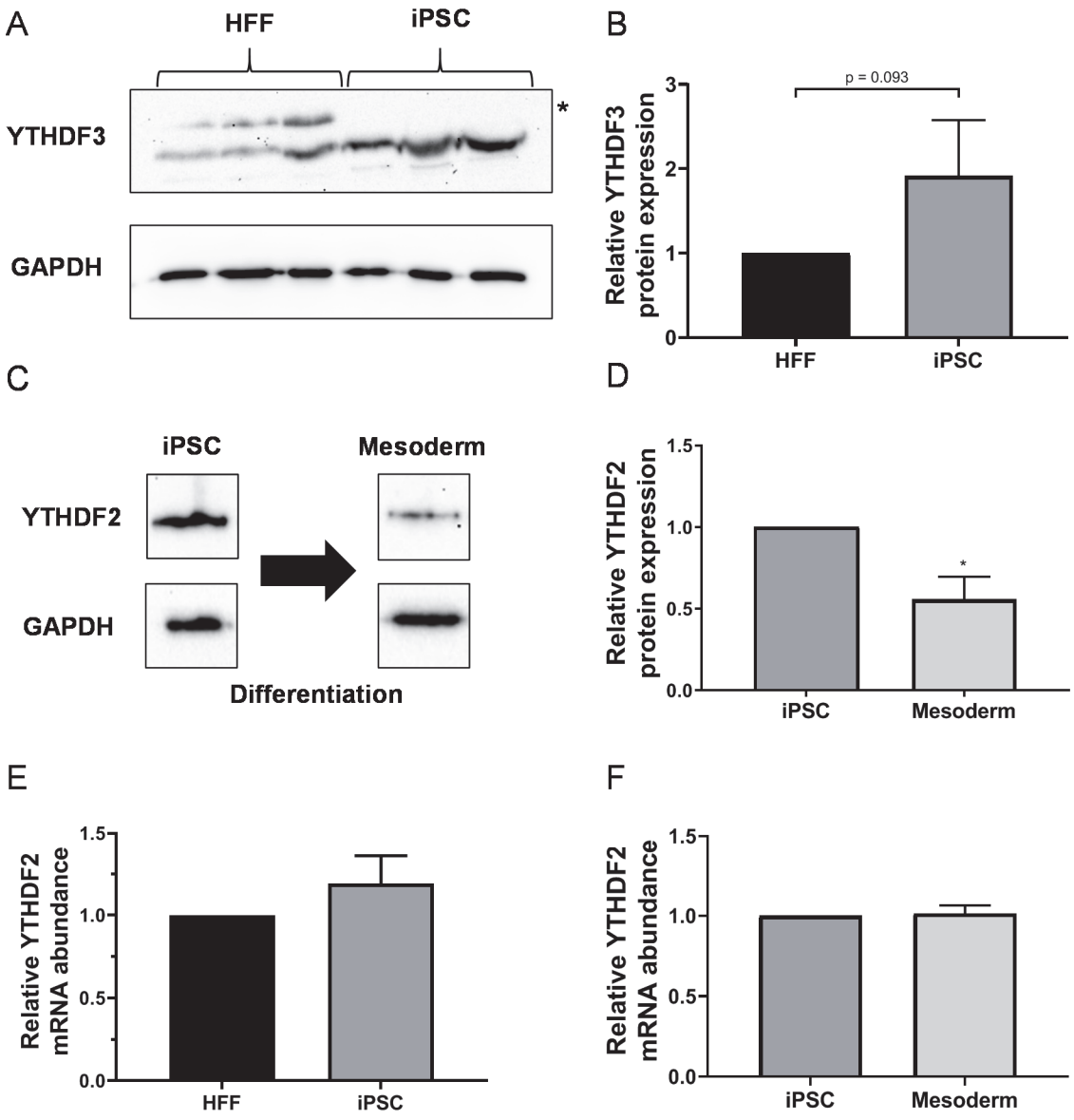

Figure 4.1: YTHDF2, but not YTHDF3, protein expression is differentially expressed between cell states. A: Western blot to detect YTHDF3 in three independent iPSC and HFF extracts. GAPDH was used as a loading control. Asterisk represents non-specific band. B: Quantification of (A). P-value listed is for comparison in the relative mean protein expression between iPSC and HFF samples. C: Representative image of western blots to detect YTHDF2 in untreated and mesoderm-induced iPSC extracts. GAPDH was used as a loading control. D: Quantification of (C). Asterisks indicate significant difference in the relative mean protein expression between iPSC and HFF samples (*p-value<0.05). E-F: RT-dPCR analysis of YTHDF2 mRNA abundance in untreated iPSC and HFF (E) or mesoderm-induced iPSC (F) samples normalized to GAPDH mRNA.

following five days of mesoderm induction (Fig. 4.1C,D). Thus, YTHDF2 is down-regulated during differentiation of iPSCs into two out of the three germ layers. These observations, coupled with our findings from Chapter 3 and previous studies (Li et al. 2018b; Wang et al. 2018b), suggest that YTHDF2 is a key reader of m^6A modification in pluripotency and development down multiple lineages.

4.2.2 YTHDF2 is regulated at the level of translation or protein turnover

As a first step to determine how YTHDF2 abundance is elevated in stem cells, we measured *YTHDF2* mRNA abundance in iPSCs and HFFs via RT-dPCR. As predicted from RNA-seq experiments (Gifford et al. 2013), *YTHDF2* mRNA abundance exhibited no change between HFFs and iPSCs (Fig. 4.1E). Similarly there was no change in YTHDF2 mRNA levels following differentiation down the mesoderm lineage (Fig. 4.1F). Based on these results, we inferred that the increased expression of YTHDF2 in iPSCs is mediated at the level of translation or protein stability.

4.2.3 YTHDF2 3'UTR is sufficient to enhance translation in iPSCs and HeLa cells

It is well-known that the 3' UTR contains elements that can influence mRNA metabolism including translation efficiency. Therefore, we evaluated the capacity of the YTHDF2 3' UTR to regulate translation via a luciferase reporter system. Briefly, the YTHDF2 3' UTR was cloned into a Renilla luciferase reporter plasmid immediately downstream of the Renilla ORF. The YTHDF2 3' UTR construct or an empty vector control were then transfected into cells along with a Firefly luciferase plasmid to control for transfection efficiency. Renilla luciferase activity was also adjusted to account for differences in mRNA abundance (Fig. 4.2A). As predicted, the presence of the YTHDF2 3' UTR significantly increased the relative luciferase activity compared to an empty vector control by approximately 6-fold in iPSCs and showed no significant effect in HFFs (Fig. 4.2B). Thus the YTHDF2 3' UTR enhances translation in iPSCs but not in HFFs.

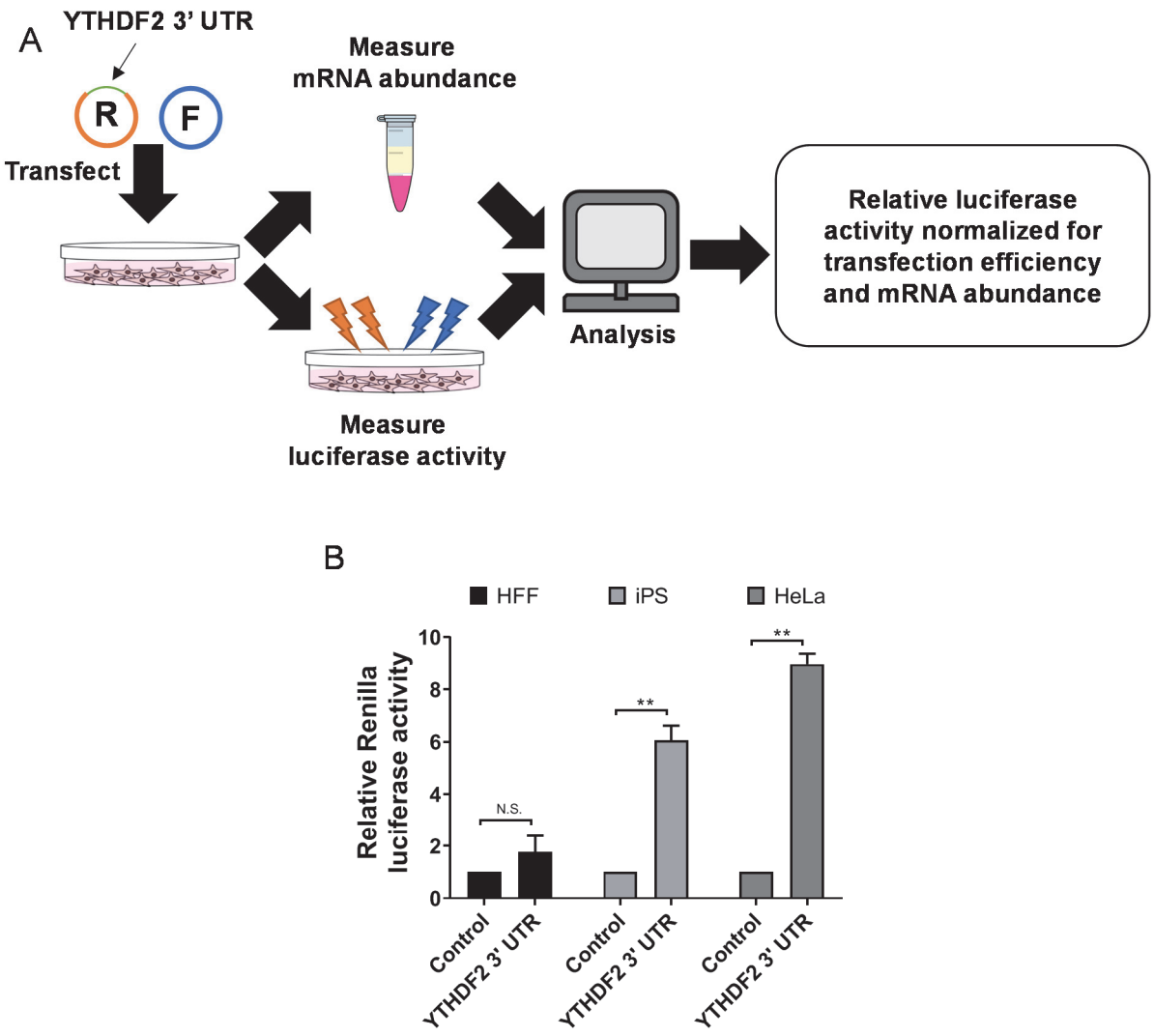

Figure 4.2: The YTHDF2 3' UTR enhances translation in iPSCs and HeLa cells. A: Diagram of the workflow for our luciferase assay. Samples were transfected with an experimental Renilla luciferase construct that contained different 3' UTRs and a Firefly luciferase construct to normalize for transfection efficiency. Approximately 24 hours after transfection, cells were assessed for luciferase activity or mRNA abundance. Renilla luciferase activity was normalized to transfection efficiency and mRNA abundance and reported as relative luciferase activity. B: Relative Renilla luciferase activity of HFF, iPSC or HeLa cells transfected with an empty vector control or full length YTHDF2 3' UTR construct. Asterisks indicate significant difference in the relative mean luciferase activity. (**p-value<0.005).

Interestingly, we also observed that the YTHDF2 3' UTR enhances translation in HeLa cells (Fig. 4.2B). Although they are not pluripotent, HeLa cells have some characteristics, like self-renewal, in common with iPSCs. More importantly, HeLa are much easier to work with in terms of cost, maintenance and transfection efficiency. Thus, we chose to utilize HeLa cells as a model system to explore how the 3' UTR of YTHDF2 promotes translation.

4.2.4 miR-145 is not a significant regulator of YTHDF2 translation in iPSCs or HeLa cells

During the course of this study, a regulatory role for miRNA-145-5p (miR-145) on YTHDF2 expression in human embryonic kidney 293 (HEK293) cells was reported (Yang et al. 2017). Two miR-145 binding sites are located in the 3' UTR of YTHDF2 (Fig. 4.3A). This caught our attention, as a previous study reported that miR-145 expression increases during differentiation of ESCs and miR-145 negatively regulates expression of the major pluripotency factors OCT4, SOX2 and KLF4 (Xu et al. 2009). Moreover, inhibition of miR-145 enhances iPSC reprogramming (Barta et al. 2016). Based on these observations, we hypothesized miR-145 negatively regulates YTHDF2 expression and the change in YTHDF2 protein levels between iPSCs and HFFs is due to increased abundance of miR-145 in HFFs. Indeed, preliminary data suggests miR-145 expression is significantly higher in HFFs compared to iPSCs (Appendix 1). If YTHDF2 were regulated by the same mechanism as some of the major pluripotency factors, it would be another piece of evidence that YTHDF2 plays a crucial role in stem cell maintenance. To address this, we evaluated the impact of miR145 on the YTHDF2 3'UTR reporter in HeLa cells. We predicted that transfection of a miR-145 mimic would abrogate the effects of the YTHDF2 3' UTR had on luciferase activity. miR-145 over-expression was verified via RT-dPCR (Fig. 4.3B). Additionally, we measured the mRNA abundance of three known targets of miR-145 (Huang et al. 2015a) in control and miR-145 over expression samples (Fig. 4.3C) and saw a decrease in all three targets, demonstrating the miR-145 mimic is active and effective.

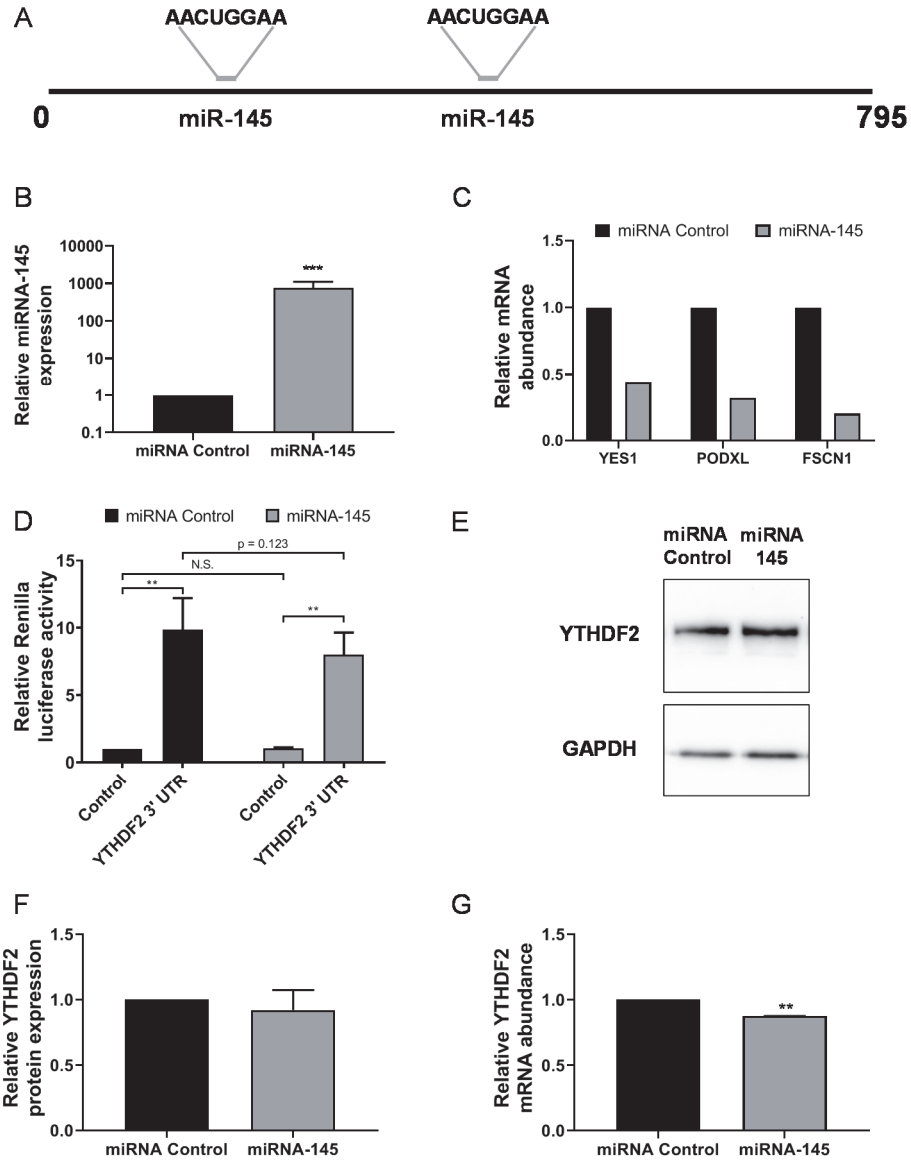

Figure 4.3: Over expression of miR-145 in HeLa or iPSCs does not significantly influence YTHDF2 expression. A: Diagram of the YTHDF2 3' UTR with the relative position and target sequence of the two miR-145 binding sites. B: RT-dPCR analysis of miR-145 abundance in iPSCs transfected with a miRNA control or miR-145 mimic normalized to 5S rRNA. Asterisks indicate significant difference in the relative mean abundance. (***p-value<0.0005). C: RT-dPCR analysis of three miR-145 targets in iPSCs transfected with a miRNA control or miR-145 mimic normalized to GAPDH. No statistical analysis was performed because this is preliminary data and n=1. D: Relative Renilla luciferase activity of HeLa cells transfected with different combinations of empty vector control or full length YTHDF2 3' UTR constructs and miRNA control or miR-145 mimic. Asterisks indicate significant difference in the relative mean luciferase activity. (**p-value<0.005). E: Representative image of western blots to detect YTHDF2 in miRNA control or miR-145 mimic transfected iPSC extracts. GAPDH was used as a loading control. F: Quantification of (E). No significant difference was observed in the relative mean protein expression between miRNA control and miR-145 mimic samples. G: RT-dPCR analysis of YTHDF2 mRNA abundance in miRNA control or miR-145 mimic transfected iPSC samples normalized to GAPDH mRNA. Asterisks indicate significant difference in the relative mean mRNA abundance between miRNA control or miR-145 mimic transfected samples (*p-value<0.005).

Surprisingly, the luciferase activity generated by the YTHDF2 3' UTR reporter was unaffected by transfection of miR-145 mimic (Fig. 4.3D). We also measured endogenous YTHDF2 protein expression and mRNA abundance in iPSCs following transfection of miR145 mimic or control miRNA. Over expression of miR-145 in iPSCs had no effect on YTHDF2 protein expression (Figures 4.3E,F) and induced only a slight (~10%) decrease in mRNA abundance (Fig. 4.3G). Thus, our results do not support the notion that miR-145 is a major player in regulation of YTHDF2 expression in iPSCs or HeLa cells.

Analysis of the YTHDF2 3' UTR sequence in TargetScan (Agarwal et al. 2015) revealed miR-145 is not the only miRNA capable of binding; other miRNAs including miR-19-3p, miR-130-3p, miR-141-3p and miR-181-5p also have potential binding sites within the YTHDF2 3' UTR. Although miRNAs are typically thought of as negative regulators of translation, as was observed in Yang et al., 2017, it is important to note there is evidence that miRNAs can promote translation as well (Vasudevan et al. 2007). Thus, YTHDF2 expression may be influenced, in either direction, by up-regulation of one or a combination of these miRNAs during differentiation. To determine if any miRNAs had a major influence on YTHDF2, we assessed YTHDF2 protein expression in control and DICER KD HeLa cell lines (Russo et al. 2018). DICER is required for miRNA maturation (Bernstein et al. 2001). We predicted a change in YTHDF2 protein expression following DICER KD would indicate at least one, if not more, miRNA(s) had a regulatory effect on YTHDF2 expression. As can be seen in Appendix 2, there was no significant difference in YTHDF2 protein expression between control and DICER KD samples.

In summary, miR-145 and/or other miRNAs may repress YTHDF2 translation in some cell types, including HEK293 (Yang et al. 2017) and perhaps HFFs. However, based on the observation that excess miR-145 does not down-regulate YTHDF2 in Hela or iPSCs, differential abundance of miR-145 is unlikely to explain the elevated translation of the reporter in these cell lines.

4.2.5 The first 300 nucleotides of the YTHDF2 3' UTR enhances translation in HeLa cells

We took a systematic approach to narrow down the region of the YTHDF2 3'UTR responsible for enhancing translation. We created Renilla luciferase constructs with overlapping 200 nucleotide segments that spanned the YTHDF2 3' UTR (Fig. 4.4A). As can be seen in Figure 4.4A, the first two segments, 0-200 and 100-300, significantly enhanced luciferase activity, albeit, not to the same extent as the full length 3' UTR. Interestingly, the 200-400 and 400-600 segments somewhat repressed luciferase activity.

The results from our initial assays showed the 0-200 and 100-300 segments of the YTHDF2 3' UTR increased luciferase activity, but not to the same extent as the full length 3' UTR (Fig. 4.4A). This suggested there may be multiple elements interspersed throughout the first 300 nucleotides that enhance translation in an additive manner. To further explore this, we created two additional luciferase constructs containing the 100-200 and 0-300 nucleotide regions. We hypothesized that if there were multiple elements enhancing luciferase activity in first 300 nucleotides, then the 0-300 region would fully recapitulate the activity of the full length 3' UTR. As predicted, the insertion of the 0-300 region of the YTHDF2 3' UTR enhanced luciferase activity to the same degree as the full length 3' UTR (Fig. 4.4B). Moreover, each smaller fragment (0-200, 100-200 and 100-300) exhibited partial increase in luciferase activity. Taken together, these results indicated there are likely multiple elements in the first 300 nucleotides of the YTDHF2 3' UTR that facilitate translation.

In an attempt to identify promising candidates that might enhance translation of YTHDF2, we performed a motif analysis of the 0-300 region using the online platforms RBPDB (Cook et al. 2011) and ATtRACT (Giudice et al. 2016). This analysis yielded a plethora of RBPs that had validated or predicted binding sites within the region. Moreover, there were also two m^6A sites according to the m6AVar database (Zheng et al. 2018), which can be bound by all three YTHDF readers (Wang et al. 2015b, 2014b; Shi et al. 2017).

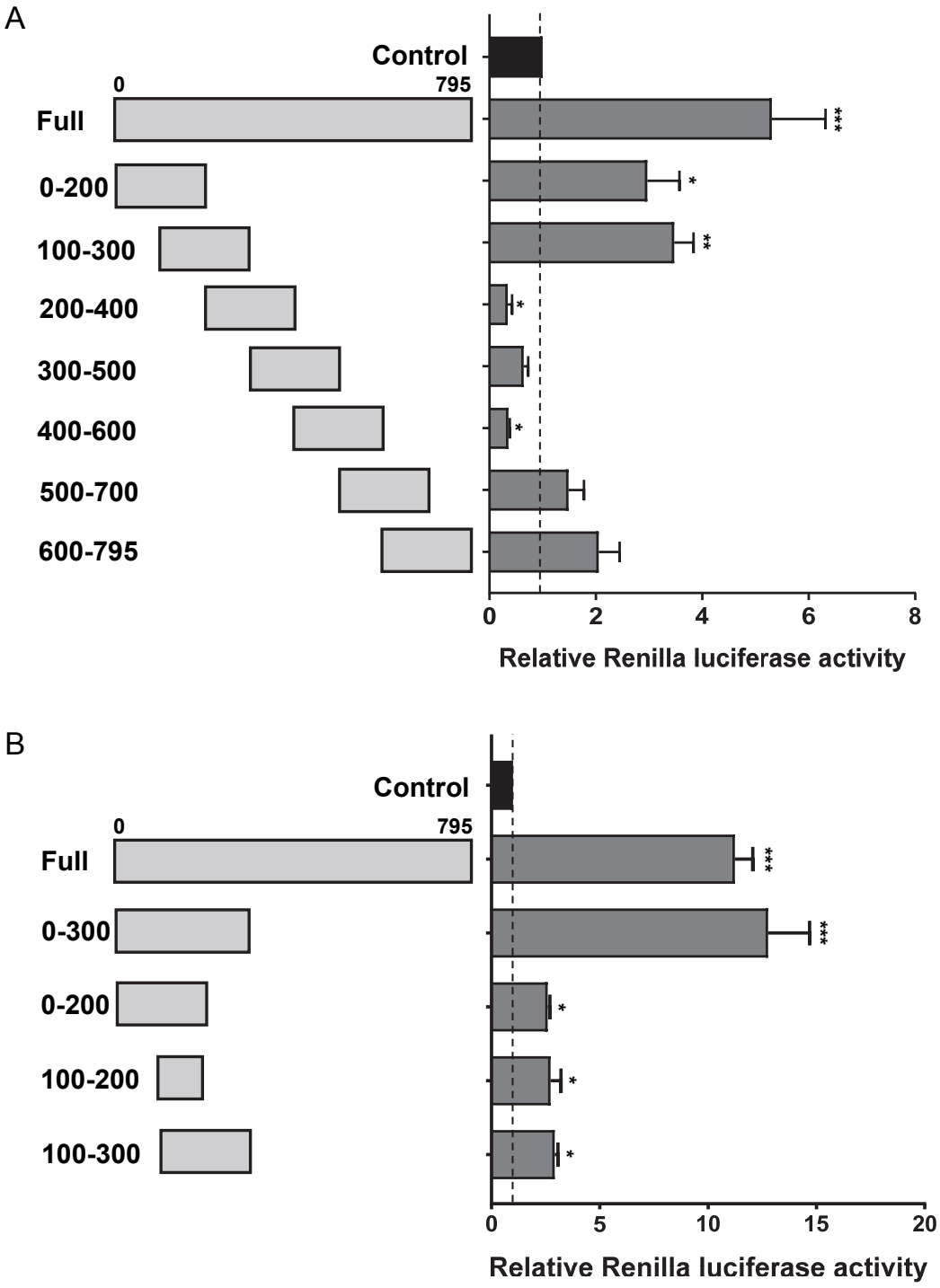

Figure 4.4: The first 300 nucleotides of the YTHDF2 3' UTR enhance Renilla luciferase activity. A-B: Relative Renilla luciferase activity of HeLa cells transfected with an empty vector control or various regions of the YTHDF2 3' UTR. Asterisks indicate significant difference in the relative mean luciferase activity between the specified construct and the empty vector control. (*p-value<0.05, **p-value<0.005, ***p-value<0.0005). Black dotted line represents a relative Renilla luciferase activity of 1.

Due to the large number of candidates these analyses produced, we opted for an experimental approach in an effort to narrow down the list of candidates.

4.2.6 Several RBPs specifically interact with the first 300 nucleotides of the YTHDF2 3' UTR

To explore what RBPs were specifically interacting with the first 300 nucleotides of the YTHDF2 3' UTR, we performed biotinylated RNA pulldowns coupled with mass spectrometry (MS). Briefly, an RNA consisting of the 0-300 nucleotide region and a size matched control derived from plasmid sequences were synthesized via *in vitro* transcription with biotin-CTP. The biotinylated RNAs were incubated with HeLa cytoplasmic cell extracts and protein-RNA complexes were isolated using magnetic streptavidin beads. After washing at increasing KCl concentrations RNPs were retrieved by a final wash with 1M NaCl, separated by SDS-PAGE and visualized through silver staining (Fig 4.5A). Ultimately, a 250 mM KCl wash buffer concentration was selected because it was stringent enough to remove a majority of the background bands seen in the control lane, yet had little impact on the specific interactions seen only in the YTHDF2 3' UTR lane. When comparing the 250 mM KCl samples prior to submission for MS, we noted the YTHDF2 3' UTR RNA had a strong interaction with a protein(s) migrating at approximately 70 kDa (Fig. 4.5B). Analysis of the MS data revealed ~40 RNA-protein interactions for 0-300 region of the YTHDF2 3' UTR, 30 of which were unique to the YTHDF2 3' UTR RNA and not seen in the control (Fig. 4.5C). The 30 proteins that uniquely bound to the YTHDF2 3' UTR were filtered to remove keratin contaminants, and were compared to the Crapome database of common MS contaminants (Mellacheruvu et al. 2013). Detailed information about the proteins identified including size, Crapome results and spectral counts can be found in Table 4.1. We evaluated the identified proteins based on a set of criteria that took into account Crapome results (present in <50% of database experiments), known functions connected to translation, protein size (preference was given to those ~70 kDa based on Fig. 4.5B) and evidence for binding sites within the 300 nucleotide region of interest based on our

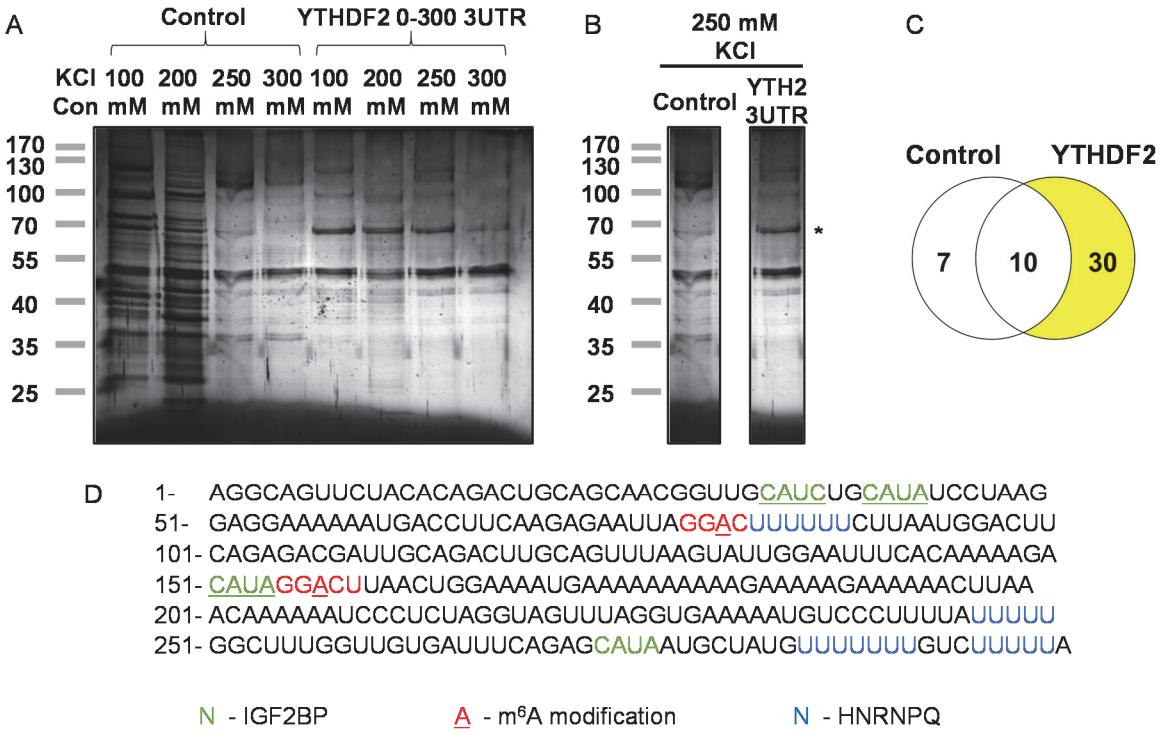

Figure 4.5: RNA pulldown coupled with mass spectrometry reveals 30 RBPs specifically interact with the YTHDF2 3' UTR. A: Silver-stained SDS PAGE gel of RNA pulldown experiments using either a size-matched control or 0-300 nucleotide region of the YTHDF2 3' UTR performed with varying concentrations (100-300 mM) of KCl wash buffer. B: Detailed view of the 250 mM KCl wash buffer lanes. Asterisk indicates an RBP interaction around 70 kDa that is specific to the YTHDF2 3' UTR RNA. D: Sequence of the first 300 nucleotides of the YTHDF2 3' UTR. IGF2BP binding sites are highlighted in green, underlined sites indicate CLIP-seq validation, m^{6}A sites are highlighted in red, predicted HNRNPQ binding sites are highlighted in blue.

Table 4.1: Proteins that specifically interacted with the first 300 nucleotides of the YTHDF2 3' UTR. Detailed information including gene symbol, accession number, protein size (in kDa), number of times protein was found in Crapome database experiments and number of spectral counts in YTHDF2 3' UTR sample.

Gene Symbol	Accession Number	Protein Size (kDa)	Crapome Results	Spectral Counts (YTH2 3' UTR)
ACTB	ACTB_HUMAN	41.7	363/411	164
NHP2	D6RC52_HUMAN	17.2	29/411	6
HSPA8	sp|P11142|HSP7C_HUMAN	70.8	396/411	13
HNRNPAB	D6R9P3_HUMAN	36.2	206/411	14
HNRNPA1	F8W6I7_HUMAN	38.7	268/411	22
HNRNPD	D6RAF8_HUMAN	38.4	216/411	27
HNRNPM	A0A087X0X3_HUMAN	77.5	220/411	49
HNRNPU	A0A1W2PP35_HUMAN	90.5	280/411	7
IGF2BP1	sp|Q9NZI8|IF2B1_HUMAN	63.4	114/411	31
IGF2BP3	sp|O00425|IF2B3_HUMAN	63.7	87/411	38
ILF2	B4DY09_HUMAN	43	152/411	31
HNRNPR	sp|O43390-2|HNRPR_HUMAN	70.9	188/411	193
EIF2AK2	sp|P19525-2|E2AK2_HUMAN	62	14/411	9
ILF3	sp|Q12906-2|ILF3_HUMAN	95.3	158/411	80
DDX21	sp|Q9NR30-2|DDX21_HUMAN	87.3	179/411	20
TGF	sp|Q92734-2|TFG_HUMAN	55.9	44/411	23
YBX3	sp|P16989-2|YBOX3_HUMAN	40	179/411	51
SYNCRIP	sp|O60506-3|HNRPQ_HUMAN	69.6	197/411	617
SSB	LA_HUMAN	46.8	102/411	245
YBX1	YBOX1_HUMAN	35.9	233/411	66
NCL	NUCL_HUMAN	76.6	261/411	169
SEC13	A8MXL6_HUMAN	35.5	61/411	3
PURA	PURA_HUMAN	34.9	27/411	7
TPM2	sp|P07951|TPM2_HUMAN	32.8	113/411	4
TUBA1B	sp|P68363|TBA1B_HUMAN	50.1	389/411	39
TUBB	Q5JP53_HUMAN	49.5	382/411	37
TUBB4B	TBB4B_HUMAN	49.8	376/411	25

motif analysis (Fig. 4.5D). Based on these conditions, we identified IGF2BP1, IGF2BP3 and HNRNPQ as the most promising candidates.

4.2.7 IGF2BP1 and IGF2BP3 are expressed highly in iPSCs

We followed up on IGF2BP1 and IGF2BP3 (hereafter referred to as IGF2BP1/3) first due to their molecular weight (~63.4 and 63.7 kDa, respectively; Fig. 4.5B), as well as existing evidence that they may bind the YTHDF2 3' UTR (Cook et al. 2011) and are upregulated in hESCs (Conway et al. 2016). The IGF2BP family has also previously been implicated in stem cell maintenance (Degrauwe et al. 2016). Interestingly, the IGF2BP family of proteins binds m^6A methylated transcripts to promote mRNA stability and translation (Huang et al. 2018a).

Our RNA sequencing data from Chapter 3 showed that *IGF2BP1*/*3* mRNAs are in the top 15^{th} percentile of expression for all genes expressed in iPSCs (See GSE133898). Western blots show that both IGF2BP1/3 proteins are expressed in iPSCs and essentially undetectable in HFFs (Fig. 4.6A,B). These findings, coupled with our results, lead to the intriguing notion that YTHDF2, a protein which targets m^6A methylated transcripts for degradation, might itself be regulated by the same epigenetic modification. It is important to note there is a third member of the IGF2BP family, IGF2BP2. Initially we focused on IGF2BP1/3, as they were present in our MS data, and are expressed highly in hESCs compared to differentiated fibroblasts, whereas IGF2BP2 protein expression does not change (Conway et al. 2016).

4.2.8 Depletion of IGF2BP1/3 has a modest effect on YTHDF2 protein expression

Sequence analysis of the 0-300 region of the YTHDF2 3' UTR revealed there were six potential IGF2BP1/3 binding sites. Of these, previous PAR-CLIP and eCLIP sequencing experiments identified peaks at the two m^6A sites and the underlined consensus binding motifs (Fig. 4.5D) (Hafner et al. 2010; Huang et al. 2018a; Dunham et al. 2012). Intriguingly, one of these motifs was located directly adjacent to an m^6A site, suggesting IGF2BP1/3 may be able to

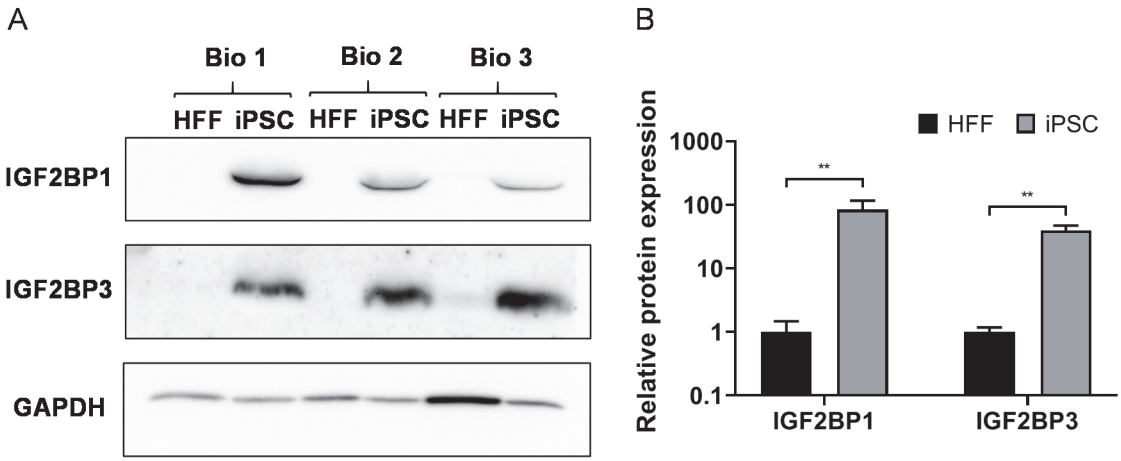

Figure 4.6: IGF2BP1/3 are highly expressed in iPSCs and feature multiple binding sites in the first 300 nucleotides of the YTHDF2 3' UTR. A: Western blot to detect IGF2BP1/3 in three independent iPSC and HFF extracts. GAPDH was used as a loading control. Asterisk represents non-specific band. B: Quantification of (A). Asterisks indicate significant difference in the relative mean protein expression between iPSC and HFF samples (**p-value<0.005).

bind to this section in the presence or absence of m^{6}A. To efficiently evaluate both IGF2BP1/3, we depleted their expression via siRNA-mediated knockdown in HeLa cells. We performed individual and combined depletions of IGF2BP1/3 because of the homology between them (73% amino acid sequence identity), which results in some redundant function (Bell et al. 2013). Knockdown efficiency of IGF2BP1/3 varied for each siRNA treatment compared to a negative siRNA control (Fig. 4.7A-D). However, the siRNA targeting IGF2BP3 elicited the highest knockdown efficiency of both IGF2BP1/3 at >80% and >60%, respectively. Thus, this was the treatment we were most interested in. If translation of *YTHDF2* mRNA in HeLa cells is enhanced by recruitment of one or both of IGF2BPs, then we would expect to see a decrease in YTHDF2 protein expression following knockdown. We observed a modest (~25-30%) but statistically significant decrease in YTHDF2 expression following treatment with the siRNA targeting IGF2BP3, but no statistically significance in samples treated with the siRNA targeting IGF2BP1 or the combined siRNAs (Fig. 4.8A,B). This was not unexpected, as the knockdown efficiency of both IGF2BP1/3 was most robust with IGF2BP3 siRNA. However, this is a small change compared to the difference in YTHDF2 expression between iPSCs and HFFs (Fig. 3.1). We also assessed the luciferase activity produced from our reporter containing the full length YTHDF2 3' UTR following IGF2BP KD and observed no significant changes in luciferase activity (Fig. 4.8C). Thus, these findings suggest that IGF2BP1/3 are not the primary factor(s) enhancing translation of YTHDF2.

4.2.9 Depletion of m^{6}A deposition also has a modest effect on YTHDF2 protein expression

Although the nominal reduction in YTHDF2 protein expression following IGF2BP1/3 depletion cannot explain the difference in YTHDF2 expression between iPSCs and HFFs (Fig. 3.1), m^{6}A might influence translation of *YTHDF2* mRNA through a different reader protein. To investigate this idea, we interfered with m^{6}A deposition in HeLa cells via siRNA-mediated knockdown of METTL3 and WTAP (Batista et al. 2014; Ping et al. 2014; Yoon et al. 2017).

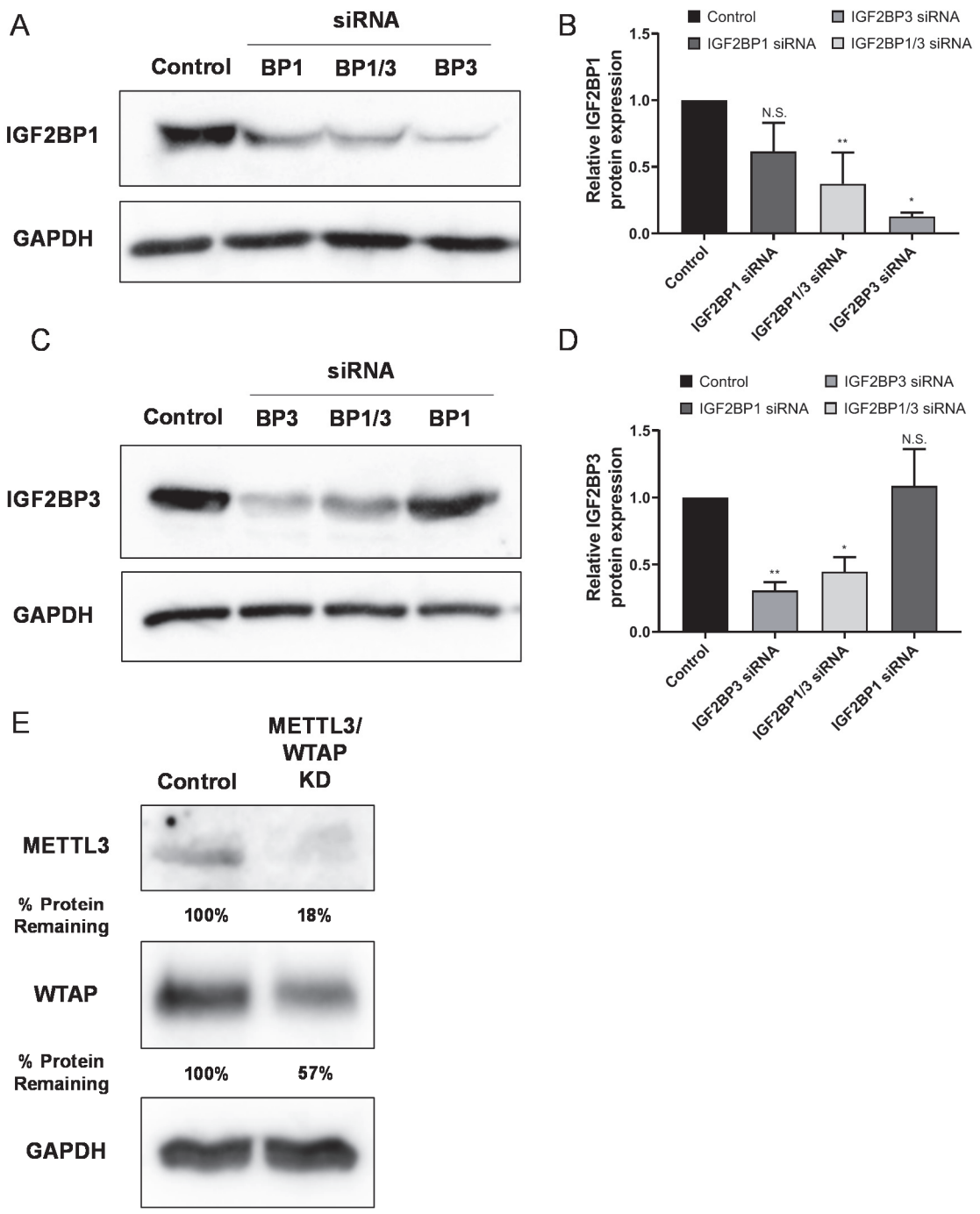

Figure 4.7: Depletion of IGF2BP1/3 or the methyltransferase components METTL3 and WTAP in iPSCs. A-D: A and C are representative image of western blots to detect IGF2BP1 and IGF2BP3, respectively, in iPSC extracts transfected with a negative control or IGF2BP1, IGF2BP3 or both siRNA(s). GAPDH was used as a loading control. B and D are quantification of (A) and (C), respectively. Asterisks indicate significant difference in the relative mean protein expression between negative control and target-specific samples (*p-value<0.05, **p-value<0.005). E: Western blots to detect METTL3 or WTAP in iPSC extracts transfected with a negative control or combination of METTL3 and WTAP siRNA(s). GAPDH was used as a loading control. Percent protein remaining is listed below each. No statistical analysis was performed because this is preliminary data and n=1.

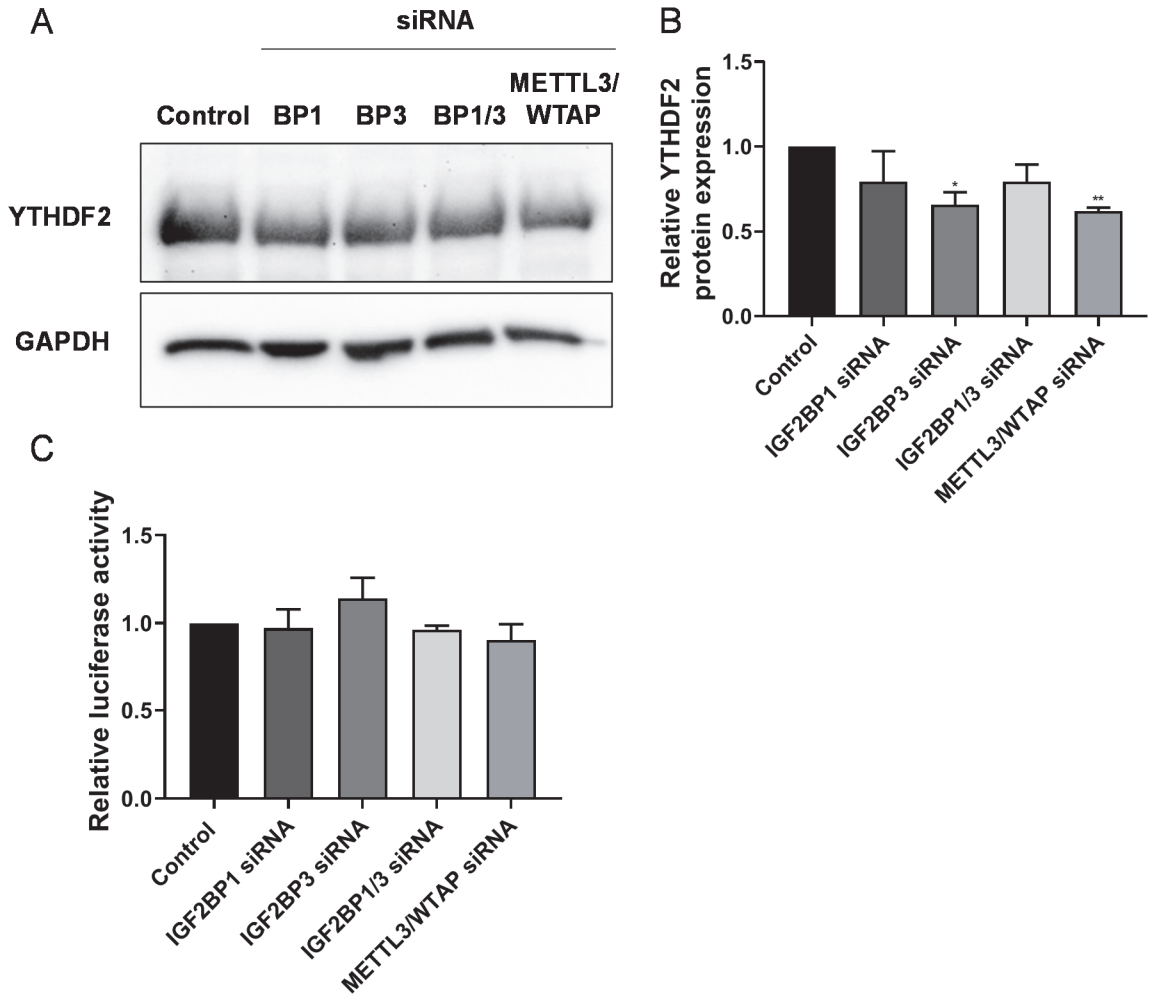

Figure 4.8: Depletion of IGF2BP1/3 or METTL3 and WTAP has a modest effect on YTHDF2 expression. A: Representative image of western blots to detect YTHDF2 in iPSC extracts transfected with a negative control or IGF2BP1, IGF2BP3, both or METTL3 and WTAP siRNA(s). GAPDH was used as a loading control. B: Quantification of (A). Asterisks indicate significant difference in the relative mean protein expression between negative control and target-specific samples (*p-value<0.05, **p-value<0.005). C: Relative Renilla luciferase activity of HeLa cells transfected with a construct containing the first 300 nucleotides of the YTHDF2 3' UTR and a negative control or IGF2BP1, IGF2BP3, both or METTL3 and WTAP siRNA(s). No significant difference was observed in the relative mean luciferase activity.

We validated the knockdown efficiency of concurrent METTL3 and WTAP siRNA treatment compared to a negative siRNA control via western blots (Fig. 4.7E). If enhanced translation of *YTHDF2* mRNA is m^{6}A-dependent, then we would predict inhibiting methylation via METTL3-WTAP knockdown would decrease YTHDF2 protein expression. Again, we observed a modest (~30%) but statistically significant decrease in YTHDF2 expression following siRNA treatment, similar to that of IGF2BP3 depletion (Fig. 4.8A,B). Moreover, we observed no significant change in the luciferase activity produced from our reporter containing the full length YTHDF2 3' UTR following METTL3-WTAP depletion (Fig. 4.8C). These findings, coupled with our results above (section 4.3.8), indicate that neither IGF2BP1/3 nor m^{6}A methylation are solely responsible for enhancing translation of YTHDF2.

4.2.9 YTHDF2 expression is not influenced by changes in HNRNPQ expression

Finally, we evaluated HNRNPQ as a potential regulator of YTHDF2 translation. Like IGF2BP1/3, HNRNPQ is approximately 70 kDa in size and promotes translation (Svitkin et al. 2013). Moreover, HNRNPQ also has several predicted binding sites within the first 300 nucleotides of the YTHDF2 3' UTR (Fig. 4.5C). We knocked down HNRNPQ in HeLa cells and achieved a ~75% decrease in expression when compared to a negative control siRNA (Fig. 4.9A,B). Again, we predicted that if HNRNPQ enhanced the translation of *YTHDF2* mRNA we would expect to see a decrease in YTHDF2 expression following depletion of HNRNPQ. Regrettably, we observed no change in endogenous YTHDF2 expression following depletion of HNRNPQ when compared control samples (Fig. 4.9C,D). Moreover, there was no change in luciferase activity of the full length YTHDF2 3' UTR construct (Fig. 4.9E). In sum, HNRNPQ does not appear to regulate the translation of YTHDF2.

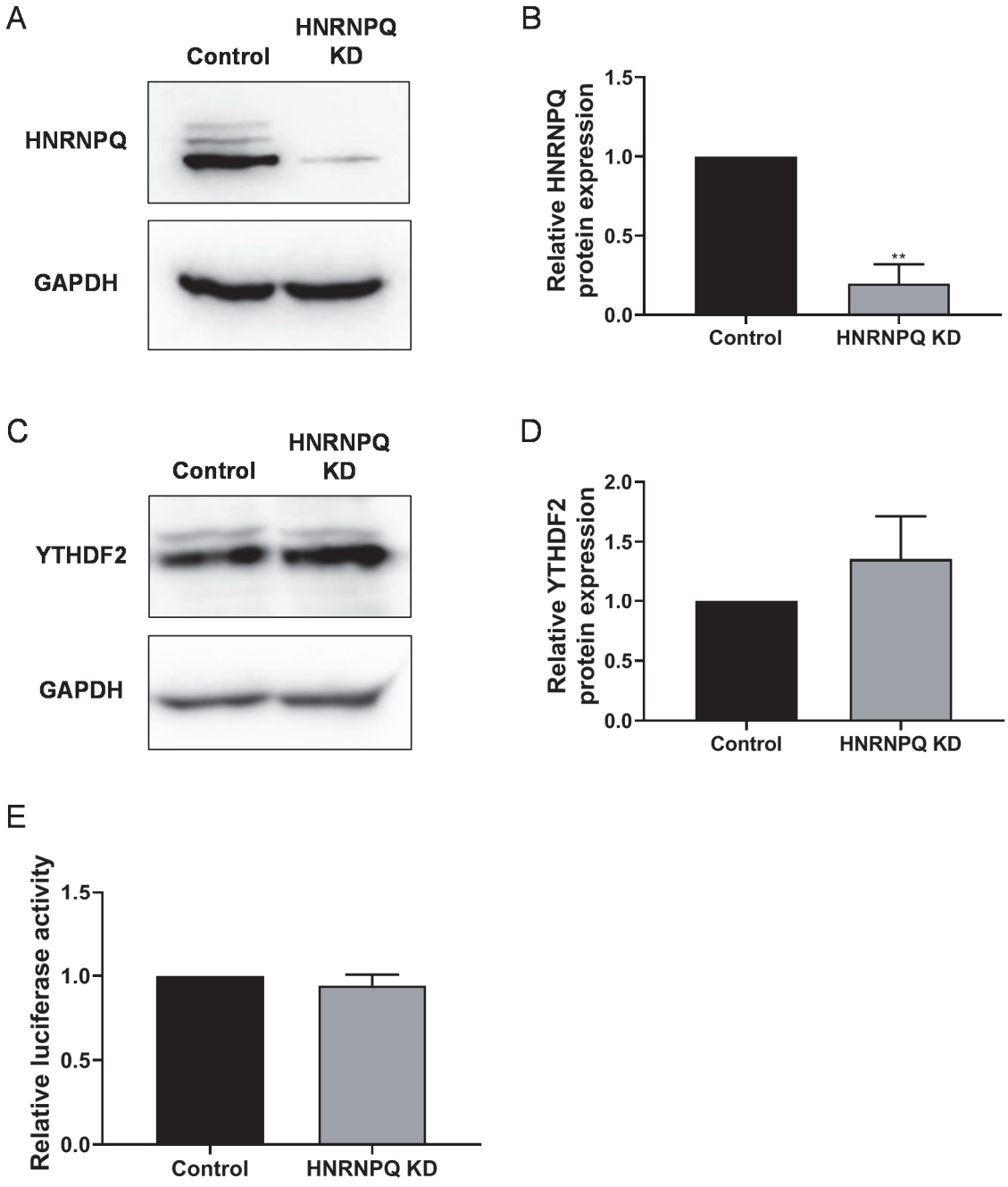

Figure 4.9: Depletion of HNRNPQ has no effect on YTHDF2 expression. A-D: A and C are representative image of western blots to detect HNRNPQ and YTHDF2, respectively, in iPSC extracts transfected with a negative control or HNRNPQ siRNA. GAPDH was used as a loading control. B and D are quantification of (A) and (C), respectively. Asterisks indicate significant difference in the relative mean protein expression between siRNA negative control or HNRNPQ depleted samples (**p-value<0.005). No significant decrease was observed in D. E: Relative Renilla luciferase activity of HeLa cells transfected with a construct containing the first 300 nucleotides of the YTHDF2 3' UTR and a negative control or HNRNPQ-targeting siRNAs. No significant difference was observed in the relative mean luciferase activity.

4.3 Discussion

In the experiments described above, we identified a 300 nt region of the YTHDF2 3' UTR which enhances translation and presumably is responsible for increased expression of YTHDF2 in iPSCs. We showed that YTHDF3, which can also facilitate degradation of m^6A-modified transcripts (Shi et al. 2017), has relatively constant protein abundance throughout differentiation. Moreover, the transition out of a pluripotent state down either the neural or mesoderm lineage reduces YTHDF2 protein expression. YTHDF2 protein expression (Fig. 3.1), but not mRNA abundance, is dramatically higher in iPSCs compared to HFFs. This suggests YTHDF2 is being regulated at the level of translation or protein stability. To this end, we discovered that the 0-300 nucleotide region of the YTHDF2 3' UTR contains elements which enhance the translation of a luciferase reporter RNA. Through MS, we identified 30 RBPs that uniquely associate with this region of the YTDHF2 3' UTR. Based on our MS data and previous reports in the literature (Yang et al. 2017; Huang et al. 2018a), we screened several potential candidates as regulators of YTHDF2 expression including miR-145, m^6A methylation, IGF2BP1/3 and HNRNPQ. Some of these factors had a modest effect on YTHDF2 expression, however, none were potent enough to be considered the primary mechanism of mediating translation of YTHDF2. Overall, our data support the idea that YTHDF2 is a key m^6A reader that is up-regulated in pluripotent stem cells via translational mechanisms to help iPSCs maintain a pluripotent state until a differentiation signal is received.

Although the candidates we have screened so far as regulators of YTHDF2 translation have exhibited a modest effect at best, we do need to address some caveats in the experiments which do not allow us to rule them out completely. The previous study which characterized miR-145 as a regulatory of YTHDF2 found that both mRNA and protein expression were affected by miR-145 expression (Yang et al. 2017). This finding is contrary to our observations that YTHDF2 protein expression fluctuates but mRNA abundance remains unchanged between iPSCs and differentiated cell types. Moreover, the experiments Yang et al., 2017 were

performed exclusively in cancer cell lines, whereas our experiments were done in a combination of stem cell and cancer cell lines. Indeed, there are differences in gene expression between the two cell types (Cantz et al. 2008; Sánchez et al. 2016; Ye et al. 2015), which can influence regulatory mechanisms. Thus, the lack of a decrease in *YTHDF2* mRNA abundance following overexpression of miR-145 in iPSCs we observed may be due to factor(s) that regulate YTHDF2 in addition to miR-145. Moreover, these factor(s), presumably enhancing YTHDF2 translation in iPSCs, may be highly abundant and/or able to outcompete miR-145, even upon over expression.

In regards to the follow up experiments on our MS data, the level of depletion we achieved for IGF2BP1/3, HNRNPQ and/or METTL3 and WTAP was perhaps not enough to elicit a biological effect. Indeed, our sequencing analysis and previous reports have suggested the IGF2BP family are highly expressed in stem cells. Thus, even though we achieved ~70% knockdown of both proteins (Fig. 4.7), there may be enough protein still remaining to regulate YTHDF2. Future experiments using knockout cell lines generated via CRISPR/Cas9 would likely provide better insight into this matter. Additionally, IGF2BP2 may also influence YTHDF2 expression. Although our MS results indicated only IGF2BP1/3 uniquely interacted with the YTHDF2 3' UTR, there is almost 60% amino acid sequence identity between the three proteins (Bell et al. 2013), which results in a fair amount of target overlap according to previous CLIP-seq experiments (Huang et al. 2018a; Conway et al. 2016). Moreover, the IGF2BP proteins are able to heterodimerize with each other (Nielsen et al. 2004), suggesting that even if IGF2BP2 does not directly bind to *YTHDF2* mRNA, it may still have an effect on its regulation. Based on this information, future experiments should take into account all the IGF2BP proteins when assessing the potential to regulate YTHDF2.

Similar to the IGF2BPs, the ~75% knockdown efficiency of HNRNPQ we achieved may not be enough to impact translation of YTHDF2. We did observe in preliminary data that the mRNA abundance of two known targets of HNRNPQ, GAP43 and SYT1, was down- and up-regulated,

respectively, as expected based on previous reports (Williams et al. 2016; Mizutani et al. 2000) (Appendix 3). This suggests there was some biological effect from the knockdown. However, evaluation of YTHDF2 expression in a knockout cell line is necessary to fully eliminate HNRNPQ as a potential regulator of YTHDF2 expression. In addition, RIPs can be utilized to validate the RNA-protein interaction reported in our MS data.

Finally, the knockdown efficiency of WTAP and METTL3 in HeLa cells appears to be on par with that of what we achieved in iPSCs in Chapter 3 (Fig. 3.9). Thus, we would predict a similar effect on m^6A deposition. However, the experiments were performed in two different cell types, thus the impact on global m^6A levels may differ. Assessment of global m^6A levels via dot blot in control and siRNA-treated cells would be necessary to ensure that sufficient depletion was achieved. As mentioned above, there are differences in gene expression and regulatory mechanisms between cancer cell lines, like HeLa cells, and endogenous stem cells that also need to be taken into account when investigating factors that may enhance YTHDF2 translation (Cantz et al. 2008; Sánchez et al. 2016; Ye et al. 2015). Thus, the results of any future experiments performed in HeLa cells, positive or negative, need to be validated at some level in iPSCs. In sum, the results from our experiments indicate the IGF2BPs, HNRNPQ and m^6A methylation are not high priority candidates as regulators of translation of YTHDF2. However, until the points above are addressed, we cannot rule these factors out completely.

There are still other promising candidates from our list we have yet to follow up on including YXB1 (aka YB-1 or p50) and La (aka SSB). Both of these proteins have previously been implicated as regulators of mRNA translation (Evdokimova et al. 2009, 2006; Kim 2001; Brenet et al. 2009). Phosphorylation of YXB1 via AKT1 inhibits association of YXB1 with the 5’ cap, which represses translation (Nekrasov et al. 2003), and promotes interactions with mRNA UTRs where YXB1 promotes translation (Evdokimova et al. 2006, 2009). Intriguingly, YBX1 interacts with the major pluripotency factor *NANOG* mRNA to up-regulate mRNA and protein expression in mESCs (Guo et al. 2016). Moreover, YBX1 is highly expressed in certain areas of mouse

fetal brain tissue and is important for neural tube closure during the early stages of embryonic development (Fotovati et al. 2011; Uchiumi et al. 2006). Both of these observations are in line with the activity we predict a regulator of YTHDF2 might exhibit. Alternatively, La was initially found to regulate translation of viral RNAs (Svitkin et al. 1994). However, several studies have since described its impact on endogenous mRNA translation (Kim 2001; Trotta et al. 2003). Like YBX1, La-mediated translational regulation can be influenced by phosphorylation via AKT1 (Brenet et al. 2009). Moreover, La is important for the establishment and maintenance of mESCs during early development (Park et al. 2006). Based on the evidence outlined above, both YBX1 and La appear to be promising candidates and future experiments may implicate one of these two proteins as the primary regulator of YTHDF2 translation in iPSCs. However, it will be important to take into account PTMs during these future experiments, as the regulatory activity of both proteins can be influenced by phosphorylation (Evdokimova et al. 2006; Brenet et al. 2009).

It is also important to note that the regulation of YTHDF2 translation in iPSCs may be influenced by multiple factors. Indeed, two miRNAs have already been identified as regulators of YTHDF2 expression (Yang et al. 2017; Li et al. 2018a). Expression of miR-145, which regulates several of the major pluripotency factors, is increased upon stem cells exit from pluripotency (Xu et al. 2009) and its expression and regulatory activity continue to influence gene expression as NPC differentiate further down the neural lineage (Morgado et al. 2016). Perhaps then, an unidentified factor enhances the translation of *YTHDF2* mRNA in a pluripotent state and, upon exiting pluripotency, miR-145 takes over as a repressor of translation. Alternatively, two or more RBPs may concomitantly regulate YTHDF2 translation. This is not an uncommon occurrence, both the IGF2BPs as well as YTHDF1 and YTHDF3 have redundant functions and targets (Bell et al. 2013; Li et al. 2017; Shi et al. 2017). However, the ability to tease this out in regards to regulation of YTHDF2 would require more rigorous experiments.

In conclusion, YTHDF2 protein expression decreases as pluripotent stem cells differentiate into other cell types. We believe elements in the 3' UTR of *YTHDF2* mRNA facilitate these changes in expression through recruitment of trans-acting factors that remain to be identified.

Chapter 5: Mutual repression of the RNA-binding protein PCBP2 and long non-coding RNAs in induced pluripotent stem cells

5.1 Introduction

Since reprogramming of human somatic cells to create iPSCs was first achieved in 2007 (Takahashi et al. 2007), our understanding of how gene expression is regulated to maintain pluripotency and facilitate controlled differentiation has increased exponentially (Takahashi and Yamanaka 2016). It is clear that both transcriptional, and post-transcriptional events play vital roles and must be tightly coordinated. Nevertheless, the contributions of many, if not most, RBPs and lncRNAs to the establishment and maintenance of pluripotency remains largely uncharacterized.

Tight control of mRNA abundance and processing is central to achieving cell-state transitions. Changes in alternative splicing (Fiszbein and Kornblihtt 2017) and polyadenylation (Mueller et al. 2013; Ji and Tian 2009) are clearly connected with pluripotency and differentiation, and in some cases the RBPs responsible have been identified. For example, MBNL proteins are repressed in stem cells and up-regulated during differentiation to block stem cell-specific splicing events, including a switch in splicing of the FOXP1 transcription factor which in turn regulates a number of pluripotency factors (Venables et al. 2013; Cieply et al. 2016; Han et al. 2013a). Beyond mRNA processing, export (Ratnadiwakara et al. 2018), translation (Sampath et al. 2008; Sugiyama et al. 2017) and mRNA stability (Lloret-Llinares et al. 2018; Kami et al. 2018) also contribute to the tight regulation of gene expression during cell-state transitions and each of these steps are regulated by RBPs.

Previously, we and others have noticed that mRNAs containing CREs are differentially regulated in stem cells (Huang et al. 2015b; Neff et al. 2012). Several RBPs recognize C-rich sequences including the PCBP family of KH domain proteins, hnRNP K and TIAR. Among

these, PCBP2 (also known as αCP2, and hnRNP E2) influences mRNA metabolism at multiple steps including splicing (Ji et al. 2018), polyadenylation (Ji et al. 2013), nuclear export (Xia et al. 2015; Yanatori et al. 2016), translation (Smirnova et al. 2019) and decay (Han et al. 2013b; Zhang et al. 2015a), as well as regulating miRNA processing and acting as an iron chaperone (Li et al. 2012; Yanatori et al. 2016).

Given the many shared properties of stem cells and cancer cells it is relevant that PCBP2 is aberrantly expressed in a variety of (Chang et al. 2007; Chen et al. 2018; Han et al. 2013b; Perron et al. 2018) Specifically, PCBP2 is up-regulated in gastric cancer and positively regulates translation of *CDK2* mRNA via binding to the 3' UTR (Chen et al. 2018). The increase in CDK2 expression enhances the viability of gastric cancer cells. Likewise, during progression of chronic myeloid leukemia (CML), PCBP2 is up-regulated and associates with the 5'UTR of C/EBPα mRNA where it represses translation (Chang et al. 2007), preventing myeloid differentiation and favoring a cancer stem cell phenotype. PCBP2 is also up-regulated in glioma where it binds to the 3' UTR of *FHL3* mRNA (Han et al. 2013b). However, rather than influencing translation, PCBP2 facilitates decay of *FHL3* mRNA, which subsequently promotes proliferation and represses apoptosis.

Strictly speaking from a developmental biology perspective, PCBP2 is essential during embryogenesis as PCBP2 knockout is lethal at day E13.5 (Ghanem et al. 2015). Finally, PCBP2 regulates hematopoietic stem cells differentiation by modulating splicing of the master regulator RUNX1 (Ghanem et al. 2018). Based on the evidence outlined above, we hypothesized that pluripotent stem cells utilize PCBP2 to modulate differentiation and self-renewal.

Here, we report that extended depletion of PCBP2 in self-renewing iPSCs disrupts the expression of multiple pluripotency markers and leads to precocious differentiation. At the level of the transcriptome, PCBP2 depletion results in down-regulation of several transcripts associated with pluripotency and development, including LIN28B, and the up-regulation of a class of lncRNAs that contain human endogenous retrovirus subfamily H (HERV-H) elements.

Intriguingly, HERV-H lncRNA abundance also influences PCBP2 protein expression, thus regulation is reciprocal. Moreover, differentiation of iPSCs into any of the three germ layers, which dramatically reduces HERV-H lncRNAs expression, leads to increased expression of PCBP2. Taken together, our findings reveal stem cells rely on PCBP2 to exert tight control of gene expression in a pluripotent state and during differentiation, and this regulation may be achieved in part through interactions between PCBP2 protein and HERV-H lncRNAs.

5.2 Results

5.2.1 PCBP2 plays a role in modulating pluripotency in human iPSCs

To determine whether PCBP2 plays in modulating pluripotency and/or driving differentiation, we evaluated the impact of PCBP2 depletion in iPSCs. iPSCs were transfected daily for up to 6 days with either a global negative control or PCBP2-targeting siRNA. Efficient knockdown was verified at the protein (Fig. 5.1A-C) and mRNA (Fig. 5.1D) levels. Over the course of siRNA treatment, we observed interesting changes in cell and colony morphology between control and PCBP2 depleted cells. As seen in Figure 5.1E, after four and, most notably, six days we observed a loss in the structural integrity of the colonies. Specifically, cells were no longer as tightly packed together, and individual cells and cell borders could be discerned. These characteristics are indicative of differentiation (Nagasaka et al. 2017; Wakao et al. 2012). Another characteristic of stem cell differentiation is enlargement of the nucleus (Rozwadowska et al. 2013; Khatau et al. 2012). We quantified the area of nuclei from control and PCBP2 KD cells via ImageJ, and observed a significant increase, >2-fold, upon PCBP2 depletion (Fig. 5.2A and B). Together, these morphological changes suggest depletion of PCBP2 pushes stem cells to differentiate.

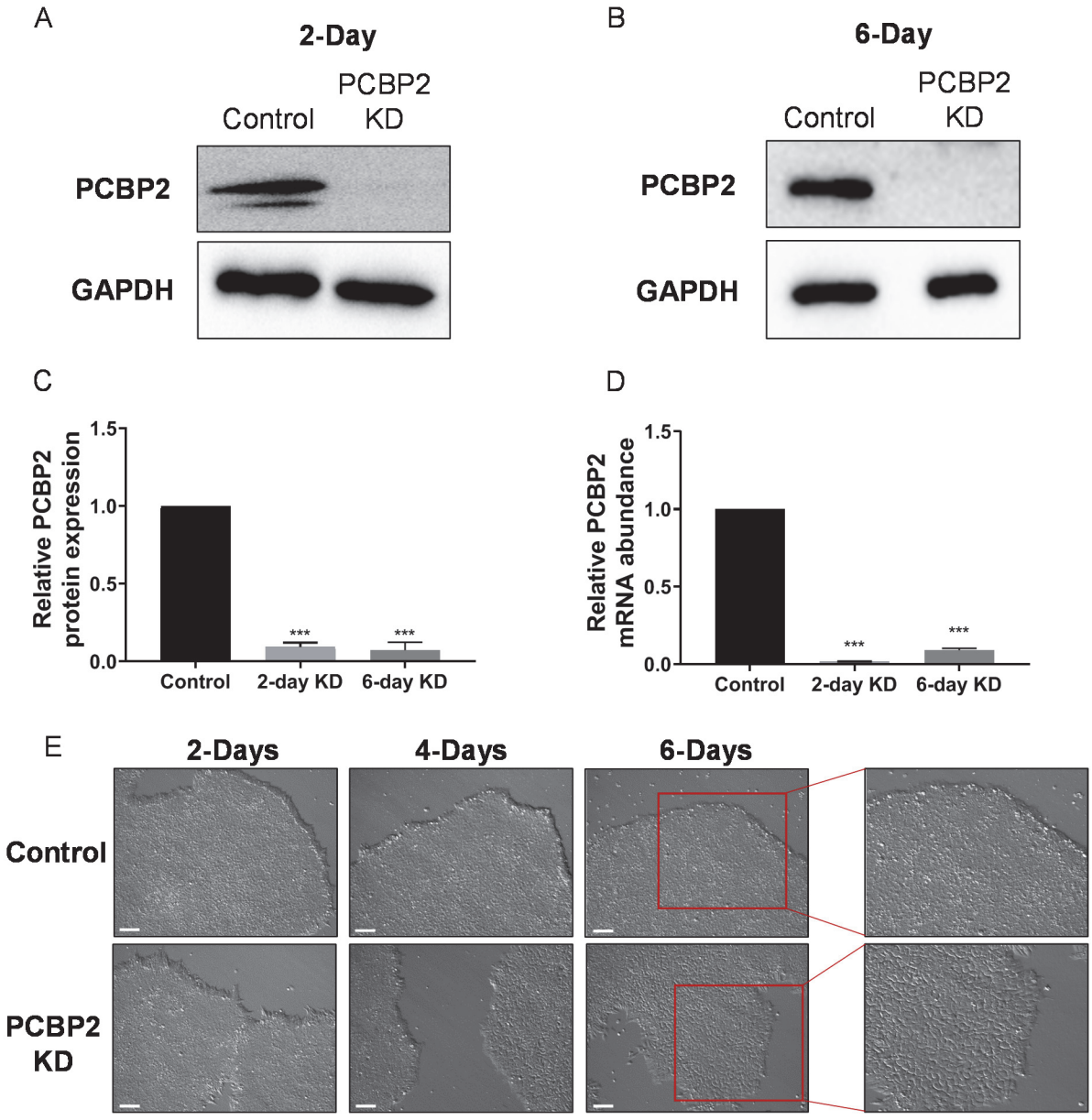

Figure 5.1: Depletion of PCBP2 effects the cell and colony morphology of iPSCs. A-B: Representative western blots using iPSC extracts to demonstrate effective depletion of PCBP2 following two (A) and six (B) days of siRNA transfection. GAPDH was used as a loading control. C: Quantification of (A) and (B). Asterisks indicate significant difference in the relative mean protein expression between siRNA negative control and PCBP2 depleted samples (***p-value<0.0005). D: RT-dPCR analysis of PCBP2 mRNA abundance in siRNA negative control and PCBP2 depleted samples normalized to GAPDH mRNA. Asterisks indicate significant difference in mean abundance between control and PCBP2 KD samples (***p-value<0.0005). E: iPSCs were subjected to two, four and six days of treatment with control or PCBP2 siRNAs. Bright field images of siRNA negative control and PCBP2-depleted iPSC colonies were taken at each time point. Scale bars indicate 100 µm.

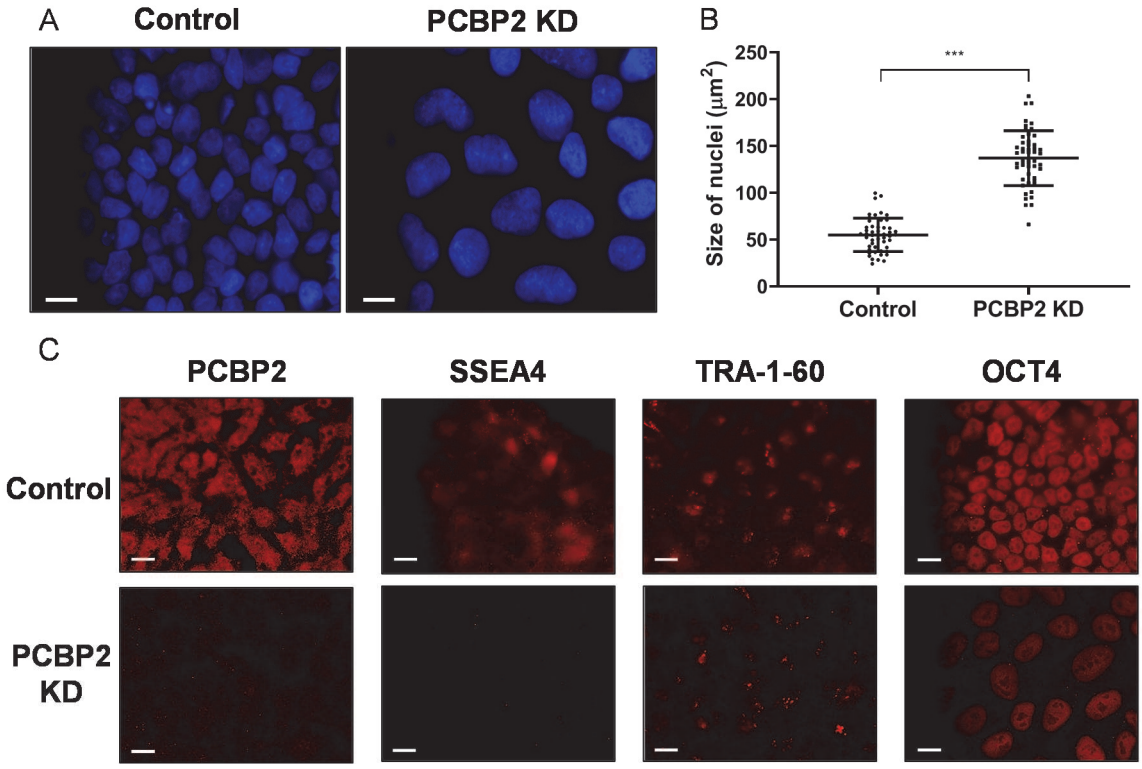

Figure 5.2: PCBP2 knockdown in iPSCs influences nucleus size and expression pluripotency markers. A-C: iPSCs were subjected to six days of treatment with negative control or PCBP2 siRNAs. The nucleus was stained with DAPI. (A) Representative image of nucleus size in control and PCBP2 depleted samples. (B) Nucleus size of siRNA negative control or PCBP2 depleted cells (n=50) was quantified via ImageJ. *p-value <0.05. (C) The indicated protein was detected by immunofluorescence (IF) staining. Scale bars indicate 10 μm.

Consistent with this, we also saw reduced expression of pluripotency factors/markers, OCT4, TRA1-60 (Grigor'eva et al. 2019; Vilà-González et al. 2019) and SSEA4 (Zhang et al. 2018b) as assessed by IF staining (Fig. 5.2C). In sum, depletion of PCBP2 in iPSCs leads to loss of pluripotency and precocious differentiation.

5.2.2 RNA-seq reveals that depletion of PCBP2 influences expression of many genes

In order to gain insight into the changes in gene expression that occur following PCBP2 depletion, we performed RNA-sequencing on control and PCBP2-depleted cells following two and six days of siRNA treatment. Filtered reads were aligned to the hg19 genome and differential expression was determined via DESeq2 (Love et al. 2014). To assess the overall structure of the RNA-seq data, samples were analyzed using a distance matrix approach and PCA (Fig. 5.3A,B and Appendix 4). As expected, both analyses grouped control and knockdown replicates together, indicating treatment was the primary differentiating factor. Moreover, PCBP2 exhibited one of the most dramatic decreases in expression. All of these observations gave us confidence in the quality of our data.

Differential expression analysis revealed depletion of PCBP2 for six days (Fig. 5.3C; 1,509 DE transcripts) resulted in over three times more differentially expressed transcripts than seen after two days (Appendix 4; 414 DE transcripts). For this reason, and because no visible phenotype was observed after two days, we focus here on the results from six day depleted samples in our follow up. For more detailed information about the two day results and analysis see Appendices 4 and 5.

5.2.3 Down-regulated mRNAs with functions connected to development are associated with PCBP2

We performed a GO-term analysis on the 853 and 656 genes that were up- and down-regulated, respectively (Fig. 5.3C), via DAVID v6.8 (Huang et al. 2009a, 2009b).

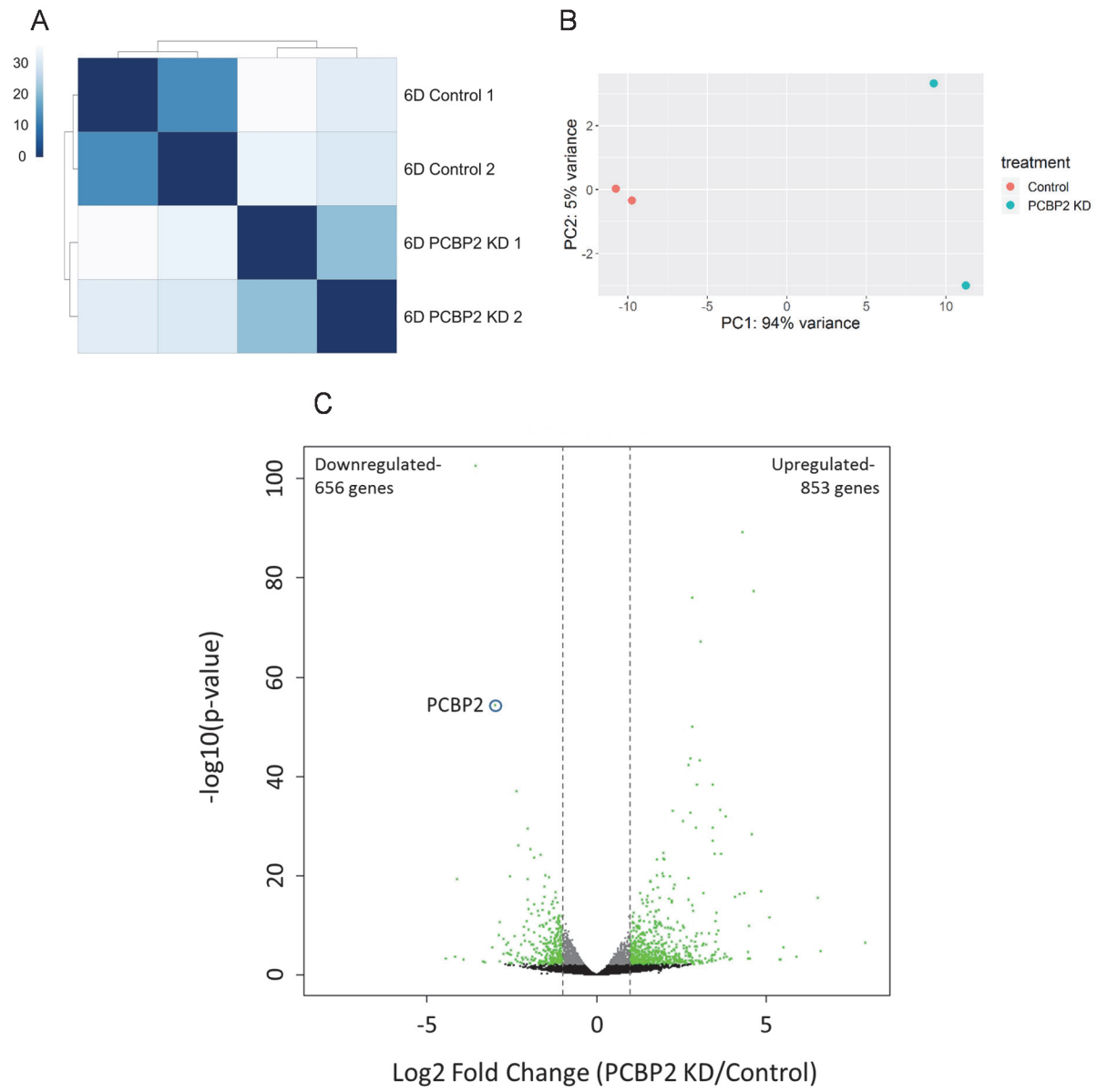

Figure 5.3: 1,509 transcripts were differentially expressed following six days of PCBP2 depletion in iPSCs. A: Distance matrix showing the Euclidean distances between RNA-seq replicates. Replicates with a lower distance (darker blue) are more closely correlated in terms of gene expression. Distances were calculated from log-stabilized normalized read counts of all detected transcripts (>5 read counts per replicate). B: PCA plot of RNA-seq replicates following DESeq2 analysis (Love et al., 2014). Control and PCBP2 depleted samples are labeled in red and blue, respectively. C: Volcano plot generated from sequencing data showing the adjusted p-value (y-axis) plotted against the fold change (x-axis) for individual genes. Differentially expressed genes are shown in green (differential expression: read counts>5, Benjamini-Hochberg adjusted p-value<0.05 and $\log_2$-fold change>1.0, represented by grey dotted lines).

GO-term analysis of the up-regulated set of transcripts revealed an enrichment of biological functions associated with the immune response (Fig. 5.4A). This is in agreement with reports that PCBP2 regulates the mitochondrial antiviral signaling protein (MAVS)-mediated signaling pathway (You et al. 2009; Xia et al. 2015; Qin et al. 2017) and interacts with viral RNAs (Hadian et al. 2009; Palusa et al. 2012; Bedard et al. 2004). However, we also noticed biological functions associated with development, indicated by red asterisk, were over-represented. Likewise, we made the same observation in regards to the down-regulated set of transcripts (Fig. 5.4B). We identified several genes that exhibited the highest levels of differential expression and were associated with GO terms connected to development and independently validated the changes in mRNA abundance following PCBP2 depletion via RT-dPCR (Fig. 5.4C,D).

Next, we performed RIPs in iPSCs to assess whether these developmental-associated transcripts directly interacted with PCBP2. Briefly, PCBP2-specific and IgG control antibodies were incubated in iPSC extracts and retrieved using protein G-conjugated magnetic beads. RNA was isolated from input, PCBP2 IP and IgG IP samples. RNA-protein interactions were evaluated by assessing fold enrichment over IgG for each mRNA via RT-dPCR. Previous reports have shown that PCBP2 protein binds its own mRNA (Ghanem et al. 2015), therefore *PCPB2* mRNA was used as a positive control. The efficiency of the RIP protocol was evaluated by measuring PCBP2 abundance in Input, PCBP2 IP and IgG IP samples via western blot (Fig. 5.5A). Intriguingly, transcripts down-regulated following PCBP2 depletion were significantly enriched in PCBP2 IPs compared to IgG (Fig. 5.5B), indicating an interaction with PCBP2 protein. However, preliminary data suggested none of the up-regulated transcripts are bound by PCBP2 (Appendix 6).

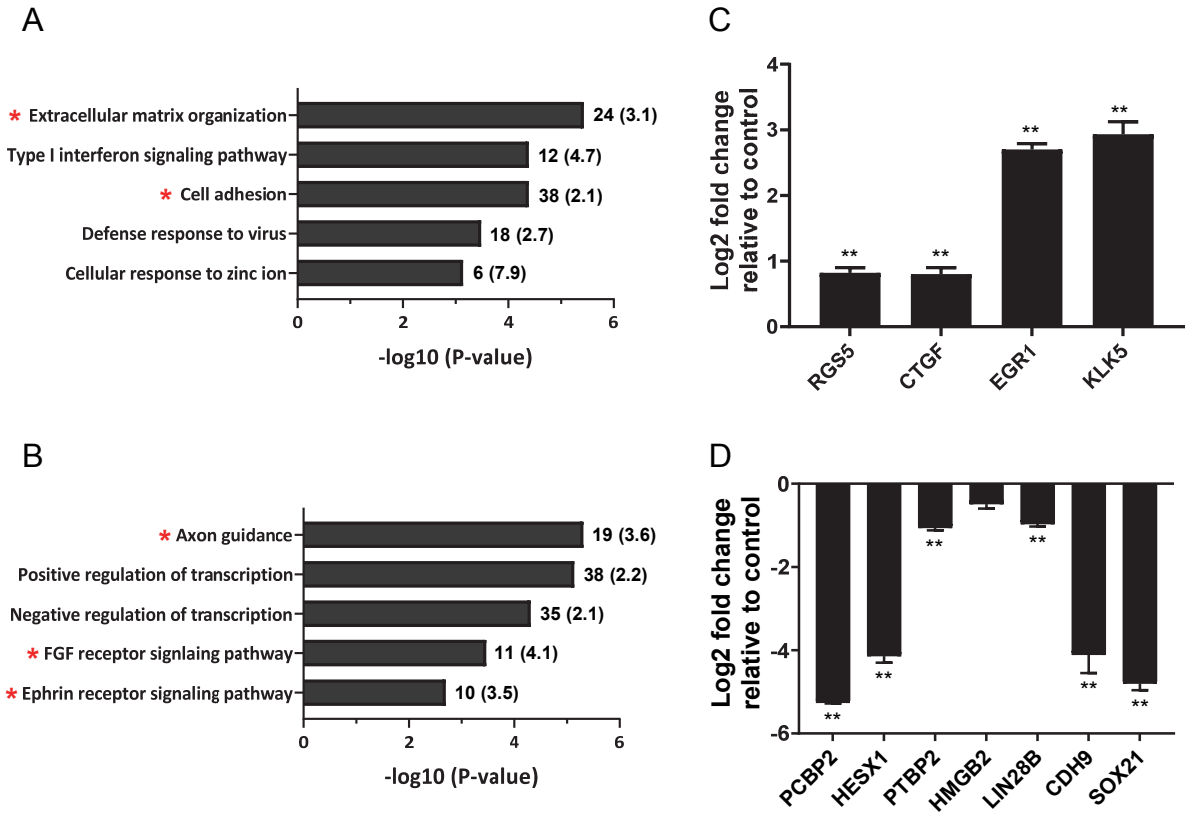

Figure 5.4: GO-term analysis reveals transcripts associated with immune response and development are up- and down-regulated, respectively, following depletion of PCBP2 in iPSCs. A and C: Functional annotation clustering of biological process performed by DAVID on genes up- (A) and down- (C) regulated following six days of PCBP2 depletion. Annotation clusters with the highest enrichment according to FDR p-value are listed. The number of genes in each cluster is shown next to the respective bar and fold enrichment over background is given in parenthesis. B and D: RT-dPCR analysis of mRNA abundances in control and PCBP2 depleted samples for transcripts identified as up- (B) and down- (D) regulated in the sequence dataset. mRNA abundance normalized to GAPDH for transcripts. Data is reported as $\log_2$ fold change (PCBP2 KD/Control). Asterisks indicate significant difference in mean abundance between control and PCBP2 KD samples (*p-value<0.05, **p-value<0.005).

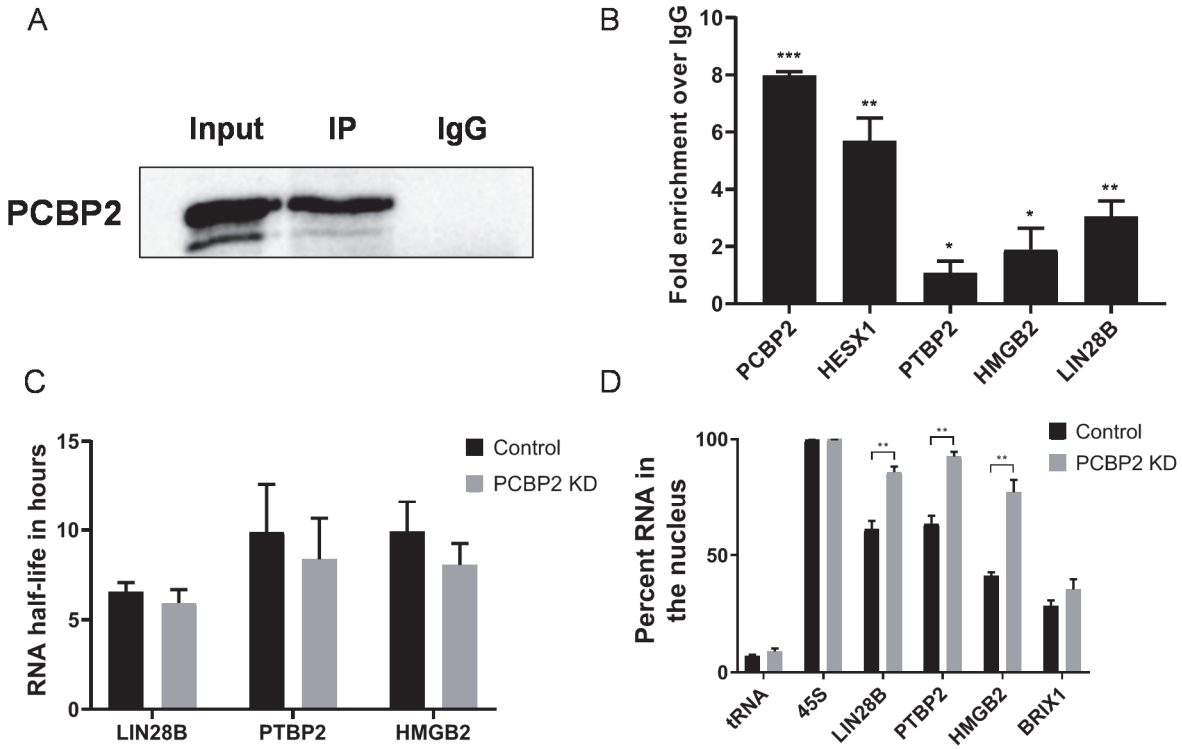

Figure 5.5: PCBP2 binds to developmental-associated transcripts and modulates their nuclear export. A: Representative western blot showing PCBP2 protein abundance in Input, IgG IP and PCBP2 IP samples from RIP experiment. B: RT-dPCR analysis of transcript abundance in IgG and PCBP2 IP samples. Data is represented as fold enrichment over IgG (PCBP2 IP/IgG IP). Asterisks indicate significant difference in mean enrichment between PCBP2 IP and IgG IP, which is set to one (*p-value<0.05, **p-value<0.005, ***p-value<0.0005). C: Half-lives of transcripts from siRNA negative control (black) and PCBP2 KD (gray) samples. No significant difference in mean half-life between control and PCBP2 KD samples was observed. D: Nuclear localization of transcripts from siRNA negative control (black) and PCBP2 KD (gray) samples. tRNA and 45S rRNA were used as cytoplasmic and nuclear controls, respectively. Asterisks indicate a significant difference in the mean percent of RNA in the nucleus between control and PCBP2 KD samples (**p-value<0.005).

5.2.4 PCBP2 modulates the nuclear export of down-regulated targets associated with development

Once we established a group of transcripts directly targeted by PCBP2, we attempted to characterize the underlying mechanism responsible for the observed changes in gene expression. To do this, we assessed the impact that PCBP2 expression had on mRNA stability and subcellular localization of mRNA targets. Of the three transcripts we tested, none exhibited a notable change in mRNA half-life when PCBP2 was depleted (Fig. 5.5C). However, we did observe that all three exhibited a significant increase in nuclear localization following PCBP2 depletion (Fig. 5.5D). In contrast localization of *BRIX1* mRNA, which exhibited no change in abundance following PCBP2 depletion (see GEO, to be determined), was unaffected.

5.2.5 Regulation of LIN28B is not solely responsible for the morphological changes in PCBP2 depleted iPSCs

Among the mRNA targets we identified, LIN28B, like its homolog the pluripotency factor LIN28A, also plays an important role in mediating self-renewal and differentiation (Copley et al. 2013; Piskounova et al. 2011; Chien et al. 2015; Oh et al. 2018; Zhang et al. 2016b). Thus, we wondered if the loss of pluripotency and morphological changes we observed following depletion of PCBP2 were due to its regulation of LIN28B. To address this, we depleted LIN28B in iPSCs for six days via siRNA transfection and evaluated the effect on cell and colony morphology compared to transfection with a negative siRNA control. We measured *LIN28B* mRNA abundance via RT-dPCR in control and knockdown samples and observed a ~90% decrease (Fig. 5.6A), a more dramatic decrease than seen in our RNA-seq analysis (~60%). However, there were no discernable cell and colony morphological changes in iPSCs after six days of LIN28B depletion (Fig. 5.6B).

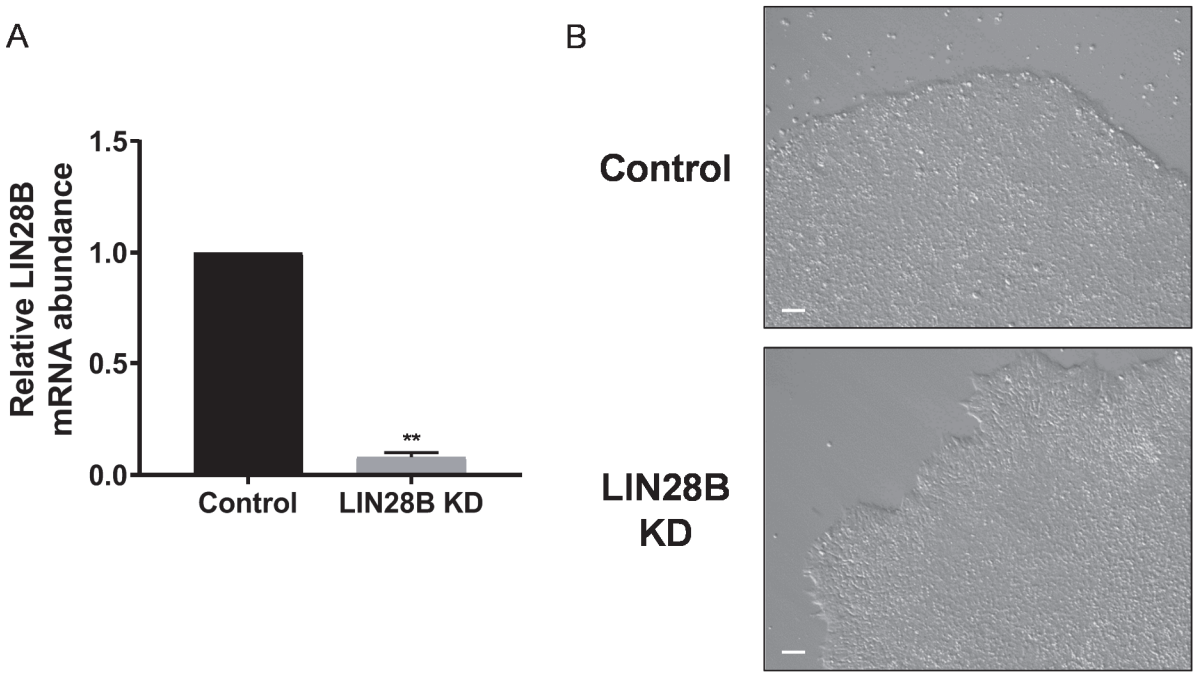

Figure 5.6: Depletion of LIN28B in iPSCs does not recapitulate the cell and colony morphology changes observed following PCBP2 depletion. iPSCs were subjected to six days of treatment with control or LIN28B siRNAs. A: RT-dPCR analysis of LIN28B mRNA abundance in siRNA negative control and LIN28B depleted samples normalized to GAPDH mRNA. Asterisks indicate significant difference in mean abundance between control and LIN28B KD samples (**p-value<0.005). B: Bright field images of siRNA negative control and LIN28B-depleted iPSC colonies. Scale bars indicate 100 μm.

To summarize, these findings show the results from our RNA-seq data is reproducible. We observed that mRNAs encoding factors associated with pluripotency are both up- and down-regulated following depletion of PCBP2, but only the down-regulated mRNAs are directly bound by PCBP2. However, we have yet to gain the full mechanistic insight into how PCBP2 regulates their expression. Furthermore, decreased LIN28B expression is not solely responsible for the loss of pluripotency during PCBP2 depletion.

In addition to mRNAs, there are a number of ncRNAs in the genome that have been reported to be involved in pluripotency. However, GO-term annotation is not as well-defined for these transcripts, thus it is important to evaluate ncRNAs separately.

5.2.6 lncRNAs with HERV-H elements are up-regulated following PCBP2 depletion and strongly interact with PCBP2 protein

When we sorted differentially expressed transcripts based on their coding potential, we found 107 out of 853 (12.5%) up-regulated transcripts were classified as ncRNAs compared to only 30 out of 656 (4.5%) down-regulated transcripts (Fig. 5.7A). When we explored the list of up-regulated ncRNAs further, we discovered several lncRNAs that contain HERV-H elements were present (Fig. 5.7B). This finding piqued our interest because HERV-H lncRNAs are expressed almost exclusively in stem cells and their transcription is driven by major pluripotency factors like OCT4 (Xie et al. 2013; Ohnuki et al. 2014; Santoni et al. 2012; Lu et al. 2014). Moreover, dynamic regulation of HERV-H lncRNAs is crucial for efficient reprogramming of iPSCs (Ohnuki et al. 2014). As a result of these findings, HERV-H RNAs have been classified as stem cell markers (Mareschi et al. 2019; Lu et al. 2014; Santoni et al. 2012), although their functions in iPSCs are not fully understood. Four of the HERV-H lncRNAs present in our dataset, indicated by red asterisk in Fig. 5.7B, have previous associations with pluripotency (Wang et al. 2013b; Loewer et al. 2010; Wang et al. 2014a; Jain et al. 2016).

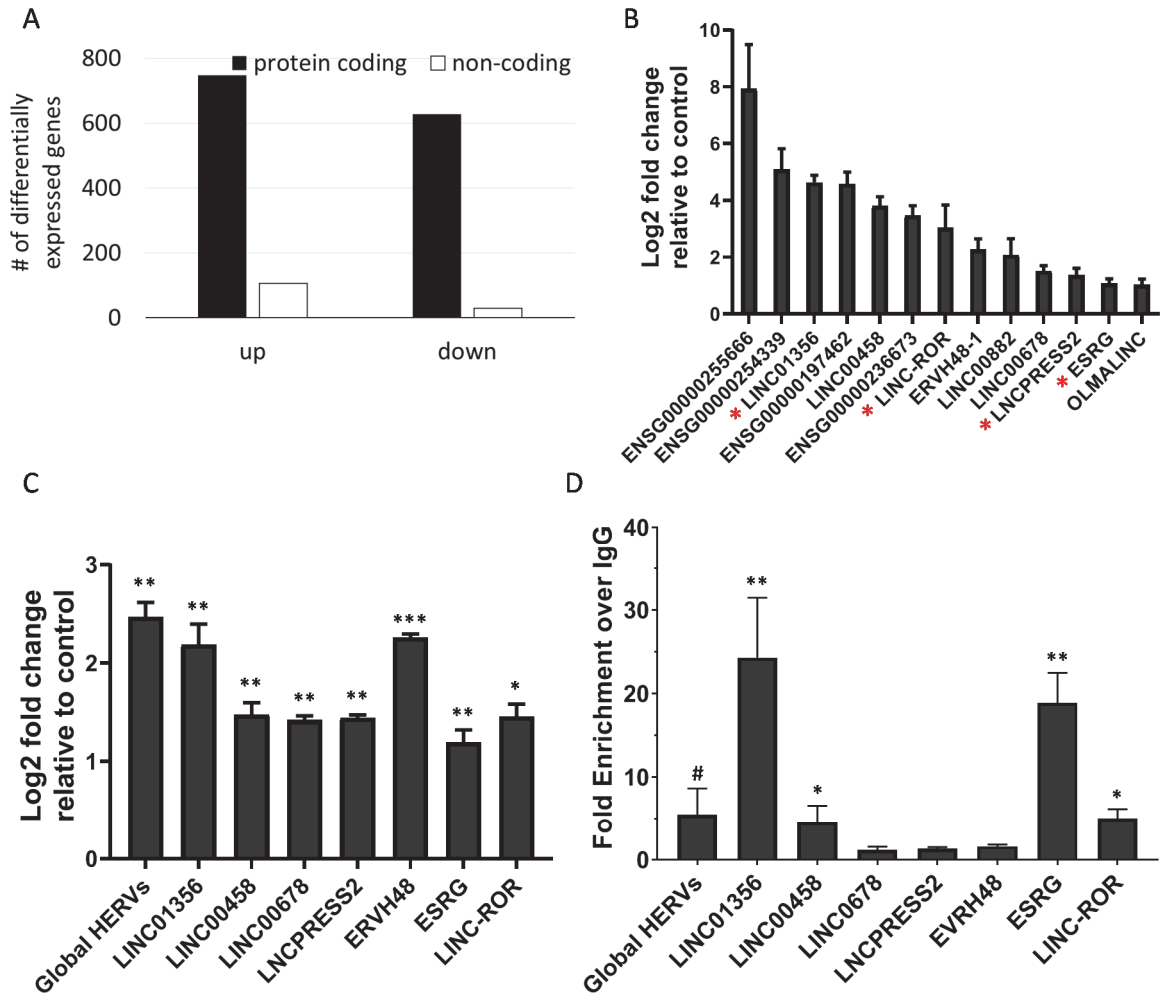

Figure 5.7: lncRNAs with HERV-H elements are up-regulated following PCBP2 depletion and strongly interact with PCBP2 protein. A: Differentially expressed transcripts were sorted based on their protein coding potential. 107 out of 853 (12.5%) of up-regulated and 30 out of 656 (4.5%) of down-regulated transcripts were classified as non-coding. B: Log_2 fold change of lncRNAs containing HERV-H elements according to DESeq2 analysis (see GSE139626). Red asterisks indicate lncRNAs with reported associations to pluripotency. C: RT-dPCR analysis of lncRNA abundances in control and PCBP2 depleted samples normalized to GAPDH for transcripts. Data is reported as log_2 fold change (PCBP2 KD/Control). Asterisks indicate significant difference in mean abundance between control and PCBP2 KD samples (*p-value<0.05, **p-value<0.005,***p-value<0.0005). D: RT-dPCR analysis of transcript abundance in IgG and PCBP2 IP samples. Data is represented as fold enrichment over IgG (PCBP2 IP/IgG IP). Asterisks indicate significant difference or trend in mean enrichment between PCBP2 IP and IgG IP, which is set to one (*p-value<0.05, **p-value<0.005, #p-value<0.06).

We selected seven HERV-H lncRNAs and validated changes in expression following PCBP2 depletion on independent replicates via RT-dPCR. We also assessed global HERV-H expression using a primer set that recognizes a region that is generally conserved between HERV-H elements (Vargiu et al. 2016). All seven of the HERV-H lncRNAs we measured and global HERV-H abundance were significantly increased in PCBP2 depleted samples compared to controls (Fig. 5.7C).

HERV-H elements are unusually C-rich (Jern et al. 2005), and PCBP2 binds to CREs. Therefore, we assessed interactions between PCBP2 protein and HERV-H lncRNAs via RIPs, as described above. We observed that four out of seven of the lncRNAs tested were significantly enriched in PCBP2 IPs compared to IgG control IPs (Fig. 5.7D). Our global HERV-H primer set did not show significant enrichment (p=0.053), perhaps because only a subset of HERV-H elements are recognized by PCBP2. The observation coupled with the fact all the HERV-lncRNAs assessed here were significantly increased following depletion of PCBP2 in iPSCs was rather curious. Intriguingly, changes in the abundance of one HERV-H lncRNA can influence the expression of several others (Zhang et al. 2019a) (see 5.3 Discussion for more details). In summary, HERV-H lncRNAs are up-regulated following depletion of PCBP2 in iPSCs and a majority directly recruit PCBP2 protein.

5.2.7 The sequence context of HERV-H elements influences PCBP2 interactions

We analyzed the distribution of cytosine across the length of each lncRNA as well as the percent overlap with the HERV-H consensus sequence (Table 5.1) (Vargiu et al. 2016). This approach failed to identify any differentiating characteristics between lncRNAs that were bound by PCBP2 (indicated by underline) and those that were not.

Next, we evaluated if specific region(s) of the HERV-H genome are present in HERV-H RNAs that interact with PCBP2. To do this, we used BLASTN under default parameters (Altschul et al. 1997) to align the lncRNAs to the HERV-H consensus sequence

Table 5.1: Sequence analysis of HERV-H lncRNAs. Information gathered from sequence analysis of the HERV-H lncRNAs includes cytosine (C) percentage across the entire HERV-H lncRNA as well as only the HERV-H regions and percent overlap with the HERV-H consensus sequence. HERV-H lncRNAs bound by PCBP2 are underlined.

HERV-H lncRNA	Percent C in total transcript	Percent C in HERV-H regions	Percent overlap with HERV-H consensus sequence
LINC01356	32.8	32.4	66.1
LINC00458	29.6	33	55.8
ESRG	30.3	33.7	63.8
LINC-ROR	24.2	32.5	51.5
LINC00678	24.4	33.3	60.9
LNCPRESS2	17	29.6	53.4
ERVH48-1	26.5	27.1	48.8

(Vargiu et al. 2016). Portions of all the lncRNAs, except ERVH48-1, which was not bound by PCBP2 (Fig. 5.7D), aligned to various regions of the HERV-H consensus sequence (Fig. 5.8). A more in-depth alignment analysis of ERVH48-1 alignment via Geneious Prime revealed numerous short regions did in fact align to the HERV-H consensus sequence, however they were discarded based on the default parameters of BLASTN. Notably, all of the other lncRNAs exhibited high alignment scores to a portion of the 5' long tandem repeat (LTR; ~500-800 nucleotide region of the consensus sequence) and moderate alignment scores to sections of the 3' LTR (~10,600-11,300 nucleotide region). Thus, these HERV-H regions likely do not influence PCBP2 interactions as they are present in both sets of lncRNAs. Intriguingly, the four lncRNAs that were bound by PCBP2 aligned to a portion of the Gag-Pro-Pol domain (~3200-3400 region of the consensus sequence) that was absent for the other lncRNAs. Moreover, LINC01356, which exhibited the strongest interaction with PCBP2, had an additional unique alignment to an upstream portion of the 5' LTR (~150-425 nucleotide region). Indeed, there are several highly C-rich stretches within these two regions which may facilitate binding of PCBP2 protein. Together, these results suggest binding of PCBP2 to HERV-H containing lncRNAs is influenced by the HERV-H region present in the lncRNA.

5.2.8 Reciprocal regulation occurs between PCBP2 protein and HERV-H lncRNAs

There is evidence that association of RBPs with ncRNAs can sequester the RBP (Lee et al. 2016; Hirose et al. 2014; Kim et al. 2016), or in some cases induce its decay (Wang et al. 2015a; Yoon et al. 2013). Moreover, a form of this regulation exists for PCBP2, as miR-328 regulates PCBP2 activity by serving as a decoy and soaking up PCBP2 protein (Eiring et al. 2010). As mentioned above, HERV-H lncRNAs are almost exclusively expressed in pluripotent stem cells (Lu et al. 2014; Wang et al. 2014a; Santoni et al. 2012).

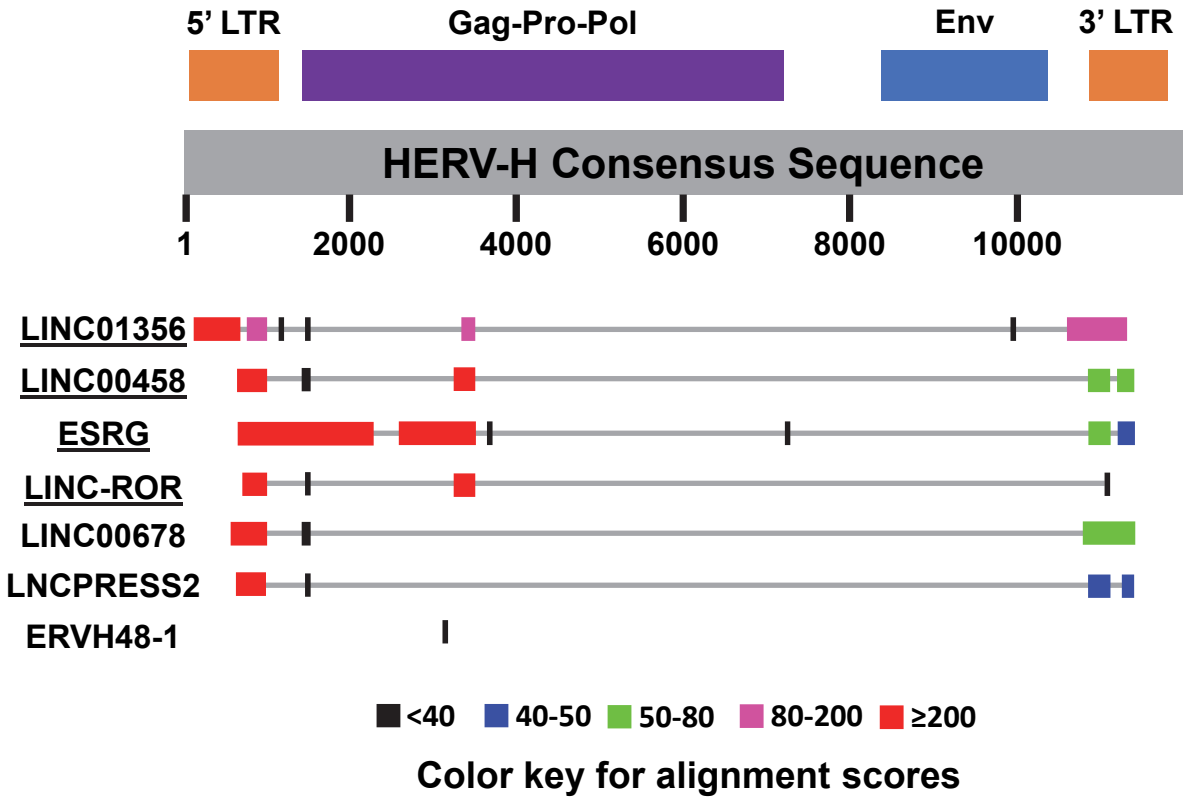

Figure 5.8: Individual HERV-H lncRNAs align to different regions of the HERV-H consensus sequence. HERV-H lncRNAs were aligned to the reported HERV-H consensus sequence (Vargiu et al., 2016) using BLASTN under default parameters (Altschul et al. 1997). A color key was used to represent the alignment scores for different regions across each HERV-H lncRNA. A higher alignment score indicates the HERV-H lncRNA and HERV-H consensus sequences are more analogous to one another. Approximate annotations for the HERV-H consensuses sequence are listed at the top.

Based on this information, we wondered if the group of HERV-H lnRNAs that interacted with PCBP2 somehow also regulated PCBP2 activity or expression.

We chose to investigate the regulation of PCBP2 expression first. To do this, we selected the lncRNA with the strongest association with PCBP2, LINC01356 (which also exhibited the third highest expression level in iPSCs relative to the other HERV-H lncRNAs in this study (See GSE139626), and reduced its expression in iPSCs via transfection of siRNAs targeting a unique region of the transcript and measured PCBP2 expression. We predicted depletion of LINC01356 in iPSCs would alter PCBP2 expression. We observed >60% knockdown of LINC01356 via RT-dPCR (Fig. 5.9A). There was no dramatic effect on the cell or colony morphology of LINC01356 depleted iPSCs and no change in OCT4 protein expression (Fig. 5.9B,C). As predicted, PCBP2 protein expression was dramatically increased in LINC01356 depleted iPSCs compared to those transfected with a negative control as determined by western blot (Fig. 5.9B,C) and IF (Fig. 5.9D). Moreover, PCBP2 mRNA levels were unchanged (Fig. 5.9F). Thus, depletion of LINC01356 results in the up-regulation of PCBP2 protein, but not mRNA, abundance. The absence of any change in mRNA abundance indicates PCBP2 repression must occur either through reduced translation or destabilization of the protein.

Given the high homology and overlap in targets between PCBP2 and PCBP1 (Ghanem et al. 2015), we evaluated whether other PCBPs were also influenced by LINC01356. Western blotting revealed that PCBP1, but not the more divergent PCBP3, was increased following depletion of LINC01356 (Fig. 5.9B,C). This indicates that binding to LINC01356, and the subsequent regulatory mechanism, is unique to PCBP1 and 2.

To directly evaluate the effects individual HERV-H lncRNAs have PCBP2 expression, we artificially introduced them into HeLa cells, which normally have no detectable HERV-H expression (Schön et al. 2001). We transfected expression plasmids for individual HERV-H lncRNAs into HeLa cells and verified expression via RT-dPCR (Fig. 5.10A).

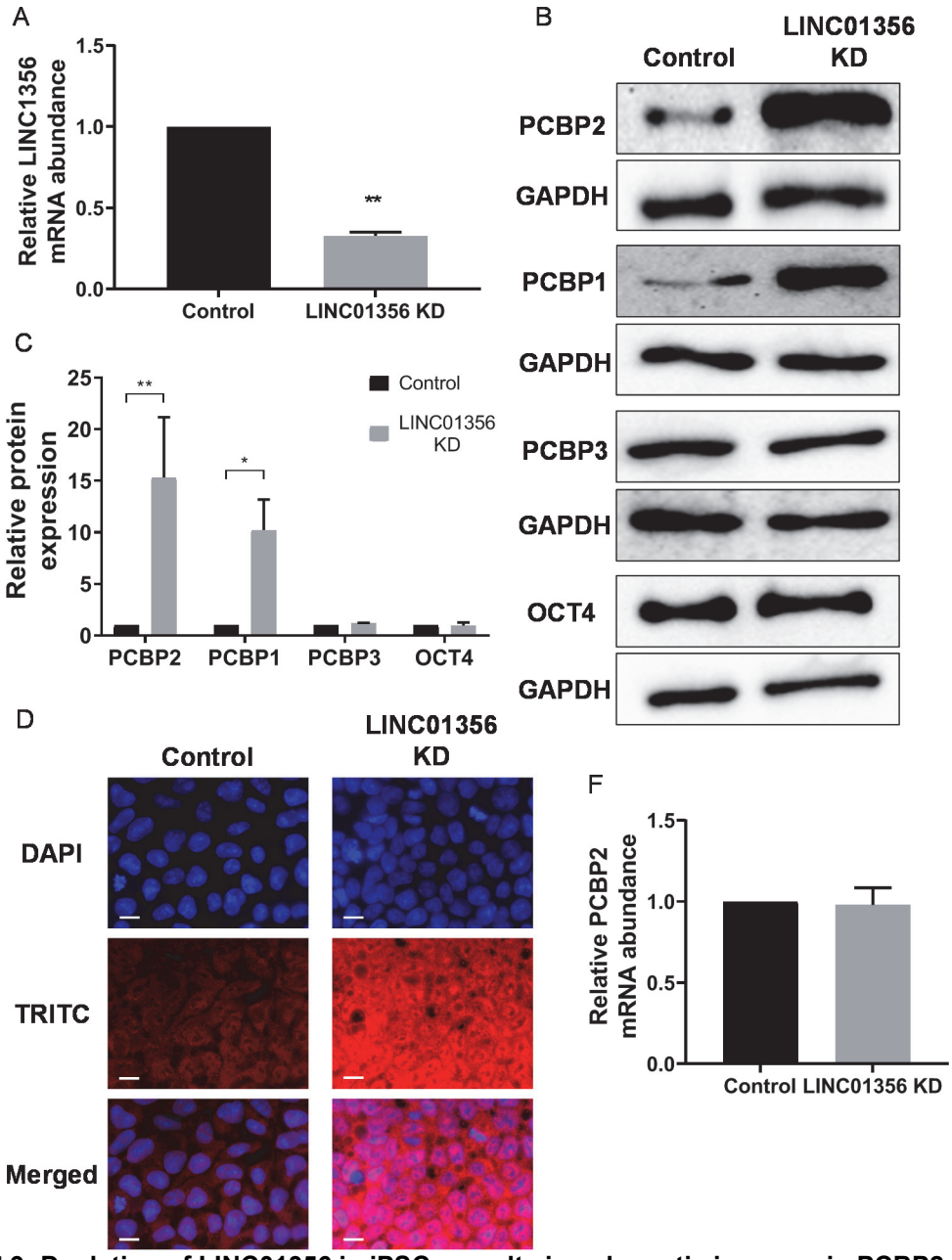

Figure 5.9: Depletion of LINC01356 in iPSCs results in a dramatic increase in PCBP2 expression. A: RT-dPCR analysis of LINC01356 abundance in siRNA negative control and LINC01356 depleted samples normalized to GAPDH mRNA. Asterisks indicate significant difference in mean abundance between control and LINC01356 KD samples (***p-value<0.0005). B,C: Representative western blots to detect PCBP2 (B) and PCBP1, PCBP3 and OCT4 (C) in negative control and LINC01356 depleted iPSC extracts. GAPDH was used as a loading control. D: Quantification of (B) and (C). Asterisks indicate significant difference in the relative mean protein expression between negative control and LINC01356 depleted samples (*p-value<0.05, **p-value<0.005). E: iPSCs were subjected to two days of treatment with negative control or LINC01356 siRNAs. The nucleus was stained with DAPI. PCBP2 protein was detected by IF staining. Scale bars indicate 10 μm. F: RT-dPCR analysis of PCBP2 abundance in siRNA negative control and LINC01356 depleted samples normalized to GAPDH mRNA. No significant difference was observed in mean abundance between control and LINC01356 KD samples.

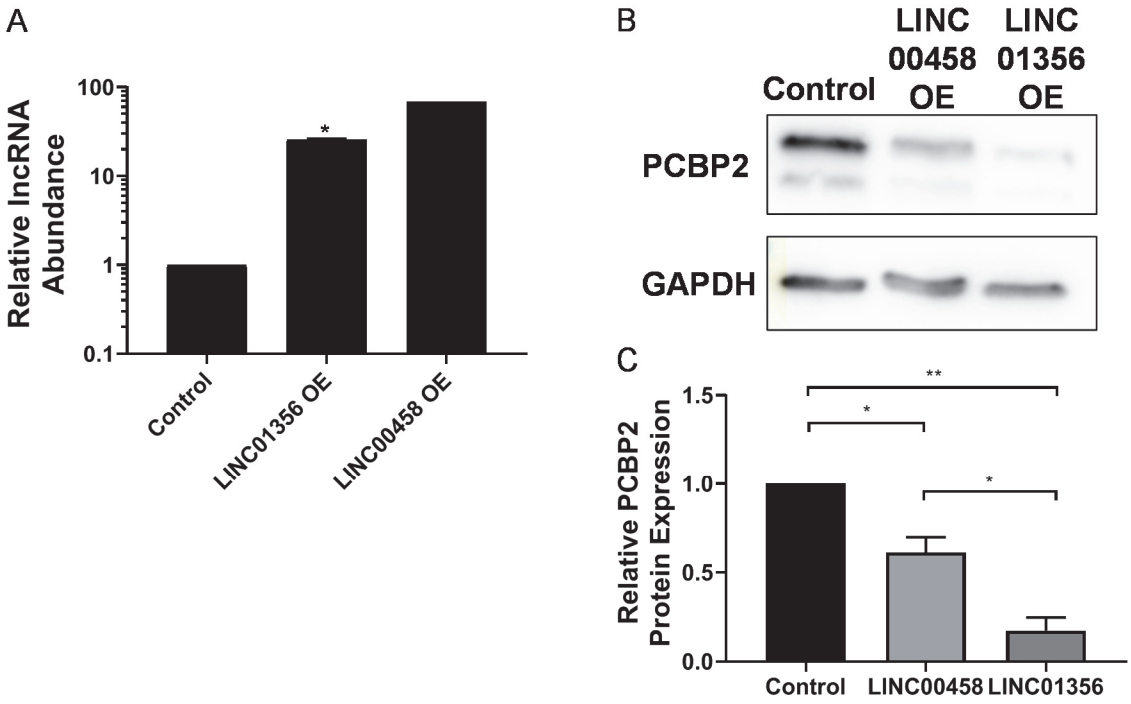

Figure 5.10: Over expression of LINC01356 or LINC00458 down-regulates PCBP2 protein expression. A: RT-dPCR analysis of lncRNA abundance in empty vector control and LINC01356 or LINC00458 over expression samples normalized to GAPDH mRNA. Asterisks indicate significant difference in mean abundance between control and LINC01356 over expression samples (*p-value<0.05).No statistical analysis was performed for LINC00458 over expression because this is preliminary data and n=1. B: Representative western blot to detect PCBP2 in empty vector control and LINC01356 or LINC00458 over expression HeLa extracts. GAPDH was used as a loading control. C: Quantification of (B). Asterisks indicate significant difference in the relative mean protein expression between empty vector control and over expression samples (*p-value<0.05, **p-value<0.005).

As expected, over-expression of LINC01356 or LINC00458 resulted in a significant decrease in PCBP2 protein expression (Fig. 5.10 B,C). However, expression of LINC01356 elicited a greater decrease in expression compared to LINC00458. These findings indicate two different HERV-H lncRNAs, LINC01356 and LINC00458, can influence PCBP2 protein expression. Taken together, our results suggest a subset of HERV-H lncRNAs, and LINC01356 in particular, may regulate PCBP2 protein expression in iPSCs.

5.2.9 PCBP2 expression increases following differentiation of iPSCs into the three germ layers

In the section above we discovered that certain HERV-H lncRNAs are able to regulate the expression PCBP2 protein. Moreover, HERV-H expression is dramatically reduced following differentiation of pluripotent stem cells into the three germ layers (Xie et al. 2013; Ohnuki et al. 2014; Santoni et al. 2012; Lu et al. 2014). Based on this information, we hypothesized that differentiation of iPSCs would result in up-regulation of PCBP2. To assess this, we assessed PCBP2 expression in iPSCs that were induced to differentiate into each of the three germ layers and observed that PCBP2 protein expression increased upon differentiation down all three lineages (Fig. 5.11A,B). Differentiation into endoderm and ectoderm elicited a large (>60-fold) increase in PCBP2 protein abundance with no detectable effect on mRNA levels (Fig. 5.11C). In contrast, differentiation into mesoderm resulted in a more modest yet significant (~6-fold) change in protein abundance which was partially accounted for by a ~2-fold change in mRNA levels. Taken together, these results suggest PCBP2 expression is up-regulated upon differentiation down any lineage and that this is primarily achieved through enhanced translation or protein stability. This change in expression correlates with the expected reduction in HERV-H expression during differentiation.

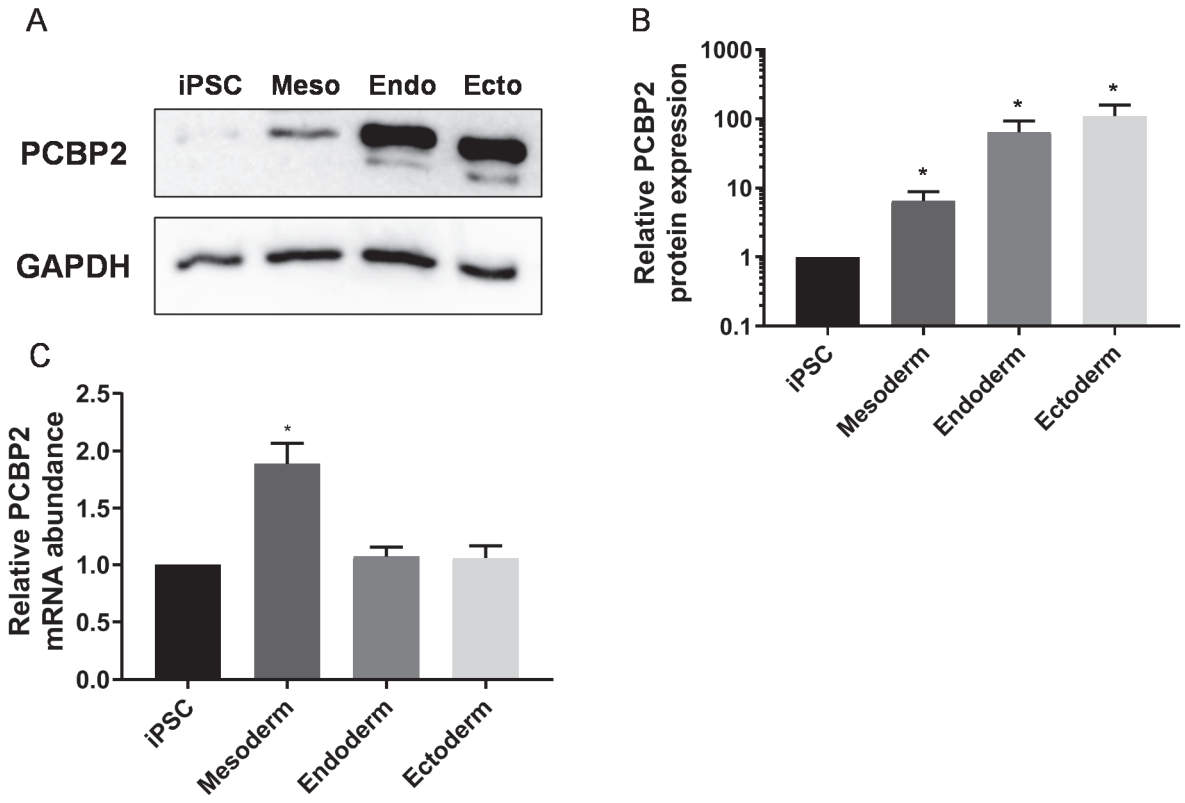

Figure 5.11: PCBP2 expression is increased following differentiation of iPSCs into all three germ layers. A: Representative western blot of PCBP2 expression in untreated or following differentiation down the three germ layers iPSC extracts. GAPDH was used as a loading control. B: Quantification of (A). Asterisks indicate significant difference in the relative mean protein expression between untreated and differentiated samples (*p-value<0.05). C: RT-dPCR analysis of PCBP2 mRNA abundance in untreated or following differentiation down the three germ layers iPSC samples. Asterisks indicate significant difference in the relative mean mRNA abundance between untreated and differentiated samples (*p-value<0.05).

5.3 Discussion

In this study, we observed that extended depletion of PCBP2 leads to changes in cell and colony morphology and reduced expression of pluripotency markers, both of which are signs of precocious differentiation. At the level of the transcriptome, transcripts associated with pluripotency and development, like LIN28B and PTBP2, are down-regulated following depletion of PCBP2, and are retained in the nucleus. In addition, HERV-H-containing lncRNAs, which play an important role in stem cell biology and are C-rich (Santoni et al. 2012; Lu et al. 2014), experience increased expression after PCBP2 knockdown and interact with PCBP2 protein. Interestingly, depletion of LINC01356, one HERV-H-containing target of PCBP2, in iPSCs results in a marked increase in PCBP2 protein expression, but does not impact PCBP2 mRNA abundance. Moreover, PCBP1, which has high homology to PCBP2, protein expression was also increased but the more divergent PCBP3 was not. In reciprocal experiments where LINC01356 or LINC00458, another HERV-H target of PCBP2, were over-expressed in HeLa cells, PCBP2 protein expression was down-regulated. These findings indicate the HERV-H-containing lncRNAs and PCBP2 protein mutually repress each other's expression. In summary, the results of our study indicate PCBP2 influences whether a pluripotent stem cell favors a state of self-renewal or begins to differentiate. To this end, the interactions between PCBP2 protein and HERV-H lncRNAs may have larger implications for stem cell biology.

As highlighted above, HERV-H lncRNAs have an important, but ill-defined, role in maintaining a pluripotent state (Xie et al. 2013; Ohnuki et al. 2014; Santoni et al. 2012; Lu et al. 2014; Mareschi et al. 2019). Stem cell-specific transcription of HERVs is driven by the presence of long-terminal repeats (LTRs), specifically LTR7 in the case of HERV-H lncRNAs, which recruits pluripotent transcription factors (Santoni et al. 2012; Xie et al. 2013; Lu et al. 2014). LTR-derived transcripts play an important role in regulating the nuclear transcriptome in stem cells and associate with enhancer regions involved in the maintenance of pluripotency (Fort et al. 2014). To this end, HERV-H lncRNAs influence the creation and boundaries of topologically

associating domains (TADs) in pluripotent stem cells (Zhang et al. 2019a). TADs are compartments within the chromatin structure that are relatively ‘open’, thus exhibit high levels of transcription and are generally conserved between cell types (Dixon et al. 2012, 2015; Jin et al. 2013). These reports indicate a key function for HERV-H lncRNAs in the nucleus. In this study, we observed that the nuclear export of several mRNAs is regulated by PCBP2 (Fig. 5.5D). Therefore, it would interesting to determine if nuclear localization of HERV-H lncRNAs is also influenced by PCBP2, as this may impact both the activity and expression of HERV-H lncRNAs. Alternatively, PCBP2 may be modulating the transcription or stability of HERV-H lncRNAs. Depletion of PCBP2 in iPSCs followed by 4sU labeling would allow us to assess both of these possibilities simultaneously. Furthermore, altered expression of an individual HERV-H abrogates formation of its associated TAD boundaries and impacts expression of genes located up to 500 kilobase pairs away (Zhang et al. 2019a). Some of the genes affected by this were other HERV-H lncRNAs, suggesting that regulating a subset of HERV-H lncRNA(s) can impact the abundance of several other HERVs. This observation may provide some clarity as to how changes in PCBP2 expression can influence global HERV-H expression, despite our findings that PCBP2 does not directly bind to every HERV-H lncRNA.

As mentioned above, HERV-H lncRNAs contain elements of a retrovirus (Jern et al. 2004). Thus, it is important to note that PCBP2 can modulate immune response, according to our findings (Fig. 5.4) as well as many other reports (Xia et al. 2015; You et al. 2009), and can also bind to several viral RNAs (Palusa et al. 2012; Blyn et al. 1997), including human immunodeficiency virus (HIV) which is also a retrovirus (Lin et al. 2014; Hadian et al. 2009). It is therefore plausible that the roles PCBP2 plays in these models may shed light its interaction and regulation of HERV-H lncRNAs. However, the majority of these works describe how PCBP2 is ‘hijacked’ by a specific virus and that binding of PCBP2 to these viral RNAs enhances translation and subsequently viral replication (Palusa et al. 2012; Lin et al. 2014; Blyn et al. 1997). Thus, on the surface, these interactions do not appear to give any mechanistic clues in

regards to how PCBP2 may be regulating HERV-H lncRNAs. Nevertheless, findings from these fields should be monitored closely, as new developments or the discovery additional interactions between viral RNAs and PCBP2 may have a more direct correlation mechanistically to the regulation of HERV-H lncRNAs.

We also observed several mRNAs associated with pluripotency that were impacted by PCBP2 depletion. As noted above, LIN28B plays a role in stem cell self-renewal and modulation of neuronal differentiation (Copley et al. 2013; Piskounova et al. 2011; Chien et al. 2015; Oh et al. 2018). Although the down-regulation of LIN28B following PCBP2 knockdown is not solely responsible for the phenotype we observed in PCBP2-depleted iPSCs (Fig. 5.6), it likely does have some impact on pluripotency. Of note, LIN28B helps to regulate Let-7 miRNA biogenesis (Piskounova et al. 2011; Copley et al. 2013) which has a plethora of downstream consequences in cancer progression and cell potency (Sun et al. 2016). Interestingly, there are two isoforms of LIN28B (long and short) that differentially regulate Let-7 biogenesis (Mizuno et al. 2018). The long-isoform binds and inhibits maturation of Let-7 miRNAs, whereas the short-isoform is able to bind but does not inhibit maturation. Thus, it would be interesting for future experiments to evaluate i). if PCBP2 differentially regulates the isoforms of LIN28B and ii). how changes in PCBP2 expression indirectly impact Let-7 expression. Based on our findings about PCBP2 expression during differentiation and what is known about Let-7-mediated regulation, we would predict that PCBP2 promotes expression of the LIN28B short-isoform, thus increasing expression of mature Let-7 miRNAs and driving differentiation.

Another target of PCBP2, PTBP2, regulates splicing patterns during embryonic development and also has ties to neural development (Li et al. 2014b; Licatalosi et al. 2012; Vuong et al. 2016). Induction of PTBP2 initiates a splicing program that is critical for neuronal maturation and survival. Little is known about the post-transcriptional regulation of PTBP2. To date, only miR-223 has been identified as a negative regulator of PTPB2 in CML (Agatheeswaran et al. 2013). Thus, our findings add to the currently limited knowledge regarding post-transcriptional

regulation of PTBP2 and present PCBP2 as a positive regulator. In future studies, it would be interesting to see if over expression of PCBP2 in iPSCs increases expression of PTBP2 and favors differentiation down the neural lineage.

Above we hypothesized that a subset of HERV-H lncRNAs is responsible for regulating PCBP2 expression in iPSCs. In support of this, we identified two HERV-H lncRNAs, LINC01356 and LINC00458, that are able to repress PCBP2 protein expression (Fig. 5.9 and 5.10). However, there are still additional questions to be addressed including: i). What differentiates HERV-Hs which are able to regulate PCBP2 vs. those that cannot? ii). By what mechanism do HERV-H lncRNAs promote degradation of PCBP2 protein?

In response to the first of question, our sequence analysis of the different HERV-H lncRNAs revealed there is a region of homology, located in the Gag-Pro-Pol domain of the consensus HERV-H sequence, that is present in the HERVs bound by PCBP2 and absent in those that are not (Fig. 5.7 and 5.8). If this region is key to PCBP2 binding and its subsequent regulation, then we would predict that over expression of a HERV-H lncRNA that lacks this region will not impact PCBP2 protein levels. We also observed that LINC01356 has a more pronounced influence on PCBP2 protein expression compared to LINC00458 (Fig. 5.9 and 5.10), despite both containing the Gag-Pro-Pol domain region of interest and able to be bound by PCBP2. As these are unlikely to be identical, it may be the sequence present in LINC01356 has a higher binding affinity for PCBP2 than the LINC00458 sequence. Additionally, LINC01356 contains a unique region of the 5' LTR in comparison to the other HERV-H lncRNAs we analyzed (Fig. 5.8). It is possible elements within this region may augment the repressive capacity of LINC01356 by enhancing interactions with PCBP2 and/or facilitating the recruitment of additional factors. We provide potential evidence for the former in this study (Fig. 5.7). However, additional research is necessary to fully support this notion. For example, we could create LINC01356 constructs with deletions of specific HERV-H regions (i.e. the Gag-Pro-Pol region and the unique portion of the 5' LTR) and measure their impact on PCBP2 binding affinity and protein expression in HeLa

cells. Based on our findings, we predict deletion of the Gag-Pro-Pol region would greatly reduce if not abrogate PCBP2 binding affinity towards LINC01356. Moreover, if a PCBP2-LINC01356 interaction is required for regulation and deletion of the Gag-Pro-Pol region alters binding affinity, we would not expect to see a change in PCBP2 protein expression. Likewise, if the unique 5' LTR region in LINC01356 enhances degradation of PCBP2 protein, then transfection of a construct with this region deleted should increase PCBP2 expression to a level on par with transfection of the LINC00458 construct, if not higher.

In regards to the second question, future experiments will seek to identify the mechanism, and other factors, responsible for changes in PCBP2 protein expression. Due to the high binding affinity of PCBP2 for some HERV-H lncRNAs and our findings that PCBP2 protein, but not mRNA, is affected by changes in HERV-H expression, we hypothesize repression of PCBP2 is being achieved through regulation of translation or stability of the protein. Although the former is possible, as PCBP2 protein is able to bind its own mRNA and HERV-H lncRNAs (Ghanem et al., 2015 and Fig. 5.7), regulation of protein stability seems more likely, as there is no evidence, to date, that PCBP2 can bind multiple mRNAs at once. Therefore, we favor initially following up on the regulation of protein stability. The first step to investigate this would be to determine if the stability of PCBP2 protein is affected following changes in LINC01356 expression (e.g. depletion in iPSCs or over expression in HeLas). This could be achieved via cyclohexamide treatment following altered LINC0136 expression and measuring PCBP2 protein levels over a time course. Additionally, it would be interesting to determine if an interaction between PCBP2 and HERV-H lncRNAs is required for regulation to occur. The experiments described above regarding LINC01356 deletion constructs may shed some light on this. However, an additional route would be to assess how deletion of the KH domains influences protein expression. We could achieve this by co-transfection of FLAG-tagged truncated versions of PCBP2 and LINC01356 or control constructs in HeLa cells. If binding of PCBP2 to HERV-H lncRNAs is required for regulation, we would predict truncated versions would be unaffected by the presence of LINC01356 compared

to the control. Some of the future experiments to characterize the regulation of PCBP2 described above are currently in progress.

In conclusion, PCBP2 helps to modulate differentiation in pluripotent stem cells by regulating the expression of specific mRNAs and ncRNAs. Specifically, the reciprocal regulation between PCBP2 protein and HERV-H lncRNAs may represent a new important aspect of stem cell biology.

Chapter 6: General Discussion

The findings in this thesis build upon previous evidence that m^{6}A modifications (Heck and Wilusz 2019; Geula et al. 2015) and CREs (Huang et al. 2015b; Neff et al. 2012) can influence mRNA decay rates and play important roles in modulating pluripotency in stem cells by beginning to characterize the roles of YTHDF2 and PCBP2, RBPs that recognize these RNA features, in the context of iPSCs. Below we provide two models that illustrate the proposed function of each RBP.

6.1 Expression of YTHDF2 helps maintains a pluripotent state in stem cells by repressing a genetic program for neural development

In Chapters 3 and 4, we provide evidence that YTHDF2 influences differentiation of pluripotent stem cells down the neural lineage. Our findings indicate YTHDF2 protein is expressed at relatively high levels in iPSCs and decreases as cells become more differentiated. Evidence suggests enhanced translation of *YTHDF2* mRNA mediated by an unknown factor that interacts with the first 300 nucleotides of the 3' UTR is the primary mechanism for increased expression of YTHDF2. In iPSCs, YTHDF2 binds to and destabilizes neural-specific transcripts in an m^{6}A-dependent manner. Moreover, depletion of YTHDF2 in iPSCs prior to induction disrupts gene expression, resulting in aberrant expression of neural and pluripotency factors as well as precocious differentiation. Based on these findings, we propose a model in which YTHDF2 is highly abundant in iPSCs and degrades m^{6}A-modified neural-specific transcripts to maintain a pluripotent state (Fig. 6.1). Upon neural induction, down-regulation of an unknown factor (referred to as 'factor X') results in decreased expression of YTHDF2, which leads to stabilization and subsequent increased expression of neural-specific transcripts. This activation of neural gene expression helps to drive differentiation down the neural lineage.

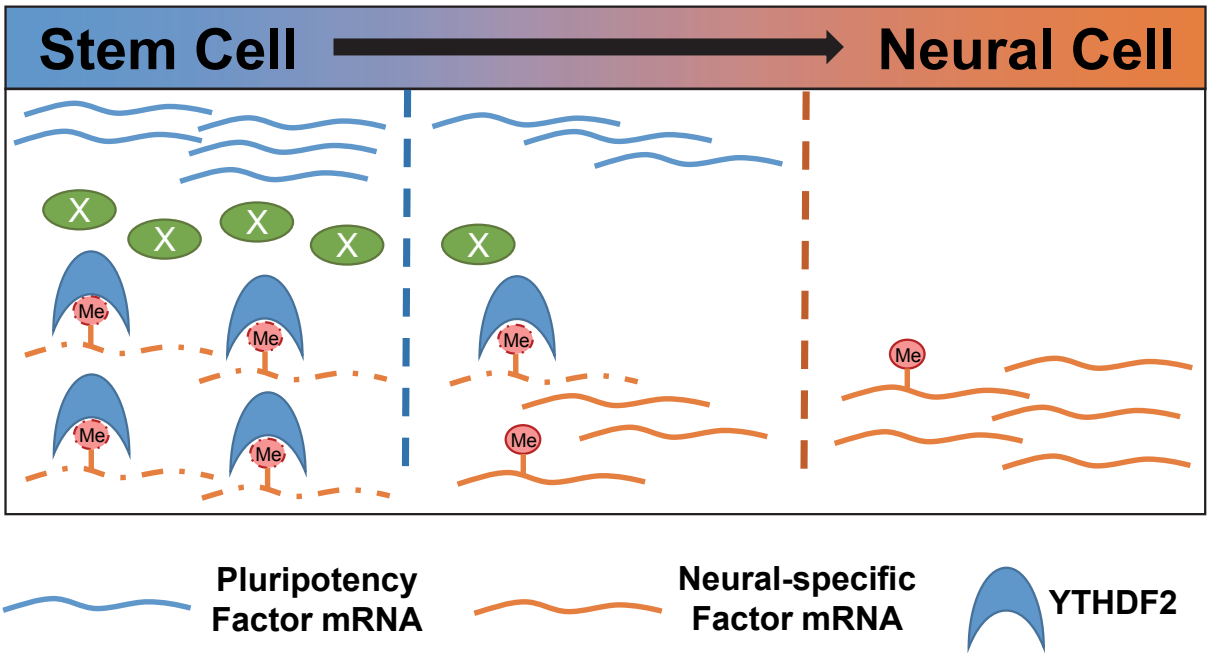

Figure 6.1: YTHDF2 modulates neural differentiation of iPSCs. Graphical representation of the role YTHDF2 plays in modulating pluripotency and neural differentiation. Stem cells utilize YTHDF2 to degrade methylated transcripts associated with neural development. Upon neural induction, YTHDF2 expression is decreased and, in some cases, the methylation status of neural associated transcripts is decreased as well. This facilitates subsequent differentiation into a neural progenitor cell.

As described in Chapters 3 and 4, future directions of study might focus on: i). identifying the factor(s) involved in enhancing translation of YTHDF2, ii). characterizing how neural-specific transcripts, out of a broad spectrum of m^6A-modified RNAs in stem cells, are selected by YTHDF2, iii) investigating the impact of YTHDF2-mediated gene expression in downstream differentiation events of the neural lineage; i.e. why does YTHDF2 appear to repress iPSC to NPC differentiation, yet promote differentiation of NPCs into glial or neuronal cell types (Li et al. 2018b)?

6.2 PCBP2 regulates multiple aspects of gene expression involved in modulating self-renewal and differentiation of pluripotent stem cells

In Chapter 5, we observed that altered expression of PCBP2 in iPSCs results in an apparent loss in pluripotency. To this end, transcripts, both mRNAs and ncRNAs, associated with pluripotency and development are differentially expressed following depletion of PCBP2 in iPSCs. Of note, we discovered lncRNAs that contain HERV-H elements, known to be important for pluripotency, are up-regulated following PCBP2 depletion and a subset are bound by PCBP2 protein. Intriguingly, this regulation is reciprocal, as changes in the expression of some HERV-H lncRNAs bound by PCBP2 can also impact PCBP2 protein expression. Overall, our data from Chapter 5 indicates that PCBP2 helps to modulate differentiation of iPSCs and the reciprocal regulation of HERV-H lncRNAs and PCBP2 protein may be an important aspect of stem cell biology. Based on this, we propose a model where PCBP2 participates in multiple regulatory mechanisms that influence self-renewal and differentiation (Fig. 6.2).

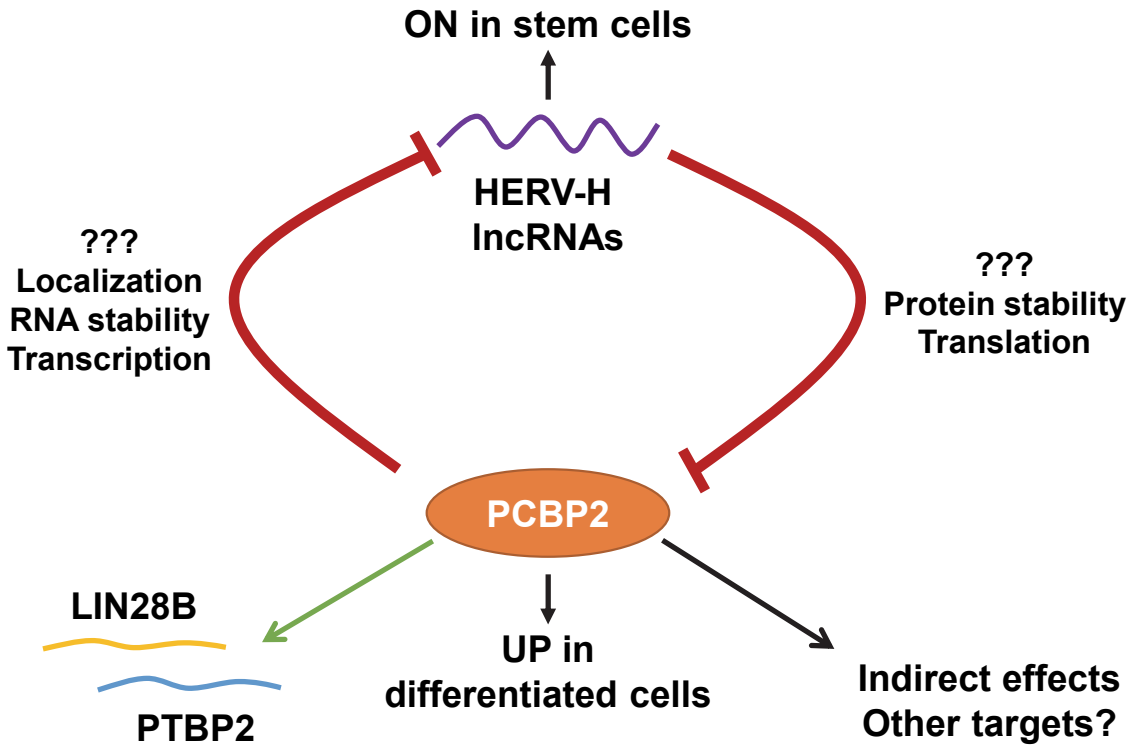

Figure 6.2: PCBP2 participates in reciprocal regulation with HERV-H lncRNAs and also modulates other aspects of pluripotency in iPSCs. Graphical representation of the roles PCBP2 plays in modulating self-renewal and differentiation in iPSCs. Notably, PCBP2 and HERV-H lncRNAs reciprocally regulate each other. HERV-H lncRNAs are expressed in stem cells and down-regulate PCBP2 at the level of translation or protein stability. PCBP2 is dramatically up-regulated in differentiated cells and may modulate localization, RNA stability or transcription to down-regulate HERV-H lncRNAs. Additionally, PCBP2 up-regulates *LIN28B* and *PTBP2* mRNAs and appears to have indirect effects on other mRNAs associated with pluripotency.

The balancing act between HERV-H lncRNAs and PCBP2 protein expression is prominent in our model. In stem cells, high expression of HERV-H lncRNAs wins out to reduce PCBP2 protein levels by decreasing protein stability or translation. Upon differentiation, an increase in PCBP2 expression may flip the scales, facilitating a decrease in HERV-H expression abrogated via mechanisms that are yet to be fully characterized. Alternatively, a down-regulation of HERV-H lncRNAs, possibly at the transcriptional level, may promote an increase in PCBP2 expression. In addition to this reciprocal regulation, PCBP2 also directly interacts with and promotes the expression of several mRNAs encoding factors associated with pluripotency and development, like LIN28B and PTBP2. Given the frequency of CREs and previous evidence from our lab and others regarding CRE the differential expression in pluripotent stem cells and differentiated fibroblasts (Neff et al. 2012; Huang et al. 2015b), it is plausible there are additional PCBP2 targets that may add to this model. Additionally, the indirect effects, some of which are presented as preliminary data here, may broaden the impact PCBP2 has on pluripotency. Thus, PCBP2 appears to have multiple roles in regards to regulating gene expression during pluripotency and differentiation.

Future directions for research in this area, as described in Chapter 5, might include: i) characterizing the mechanism by which PCBP2 modulates expression of HERV-H lncRNAs, both directly and indirectly, ii) identifying the HERV-H sequence elements and PCBP2 protein domains responsible their interaction, iii) characterizing the regulatory mechanism by which HERV-H lncRNAs modulate PCBP2 protein level.

6.3 Implications for clinical use of induced pluripotent stem cells

As described in Chapter 1, the ability to create patient-specific iPSC lines as well as less accessible cell types via differentiation of iPSCs is of great interest for gene therapy, personalized medicine and basic research (Cubillo et al. 2018; Avior et al. 2016; Karagiannis 2019). Moreover, some of these avenues are already being explored (Mandai et al. 2017; Loring

2018; Penney et al. 2019). However, additional insight into the mechanisms governing pluripotency are necessary to improve the efficiency and accuracy of reprogramming and subsequent differentiation of iPSCs to enable their full potential in the clinical setting to be reached. Based on the evidence presented in this thesis, modulation of YTHDF2 or PCBP2 may enhance the efficiency of certain reprogramming or differentiation protocols. For example, one of the more common methods of iPSC neural induction involves inhibition of the transforming growth factor-β/SMAD signaling pathway, which typically yields around 80% induction efficiency (Chambers et al. 2009; Shi et al. 2012). One of the pathways regulated by this signaling in pluripotent stem cells is m^6A methylation (Bertero et al. 2018). Thus, including a mechanism to modulate YTHDF2 expression, which represses neural programming in iPSCs according to our findings (Chapter 3), may increase the efficiency of these protocols. On the other hand, our results indicate PCBP2 is more highly expressed in differentiated cell types compared to pluripotent stem cells and negatively regulates HERV-H lncRNAs (Chapter 5). Expression of HERV-H lncRNAs is critical for reprogramming (Ohnuki et al. 2014). Therefore, the efficiency of reprogramming protocols might be enhanced by including a mechanism to down-regulate PCBP2. It is important to note these ideas are by no means guaranteed to have any effect on reprogramming or differentiation efficiencies. However, given the results of this thesis, they are worthy of consideration.

6.4 Concluding remarks

In the experiments presented here, we established that YTHDF2 plays a key role in the ability of m^6A methylation to influence self-renewal and neural differentiation of iPSCs by targeting neural-specific transcripts for degradation. Destabilization of neural-specific transcripts while iPSCs are in a pluripotent state not only prevents inappropriate activation of neural gene expression, but also enables rapid and coordinated differentiation to occur upon neural induction. Additionally, we demonstrated that YTHDF2 protein expression decreases as

pluripotent stem cells differentiate into lineage-specific cell types. Our findings indicate the change in YTHDF2 expression is primarily driven by elements in the 3' UTR of *YTHDF2* mRNA that help to enhance YTHDF2 translation.

We also identified PCBP2 as a regulator of differentiation in iPSCs. We observed PCBP2 protein expression is dramatically increased as iPSCs differentiate into the three germ layers, and this change in expression impacts mRNAs and HERV-H lncRNAs associated with pluripotency and development. Furthermore, a subset of HERV-H lncRNAs can also influence PCBP2 protein expression, indicating PCBP2 and HERV-H lncRNAs participate in reciprocal regulation.

Although there are numerous regulatory factors and networks involved in pluripotency, the studies presented here further our understanding of the post-transcriptional mechanisms utilized to tightly control gene expression during self-renewal and differentiation of pluripotent stem cells.

References

Abby E, Tourpin S, Ribeiro J, Daniel K, Messiaen S, Moison D, Guerquin J, Gaillard J-C, Armengaud J, Langa F, et al. 2016. Implementation of meiosis prophase I programme requires a conserved retinoid-independent stabilizer of meiotic transcripts. *Nat Commun* **7**: 10324. doi: 10.1038/ncomms10324.

Agarwal V, Bell GW, Nam JW, Bartel DP. 2015. Predicting effective microRNA target sites in mammalian mRNAs. *Elife*. doi: 10.7554/eLife.05005.

Agarwala SD, Blitzblau HG, Hochwagen A, Fink GR. 2012. RNA Methylation by the MIS Complex Regulates a Cell Fate Decision in Yeast ed. M. Lichten. *PLoS Genet* **8**: e1002732. doi: 10.1371/journal.pgen.1002732.

Agatheeswaran S, Singh S, Biswas S, Biswas G, Chandra Pattnayak N, Chakraborty S. 2013. BCR-ABL mediated repression of miR-223 results in the activation of MEF2C and PTBP2 in chronic myeloid leukemia. *Leukemia*. doi: 10.1038/leu.2012.339.

Aguilo F, Zhang F, Sancho A, Fidalgo M, Di Cecilia S, Vashisht A, Lee D-F, Chen C-H, Rengasamy M, Andino B, et al. 2015. Coordination of m(6)A mRNA Methylation and Gene Transcription by ZFP217 Regulates Pluripotency and Reprogramming. *Cell Stem Cell* **17**: 689–704. doi: 10.1016/j.stem.2015.09.005.

Akichika S, Hirano S, Shichino Y, Suzuki T, Nishimasu H, Ishitani R, Sugita A, Hirose Y, Iwasaki S, Nureki O, et al. 2019. Cap-specific terminal N 6 -methylation of RNA by an RNA polymerase II–associated methyltransferase. *Science (80-)* **363**. doi: 10.1126/science.aav0080.

Al-Khalaf HH, Aboussekhra A. 2019. AUF1 positively controls angiogenesis through mRNA stabilization-dependent up-regulation of HIF-1α and VEGF-A in human osteosarcoma. *Oncotarget* **10**: 4868–4879. doi: 10.18632/oncotarget.27115.

Alajem A, Biran A, Harikumar A, Sailaja BS, Aaronson Y, Livyatan I, Nissim-Rafinia M, Sommer AG, Mostoslavsky G, Gerbasi VR, et al. 2015. Differential Association of Chromatin Proteins Identifies BAF60a/SMARCD1 as a Regulator of Embryonic Stem Cell Differentiation. *Cell Rep* **10**: 2019–2031. doi: 10.1016/J.CELREP.2015.02.064.

Alshawaf AJ, Antonic A, Skafidas E, Ng DCH, Dottori M. 2017. WDR62 Regulates Early Neural and Glial Progenitor Specification of Human Pluripotent Stem Cells. *Stem Cells Int*. doi: 10.1155/2017/7848932.

Altschul SF, Madden TL, Schäffer AA, Zhang J, Zhang Z, Miller W, Lipman DJ. 1997. Gapped BLAST and PSI-BLAST: A new generation of protein database search programs. *Nucleic Acids Res*. doi: 10.1093/nar/25.17.3389.

Anders S, Pyl PT, Huber W. 2015. HTSeq--a Python framework to work with high-throughput sequencing data. *Bioinformatics* **31**: 166–169. doi: 10.1093/bioinformatics/btu638.

Arguello AE, DeLiberto AN, Kleiner RE. 2017. RNA Chemical Proteomics Reveals the N ^{6} -Methyladenosine (m ^{6} A)-Regulated Protein–RNA Interactome. *J Am Chem Soc* **139**: 17249–17252. doi: 10.1021/jacs.7b09213.

Arguello AE, Leach RW, Kleiner RE. 2019. In Vitro Selection with a Site-Specifically Modified RNA Library Reveals the Binding Preferences of N 6 -Methyladenosine Reader Proteins . *Biochemistry*. doi: 10.1021/acs.biochem.9b00485.

Avior Y, Sagi I, Benvenisty N. 2016. Pluripotent stem cells in disease modelling and drug discovery. *Nat Rev Mol Cell Biol* **17**: 170–182. doi: 10.1038/nrm.2015.27.

Babaie Y, Herwig R, Greber B, Brink TC, Wruck W, Groth D, Lehrach H, Burdon T, Adjaye J. 2007. Analysis of Oct4-Dependent Transcriptional Networks Regulating Self-Renewal and Pluripotency in Human Embryonic Stem Cells. *Stem Cells*. doi: 10.1634/stemcells.2006-0426.

Bailey AS, Batista PJ, Gold RS, Chen YG, de Rooij DG, Chang HY, Fuller MT. 2017. The conserved RNA helicase YTHDC2 regulates the transition from proliferation to differentiation in the germline. *Elife* **6**. doi: 10.7554/eLife.26116.

Baltz AG, Munschauer M, Schwanhäusser B, Vasile A, Murakawa Y, Schueler M, Youngs N, Penfold-Brown D, Drew K, Milek M, et al. 2012. The mRNA-Bound Proteome and Its Global Occupancy Profile on Protein-Coding Transcripts. *Mol Cell* **46**: 674–690. doi: 10.1016/j.molcel.2012.05.021.

Barbieri I, Tzelepis K, Pandolfini L, Shi J, Millán-Zambrano G, Robson SC, Aspris D, Migliori V, Bannister AJ, Han N, et al. 2017. Promoter-bound METTL3 maintains myeloid leukaemia by m6A-dependent translation control. *Nature* **552**: 126–131. doi: 10.1038/nature24678.

Barta T, Peskova L, Collin J, Montaner D, Neganova I, Armstrong L, Lako M. 2016. Brief Report: Inhibition of miR-145 Enhances Reprogramming of Human Dermal Fibroblasts to Induced Pluripotent Stem Cells. *Stem Cells* **34**: 246–51. doi: 10.1002/stem.2220.

Bartel DP. 2018. Metazoan MicroRNAs. *Cell*. doi: 10.1016/j.cell.2018.03.006.

Bartosovic M, Molares HC, Gregorova P, Hrossova D, Kudla G, Vanacova S. 2017. N6-methyladenosine demethylase FTO targets pre-mRNAs and regulates alternative splicing and 3′-end processing. *Nucleic Acids Res* **45**: 11356–11370. doi: 10.1093/nar/gkx778.

Basquin J, Roudko V V., Rode M, Basquin C, S?raphin B, Conti E. 2012. Architecture of the Nuclease Module of the Yeast Ccr4-Not Complex: the Not1-Caf1-Ccr4 Interaction. *Mol Cell* **48**: 207–218. doi: 10.1016/j.molcel.2012.08.014.

Batista PJ, Molinie B, Wang J, Qu K, Zhang J, Li L, Bouley DM, Lujan E, Haddad B, Daneshvar K, et al. 2014. m(6)A RNA modification controls cell fate transition in mammalian embryonic stem cells. *Cell Stem Cell* **15**: 707–19. doi: 10.1016/j.stem.2014.09.019.

Bedard KM, Walter BL, Semler BL. 2004. Multimerization of poly(rC) binding protein 2 is required for translation initiation mediated by viral IRES. *RNA*. doi: 10.1261/rna.7070304.

Behm-Ansmant I, Rehwinkel J, Doerks T, Stark A, Bork P, Izaurralde E. 2006. mRNA degradation by miRNAs and GW182 requires both CCR4:NOT deadenylase and DCP1:DCP2 decapping complexes. *Genes Dev* **20**: 1885–1898. doi: 10.1101/gad.1424106.

Bell JL, Wächter K, Mühleck B, Pazaitis N, Köhn M, Lederer M, Hüttelmaier S. 2013. Insulin-like growth factor 2 mRNA-binding proteins (IGF2BPs): post-transcriptional drivers of cancer progression? *Cell Mol Life Sci* **70**: 2657–2675. doi: 10.1007/s00018-012-1186-z.

Benjamini Y, Krieger AM, Yekutieli D. 2006. *Adaptive linear step-up procedures that control the false discovery rate*.

Bernstein E, Caudy AA, Hammond SM, Hannon GJ. 2001. Role for a bidentate ribonuclease in the initiation step of RNA interference. *Nature*. doi: 10.1038/35053110.

Berry AM, Flock KE, Loh HH, Ko JL. 2006. Molecular basis of cellular localization of poly C binding protein 1 in neuronal cells. *Biochem Biophys Res Commun*. doi: 10.1016/j.bbrc.2006.09.012.

Bertero A, Brown S, Madrigal P, Osnato A, Ortmann D, Yiangou L, Kadiwala J, Hubner NC, de los Mozos IR, Sadée C, et al. 2018. The SMAD2/3 interactome reveals that TGFβ controls m6A mRNA methylation in pluripotency. *Nature* **555**: 256–259. doi: 10.1038/nature25784.

Bibel M, Richter J, Schrenk K, Tucker KL, Staiger V, Korte M, Goetz M, Barde YA. 2004. Differentiation of mouse embryonic stem cells into a defined neuronal lineage. *Nat Neurosci*. doi: 10.1038/nn1301.

Bilgüvar K, Öztürk AK, Louvi A, Kwan KY, Choi M, Tatli B, Yalnizoğlu D, Tüysüz B, Çağlayan AO, Gökben S, et al. 2010. Whole-exome sequencing identifies recessive WDR62 mutations in severe brain malformations. *Nature*. doi: 10.1038/nature09327.

Blyn LB, Towner JS, Semler BL, Ehrenfeld E. 1997. Requirement of poly(rC) binding protein 2 for translation of poliovirus RNA. *J Virol*.

Bodi Z, Bottley A, Archer N, May ST, Fray RG. 2015. Yeast m6A Methylated mRNAs Are Enriched on Translating Ribosomes during Meiosis, and under Rapamycin Treatment ed. S. Granneman. *PLoS One* **10**: e0132090. doi: 10.1371/journal.pone.0132090.

Bodi Z, Button JD, Grierson D, Fray RG. 2010. Yeast targets for mRNA methylation. *Nucleic Acids Res* **38**: 5327–5335. doi: 10.1093/nar/gkq266.

Bodi Z, Zhong S, Mehra S, Song J, Graham N, Li H, May S, Fray RG. 2012. Adenosine Methylation in Arabidopsis mRNA is Associated with the 3′ End and Reduced Levels Cause Developmental Defects. *Front Plant Sci* **3**: 48. doi: 10.3389/fpls.2012.00048.

Bolger AM, Lohse M, Usadel B. 2014. Trimmomatic: A flexible trimmer for Illumina sequence data. *Bioinformatics*. doi: 10.1093/bioinformatics/btu170.

Boyer LA, Tong IL, Cole MF, Johnstone SE, Levine SS, Zucker JP, Guenther MG, Kumar RM,

Murray HL, Jenner RG, et al. 2005. Core transcriptional regulatory circuitry in human embryonic stem cells. *Cell*. doi: 10.1016/j.cell.2005.08.020.

Braun JE, Truffault V, Boland A, Huntzinger E, Chang C-T, Haas G, Weichenrieder O, Coles M, Izaurralde E. 2012. A direct interaction between DCP1 and XRN1 couples mRNA decapping to 5′ exonucleolytic degradation. *Nat Struct Mol Biol* **19**: 1324–1331. doi: 10.1038/nsmb.2413.

Brenet F, Socci ND, Sonenberg N, Holland EC. 2009. Akt phosphorylation of La regulates specific mRNA translation in glial progenitors. *Oncogene*. doi: 10.1038/onc.2008.376.

Brewer BY, Malicka J, Blackshear PJ, Wilson GM. 2004. RNA sequence elements required for high affinity binding by the zinc finger domain of tristetraprolin. Conformational changes coupled to the bipartite nature of AU-rich mRNA-destabilizing motifs. *J Biol Chem*. doi: 10.1074/jbc.M402551200.

Brown JA, Kinzig CG, DeGregorio SJ, Steitz JA. 2016. Methyltransferase-like protein 16 binds the 3′-terminal triple helix of MALAT1 long noncoding RNA. *Proc Natl Acad Sci* **113**: 14013–14018. doi: 10.1073/pnas.1614759113.

Brumbaugh J, Di Stefano B, Wang X, Borkent M, Forouzmand E, Clowers KJ, Ji F, Schwarz BA, Kalocsay M, Elledge SJ, et al. 2018. Nudt21 Controls Cell Fate by Connecting Alternative Polyadenylation to Chromatin Signaling. *Cell*. doi: 10.1016/j.cell.2017.11.023.

Cacchiarelli D, Trapnell C, Ziller MJ, Soumillon M, Cesana M, Karnik R, Donaghey J, Smith ZD, Ratanasirintrawoot S, Zhang X, et al. 2015. Integrative Analyses of Human Reprogramming Reveal Dynamic Nature of Induced Pluripotency. *Cell*. doi: 10.1016/j.cell.2015.06.016.

Cantz T, Key G, Bleidißel M, Gentile L, Han DW, Brenne A, Schöler HR. 2008. Absence of OCT4 Expression in Somatic Tumor Cell Lines. *Stem Cells*. doi: 10.1634/stemcells.2007-0657.

Carelli S, Giallongo T, Rey F, Latorre E, Bordoni M, Mazzucchelli S, Gorio MC, Pansarasa O, Provenzani A, Cereda C, et al. 2019. HuR interacts with lincBRN1a and lincBRN1b during neuronal stem cells differentiation. *RNA Biol*. doi: 10.1080/15476286.2019.1637698.

Castelo-Branco P, Furger A, Wollerton M, Smith C, Moreira A, Proudfoot N. 2004. Polypyrimidine Tract Binding Protein Modulates Efficiency of Polyadenylation. *Mol Cell Biol*. doi: 10.1128/mcb.24.15.6889.2004.

Chambers SM, Fasano CA, Papapetrou EP, Tomishima M, Sadelain M, Studer L. 2009. Highly efficient neural conversion of human ES and iPS cells by dual inhibition of SMAD signaling. *Nat Biotechnol* **27**: 275–280. doi: 10.1038/nbt.1529.

Chang C-T, Muthukumar S, Weber R, Levdansky Y, Chen Y, Bhandari D, Igreja C, Wohlbold L, Valkov E, Izaurralde E. 2019. A low-complexity region in human XRN1 directly recruits deadenylation and decapping factors in 5′–3′ messenger RNA decay. *Nucleic Acids Res*. doi: 10.1093/nar/gkz633.

Chang JS, Santhanam R, Trotta R, Neviani P, Eiring AM, Briercheck E, Ronchetti M, Roy DC, Calabretta B, Caligiuri MA, et al. 2007. High levels of the BCR/ABL oncoprotein are required for the MAPK-hnRNP-E2-dependent suppression of C/EBPα-driven myeloid differentiation. *Blood*. doi: 10.1182/blood-2007-03-078303.

Chapman EG, Costantino DA, Rabe JL, Moon SL, Wilusz J, Nix JC, Kieft JS. 2014. The Structural Basis of Pathogenic Subgenomic Flavivirus RNA (sfRNA) Production. *Science (80-)* **344**: 307–310. doi: 10.1126/science.1250897.

Chavèz S, Garcia-Martinez J, Delgado-Ramos L, Pèrez-Ortin JE. 2016. The importance of controlling mRNA turnover during cell proliferation. *Curr Genet* **62**: 701–710. doi: 10.1007/s00294-016-0594-2.

Chen C-YA, Shyu A-B. 2017. Emerging Themes in Regulation of Global mRNA Turnover in cis. *Trends Biochem Sci* **42**: 16–27. doi: 10.1016/j.tibs.2016.08.014.

Chen C, Lei J, Zheng Q, Tan S, Ding K, Yu C. 2018. Poly(rC) binding protein 2 (PCBP2) promotes the viability of human gastric cancer cells by regulating CDK2. *FEBS Open Bio*. doi: 10.1002/2211-5463.12408.

Chen H. 2018. VennDiagram: Generate High-Resolution Venn and Euler PlotsPackage "VennDiagram."

Chen J, Sun Y, Xu X, Wang D, He J, Zhou H, Lu Y, Zeng J, Du F, Gong A, et al. 2017. YTH domain family 2 orchestrates epithelial-mesenchymal transition/proliferation dichotomy in pancreatic cancer cells. *Cell Cycle* **16**: 2259–2271. doi: 10.1080/15384101.2017.1380125.

Chen J, Zhang YC, Huang C, Shen H, Sun B, Cheng X, Zhang YJ, Yang YG, Shu Q, Yang Y, et al. 2019. m6A Regulates Neurogenesis and Neuronal Development by Modulating Histone Methyltransferase Ezh2. *Genomics, Proteomics Bioinforma*. doi: 10.1016/j.gpb.2018.12.007.

Chen JF, Zhang Y, Wilde J, Hansen KC, Lai F, Niswander L. 2014. Microcephaly disease gene Wdr62 regulates mitotic progression of embryonic neural stem cells and brain size. *Nat Commun*. doi: 10.1038/ncomms4885.

Chen K, Lu Z, Wang X, Fu Y, Luo G-Z, Liu N, Han D, Dominissini D, Dai Q, Pan T, et al. 2015a. High-resolution N(6) -methyladenosine (m(6) A) map using photo-crosslinking-assisted m(6) A sequencing. *Angew Chem Int Ed Engl* **54**: 1587–90. doi: 10.1002/anie.201410647.

Chen Q, Cai ZK, Chen YB, Gu M, Zheng DC, Zhou J, Wang Z. 2015b. Poly r(C) binding protein-1 is central to maintenance of cancer stem cells in prostate cancer cells. *Cell Physiol Biochem*. doi: 10.1159/000373931.

Chen T, Hao Y-J, Zhang Y, Li M-M, Wang M, Han W, Wu Y, Lv Y, Hao J, Wang L, et al. 2015c. m6A RNA Methylation Is Regulated by MicroRNAs and Promotes Reprogramming to Pluripotency. *Cell Stem Cell* **16**: 289–301. doi: 10.1016/j.stem.2015.01.016.

Chi Z, Byrne ST, Dolinko A, Harraz MM, Kim MS, Umanah G, Zhong J, Chen R, Zhang J, Xu J,

et al. 2014. Botch Is a γ-Glutamyl Cyclotransferase that Deglycinates and Antagonizes Notch. *Cell Rep*. doi: 10.1016/j.celrep.2014.03.048.

Chi Z, Zhang J, Tokunaga A, Harraz MM, Byrne ST, Dolinko A, Xu J, Blackshaw S, Gaiano N, Dawson TM, et al. 2012. Botch Promotes Neurogenesis by Antagonizing Notch. *Dev Cell*. doi: 10.1016/j.devcel.2012.02.011.

Chia M, van Werven FJ. 2016. Temporal Expression of a Master Regulator Drives Synchronous Sporulation in Budding Yeast. *G3 (Bethesda)* **6**: 3553–3560. doi: 10.1534/g3.116.034983.

Chien CS, Wang ML, Chu PY, Chang YL, Liu WH, Yu CC, Lan YT, Huang PI, Lee YY, Chen YW, et al. 2015. Lin28B/Let-7 regulates expression of Oct4 and Sox2 and reprograms oral squamous cell carcinoma cells to a stem-like state. *Cancer Res*. doi: 10.1158/0008-5472.CAN-14-2215.

Chkheidze AN, Liebhaber SA. 2003. A Novel Set of Nuclear Localization Signals Determine Distributions of the CP RNA-Binding Proteins. *Mol Cell Biol*. doi: 10.1128/mcb.23.23.8405-8415.2003.

Choi HS, Hwang CK, Song KY, Law P-Y, Wei L-N, Loh HH. 2009. Poly(C)-binding proteins as transcriptional regulators of gene expression. *Biochem Biophys Res Commun* **380**: 431–6. doi: 10.1016/j.bbrc.2009.01.136.

Choi HS, Song KY, Hwang CK, Kim CS, Law PY, Wei LN, Loh HH. 2008. A proteomics approach for identification of single strand DNA-binding proteins involved in transcriptional regulation of mouse μ opioid receptor gene. *Mol Cell Proteomics*. doi: 10.1074/mcp.M800052-MCP200.

Church C, Moir L, McMurray F, Girard C, Banks GT, Teboul L, Wells S, Brüning JC, Nolan PM, Ashcroft FM, et al. 2010. Overexpression of Fto leads to increased food intake and results in obesity. *Nat Genet* **42**: 1086–1092. doi: 10.1038/ng.713.

Cieply B, Park JW, Nakauka-Ddamba A, Bebee TW, Guo Y, Shang X, Lengner CJ, Xing Y, Carstens RP. 2016. Multiphasic and Dynamic Changes in Alternative Splicing during Induction of Pluripotency Are Coordinated by Numerous RNA-Binding Proteins. *Cell Rep*. doi: 10.1016/j.celrep.2016.03.025.

Clancy MJ, Shambaugh ME, Timpte CS, Bokar JA. 2002. Induction of sporulation in Saccharomyces cerevisiae leads to the formation of N6-methyladenosine in mRNA: a potential mechanism for the activity of the IME4 gene. *Nucleic Acids Res* **30**: 4509–18.

Collart MA, Panasenko OO. 2017. The Ccr4-Not Complex: Architecture and Structural Insights. In *Sub-cellular biochemistry*, Vol. 83 of, pp. 349–379 doi: 10.1007/978-3-319-46503-6_13.

Collier AJ, Panula SP, Schell JP, Chovanec P, Plaza Reyes A, Petropoulos S, Corcoran AE, Walker R, Douagi I, Lanner F, et al. 2017. Comprehensive Cell Surface Protein Profiling Identifies Specific Markers of Human Naive and Primed Pluripotent States. *Cell Stem Cell*. doi: 10.1016/j.stem.2017.02.014.

Conway AE, Van Nostrand EL, Pratt GA, Aigner S, Wilbert ML, Sundararaman B, Freese P, Lambert NJ, Sathe S, Liang TY, et al. 2016. Enhanced CLIP Uncovers IMP Protein-RNA Targets in Human Pluripotent Stem Cells Important for Cell Adhesion and Survival. *Cell Rep* **15**: 666–679. doi: 10.1016/j.celrep.2016.03.052.

Cook KB, Kazan H, Zuberi K, Morris Q, Hughes TR. 2011. RBPDB: A database of RNA-binding specificities. *Nucleic Acids Res* **39**. doi: 10.1093/nar/gkq1069.

Copley MR, Babovic S, Benz C, Knapp DJHF, Beer PA, Kent DG, Wohrer S, Treloar DQ, Day C, Rowe K, et al. 2013. The Lin28b-let-7-Hmga2 axis determines the higher self-renewal potential of fetal haematopoietic stem cells. *Nat Cell Biol*. doi: 10.1038/ncb2783.

Cowling VH. 2019. CAPAM: The mRNA Cap Adenosine N6-Methyltransferase. *Trends Biochem Sci* **44**: 183–185. doi: 10.1016/j.tibs.2019.01.002.

Crane GM, Jeffery E, Morrison SJ. 2017. Adult haematopoietic stem cell niches. *Nat Rev Immunol* **17**: 573–590. doi: 10.1038/nri.2017.53.

Crisp PA, Ganguly DR, Smith AB, Murray KD, Estavillo GM, Searle I, Ford E, Bogdanović O, Lister R, Borevitz JO, et al. 2017. Rapid Recovery Gene Downregulation during Excess-Light Stress and Recovery in Arabidopsis. *Plant Cell* **29**: 1836–1863. doi: 10.1105/tpc.16.00828.

Cubillo EJ, Ngo SM, Juarez A, Gagan J, Lopez GD, Stout DA. 2018. Embryonic stem cell therapy applications for autoimmune, cardiovascular, and neurological diseases: A review. *AIMS Cell Tissue Eng* **1**: 191–223. doi: 10.3934/celltissue.2017.3.191.

Dai X, Wang T, Gonzalez G, Wang Y. 2018. Identification of YTH Domain-Containing Proteins as the Readers for *N* 1-Methyladenosine in RNA. *Anal Chem* **90**: 6380–6384. doi: 10.1021/acs.analchem.8b01703.

Darnell RB, Ke S, Darnell JE. 2018. Pre-mRNA processing includes N6 methylation of adenosine residues that are retained in mRNA exons and the fallacy of “RNA epigenetics”. *RNA* **24**: 262–267. doi: 10.1261/rna.065219.117.

Degrauwe N, Suvà M-LL, Janiszewska M, Riggi N, Stamenkovic I. 2016. *Imps: An RNA-binding protein family that provides a link between stem cell maintenance in normal development and cancer*. Cold Spring Harbor Laboratory Press doi: 10.1101/gad.287540.116.

Desrosiers R, Friderici K, Rottman F. 1974. Identification of methylated nucleosides in messenger RNA from Novikoff hepatoma cells. *Proc Natl Acad Sci U S A* **71**: 3971–5.

Dixon JR, Jung I, Selvaraj S, Shen Y, Antosiewicz-Bourget JE, Lee AY, Ye Z, Kim A, Rajagopal N, Xie W, et al. 2015. Chromatin architecture reorganization during stem cell differentiation. *Nature*. doi: 10.1038/nature14222.

Dixon JR, Selvaraj S, Yue F, Kim A, Li Y, Shen Y, Hu M, Liu JS, Ren B. 2012. Topological domains in mammalian genomes identified by analysis of chromatin interactions. *Nature*. doi: 10.1038/nature11082.

Dodson AE, Kennedy S. 2019. Germ Granules Coordinate RNA-Based Epigenetic Inheritance Pathways. *Dev Cell*. doi: 10.1016/J.DEVCEL.2019.07.025.

Domingues RG, Lago-Baldaia I, Pereira-Castro I, Fachini JM, Oliveira L, Drpic D, Lopes N, Henriques T, Neilson JR, Carmo AM, et al. 2016. CD5 expression is regulated during human T-cell activation by alternative polyadenylation, PTBP1, and miR-204. *Eur J Immunol*. doi: 10.1002/eji.201545663.

Dominissini D, Moshitch-Moshkovitz S, Schwartz S, Salmon-Divon M, Ungar L, Osenberg S, Cesarkas K, Jacob-Hirsch J, Amariglio N, Kupiec M, et al. 2012. Topology of the human and mouse m6A RNA methylomes revealed by m6A-seq. *Nature* **485**: 201–6. doi: 10.1038/nature11112.

Doxtader KA, Wang P, Scarborough AM, Seo D, Conrad NK, Nam Y. 2018. Structural Basis for Regulation of METTL16, an S-Adenosylmethionine Homeostasis Factor. *Mol Cell* **71**: 1001-1011.e4. doi: 10.1016/J.MOLCEL.2018.07.025.

Du H, Zhao Y, He J, Zhang Y, Xi H, Liu M, Ma J, Wu L. 2016a. YTHDF2 destabilizes m(6)A-containing RNA through direct recruitment of the CCR4-NOT deadenylase complex. *Nat Commun* **7**: 12626. doi: 10.1038/ncomms12626.

Du H, Zhao Y, He J, Zhang Y, Xi H, Liu M, Ma J, Wu L. 2016b. YTHDF2 destabilizes m6A-containing RNA through direct recruitment of the CCR4–NOT deadenylase complex. *Nat Commun* **7**: 12626. doi: 10.1038/ncomms12626.

Du M, Zhang Y, Mao Y, Mou J, Zhao J, Xue Q, Wang D, Huang J, Gao S, Gao Y. 2017. MiR-33a suppresses proliferation of NSCLC cells via targeting METTL3 mRNA. *Biochem Biophys Res Commun* **482**: 582–589. doi: 10.1016/J.BBRC.2016.11.077.

Du Y, Hou G, Zhang H, Dou J, He J, Guo Y, Li L, Chen R, Wang Y, Deng R, et al. 2018. SUMOylation of the m6A-RNA methyltransferase METTL3 modulates its function. *Nucleic Acids Res*. doi: 10.1093/nar/gky156.

Du Z, Fenn S, Tjhen R, James TL. 2008. Structure of a construct of a human poly(C)-binding protein containing the first and second KH domains reveals insights into its regulatory mechanisms. *J Biol Chem* **283**: 28757–66. doi: 10.1074/jbc.M803046200.

Du Z, Lee JK, Fenn S, Tjhen R, Stroud RM, James TL. 2007. X-ray crystallographic and NMR studies of protein-protein and protein-nucleic acid interactions involving the KH domains from human poly(C)-binding protein-2. *RNA*. doi: 10.1261/rna.410107.

Du Z, Lee JK, Tjhen R, Li S, Pan H, Stroud RM, James TL. 2005. Crystal structure of the first KH domain of human poly(C)-binding protein-2 in complex with a C-rich strand of human telomeric DNA at 1.7 A. *J Biol Chem* **280**: 38823–30. doi: 10.1074/jbc.M508183200.

Duan H-C, Wei L-H, Zhang C, Wang Y, Chen L, Lu Z, Chen PR, He C, Jia G. 2017. ALKBH10B Is an RNA N^6 -Methyladenosine Demethylase Affecting Arabidopsis Floral Transition. *Plant Cell* **29**: 2995–3011. doi: 10.1105/tpc.16.00912.

Dunham I, Kundaje A, Aldred SF, Collins PJ, Davis CA, Doyle F, Epstein CB, Frietze S, Harrow J, Kaul R, et al. 2012. An integrated encyclopedia of DNA elements in the human genome. *Nature*. doi: 10.1038/nature11247.

Durinck S, Spellman PT, Birney E, Huber W. 2009. Mapping identifiers for the integration of genomic datasets with the R/ Bioconductor package biomaRt. *Nat Protoc*. doi: 10.1038/nprot.2009.97.

Ebert MS, Sharp PA. 2012. Roles for MicroRNAs in Conferring Robustness to Biological Processes. *Cell* **149**: 515–524. doi: 10.1016/j.cell.2012.04.005.

Eckersley-Maslin MA, Alda-Catalinas C, Reik W. 2018. Dynamics of the epigenetic landscape during the maternal-to-zygotic transition. *Nat Rev Mol Cell Biol* **19**: 436–450. doi: 10.1038/s41580-018-0008-z.

Edens BM, Vissers C, Su J, Arumugam S, Xu Z, Shi H, Miller N, Rojas Ringeling F, Ming G, He C, et al. 2019. FMRP Modulates Neural Differentiation through m6A-Dependent mRNA Nuclear Export. *Cell Rep*. doi: 10.1016/j.celrep.2019.06.072.

Edupuganti RR, Geiger S, Lindeboom RGH, Shi H, Hsu PJ, Lu Z, Wang S-Y, Baltissen MPA, Jansen PWTC, Rossa M, et al. 2017. N6-methyladenosine (m6A) recruits and repels proteins to regulate mRNA homeostasis. *Nat Struct Mol Biol* **24**: 870–878. doi: 10.1038/nsmb.3462.

Eichelbaum K, Krijgsveld J. 2014. Rapid temporal dynamics of transcription, protein synthesis, and secretion during macrophage activation. *Mol Cell Proteomics* **13**: 792–810. doi: 10.1074/mcp.M113.030916.

Eiring AM, Harb JG, Neviani P, Garton C, Oaks JJ, Spizzo R, Liu S, Schwind S, Santhanam R, Hickey CJ, et al. 2010. miR-328 Functions as an RNA Decoy to Modulate hnRNP E2 Regulation of mRNA Translation in Leukemic Blasts. *Cell*. doi: 10.1016/j.cell.2010.01.007.

Emani MR, Närvä E, Stubb A, Chakroborty D, Viitala M, Rokka A, Rahkonen N, Moulder R, Denessiouk K, Trokovic R, et al. 2015. The L1TD1 protein interactome reveals the importance of post-transcriptional regulation in human pluripotency. *Stem Cell Reports*. doi: 10.1016/j.stemcr.2015.01.014.

Engel M, Eggert C, Kaplick PM, Eder M, Röh S, Tietze L, Namendorf C, Arloth J, Weber P, Rex-Haffner M, et al. 2018. The Role of m6A/m-RNA Methylation in Stress Response Regulation. *Neuron* **99**: 389-403.e9. doi: 10.1016/j.neuron.2018.07.009.

Espinoza-Lewis RA, Yang Q, Liu J, Huang ZP, Hu X, Chen D, Wang DZ. 2017. Poly(C)-binding protein 1 (Pcbp1) regulates skeletal muscle differentiation by modulating microRNA processing in myoblasts. *J Biol Chem*. doi: 10.1074/jbc.M116.773671.

Evdokimova V, Ruzanov P, Anglesio MS, Sorokin A V., Ovchinnikov LP, Buckley J, Triche TJ, Sonenberg N, Sorensen PHB. 2006. Akt-Mediated YB-1 Phosphorylation Activates Translation of Silent mRNA Species. *Mol Cell Biol*. doi: 10.1128/mcb.26.1.277-292.2006.

Evdokimova V, Tognon C, Ng T, Ruzanov P, Melnyk N, Fink D, Sorokin A, Ovchinnikov LP, Davicioni E, Triche TJ, et al. 2009. Translational Activation of Snail1 and Other Developmentally Regulated Transcription Factors by YB-1 Promotes an Epithelial-Mesenchymal Transition. *Cancer Cell*. doi: 10.1016/j.ccr.2009.03.017.

Fawcett KA, Barroso I. 2010. The genetics of obesity: FTO leads the way. *Trends Genet* **26**: 266–274. doi: 10.1016/J.TIG.2010.02.006.

Fedeles BI, Singh V, Delaney JC, Li D, Essigmann JM. 2015. The AlkB Family of Fe(II)/α-Ketoglutarate-dependent Dioxygenases: Repairing Nucleic Acid Alkylation Damage and Beyond. *J Biol Chem* **290**: 20734–20742. doi: 10.1074/jbc.R115.656462.

Feng C, Liu Y, Wang G, Deng Z, Zhang Q, Wu W, Tong Y, Cheng C, Chen Z. 2014a. Crystal structures of the human RNA demethylase Alkbh5 reveal basis for substrate recognition. *J Biol Chem* **289**: 11571–83. doi: 10.1074/jbc.M113.546168.

Feng N, Han Q, Li J, Wang S, Li H, Yao X, Zhao RC. 2014b. Generation of Highly Purified Neural Stem Cells from Human Adipose-Derived Mesenchymal Stem Cells by *Sox1* Activation. *Stem Cells Dev* **23**: 515–529. doi: 10.1089/scd.2013.0263.

Fenger-Grøn M, Fillman C, Norrild B, Lykke-Andersen J. 2005. Multiple processing body factors and the ARE binding protein TTP activate mRNA decapping. *Mol Cell*. doi: 10.1016/j.molcel.2005.10.031.

Fenn S, Du Z, Lee JK, Tjhen R, Stroud RM, James TL. 2007. Crystal structure of the third KH domain of human poly(C)-binding protein-2 in complex with a C-rich strand of human telomeric DNA at 1.6 A resolution. *Nucleic Acids Res* **35**: 2651–2660. doi: 10.1093/nar/gkm139.

Festuccia N, Osorno R, Halbritter F, Karwacki-Neisius V, Navarro P, Colby D, Wong F, Yates A, Tomlinson SR, Chambers I. 2012. Esrrb is a direct Nanog target gene that can substitute for Nanog function in pluripotent cells. *Cell Stem Cell*. doi: 10.1016/j.stem.2012.08.002.

Fisher CL, Fisher AG. 2011. Chromatin states in pluripotent, differentiated, and reprogrammed cells. *Curr Opin Genet Dev*. doi: 10.1016/j.gde.2011.01.015.

Fiszbein A, Kornblihtt AR. 2017. Alternative splicing switches: Important players in cell differentiation. *BioEssays*. doi: 10.1002/bies.201600157.

Ford LP, Watson J, Keene JD, Wilusz J. 1999. ELAV proteins stabilize deadenylated intermediates in a novel in vitro mRNA deadenylation/degradation system. *Genes Dev*. doi: 10.1101/gad.13.2.188.

Fort A, Hashimoto K, Yamada D, Salimullah M, Keya CA, Saxena A, Bonetti A, Voineagu I, Bertin N, Kratz A, et al. 2014. Deep transcriptome profiling of mammalian stem cells supports a regulatory role for retrotransposons in pluripotency maintenance. *Nat Genet*. doi: 10.1038/ng.2965.

Fotovati A, Abu-Ali S, Wang PS, Deleyrolle LP, Lee C, Triscott J, Chen JY, Franciosi S,

Nakamura Y, Sugita Y, et al. 2011. YB-1 bridges neural stem cells and brain tumor-initiating cells via its roles in differentiation and cell growth. *Cancer Res*. doi: 10.1158/0008-5472.CAN-10-2805.

Franks TM, Lykke-Andersen J. 2007. TTP and BRF proteins nucleate processing body formation to silence mRNAs with AU-rich elements. *Genes Dev*. doi: 10.1101/gad.1494707.

Fu Y, Jia G, Pang X, Wang RN, Wang X, Li CJ, Smemo S, Dai Q, Bailey KA, Nobrega MA, et al. 2013. FTO-mediated formation of N6-hydroxymethyladenosine and N6-formyladenosine in mammalian RNA. *Nat Commun* **4**: 1798. doi: 10.1038/ncomms2822.

Fu Y, Zhuang X. 2019. m6A-binding YTHDF proteins promote stress granule formation by modulating phase separation of stress granule proteins. *bioRxiv* 694455. doi: 10.1101/694455.

Gafni O, Weinberger L, Mansour AA, Manor YS, Chomsky E, Ben-Yosef D, Kalma Y, Viukov S, Maza I, Zviran A, et al. 2013. Derivation of novel human ground state naive pluripotent stem cells. *Nature*. doi: 10.1038/nature12745.

Galganski L, Urbanek MO, Krzyzosiak WJ. 2017. Nuclear speckles: molecular organization, biological function and role in disease. *Nucleic Acids Res* **45**: 10350–10368. doi: 10.1093/nar/gkx759.

Gao FB, Keene JD. 1996. Hel-N1/Hel-N2 proteins are bound to poly(A)+ mRNA in granular RNP structures and are implicated in neuronal differentiation. *J Cell Sci*.

Gao Y, Pei G, Li D, Li R, Shao Y, Zhang QC, Li P. 2019. Multivalent m6A motifs promote phase separation of YTHDF proteins. *Cell Res* 1–3. doi: 10.1038/s41422-019-0210-3.

Garcia-Campos MA, Edelheit S, Toth U, Safra M, Shachar R, Viukov S, Winkler R, Nir R, Lasman L, Brandis A, et al. 2019a. Deciphering the “m6A Code” via Antibody-Independent Quantitative Profiling. *Cell*. doi: 10.1016/j.cell.2019.06.013.

Garcia-Campos MA, Edelheit S, Toth U, Shachar R, Nir R, Lasman L, Brandis A, Hanna JH, Rossmanith W, Schwartz S. 2019b. Deciphering the ‘m6A code’ via quantitative profiling of m6A at single-nucleotide resolution. *bioRxiv* 571679. doi: 10.1101/571679.

Gerstberger S, Hafner M, Tuschl T. 2014. A census of human RNA-binding proteins. *Nat Rev Genet*. doi: 10.1038/nrg3813.

Geula S, Moshitch-Moshkovitz S, Dominissini D, Mansour AA, Kol N, Salmon-Divon M, Hershkovitz V, Peer E, Mor N, Manor YS, et al. 2015. m6A mRNA methylation facilitates resolution of naïve pluripotency toward differentiation. *Science* **347**: 1002–6. doi: 10.1126/science.1261417.

Ghanem LR, Kromer A, Silverman IM, Chatterji P, Traxler E, Penzo-Mendez A, Weiss MJ, Stanger BZ, Liebhaber SA. 2015. The Poly(C) binding protein Pcbp2, and its retrotransposed derivative Pcbp1, are independently essential to mouse development. *Mol*

Cell Biol. doi: 10.1128/mcb.00936-15.

Ghanem LR, Kromer A, Silverman IM, Ji X, Gazzara M, Nguyen N, Aguilar G, Martinelli M, Barash Y, Liebhaber SA. 2018. The Poly(C)-binding protein, Pcbp2, enables differentiation of definitive erythropoiesis by directing functional splicing of the Runx1 transcript. *Mol Cell Biol*. doi: 10.1128/mcb.00175-18.

Gifford CA, Ziller MJ, Gu H, Trapnell C, Donaghey J, Tsankov A, Shalek AK, Kelley DR, Shishkin AA, Issner R, et al. 2013. Transcriptional and epigenetic dynamics during specification of human embryonic stem cells. *Cell*. doi: 10.1016/j.cell.2013.04.037.

Gilbertson S, Federspiel JD, Hartenian E, Cristea IM, Glaunsinger B. 2018. Changes in mRNA abundance drive shuttling of RNA binding proteins, linking cytoplasmic RNA degradation to transcription. *Elife*. doi: 10.7554/eLife.37663.

Git A, Dvinge H, Salmon-Divon M, Osborne M, Kutter C, Hadfield J, Bertone P, Caldas C. 2010. Systematic comparison of microarray profiling, real-time PCR, and next-generation sequencing technologies for measuring differential microRNA expression. *RNA* **16**: 991–1006. doi: 10.1261/rna.1947110.

Giudice G, Sánchez-Cabo F, Torroja C, Lara-Pezzi E. 2016. ATtRACT-a database of RNA-binding proteins and associated motifs. *Database*. doi: 10.1093/database/baw035.

Godoy P, Schmidt-Heck W, Hellwig B, Nell P, Feuerborn D, Rahnenführer J, Kattler K, Walter J, Blüthgen N, Hengstler JG. 2018. Assessment of stem cell differentiation based on genome-wide expression profiles. *Philos Trans R Soc B Biol Sci* **373**: 20170221. doi: 10.1098/rstb.2017.0221.

Grigor'eva EV, Malankhanova TB, Surumbayeva A, Minina JM, Morozov VV, Abramycheva NY, Illarioshkin SN, Malakhova AA, Zakian SM. 2019. Generation of induced pluripotent stem cell line, ICGi007-A, by reprogramming peripheral blood mononuclear cells from a patient with Huntington's disease. *Stem Cell Res* **34**: 101382. doi: 10.1016/j.scr.2018.101382.

Grudzien-Nogalska E, Kiledjian M. 2017. New insights into decapping enzymes and selective mRNA decay. *Wiley Interdiscip Rev RNA* **8**: e1379. doi: 10.1002/wrna.1379.

Guo C, Xue Y, Yang G, Yin S, Shi W, Cheng Y, Yan X, Fan S, Zhang H, Zeng F. 2016. Nanog RNA-binding proteins YBX1 and ILF3 affect pluripotency of embryonic stem cells. *Cell Biol Int*. doi: 10.1002/cbin.10539.

Guo J, Tang H-W, Li J, Perrimon N, Yan D. 2018. Xio is a component of the Drosophila sex determination pathway and RNA N6-methyladenosine methyltransferase complex. *Proc Natl Acad Sci U S A* **115**: 3674–3679. doi: 10.1073/pnas.1720945115.

Guttman M, Donaghey J, Carey BW, Garber M, Grenier JK, Munson G, Young G, Lucas AB, Ach R, Bruhn L, et al. 2011. LincRNAs act in the circuitry controlling pluripotency and differentiation. *Nature*. doi: 10.1038/nature10398.

Hadian K, Vincendeau M, Mäusbacher N, Nagel D, Hauck SM, Ueffing M, Loyter A, Werner T,

Wolff H, Brack-Werner R. 2009. Identification of a heterogeneous nuclear ribonucleoprotein-recognition region in the HIV rev protein. *J Biol Chem*. doi: 10.1074/jbc.M109.021659.

Hafner M, Landthaler M, Burger L, Khorshid M, Hausser J, Berninger P, Rothballer A, Ascano M, Jungkamp A-C, Munschauer M, et al. 2010. Transcriptome-wide Identification of RNA-Binding Protein and MicroRNA Target Sites by PAR-CLIP. *Cell* **141**: 129–141. doi: 10.1016/j.cell.2010.03.009.

Hainer SJ, Bošković A, McCannell KN, Rando OJ, Fazzio TG. 2019. Profiling of Pluripotency Factors in Single Cells and Early Embryos. *Cell*. doi: 10.1016/j.cell.2019.03.014.

Han H, Irimia M, Ross PJ, Sung HK, Alipanahi B, David L, Golipour A, Gabut M, Michael IP, Nachman EN, et al. 2013a. MBNL proteins repress ES-cell-specific alternative splicing and reprogramming. *Nature*. doi: 10.1038/nature12270.

Han W, Xin Z, Zhao Z, Bao W, Lin X, Yin B, Zhao J, Yuan J, Qiang B, Peng X. 2013b. RNA-binding protein PCBP2 modulates glioma growth by regulating FHL3. *J Clin Invest*. doi: 10.1172/JCI61820.

Harikumar A, Meshorer E. 2015. Chromatin remodeling and bivalent histone modifications in embryonic stem cells. *EMBO Rep*. doi: 10.15252/embr.201541011.

Harvey RF, Smith TS, Mulroney T, Queiroz RML, Pizzinga M, Dezi V, Villenueva E, Ramakrishna M, Lilley KS, Willis AE. 2018. Trans-acting translational regulatory RNA binding proteins. *Wiley Interdiscip Rev RNA*. doi: 10.1002/wrna.1465.

Hau HH, Walsh RJ, Ogilvie RL, Williams DA, Reilly CS, Bohjanen PR. 2007. Tristetraprolin recruits functional mRNA decay complexes to ARE sequences. *J Cell Biochem*. doi: 10.1002/jcb.21130.

Hausburg MA, Doles JD, Clement SL, Cadwallader AB, Hall MN, Blackshear PJ, Lykke-Andersen J, Olwin BB. 2015. Post-transcriptional regulation of satellite cell quiescence by TTP-mediated mRNA decay. *Elife*. doi: 10.7554/eLife.03390.

Haussmann IU, Bodi Z, Sanchez-Moran E, Mongan NP, Archer N, Fray RG, Soller M. 2016. m6A potentiates Sxl alternative pre-mRNA splicing for robust Drosophila sex determination. *Nature* **540**: 301–304. doi: 10.1038/nature20577.

Heck AM, Wilusz CJ. 2019. Small changes, big implications: The impact of m6A RNA methylation on gene expression in pluripotency and development. *Biochim Biophys Acta - Gene Regul Mech*. doi: 10.1016/j.bbagrm.2019.07.003.

Hentze MW, Castello A, Schwarzl T, Preiss T. 2018. A brave new world of RNA-binding proteins. *Nat Rev Mol Cell Biol*. doi: 10.1038/nrm.2017.130.

Hess ME, Hess S, Meyer KD, Verhagen LAW, Koch L, Brönneke HS, Dietrich MO, Jordan SD, Saletore Y, Elemento O, et al. 2013. The fat mass and obesity associated gene (Fto) regulates activity of the dopaminergic midbrain circuitry. *Nat Neurosci* **16**: 1042–1048. doi:

10.1038/nn.3449.

Hirose T, Virnicchi G, Tanigawa A, Naganuma T, Li R, Kimura H, Yokoi T, Nakagawa S, Bénard M, Fox AH, et al. 2014. NEAT1 long noncoding RNA regulates transcription via protein sequestration within subnuclear bodies. *Mol Biol Cell*. doi: 10.1091/mbc.E13-09-0558.

Ho JJD, Robb GB, Tai SC, Turgeon PJ, Mawji IA, Man HSJ, Marsden PA. 2013. Active Stabilization of Human Endothelial Nitric Oxide Synthase mRNA by hnRNP E1 Protects against Antisense RNA and MicroRNAs. *Mol Cell Biol*. doi: 10.1128/mcb.01257-12.

Hong S. 2017. RNA Binding Protein as an Emerging Therapeutic Target for Cancer Prevention and Treatment. *J Cancer Prev*. doi: 10.15430/jcp.2017.22.4.203.

Hongay CF, Orr-Weaver TL. 2011. Drosophila Inducer of MEiosis 4 (IME4) is required for Notch signaling during oogenesis. *Proc Natl Acad Sci* **108**: 14855–14860. doi: 10.1073/pnas.1111577108.

Hou P, Li L, Chen F, Chen Y, Liu H, Li J, Bai J, Zheng J. 2018. PTBP3-Mediated regulation of zeb1 mRNA stability promotes epithelial–mesenchymal transition in breast cancer. *Cancer Res*. doi: 10.1158/0008-5472.CAN-17-0883.

Hsu PJ, Zhu Y, Ma H, Guo Y, Shi X, Liu Y, Qi M, Lu Z, Shi H, Wang J, et al. 2017. Ythdc2 is an N6-methyladenosine binding protein that regulates mammalian spermatogenesis. *Cell Res*. doi: 10.1038/cr.2017.99.

Huang DW, Sherman BT, Lempicki RA. 2009a. Bioinformatics enrichment tools: paths toward the comprehensive functional analysis of large gene lists. *Nucleic Acids Res* **37**: 1–13. doi: 10.1093/nar/gkn923.

Huang DW, Sherman BT, Lempicki RA. 2009b. Systematic and integrative analysis of large gene lists using DAVID bioinformatics resources. *Nat Protoc* **4**: 44–57. doi: 10.1038/nprot.2008.211.

Huang H, Weng H, Sun W, Qin X, Shi H, Wu H, Zhao BS, Mesquita A, Liu C, Yuan CL, et al. 2018a. Recognition of RNA N6-methyladenosine by IGF2BP proteins enhances mRNA stability and translation. *Nat Cell Biol* **20**: 285–295. doi: 10.1038/s41556-018-0045-z.

Huang H, Weng H, Zhou K, Wu T, Zhao BS, Sun M, Chen Z, Deng X, Xiao G, Auer F, et al. 2019. Histone H3 trimethylation at lysine 36 guides m6A RNA modification co-transcriptionally. *Nature* 1. doi: 10.1038/s41586-019-1016-7.

Huang J, Dong X, Gong Z, Qin L-Y, Yang S, Zhu Y-L, Wang X, Zhang D, Zou T, Yin P, et al. 2018b. Solution structure of the RNA recognition domain of METTL3-METTL14 N6-methyladenosine methyltransferase. *Protein Cell* 1–13. doi: 10.1007/s13238-018-0518-7.

Huang T-C, Renuse S, Pinto S, Kumar P, Yang Y, Chaerkady R, Godsey B, Mendell JT, Halushka MK, Civin CI, et al. 2015a. Identification of miR-145 targets through an integrated omics analysis. *Mol Biosyst* **11**: 197–207. doi: 10.1039/c4mb00585f.

Huang Y, Xiong Y, Lin Z, Feng X, Jiang X, Songyang Z, Huang J. 2015b. Specific tandem 3'UTR patterns and gene expression profiles in mouse Thy1+ germline stem cells. *PLoS One*. doi: 10.1371/journal.pone.0145417.

Huntzinger E, Kuzuoğlu-Öztürk D, Braun JE, Eulalio A, Wohlbold L, Izaurralde E. 2013. The interactions of GW182 proteins with PABP and deadenylases are required for both translational repression and degradation of miRNA targets. *Nucleic Acids Res*. doi: 10.1093/nar/gks1078.

Hurrell T, Segeritz CP, Vallier L, Lilley KS, Cromarty AD. 2019. A proteomic time course through the differentiation of human induced pluripotent stem cells into hepatocyte-like cells. *Sci Rep*. doi: 10.1038/s41598-019-39400-1.

Hwang CK, Wagley Y, Law PY, Wei LN, Loh HH. 2017. Phosphorylation of poly(rC) binding protein 1 (PCBP1) contributes to stabilization of mu opioid receptor (MOR) mRNA via interaction with AU-rich element RNA-binding protein 1 (AUF1) and poly A binding protein (PABP). *Gene*. doi: 10.1016/j.gene.2016.11.003.

Imai Y, Matsuo N, Ogawa S, Tohyama M, Takagi T. 1998. Cloning of a gene, YT521, for a novel RNA splicing-related protein induced by hypoxia/reoxygenation. *Mol Brain Res* **53**: 33–40. doi: 10.1016/S0169-328X(97)00262-3.

Ishiguro K, Watanabe O, Nakamura M, Yamamura T, Matsushita M, Goto H, Hirooka Y. 2017. Combinational use of lipid-based reagents for efficient transfection of primary fibroblasts and hepatoblasts. *Biotechniques*. doi: 10.2144/000114569.

Itskovitz-Eldor J, Schuldiner M, Karsenti D, Eden A, Yanuka O, Amit M, Soreq H, Benvenisty N. 2000. Differentiation of human embryonic stem cells into embryoid bodies compromising the three embryonic germ layers. *Mol Med*.

Ivanova I, Much C, Di Giacomo M, Azzi C, Morgan M, Moreira PN, Monahan J, Carrieri C, Enright AJ, O'Carroll D. 2017. The RNA m 6 A Reader YTHDF2 Is Essential for the Post-transcriptional Regulation of the Maternal Transcriptome and Oocyte Competence. *Mol Cell*. doi: 10.1016/j.molcel.2017.08.003.

Iwakawa H oki, Tomari Y. 2015. The Functions of MicroRNAs: mRNA Decay and Translational Repression. *Trends Cell Biol*. doi: 10.1016/j.tcb.2015.07.011.

Jain AK, Xi Y, McCarthy R, Allton K, Akdemir KC, Patel LR, Aronow B, Lin C, Li W, Yang L, et al. 2016. LncPRESS1 Is a p53-Regulated LncRNA that Safeguards Pluripotency by Disrupting SIRT6-Mediated De-acetylation of Histone H3K56. *Mol Cell*. doi: 10.1016/j.molcel.2016.10.039.

James D, Levine AJ, Besser D, Hemmati-Brivanlou A. 2005. TGFβ/activin/nodal signaling is necessary for the maintenance of pluripotency in human embryonic stem cells. *Development*. doi: 10.1242/dev.01706.

Jern P, Sperber GO, Ahlsen G, Blomberg J. 2005. Sequence Variability, Gene Structure, and Expression of Full-Length Human Endogenous Retrovirus H. *J Virol*. doi: 10.1128/jvi.79.10.6325-6337.2005.

Jern P, Sperber GO, Blomberg J. 2004. Definition and variation of human endogenous retrovirus H. *Virology*. doi: 10.1016/j.virol.2004.06.023.

Ji X, Humenik J, Yang D, Liebhaber SA. 2018. PolyC-binding proteins enhance expression of the CDK2 cell cycle regulatory protein via alternative splicing. *Nucleic Acids Res*. doi: 10.1093/nar/gkx1255.

Ji X, Wan J, Vishnu M, Xing Y, Liebhaber SA. 2013. αCP Poly(C) Binding Proteins Act as Global Regulators of Alternative Polyadenylation. *Mol Cell Biol*. doi: 10.1128/mcb.01380-12.

Ji Z, Tian B. 2009. Reprogramming of 3' Untranslated Regions of mRANs by Alternative Polyadenylation in Generation of Pluripotent Stem Cells from Different Cell Types. *PLoS One*. doi: 10.1371/journal.pone.0008419.

Jia G, Fu Y, Zhao X, Dai Q, Zheng G, Yang YY-G, Yi C, Lindahl T, Pan T, Yang YY-G, et al. 2011. N6-methyladenosine in nuclear RNA is a major substrate of the obesity-associated FTO. *Nat Chem Biol* **7**: 885–7. doi: 10.1038/nchembio.687.

Jiao X, Doamekpor SK, Bird JG, Nickels BE, Tong L, Hart RP, Kiledjian M. 2017. 5' End Nicotinamide Adenine Dinucleotide Cap in Human Cells Promotes RNA Decay through DXO-Mediated deNADding. *Cell* **168**: 1015-1027.e10. doi: 10.1016/j.cell.2017.02.019.

Jin F, Li Y, Dixon JR, Selvaraj S, Ye Z, Lee AY, Yen CA, Schmitt AD, Espinoza CA, Ren B. 2013. A high-resolution map of the three-dimensional chromatin interactome in human cells. *Nature*. doi: 10.1038/nature12644.

Jing Q, Huang S, Guth S, Zarubin T, Motoyama A, Chen J, Di Padova F, Lin SC, Gram H, Han J. 2005. Involvement of MicroRNA in AU-Rich Element-Mediated mRNA Instability. *Cell* **120**: 623–634. doi: 10.1016/j.cell.2004.12.038.

Jonas S, Christie M, Peter D, Bhandari D, Loh B, Huntzinger E, Weichenrieder O, Izaurralde E. 2014. An asymmetric PAN3 dimer recruits a single PAN2 exonuclease to mediate mRNA deadenylation and decay. *Nat Struct Mol Biol* **21**: 599–608. doi: 10.1038/nsmb.2837.

Jonas S, Izaurralde E. 2015. Towards a molecular understanding of microRNA-mediated gene silencing. *Nat Rev Genet*. doi: 10.1038/nrg3965.

Jones CI, Zabolotskaya MV, Newbury SF. 2012. The 5′ → 3′ exoribonuclease XRN1/Pacman and its functions in cellular processes and development. *Wiley Interdiscip Rev RNA* **3**: 455–468. doi: 10.1002/wrna.1109.

Ju Lee H, Bartsch D, Xiao C, Guerrero S, Ahuja G, Schindler C, Moresco JJ, Yates JR, Gebauer F, Bazzi H, et al. 2017. A post-transcriptional program coordinated by CSDE1 prevents intrinsic neural differentiation of human embryonic stem cells. *Nat Commun*. doi: 10.1038/s41467-017-01744-5.

Kalkan T, Olova N, Roode M, Mulas C, Lee HJ, Nett I, Marks H, Walker R, Stunnenberg HG, Lilley KS, et al. 2017. Tracking the embryonic stem cell transition from ground state

pluripotency. *Dev*. doi: 10.1242/dev.142711.

Kami D, Kitani T, Nakamura A, Wakui N, Mizutani R, Ohue M, Kametani F, Akimitsu N, Gojo S. 2018. The DEAD-box RNA-binding protein DDX6 regulates parental RNA decay for cellular reprogramming to pluripotency ed. Y.K. Kim. *PLoS One* **13**: e0203708. doi: 10.1371/journal.pone.0203708.

Kan L, Grozhik A V., Vedanayagam J, Patil DP, Pang N, Lim K-S, Huang Y-C, Joseph B, Lin C-J, Despic V, et al. 2017. The m6A pathway facilitates sex determination in Drosophila. *Nat Commun* **8**: 15737. doi: 10.1038/ncomms15737.

Karagiannis P. 2019. Clinical Potential of Induced Pluripotent Stem Cells. In *Medical Applications of iPS Cells* (eds. H. Inoue and Y. Nakamura), pp. 3–12, Springer, Singapore doi: 10.1007/978-981-13-3672-0_1.

Kasowitz SD, Ma J, Anderson SJ, Leu NA, Xu Y, Gregory BD, Schultz RM, Wang PJ. 2018. Nuclear m6A reader YTHDC1 regulates alternative polyadenylation and splicing during mouse oocyte development ed. W. Yan. *PLOS Genet* **14**: e1007412. doi: 10.1371/journal.pgen.1007412.

Ke S, Pandya-Jones A, Saito Y, Fak JJ, Vågbø CB, Geula S, Hanna JH, Black DL, Darnell JE, Darnell RB. 2017. m(6)A mRNA modifications are deposited in nascent pre-mRNA and are not required for splicing but do specify cytoplasmic turnover. *Genes Dev* **31**: 990–1006. doi: 10.1101/gad.301036.117.

Khatau SB, Kusuma S, Hanjaya-Putra D, Mali P, Cheng L, Lee JSH, Gerecht S, Wirtz D. 2012. The differential formation of the LINC-mediated perinuclear actin cap in pluripotent and somatic cells. *PLoS One* **7**: e36689. doi: 10.1371/journal.pone.0036689.

Kim D, Pertea G, Trapnell C, Pimentel H, Kelley R, Salzberg SL. 2013. TopHat2: accurate alignment of transcriptomes in the presence of insertions, deletions and gene fusions. *Genome Biol* **14**: R36. doi: 10.1186/gb-2013-14-4-r36.

Kim J, Abdelmohsen K, Yang X, De S, Grammatikakis I, Noh JH, Gorospe M. 2016. LncRNA OIP5-AS1/cyrano sponges RNA-binding protein HuR. *Nucleic Acids Res*. doi: 10.1093/nar/gkw017.

Kim YK. 2001. La autoantigen enhances translation of BiP mRNA. *Nucleic Acids Res*. doi: 10.1093/nar/29.24.5009.

Knuckles P, Carl SH, Musheev M, Niehrs C, Wenger A, Bühler M. 2017. RNA fate determination through cotranscriptional adenosine methylation and microprocessor binding. *Nat Struct Mol Biol*. doi: 10.1038/nsmb.3419.

Knuckles P, Lence T, Haussmann IU, Jacob D, Kreim N, Carl SH, Masiello I, Hares T, Villaseñor R, Hess D, et al. 2018. Zc3h13/Flacc is required for adenosine methylation by bridging the mRNA-binding factor Rbm15/Spenito to the m ^{6} A machinery component Wtap/Fl(2)d. *Genes Dev*. doi: 10.1101/gad.309146.117.

Knutson AK, Egelhofer T, Rechtsteiner A, Strome S. 2017. Germ granules prevent accumulation of somatic transcripts in the adult Caenorhabditis elegans germline. *Genetics*. doi: 10.1534/genetics.116.198549.

Kowalinski E, Kögel A, Ebert J, Reichelt P, Stegmann E, Habermann B, Conti E. 2016. Structure of a Cytoplasmic 11-Subunit RNA Exosome Complex. *Mol Cell* **63**: 125–134. doi: 10.1016/j.molcel.2016.05.028.

Kretschmer J, Rao H, Hackert P, Sloan KE, Höbartner C, Bohnsack MT. 2018. The m6A reader protein YTHDC2 interacts with the small ribosomal subunit and the 5'-3' exoribonuclease XRN1. *RNA* rna.064238.117. doi: 10.1261/rna.064238.117.

Kuang YL, Munoz A, Nalula G, Santostefano KE, Sanghez V, Sanchez G, Terada N, Mattis AN, Iacovino M, Iribarren C, et al. 2019. Evaluation of commonly used ectoderm markers in iPSC trilineage differentiation. *Stem Cell Res*. doi: 10.1016/j.scr.2019.101434.

Kurimoto K, Yabuta Y, Hayashi K, Ohta H, Kiyonari H, Mitani T, Moritoki Y, Kohri K, Kimura H, Yamamoto T, et al. 2015. Quantitative dynamics of chromatin remodeling during germ cell specification from mouse embryonic stem cells. *Cell Stem Cell*. doi: 10.1016/j.stem.2015.03.002.

Küspert M, Murakawa Y, Schäffler K, Vanselow JT, Wolf E, Juranek S, Schlosser A, Landthaler M, Fischer U. 2015. LARP4B is an AU-rich sequence associated factor that promotes mRNA accumulation and translation. *RNA*. doi: 10.1261/rna.051441.115.

Łabno A, Tomecki R, Dziembowski A. 2016. Cytoplasmic RNA decay pathways - Enzymes and mechanisms. *Biochim Biophys Acta - Mol Cell Res* **1863**: 3125–3147. doi: 10.1016/j.bbamcr.2016.09.023.

Lackford B, Yao C, Charles GM, Weng L, Zheng X, Choi EA, Xie X, Wan J, Xing Y, Freudenberg JM, et al. 2014. Fip1 regulates mRNA alternative polyadenylation to promote stem cell self-renewal. *EMBO J*. doi: 10.1002/embj.201386537.

Lafontaine D, Vandenhaute J, Tollervey D. 1995. The 18S rRNA dimethylase Dim1p is required for pre-ribosomal RNA processing in yeast. *Genes Dev* **9**: 2470–81.

Lai WS, Carrick DM, Blackshear PJ. 2005. Influence of nonameric AU-rich tristetraprolin-binding sites on mRNA deadenylation and turnover. *J Biol Chem*. doi: 10.1074/jbc.M506757200.

Langmead B, Salzberg SL. 2012. Fast gapped-read alignment with Bowtie 2. *Nat Methods* **9**: 357–359. doi: 10.1038/nmeth.1923.

Lao N, Barron N. 2019. Cross-talk between m6A and m1A regulators, YTHDF2 and ALKBH3 fine-tunes mRNA expression. *bioRxiv* 589747. doi: 10.1101/589747.

Latos PA, Goncalves A, Oxley D, Mohammed H, Turro E, Hemberger M. 2015. Fgf and Esrrb integrate epigenetic and transcriptional networks that regulate self-renewal of trophoblast stem cells. *Nat Commun*. doi: 10.1038/ncomms8776.

Le Sommer C, Lesimple M, Mereau A, Menoret S, Allo M-R, Hardy S. 2005. PTB Regulates the Processing of a 3'-Terminal Exon by Repressing both Splicing and Polyadenylation. *Mol Cell Biol*. doi: 10.1128/mcb.25.21.9595-9607.2005.

Lee G, Kim H, Elkabetz Y, Al Shamy G, Panagiotakos G, Barberi T, Tabar V, Studer L. 2007. Isolation and directed differentiation of neural crest stem cells derived from human embryonic stem cells. *Nat Biotechnol*. doi: 10.1038/nbt1365.

Lee S, Kopp F, Chang TC, Sataluri A, Chen B, Sivakumar S, Yu H, Xie Y, Mendell JT. 2016. Noncoding RNA NORAD Regulates Genomic Stability by Sequestering PUMILIO Proteins. *Cell*. doi: 10.1016/j.cell.2015.12.017.

Leffers H, Dejgaard K, Celis JE. 1995. Characterisation of two major cellular poly(rC)-binding human proteins, each containing three K-homologous (KH) domains. *Eur J Biochem* **230**: 447–53.

Leidgens S, Bullough KZ, Shi H, Li F, Shakoury-Elizeh M, Yabe T, Subramanian P, Hsu E, Natarajan N, Nandal A, et al. 2013. Each member of the poly-r(C)-binding protein 1 (PCBP) family exhibits iron chaperone activity toward ferritin. *J Biol Chem*. doi: 10.1074/jbc.M113.460253.

Lence T, Paolantoni C, Worpenberg L, Roignant J-Y. 2018. Mechanistic insights into m6A RNA enzymes. *Biochim Biophys Acta - Gene Regul Mech*. doi: 10.1016/J.BBAGRM.2018.10.014.

Lence T, Soller M, Roignant J-Y. 2017. A fly view on the roles and mechanisms of the m6A mRNA modification and its players. *RNA Biol* **14**: 1232. doi: 10.1080/15476286.2017.1307484.

Lewis BP, Burge CB, Bartel DP. 2005. Conserved Seed Pairing , Often Flanked by Adenosines , Indicates that Thousands of Human Genes are MicroRNA Targets We predict regulatory targets of vertebrate microRNAs. *Cell*. doi: 10.1016/j.cell.2004.12.035.

Li A, Chen Y-S, Ping X-L, Yang X, Xiao W, Yang Y, Sun H-Y, Zhu Q, Baidya P, Wang X, et al. 2017. Cytoplasmic m6A reader YTHDF3 promotes mRNA translation. *Cell Res* **27**: 444–447. doi: 10.1038/cr.2017.10.

Li F, Bullough KZ, Vashisht AA, Wohlschlegel JA, Philpott CC. 2016. Poly(rC)-Binding Protein 2 Regulates Hippo Signaling To Control Growth in Breast Epithelial Cells. *Mol Cell Biol*. doi: 10.1128/mcb.00104-16.

Li F, Zhao D, Wu J, Shi Y. 2014a. Structure of the YTH domain of human YTHDF2 in complex with an m6A mononucleotide reveals an aromatic cage for m6A recognition. *Cell Res* **24**: 1490–1492. doi: 10.1038/cr.2014.153.

Li H, Handsaker B, Wysoker A, Fennell T, Ruan J, Homer N, Marth G, Abecasis G, Durbin R, 1000 Genome Project Data Processing Subgroup. 2009. The Sequence Alignment/Map format and SAMtools. *Bioinformatics* **25**: 2078–2079. doi: 10.1093/bioinformatics/btp352.

Li J, Meng S, Xu M, Wang S, He L, Xu X, Wang X, Xie L. 2018a. Downregulation of N6-methyladenosine binding YTHDF2 protein mediated by miR-493-3p suppresses prostate cancer by elevating N6-methyladenosine levels. *Oncotarget* **9**: 3752–3764. doi: 10.18632/oncotarget.23365.

Li M, Zhao X, Wang W, Shi H, Pan Q, Lu Z, Perez SP, Suganthan R, He C, Bjørås M, et al. 2018b. Ythdf2-mediated m6A mRNA clearance modulates neural development in mice. *Genome Biol* **19**: 69. doi: 10.1186/s13059-018-1436-y.

Li Q, Zheng S, Han A, Lin CH, Stoilov P, Fu XD, Black DL. 2014b. The splicing regulator PTBP2 controls a program of embryonic splicing required for neuronal maturation. *Elife*. doi: 10.7554/eLife.01201.001.

Li Y, Lin L, Li Z, Ye X, Xiong K, Aryal B, Xu Z, Paroo Z, Liu Q, He C, et al. 2012. Iron homeostasis regulates the activity of the microRNA pathway through poly(C)-binding protein 2. *Cell Metab*. doi: 10.1016/j.cmet.2012.04.021.

Li Y, Wang Y, Zhang Z, Zamudio AV, Zhao JC. 2015. Genome-wide detection of high abundance N6-methyladenosine sites by microarray. *RNA*. doi: 10.1261/rna.051474.115.

Li Z, Qian P, Shao W, Shi H, He XC, Gogol M, Yu Z, Wang Y, Qi M, Zhu Y, et al. 2018c. Suppression of m6A reader Ythdf2 promotes hematopoietic stem cell expansion. *Cell Res*. doi: 10.1038/s41422-018-0072-0.

Licatalosi DD, Yano M, Fak JJ, Mele A, Grabinski SE, Zhang C, Darnell RB. 2012. Ptbp2 represses adult-specific splicing to regulate the generation of neuronal precursors in the embryonic brain. *Genes Dev*. doi: 10.1101/gad.191338.112.

Lin JC, Tarn WY. 2009. RNA-binding motif Protein 4 translocates to cytoplasmic granules and suppresses translation via argonaute2 duringmuscle cell differentiation. *J Biol Chem*. doi: 10.1074/jbc.M109.032946.

Lin MH, Sivakumaran H, Jones A, Li D, Harper C, Wei T, Jin H, Rustanti L, Meunier FA, Spann K, et al. 2014. A HIV-1 Tat mutant protein disrupts HIV-1 Rev function by targeting the DEAD-box RNA helicase DDX1. *Retrovirology*. doi: 10.1186/s12977-014-0121-9.

Lin Z, Hsu PJ, Xing X, Fang J, Lu Z, Zou Q, Zhang K-J, Zhang X, Zhou Y, Zhang T, et al. 2017. Mettl3-/Mettl14-mediated mRNA N6-methyladenosine modulates murine spermatogenesis. *Cell Res* **27**: 1216–1230. doi: 10.1038/cr.2017.117.

Linder B, Grozhik A V, Olarerin-George AO, Meydan C, Mason CE, Jaffrey SR. 2015. Single-nucleotide-resolution mapping of m6A and m6Am throughout the transcriptome. *Nat Methods* **12**: 767–772. doi: 10.1038/nmeth.3453.

Liu J, Yue Y, Han D, Wang X, Fu Y, Zhang L, Jia G, Yu M, Lu Z, Deng X, et al. 2014. A METTL3-METTL14 complex mediates mammalian nuclear RNA N6-adenosine methylation. *Nat Chem Biol* **10**: 93–5. doi: 10.1038/nchembio.1432.

Liu N, Dai Q, Zheng G, He C, Parisien M, Pan T. 2015a. N(6)-methyladenosine-dependent RNA

structural switches regulate RNA-protein interactions. *Nature* **518**: 560–4. doi: 10.1038/nature14234.

Liu N, Dai Q, Zheng G, He C, Parisien M, Pan T. 2015b. N6-methyladenosine-dependent RNA structural switches regulate RNA–protein interactions. *Nature* **518**: 560–564. doi: 10.1038/nature14234.

Liu N, Zhou KI, Parisien M, Dai Q, Diatchenko L, Pan T. 2017. N 6-methyladenosine alters RNA structure to regulate binding of a low-complexity protein. *Nucleic Acids Res* **45**: 6051–6063. doi: 10.1093/nar/gkx141.

Lloret-Llinares M, Karadoulama E, Chen Y, Wojenski LA, Villafano GJ, Bornholdt J, Andersson R, Core L, Sandelin A, Jensen TH. 2018. The RNA exosome contributes to gene expression regulation during stem cell differentiation. *Nucleic Acids Res* **46**: 11502–11513. doi: 10.1093/nar/gky817.

Loewer S, Cabili MN, Guttman M, Loh YH, Thomas K, Park IH, Garber M, Curran M, Onder T, Agarwal S, et al. 2010. Large intergenic non-coding RNA-RoR modulates reprogramming of human induced pluripotent stem cells. *Nat Genet*. doi: 10.1038/ng.710.

Loring JF. 2018. Autologous induced pluripotent stem cell-derived neurons to treat Parkinson's disease. *Stem Cells Dev*. doi: 10.1089/scd.2018.0107.

Lou CH, Shao A, Shum EY, Espinoza JL, Huang L, Karam R, Wilkinson MF. 2014. Posttranscriptional Control of the Stem Cell and Neurogenic Programs by the Nonsense-Mediated RNA Decay Pathway. *Cell Rep*. doi: 10.1016/j.celrep.2014.01.028.

Love MI, Huber W, Anders S. 2014. Moderated estimation of fold change and dispersion for RNA-seq data with DESeq2. *Genome Biol* **15**: 550. doi: 10.1186/s13059-014-0550-8.

Lu X, Sachs F, Ramsay LA, Jacques PÉ, Göke J, Bourque G, Ng HH. 2014. The retrovirus HERVH is a long noncoding RNA required for human embryonic stem cell identity. *Nat Struct Mol Biol*. doi: 10.1038/nsmb.2799.

Luo G-Z, MacQueen A, Zheng G, Duan H, Dore LC, Lu Z, Liu J, Chen K, Jia G, Bergelson J, et al. 2014. Unique features of the m6A methylome in Arabidopsis thaliana. *Nat Commun* **5**: 5630. doi: 10.1038/ncomms6630.

Luo Y, Na Z, Slavoff SA. 2018. P-Bodies: Composition, Properties, and Functions. *Biochemistry*. doi: 10.1021/acs.biochem.7b01162.

Lv J, Zhang Y, Gao S, Zhang C, Chen Y, Li W, Yang Y-G, Zhou Q, Liu F. 2018. Endothelial-specific m6A modulates mouse hematopoietic stem and progenitor cell development via Notch signaling. *Cell Res* **28**: 249–252. doi: 10.1038/cr.2017.143.

Lykke-Andersen J, Wagner E. 2005. Recruitment and activation of mRNA decay enzymes by two ARE-mediated decay activation domains in the proteins TTP and BRF-1. *Genes Dev* **19**: 351–361. doi: 10.1101/gad.1282305.

Ma C, Chang M, Lv H, Zhang Z-W, Zhang W, He X, Wu G, Zhao S, Zhang Y, Wang D, et al. 2018. RNA m6A methylation participates in regulation of postnatal development of the mouse cerebellum. *Genome Biol* **19**: 68. doi: 10.1186/s13059-018-1435-z.

Makeyev A V., Chkheidze AN, Liebhaber SA. 1999. A set of highly conserved RNA-binding proteins, αCP-1 and αCP-2, implicated in mRNA stabilization, are coexpressed from an intronless gene and its intron-containing paralog. *J Biol Chem* **274**: 24849–24857. doi: 10.1074/jbc.274.35.24849.

Makeyev A V., Liebhaber SA. 2000. Identification of Two Novel Mammalian Genes Establishes a Subfamily of KH-Domain RNA-Binding Proteins. *Genomics* **67**: 301–316. doi: 10.1006/geno.2000.6244.

Makeyev A V., Liebhaber SA. 2002. The poly(C)-binding proteins: A multiplicity of functions and a search for mechanisms. *RNA*. doi: 10.1017/S1355838202024627.

Makeyev E V., Zhang J, Carrasco MA, Maniatis T. 2007. The MicroRNA miR-124 Promotes Neuronal Differentiation by Triggering Brain-Specific Alternative Pre-mRNA Splicing. *Mol Cell*. doi: 10.1016/j.molcel.2007.07.015.

Malchenko S, Xie J, de Fatima Bonaldo M, Vanin EF, Bhattacharyya BJ, Belmadani A, Xi G, Galat V, Goossens W, Seftor REB, et al. 2014. Onset of rosette formation during spontaneous neural differentiation of hESC and hiPSC colonies. *Gene* **534**: 400–407. doi: 10.1016/j.gene.2013.07.101.

Mandai M, Watanabe A, Kurimoto Y, Hirami Y, Morinaga C, Daimon T, Fujihara M, Akimaru H, Sakai N, Shibata Y, et al. 2017. Autologous induced stem-cell-derived retinal cells for macular degeneration. *N Engl J Med*. doi: 10.1056/NEJMoa1608368.

Mareschi K, Montanari P, Rassu M, Galliano I, Daprà V, Adamini A, Castiglia S, Fagioli F, Bergallo M. 2019. Human Endogenous Retrovirus-H and K Expression in Human Mesenchymal Stem Cells as Potential Markers of Stemness. *Intervirology* **62**: 9–14. doi: 10.1159/000499185.

Martínez-Pérez M, Aparicio F, López-Gresa MP, Bellés JM, Sánchez-Navarro JA, Pallás V. 2017. *Arabidopsis* m ^{6} A demethylase activity modulates viral infection of a plant virus and the m ^{6} A abundance in its genomic RNAs. *Proc Natl Acad Sci* **114**: 10755–10760. doi: 10.1073/pnas.1703139114.

Maryati M, Airhihen B, Winkler GS. 2015. The enzyme activities of Caf1 and Ccr4 are both required for deadenylation by the human Ccr4-Not nuclease module. *Biochem J* **469**: 169–176. doi: 10.1042/BJ20150304.

Mauer J, Jaffrey SR. 2018. FTO, m ^{6} A $_{m}$, and the hypothesis of reversible epitranscriptomic mRNA modifications. *FEBS Lett* **592**: 2012–2022. doi: 10.1002/1873-3468.13092.

Mauer J, Luo X, Blanjoie A, Jiao X, Grozhik A V., Patil DP, Linder B, Pickering BF, Vasseur J-J, Chen Q, et al. 2017. Reversible methylation of m6Am in the 5′ cap controls mRNA stability. *Nature* **541**: 371–375. doi: 10.1038/nature21022.

Mauer J, Sindelar M, Despic V, Guez T, Hawley BR, Vasseur J-J, Rentmeister A, Gross SS, Pellizzoni L, Debart F, et al. 2019. FTO controls reversible m6Am RNA methylation during snRNA biogenesis. *Nat Chem Biol* **15**. doi: 10.1038/s41589-019-0231-8.

McDermott BT, Johnson KA, Hayati HF, Tew SR. 2018. The RNA binding protein HuR is critical for effective differentiation of bone marrow derived stem cells. *Osteoarthr Cartil* **26**: S149–S150. doi: 10.1016/j.joca.2018.02.322.

McIntyre ABR, Gokhale NS, Cerchietti L, Jaffrey SR, Horner SM, Mason CE. 2019. Limits in the detection of m6A changes using MeRIP/m6A-seq. *bioRxiv* 657130. doi: 10.1101/657130.

Mellacheruvu D, Wright Z, Couzens AL, Lambert JP, St-Denis NA, Li T, Miteva Y V., Hauri S, Sardiu ME, Low TY, et al. 2013. The CRAPome: A contaminant repository for affinity purification-mass spectrometry data. *Nat Methods* **10**: 730–736. doi: 10.1038/nmeth.2557.

Melton C, Judson RL, Blelloch R. 2010. Opposing microRNA families regulate self-renewal in mouse embryonic stem cells. *Nature*. doi: 10.1038/nature08725.

Meyer KD, Patil DP, Zhou J, Zinoviev A, Skabkin MA, Elemento O, Pestova TV, Qian S-B, Jaffrey SR. 2015. 5′ UTR m6A Promotes Cap-Independent Translation. *Cell* **163**: 999–1010. doi: 10.1016/j.cell.2015.10.012.

Meyer KD, Saletore Y, Zumbo P, Elemento O, Mason CE, Jaffrey SR. 2012. Comprehensive analysis of mRNA methylation reveals enrichment in 3' UTRs and near stop codons. *Cell* **149**: 1635–46. doi: 10.1016/j.cell.2012.05.003.

Michalski D, Ontiveros JG, Russo J, Charley PA, Anderson JR, Heck AM, Geiss BJ, Wilusz J. 2019. Zika virus noncoding sfRNAs sequester multiple host-derived RNA-binding proteins and modulate mRNA decay and splicing during infection. *J Biol Chem*. doi: 10.1074/jbc.RA119.009129.

Mitsumori K, Takei Y, Hirokawa N. 2017. Components of RNA granules affect their localization and dynamics in neuronal dendrites. *Mol Biol Cell*. doi: 10.1091/mbc.E16-07-0497.

Mizuno R, Chatterji P, Andres S, Hamilton K, Simon L, Foley SW, Jeganathan A, Gregory BD, Madison B, Rustgi AK. 2018. Differential regulation of LET-7 by LIN28B isoform-specific functions. *Mol Cancer Res*. doi: 10.1158/1541-7786.MCR-17-0514.

Mizutani A, Fukuda M, Ibata K, Shiraishi Y, Mikoshiba K. 2000. SYNCRIP, a cytoplasmic counterpart of heterogeneous nuclear ribonucleoprotein R, interacts with ubiquitous synaptotagmin isoforms. *J Biol Chem*. doi: 10.1074/jbc.275.13.9823.

Moon SL, Anderson JR, Kumagai Y, Wilusz CJ, Akira S, Khromykh AA, Wilusz J. 2012. A noncoding RNA produced by arthropod-borne flaviviruses inhibits the cellular exoribonuclease XRN1 and alters host mRNA stability. *RNA* **18**: 2029–2040. doi: 10.1261/rna.034330.112.

Moon SL, Blackinton JG, Anderson JR, Dozier MK, Dodd BJT, Keene JD, Wilusz CJ, Bradrick SS, Wilusz J. 2015. XRN1 Stalling in the 5' UTR of Hepatitis C Virus and Bovine Viral

Diarrhea Virus Is Associated with Dysregulated Host mRNA Stability ed. A. Siddiqui. *PLOS Pathog* **11**: e1004708. doi: 10.1371/journal.ppat.1004708.

Morgado AL, Rodrigues CMPP, Solá S. 2016. MicroRNA-145 Regulates Neural Stem Cell Differentiation Through the Sox2-Lin28/let-7 Signaling Pathway. *Stem Cells*. doi: 10.1002/stem.2309.

Mueller AA, Cheung TH, Rando TA. 2013. All's well that ends well: Alternative polyadenylation and its implications for stem cell biology. *Curr Opin Cell Biol*. doi: 10.1016/j.ceb.2012.12.008.

Müller S, Glaß M, Singh AK, Haase J, Bley N, Fuchs T, Lederer M, Dahl A, Huang H, Chen J, et al. 2018. IGF2BP1 promotes SRF-dependent transcription in cancer in a m6A- and miRNA-dependent manner. *Nucleic Acids Res*. doi: 10.1093/nar/gky1012.

Nagasaka R, Matsumoto M, Okada M, Sasaki H, Kanie K, Kii H, Uozumi T, Kiyota Y, Honda H, Kato R. 2017. Visualization of morphological categories of colonies for monitoring of effect on induced pluripotent stem cell culture status. *Regen Ther* **6**: 41–51. doi: 10.1016/J.RETH.2016.12.003.

Nazarov IB, Bakhmet EI, Tomilin AN. 2019. KH-Domain Poly(C)-Binding Proteins as Versatile Regulators of Multiple Biological Processes. *Biochem* **84**: 205–219. doi: 10.1134/S0006297919030039.

Neff AT, Lee JY, Wilusz J, Tian B, Wilusz CJ. 2012. Global analysis reveals multiple pathways for unique regulation of mRNA decay in induced pluripotent stem cells. *Genome Res* **22**: 1457–67. doi: 10.1101/gr.134312.111.

Nekrasov MP, Ivshina MP, Chernov KG, Kovrigina EA, Evdokimova VM, Thomas AAM, Hershey JWB, Ovchinnikov LP. 2003. The mRNA-binding protein YB-1 (p50) prevents association of the eukaryotic initiation factor eIF4G with mRNA and inhibits protein synthesis at the initiation stage. *J Biol Chem*. doi: 10.1074/jbc.M209145200.

Nicholas AK, Khurshid M, Désir J, Carvalho OP, Cox JJ, Thornton G, Kausar R, Ansar M, Ahmad W, Verloes A, et al. 2010. WDR62 is associated with the spindle pole and is mutated in human microcephaly. *Nat Genet*. doi: 10.1038/ng.682.

Nichols J, Smith A. 2009. Naive and Primed Pluripotent States. *Cell Stem Cell* **4**: 487–92. doi: 10.1016/j.stem.2009.05.015.

Niedzwiecka A, Nilsson P, Worch R, Stepinski J, Darzynkiewicz E, Virtanen A. 2016. Molecular recognition of mRNA 5' cap by 3' poly(A)-specific ribonuclease (PARN) differs from interactions known for other cap-binding proteins. *Biochim Biophys Acta - Proteins Proteomics* **1864**: 331–345. doi: 10.1016/j.bbapap.2016.01.002.

Nielsen J, Kristensen MA, Willemoës M, Nielsen FC, Christiansen J. 2004. Sequential dimerization of human zipcode-binding protein IMP1 on RNA: A cooperative mechanism providing RNP stability. *Nucleic Acids Res*. doi: 10.1093/nar/gkh754.

Niinuma S, Fukaya T, Tomari Y. 2016. CCR4 and CAF1 deadenylases have an intrinsic activity to remove the post-poly(A) sequence. *RNA* **22**: 1550–1559. doi: 10.1261/rna.057679.116.

Nishihara T, Zekri L, Braun JE, Izaurralde E. 2013. MiRISC recruits decapping factors to miRNA targets to enhance their degradation. *Nucleic Acids Res*. doi: 10.1093/nar/gkt619.

O'Brien J, Hayder H, Zayed Y, Peng C. 2018. Overview of microRNA biogenesis, mechanisms of actions, and circulation. *Front Endocrinol (Lausanne)*. doi: 10.3389/fendo.2018.00402.

Odorico JS, Kaufman DS, Thomson JA. 2001. Multilineage Differentiation from Human Embryonic Stem Cell Lines. *Stem Cells* **19**: 193–204. doi: 10.1634/stemcells.19-3-193.

Oh Y, Park J, Kim J-I, Chang M-Y, Lee S-H, Cho Y-H, Hwang J. 2018. Lin28B and miR-142-3p regulate neuronal differentiation by modulating Staufen1 expression. *Cell Death Differ* **25**: 432–443. doi: 10.1038/cdd.2017.182.

Ohnuki M, Tanabe K, Sutou K, Teramoto I, Sawamura Y, Narita M, Nakamura M, Tokunaga Y, Nakamura M, Watanabe A, et al. 2014. Dynamic regulation of human endogenous retroviruses mediates factor-induced reprogramming and differentiation potential. *Proc Natl Acad Sci U S A* **111**: 12426–31. doi: 10.1073/pnas.1413299111.

Ostareck DH, Ostareck-Lederer A, Shatsky IN, Hentze MW. 2001. Lipoxygenase mRNA silencing in erythroid differentiation: The 3′UTR regulatory complex controls 60S ribosomal subunit joining. *Cell*. doi: 10.1016/S0092-8674(01)00212-4.

Palusa S, Ndaluka C, Bowen RA, Wilusz CJ, Wilusz J. 2012. The 3′ untranslated region of the rabies virus glycoprotein mRNA specifically interacts with cellular PCBP2 protein and promotes transcript stability. *PLoS One*. doi: 10.1371/journal.pone.0033561.

Pan G, Thomson JA. 2007. Nanog and transcriptional networks in embryonic stem cell pluripotency. *Cell Res*. doi: 10.1038/sj.cr.7310125.

Paris J, Morgan M, Campos J, Spencer GJ, Shmakova A, Ivanova I, Mapperley C, Lawson H, Wotherspoon DA, Sepulveda C, et al. 2019. Targeting the RNA m6A Reader YTHDF2 Selectively Compromises Cancer Stem Cells in Acute Myeloid Leukemia. *Cell Stem Cell*. doi: 10.1016/j.stem.2019.03.021.

Park J-M, Kohn MJ, Bruinsma MW, Vech C, Intine R V., Fuhrmann S, Grinberg A, Mukherjee I, Love PE, Ko MS, et al. 2006. The Multifunctional RNA-Binding Protein La Is Required for Mouse Development and for the Establishment of Embryonic Stem Cells. *Mol Cell Biol*. doi: 10.1128/mcb.26.4.1445-1451.2006.

Park JH, Shin C. 2014. MicroRNA-directed cleavage of targets: mechanism and experimental approaches. *BMB Rep* **47**: 417–23.

Park OH, Ha H, Lee Y, Boo SH, Kwon DH, Song HK, Kim YK. 2019. Endoribonucleolytic Cleavage of m6A-Containing RNAs by RNase P/MRP Complex. *Mol Cell*. doi: 10.1016/J.MOLCEL.2019.02.034.

Patil DP, Chen C-K, Pickering BF, Chow A, Jackson C, Guttman M, Jaffrey SR. 2016. m6A RNA methylation promotes XIST-mediated transcriptional repression. *Nature* **537**: 369–373. doi: 10.1038/nature19342.

Patil DP, Pickering BF, Jaffrey SR. 2018. Reading m6A in the Transcriptome: m6A-Binding Proteins. *Trends Cell Biol* **28**: 113–127. doi: 10.1016/J.TCB.2017.10.001.

Pendleton KE, Chen B, Liu K, Hunter O V., Xie Y, Tu BP, Conrad NK. 2017. The U6 snRNA m6A Methyltransferase METTL16 Regulates SAM Synthetase Intron Retention. *Cell* **169**: 824-835.e14. doi: 10.1016/J.CELL.2017.05.003.

Peng SSY, Chen CYA, Xu N, Shyu A Bin. 1998. RNA stabilization by the AU-rich element binding protein, HuR, an ELAV protein. *EMBO J*. doi: 10.1093/emboj/17.12.3461.

Penney J, Ralvenius WT, Tsai L-H. 2019. Modeling Alzheimer's disease with iPSC-derived brain cells. *Mol Psychiatry*. doi: 10.1038/s41380-019-0468-3.

Perron G, Jandaghi P, Solanki S, Safisamghabadi M, Storoz C, Karimzadeh M, Papadakis AI, Arseneault M, Scelo G, Banks RE, et al. 2018. A General Framework for Interrogation of mRNA Stability Programs Identifies RNA-Binding Proteins that Govern Cancer Transcriptomes. *Cell Rep*. doi: 10.1016/j.celrep.2018.04.031.

Perry RP, Kelley DE. 1974. Existence of methylated messenger RNA in mouse L cells. *Cell* **1**: 37–42. doi: 10.1016/0092-8674(74)90153-6.

Picelli S, Björklund ÅK, Reinius B, Sagasser S, Winberg G, Sandberg R. 2014. Tn5 transposase and tagmentation procedures for massively scaled sequencing projects. *Genome Res* **24**: 2033–2040. doi: 10.1101/gr.177881.114.

Ping X-L, Sun B-F, Wang L, Xiao W, Yang X, Wang W-J, Adhikari S, Shi Y, Lv Y, Chen Y-S, et al. 2014. Mammalian WTAP is a regulatory subunit of the RNA N6-methyladenosine methyltransferase. *Cell Res* **24**: 177–89. doi: 10.1038/cr.2014.3.

Pio R, Zudaire I, Pino I, Castaño Z, Zabalegui N, Vicent S, Garcia-Amigot F, Odero MD, Lozano MD, Garcia-Foncillas J, et al. 2004. αCP-4, encoded by a putative tumor suppressor gene at 3p21, but not its alternative splice variant αCP-4a, is underexpressed in lung cancer. *Cancer Res*. doi: 10.1158/0008-5472.CAN-03-2982.

Piskounova E, Polytarchou C, Thornton JE, Lapierre RJ, Pothoulakis C, Hagan JP, Iliopoulos D, Gregory RI. 2011. Lin28A and Lin28B inhibit let-7 MicroRNA biogenesis by distinct mechanisms. *Cell*. doi: 10.1016/j.cell.2011.10.039.

Pruszak J, Sonntag K-C, Aung MH, Sanchez-Pernaute R, Isacson O. 2007. Markers and Methods for Cell Sorting of Human Embryonic Stem Cell-Derived Neural Cell Populations. *Stem Cells*. doi: 10.1634/stemcells.2006-0744.

Pyle AD, Lock LF, Donovan PJ. 2006. Neurotrophins mediate human embryonic stem cell survival. *Nat Biotechnol*. doi: 10.1038/nbt1189.

Qin Y, Xue B, Liu C, Wang X, Tian R, Xie Q, Guo M, Li G, Yang D, Zhu H. 2017. NLRX1 Mediates MAVS Degradation To Attenuate the Hepatitis C Virus-Induced Innate Immune Response through PCBP2. *J Virol*. doi: 10.1128/jvi.01264-17.

R Core Team. 2018. R: A language and environment for statistical computing. R Foundation for Statistical Computing. *Vienna, Austria*. doi: 10.1108/eb003648.

Rädle B, Rutkowski AJ, Ruzsics Z, Friedel CC, Koszinowski UH, Dölken L. 2013. Metabolic labeling of newly transcribed RNA for high resolution gene expression profiling of RNA synthesis, processing and decay in cell culture. *J Vis Exp* e50195. doi: 10.3791/50195.

Rafalska I, Zhang Z, Benderska N, Wolff H, Hartmann AM, Brack-Werner R, Stamm S. 2004. The intranuclear localization and function of YT521-B is regulated by tyrosine phosphorylation. *Hum Mol Genet* **13**: 1535–1549. doi: 10.1093/hmg/ddh167.

Rath S, Donovan J, Whitney G, Chitrakar A, Wang W, Korennykh A. 2015. Human RNase L tunes gene expression by selectively destabilizing the microRNA-regulated transcriptome. *Proc Natl Acad Sci* **112**: 15916–15921. doi: 10.1073/pnas.1513034112.

Ratnadiwakara M, Archer SK, Dent CI, Ruiz De Los Mozos I, Beilharz TH, Knaupp AS, Nefzger CM, Polo JM, Anko M-LL, De Los Mozos IR, et al. 2018. SRSF3 promotes pluripotency through nanog mRNA export and coordination of the pluripotency gene expression program. *Elife* **7**: e37419. doi: 10.7554/eLife.37419.

Rehwinkel J, Behm-Ansmant I, Gatfield D, Izaurralde E. 2005. A crucial role for GW182 and the DCP1:DCP2 decapping complex in miRNA-mediated gene silencing. *RNA*. doi: 10.1261/rna.2191905.

Ren C, Zhang J, Yan W, Zhang Y, Chen X. 2016. RNA-binding protein PCBP2 regulates p73 expression and p73-dependent antioxidant defense. *J Biol Chem*. doi: 10.1074/jbc.M115.712125.

Ries RJ, Zaccara S, Klein P, Olarerin-George A, Namkoong S, Pickering BF, Patil DP, Kwak H, Lee JH, Jaffrey SR. 2019. m6A enhances the phase separation potential of mRNA. *Nature* **571**: 424–428. doi: 10.1038/s41586-019-1374-1.

Rigbolt KTG, Prokhorova TA, Akimov V, Henningsen J, Johansen PT, Kratchmarova I, Kassem M, Mann M, Olsen J V., Blagoev B. 2011. System-wide temporal characterization of the proteome and phosphoproteome of human embryonic stem cell differentiation. *Sci Signal*. doi: 10.1126/scisignal.2001570.

Risso D, Ngai J, Speed TP, Dudoit S. 2014. Normalization of RNA-seq data using factor analysis of control genes or samples. *Nat Biotechnol* **32**: 896–902. doi: 10.1038/nbt.2931.

Robbens S, Rouzé P, Cock JM, Spring J, Worden AZ, Van de Peer Y. 2008. The FTO Gene, Implicated in Human Obesity, Is Found Only in Vertebrates and Marine Algae. *J Mol Evol* **66**: 80–84. doi: 10.1007/s00239-007-9059-z.

Roost C, Lynch SR, Batista PJ, Qu K, Chang HY, Kool ET. 2015. Structure and

thermodynamics of N6-methyladenosine in RNA: a spring-loaded base modification. *J Am Chem Soc* **137**: 2107–15. doi: 10.1021/ja513080v.

Rossant J, Tam PPL. 2017. New Insights into Early Human Development: Lessons for Stem Cell Derivation and Differentiation. *Cell Stem Cell*. doi: 10.1016/j.stem.2016.12.004.

Rottman FM, Bokar JA, Narayan P, Shambaugh ME, Ludwiczak R. 1994. N6-adenosine methylation in mRNA: substrate specificity and enzyme complexity. *Biochimie* **76**: 1109–14.

Roundtree IA, Luo G-Z, Zhang Z, Wang X, Zhou T, Cui Y, Sha J, Huang X, Guerrero L, Xie P, et al. 2017. YTHDC1 Mediates Nuclear Export of N6-methyladenosine Methylated mRNAs. *Elife* **6**. doi: 10.7554/eLife.31311.

Rowe BLY. 2016. futile.logger: A Logging Utility for R.

Rozwadowska N, Kolanowski T, Wiland E, Siatkowski M, Pawlak P, Malcher A, Mietkiewski T, Olszewska M, Kurpisz M. 2013. Characterisation of nuclear architectural alterations during in vitro differentiation of human stem cells of myogenic origin. *PLoS One* **8**: e73231. doi: 10.1371/journal.pone.0073231.

Russo J, Heck AM, Wilusz J, Wilusz CJ. 2017. Metabolic labeling and recovery of nascent RNA to accurately quantify mRNA stability. *Methods*. doi: 10.1016/j.ymeth.2017.02.003.

Russo J, Jalkanen AL, Heck AM, Schmidt CM, Wilusz J, Wilusz CJ. 2018. Sequences encoding C2H2 zinc fingers inhibit polyadenylation and mRNA export in human cells. *Sci Rep*. doi: 10.1038/s41598-018-35138-4.

Ruszkowska A, Ruszkowski M, Dauter Z, Brown JA. 2018. Structural insights into the RNA methyltransferase domain of METTL16. *Sci Rep* **8**: 5311. doi: 10.1038/s41598-018-23608-8.

Růžička K, Zhang M, Campilho A, Bodi Z, Kashif M, Saleh M, Eeckhout D, El-Showk S, Li H, Zhong S, et al. 2017. Identification of factors required for m ^{6} A mRNA methylation in *Arabidopsis* reveals a role for the conserved E3 ubiquitin ligase HAKAI. *New Phytol* **215**: 157–172. doi: 10.1111/nph.14586.

Ryu HG, Kim S, Lee S, Lee E, Kim HJ, Kim DY, Kim KT. 2019. HNRNP Q suppresses polyglutamine huntingtin aggregation by post-transcriptional regulation of vaccinia-related kinase 2. *J Neurochem*. doi: 10.1111/jnc.14638.

Sampath P, Pritchard DK, Pabon L, Reinecke H, Schwartz SM, Morris DR, Murry CE. 2008. A Hierarchical Network Controls Protein Translation during Murine Embryonic Stem Cell Self-Renewal and Differentiation. *Cell Stem Cell*. doi: 10.1016/j.stem.2008.03.013.

Sánchez CA, Andahur EI, Valenzuela R, Castellón EA, Fullá JA, Ramos CG, Triviño JC. 2016. Exosomes from bulk and stem cells from human prostate cancer have a differential microRNA content that contributes cooperatively over local and pre-metastatic niche. *Oncotarget*. doi: 10.18632/oncotarget.6540.

Santoni FA, Guerra J, Luban J. 2012. HERV-H RNA is abundant in human embryonic stem cells and a precise marker for pluripotency. *Retrovirology*. doi: 10.1186/1742-4690-9-111.

Saul MJ, Stein S, Grez M, Jakobsson PJ, Steinhilber D, Suess B. 2016. UPF1 regulates myeloid cell functions and S100A9 expression by the hnRNP E2/miRNA-328 balance. *Sci Rep*. doi: 10.1038/srep31995.

Schäfer IB, Rode M, Bonneau F, Schüssler S, Conti E. 2014. The structure of the Pan2–Pan3 core complex reveals cross-talk between deadenylase and pseudokinase. *Nat Struct Mol Biol* **21**: 591–598. doi: 10.1038/nsmb.2834.

Schneider CA, Rasband WS, Eliceiri KW. 2012. NIH Image to ImageJ: 25 years of image analysis. *Nat Methods* **9**: 671–5.

Schöller E, Weichmann F, Treiber T, Ringle S, Treiber N, Flatley A, Feederle R, Bruckmann A, Meister G. 2018. Interactions, localization, and phosphorylation of the m6A generating METTL3–METTL14–WTAP complex. *RNA* **24**: 499–512. doi: 10.1261/rna.064063.117.

Schön U, Seifarth W, Baust C, Hohenadl C, Erfle V, Leib-Mösch C. 2001. Cell type-specific expression and promoter activity of human endogenous retroviral long terminal repeats. *Virology*. doi: 10.1006/viro.2000.0712.

Schwartz S, Agarwala SD, Mumbach MR, Jovanovic M, Mertins P, Shishkin A, Tabach Y, Mikkelsen TS, Satija R, Ruvkun G, et al. 2013. High-Resolution Mapping Reveals a Conserved, Widespread, Dynamic mRNA Methylation Program in Yeast Meiosis. *Cell* **155**: 1409–1421. doi: 10.1016/j.cell.2013.10.047.

Schwartz S, Mumbach MR, Jovanovic M, Wang T, Maciag K, Bushkin GG, Mertins P, Ter-Ovanesyan D, Habib N, Cacchiarelli D, et al. 2014. Perturbation of m6A Writers Reveals Two Distinct Classes of mRNA Methylation at Internal and 5′ Sites. *Cell Rep* **8**: 284–296. doi: 10.1016/j.celrep.2014.05.048.

Scoumanne A, Cho SJ, Zhang J, Chen X. 2011. The cyclin-dependent kinase inhibitor p21 is regulated by RNA-binding protein PCBP4 via mRNA stability. *Nucleic Acids Res*. doi: 10.1093/nar/gkq778.

Searle BC. 2010. Scaffold: A bioinformatic tool for validating MS/MS-based proteomic studies. *Proteomics*. doi: 10.1002/pmic.200900437.

Serrano-Gomez SJ, Maziveyi M, Alahari SK. 2016. Regulation of epithelial-mesenchymal transition through epigenetic and post-translational modifications. *Mol Cancer* **15**: 18. doi: 10.1186/s12943-016-0502-x.

Sha Q-Q, Zhang J, Fan H-Y. 2019. A story of birth and death: mRNA translation and clearance at the onset of maternal-to-zygotic transition in mammals†. *Biol Reprod*. doi: 10.1093/biolre/ioz012.

Shan B, Wang X, Wu Y, Xu C, Xia Z, Dai J, Shao M, Zhao F, He S, Yang L, et al. 2017. The metabolic ER stress sensor IRE1a suppresses alternative activation of macrophages and

impairs energy expenditure in obesity. *Nat Immunol* **18**: 519–529. doi: 10.1038/ni.3709.

Shen L, Song C-X, He C, Zhang Y. 2014. Mechanism and Function of Oxidative Reversal of DNA and RNA Methylation. *Annu Rev Biochem* **83**: 585–614. doi: 10.1146/annurev-biochem-060713-035513.

Shi H, Li H, Yuan R, Guan W, Zhang X, Zhang S, Zhang W, Tong F, Li L, Song Z, et al. 2018a. PCBP1 depletion promotes tumorigenesis through attenuation of p27Kip1 mRNA stability and translation. *J Exp Clin Cancer Res*. doi: 10.1186/s13046-018-0840-1.

Shi H, Wang X, Lu Z, Zhao BS, Ma H, Hsu PJ, Liu C, He C. 2017. YTHDF3 facilitates translation and decay of N6-methyladenosine-modified RNA. *Cell Res* **27**: 315–328. doi: 10.1038/cr.2017.15.

Shi H, Zhang X, Weng Y-L, Lu Z, Liu Y, Lu Z, Li J, Hao P, Zhang Y, Zhang F, et al. 2018b. m6A facilitates hippocampus-dependent learning and memory through YTHDF1. *Nature* **563**: 249–253. doi: 10.1038/s41586-018-0666-1.

Shi Y, Kirwan P, Livesey FJ. 2012. Directed differentiation of human pluripotent stem cells to cerebral cortex neurons and neural networks. *Nat Protoc*. doi: 10.1038/nprot.2012.116.

Shibayama M, Ohno S, Osaka T, Sakamoto R, Tokunaga A, Nakatake Y, Sato M, Yoshida N. 2009. Polypyrimidine tract-binding protein is essential for early mouse development and embryonic stem cell proliferation. *FEBS J*. doi: 10.1111/j.1742-4658.2009.07380.x.

Shima H, Matsumoto M, Ishigami Y, Ebina M, Muto A, Sato Y, Kumagai S, Ochiai K, Suzuki T, Igarashi K. 2017. S-Adenosylmethionine Synthesis Is Regulated by Selective N6-Adenosine Methylation and mRNA Degradation Involving METTL16 and YTHDC1. *Cell Rep* **21**: 3354–3363. doi: 10.1016/J.CELREP.2017.11.092.

Sidiqi M, Wilce JA, Vivian JP, Porter CJ, Barker A, Leedman PJ, Wilce MCJ. 2005. Structure and RNA binding of the third KH domain of poly(C)-binding protein 1. *Nucleic Acids Res* **33**: 1213–1221. doi: 10.1093/nar/gki265.

Sieburth LE, Vincent JN. 2018. Beyond transcription factors: Roles of mRNA decay in regulating gene expression in plants. *F1000Research*. doi: 10.12688/f1000research.16203.1.

Singh P, James RS, Mee CJ, Morozov IY. 2019. mRNA levels are buffered upon knockdown of RNA decay and translation factors via adjustment of transcription rates in human HepG2 cells. *RNA Biol*. doi: 10.1080/15476286.2019.1621121.

Skeparnias I, Anastasakis D, Shaukat A-N, Grafanaki K, Stathopoulos C. 2017. Expanding the repertoire of deadenylases. *RNA Biol* 1–6. doi: 10.1080/15476286.2017.1300222.

Śledź P, Jinek M. 2016. Structural insights into the molecular mechanism of the m6A writer complex. *Elife* **5**. doi: 10.7554/eLife.18434.

Slobodin B, Han R, Calderone V, Vrielink JAFO, Loayza-Puch F, Elkon R, Agami R. 2017. Transcription Impacts the Efficiency of mRNA Translation via Co-transcriptional N6-

adenosine Methylation. *Cell* **169**: 326-337.e12.

Smirnova V V., Shestakova ED, Bikmetov D V., Chugunova AA, Osterman IA, Serebryakova M V., Sergeeva O V., Zatsepin TS, Shatsky IN, Terenin IM. 2019. eIF4G2 balances its own mRNA translation via a PCBP2-based feedback loop. *RNA*. doi: 10.1261/rna.065623.118.

Soh YQS, Mikedis MM, Kojima M, Godfrey AK, de Rooij DG, Page DC. 2017. Meioc maintains an extended meiotic prophase I in mice ed. P.E. Cohen. *PLOS Genet* **13**: e1006704. doi: 10.1371/journal.pgen.1006704.

Sokoloski K, Anderson JR, Wilusz J. 2008. Development of an in vitro mRNA decay system in insect cells. *Methods Mol Biol*. doi: 10.1007/978-1-59745-033-1_19.

Solinger JA, Pascolini D, Heyer WD. 1999. Active-site mutations in the Xrn1p exoribonuclease of Saccharomyces cerevisiae reveal a specific role in meiosis. *Mol Cell Biol* **19**: 5930–42.

Song H, Feng X, Zhang H, Luo Y, Huang J, Lin M, Jin J, Ding X, Wu S, Huang H, et al. 2019. METTL3 and ALKBH5 oppositely regulate m ^{6} A modification of *TFEB* mRNA, which dictates the fate of hypoxia/reoxygenation-treated cardiomyocytes. *Autophagy* 1–19. doi: 10.1080/15548627.2019.1586246.

Song JJ, Smith SK, Hannon GJ, Joshua-Tor L. 2004. Crystal structure of Argonaute and its implications for RISC slicer activity. *Science (80-)* **305**: 1434–1437. doi: 10.1126/science.1102514.

Sorci M, Ianniello Z, Cruciani S, Larivera S, Ginistrelli LC, Capuano E, Marchioni M, Fazi F, Fatica A. 2018. METTL3 regulates WTAP protein homeostasis. *Cell Death Dis* **9**: 796. doi: 10.1038/s41419-018-0843-z.

Stirparo GG, Boroviak T, Guo G, Nichols J, Smith A, Bertone P. 2018. Integrated analysis of single-cell embryo data yields a unified transcriptome signature for the human pre-implantation epiblast. *Dev*. doi: 10.1242/dev.158501.

Stoilov P, Rafalska I, Stamm S. 2002. YTH: a new domain in nuclear proteins. *Trends Biochem Sci* **27**: 495–7.

Stowell JAW, Webster MW, Kögel A, Wolf J, Shelley KL, Passmore LA. 2016. Reconstitution of Targeted Deadenylation by the Ccr4-Not Complex and the YTH Domain Protein Mmi1. *Cell Rep* **17**: 1978–1989. doi: 10.1016/j.celrep.2016.10.066.

Su R, Dong L, Li C, Nachtergaele S, Wunderlich M, Qing Y, Deng X, Wang Y, Weng X, Hu C, et al. 2018. R-2HG Exhibits Anti-tumor Activity by Targeting FTO/m 6 A/MYC/CEBPA Signaling. *Cell* **172**: 90-105.e23. doi: 10.1016/j.cell.2017.11.031.

Suckale J, Wendling O, Masjkur J, Jäger M, Münster C, Anastassiadis K, Stewart AF, Solimena M. 2011. PTBP1 is required for embryonic development before gastrulation. *PLoS One*. doi: 10.1371/journal.pone.0016992.

Sugiyama H, Takahashi K, Yamamoto T, Iwasaki M, Narita M, Nakamura M, Rand TA,

Nakagawa M, Watanabe A, Yamanaka S. 2017. Nat1 promotes translation of specific proteins that induce differentiation of mouse embryonic stem cells. *Proc Natl Acad Sci U S A*. doi: 10.1073/pnas.1617234114.

Sun X, Liu J, Xu C, Tang SC, Ren H. 2016. The insights of Let-7 miRNAs in oncogenesis and stem cell potency. *J Cell Mol Med*. doi: 10.1111/jcmm.12861.

Sun Y, Liu WZ, Liu T, Feng X, Yang N, Zhou HF. 2015. Signaling pathway of MAPK/ERK in cell proliferation, differentiation, migration, senescence and apoptosis. *J Recept Signal Transduct*. doi: 10.3109/10799893.2015.1030412.

Svitkin Y V., Pause A, Sonenberg N. 1994. La autoantigen alleviates translational repression by the 5' leader sequence of the human immunodeficiency virus type 1 mRNA. *J Virol*.

Svitkin Y V., Yanagiya A, Karetnikov AE, Alain T, Fabian MR, Khoutorsky A, Perreault S, Topisirovic I, Sonenberg N. 2013. Control of Translation and miRNA-Dependent Repression by a Novel Poly(A) Binding Protein, hnRNP-Q. *PLoS Biol*. doi: 10.1371/journal.pbio.1001564.

Takahashi K, Tanabe K, Ohnuki M, Narita M, Ichisaka T, Tomoda K, Yamanaka S. 2007. Induction of Pluripotent Stem Cells from Adult Human Fibroblasts by Defined Factors. *Cell*. doi: 10.1016/j.cell.2007.11.019.

Takahashi K, Yamanaka S. 2016. A decade of transcription factor-mediated reprogramming to pluripotency. *Nat Rev Mol Cell Biol* **17**: 183–193. doi: 10.1038/nrm.2016.8.

Takahashi K, Yamanaka S. 2006. Induction of pluripotent stem cells from mouse embryonic and adult fibroblast cultures by defined factors. *Cell* **126**: 663–76. doi: 10.1016/j.cell.2006.07.024.

Tanabe A, Konno J, Tanikawa K, Sahara H. 2014. Transcriptional machinery of TNF-α-inducible YTH domain containing 2 (YTHDC2) gene. *Gene* **535**: 24–32. doi: 10.1016/j.gene.2013.11.005.

Tang C, Klukovich R, Peng H, Wang Z, Yu T, Zhang Y, Zheng H, Klungland A, Yan W. 2018. ALKBH5-dependent m6A demethylation controls splicing and stability of long 3′-UTR mRNAs in male germ cells. *Proc Natl Acad Sci* **115**: E325–E333. doi: 10.1073/pnas.1717794115.

Tang TTL, Stowell JAW, Hill CH, Passmore LA. 2019. The intrinsic structure of poly(A) RNA determines the specificity of Pan2 and Caf1 deadenylases. *Nat Struct Mol Biol*. doi: 10.1038/s41594-019-0227-9.

Tavernier SJ, Osorio F, Vandersarren L, Vetters J, Vanlangenakker N, Van Isterdael G, Vergote K, De Rycke R, Parthoens E, van de Laar L, et al. 2017. Regulated IRE1-dependent mRNA decay sets the threshold for dendritic cell survival. *Nat Cell Biol* **19**: 698–710. doi: 10.1038/ncb3518.

Thakur S, Nakamura T, Calin G, Russo A, Tamburrino JF, Shimizu M, Baldassarre G, Battista

S, Fusco A, Wassell RP, et al. 2003. Regulation of BRCA1 Transcription by Specific Single-Stranded DNA Binding Factors. *Mol Cell Biol*. doi: 10.1128/mcb.23.11.3774-3787.2003.

Thalhammer A, Bencokova Z, Poole R, Loenarz C, Adam J, O'Flaherty L, Schödel J, Mole D, Giaslakiotis K, Schofield CJ, et al. 2011. Human AlkB Homologue 5 Is a Nuclear 2-Oxoglutarate Dependent Oxygenase and a Direct Target of Hypoxia-Inducible Factor 1α (HIF-1α) ed. B.C.B. Ko. *PLoS One* **6**: e16210. doi: 10.1371/journal.pone.0016210.

Thomas SP, Kim E, Kim J-S, Raines RT. 2016. Knockout of the Ribonuclease Inhibitor Gene Leaves Human Cells Vulnerable to Secretory Ribonucleases. *Biochemistry* **55**: 6359–6362. doi: 10.1021/acs.biochem.6b01003.

Thoms M, Thomson E, Baßler J, Gnädig M, Griesel S, Hurt E. 2015. The Exosome Is Recruited to RNA Substrates through Specific Adaptor Proteins. *Cell*. doi: 10.1016/j.cell.2015.07.060.

Thomson AM, Cahill CM, Cho HH, Kassachau KD, Epis MR, Bridges KR, Leedman PJ, Rogers JT. 2005. The acute box cis-element in human heavy ferritin mRNA 5′- untranslated region is a unique translation enhancer that binds poly(C)-binding proteins. *J Biol Chem*. doi: 10.1074/jbc.M502951200.

Tiedje C, Ronkina N, Tehrani M, Dhamija S, Laass K, Holtmann H, Kotlyarov A, Gaestel M. 2012. The p38/MK2-Driven Exchange between Tristetraprolin and HuR Regulates AU-Rich Element-Dependent Translation. *PLoS Genet*. doi: 10.1371/journal.pgen.1002977.

Timmers HTM, Tora L. 2018. Transcript Buffering: A Balancing Act between mRNA Synthesis and mRNA Degradation. *Mol Cell* **72**: 10–17. doi: 10.1016/j.molcel.2018.08.023.

Tommerup N, Leffers H. 1996. Assignment of the human genes encoding 14-3-3 Eta (YWHAH) to 22q12, 14-3-3 zeta (YWHAZ) to 2p25.1-p25.2, and 14-3-3 beta (YWHAB) to 20q13.1 by in situ hybridization. *Genomics*. doi: 10.1006/geno.1996.0176.

Trotta R, Vignudelli T, Candini O, Intine R V., Pecorari L, Guerzoni C, Santilli G, Byrom MW, Goldoni S, Ford LP, et al. 2003. BCR/ABL activates mdm2 mRNA translation via the La antigen. *Cancer Cell*. doi: 10.1016/S1535-6108(03)00020-5.

Tsankov AM, Gu H, Akopian V, Ziller MJ, Donaghey J, Amit I, Gnirke A, Meissner A. 2015. Transcription factor binding dynamics during human ES cell differentiation. *Nature*. doi: 10.1038/nature14233.

Tung YCL, Yeo GSH, O'Rahilly S, Coll AP. 2014. Obesity and FTO: Changing Focus at a Complex Locus. *Cell Metab* **20**: 710–718. doi: 10.1016/J.CMET.2014.09.010.

Uchiumi T, Fotovati A, Sasaguri T, Shibahara K, Shimada T, Fukuda T, Nakamura T, Izumi H, Tsuzuki T, Kuwano M, et al. 2006. YB-1 is important for an early stage embryonic development: Neural tube formation and cell proliferation. *J Biol Chem*. doi: 10.1074/jbc.M605948200.

Uehata T, Takeuchi O. 2017. Regnase-1 Is an Endoribonuclease Essential for the Maintenance

of Immune Homeostasis. *J Interf Cytokine Res* **37**: 220–229. doi: 10.1089/jir.2017.0001.

Van Driesche SJ, Martin KC. 2018. New frontiers in RNA transport and local translation in neurons. *Dev Neurobiol*. doi: 10.1002/dneu.22574.

Van Etten J, Schagat TL, Goldstrohm AC. 2013. A guide to design and optimization of reporter assays for 3' untranslated region mediated regulation of mammalian messenger RNAs. *Methods* **63**: 110–8. doi: 10.1016/j.ymeth.2013.04.020.

Vargiu L, Rodriguez-Tomé P, Sperber GO, Cadeddu M, Grandi N, Blikstad V, Tramontano E, Blomberg J. 2016. Classification and characterization of human endogenous retroviruses mosaic forms are common. *Retrovirology*. doi: 10.1186/s12977-015-0232-y.

Vasudevan S, Tong Y, Steitz JA. 2007. Switching from repression to activation: MicroRNAs can up-regulate translation. *Science (80-)*. doi: 10.1126/science.1149460.

Venables JP, Lapasset L, Gadea G, Fort P, Klinck R, Irimia M, Vignal E, Thibault P, Prinos P, Chabot B, et al. 2013. MBNL1 and RBFOX2 cooperate to establish a splicing programme involved in pluripotent stem cell differentiation. *Nat Commun*. doi: 10.1038/ncomms3480.

Vilà-González M, Kelaini S, Magee C, Caines R, Campbell D, Eleftheriadou M, Cochrane A, Drehmer D, Tsifaki M, O'Neill K, et al. 2019. Enhanced Function of Induced Pluripotent Stem Cell-Derived Endothelial Cells Through ESM1 Signaling. *Stem Cells* **37**: 226–239. doi: 10.1002/stem.2936.

Virtanen A, Henriksson N, Nilsson P, Nissbeck M. 2013. Poly(A)-specific ribonuclease (PARN): An allosterically regulated, processive and mRNA cap-interacting deadenylase. *Crit Rev Biochem Mol Biol* **48**: 192–209. doi: 10.3109/10409238.2013.771132.

Vuong JK, Lin CH, Zhang M, Chen L, Black DL, Zheng S. 2016. PTBP1 and PTBP2 Serve Both Specific and Redundant Functions in Neuronal Pre-mRNA Splicing. *Cell Rep*. doi: 10.1016/j.celrep.2016.11.034.

Wahle E, Winkler GS. 2013. RNA decay machines: Deadenylation by the Ccr4/Not and Pan2/Pan3 complexes. *Biochim Biophys Acta - Gene Regul Mech* **1829**: 561–570. doi: 10.1016/j.bbagrm.2013.01.003.

Wakao S, Kitada M, Kuroda Y, Ogura F, Murakami T, Niwa A, Dezawa M. 2012. Morphologic and Gene Expression Criteria for Identifying Human Induced Pluripotent Stem Cells ed. M. Pera. *PLoS One* **7**: e48677. doi: 10.1371/journal.pone.0048677.

Wang C-X, Cui G-S, Liu X, Xu K, Wang M, Zhang X-X, Jiang L-Y, Li A, Yang Y, Lai W-Y, et al. 2018a. METTL3-mediated m6A modification is required for cerebellar development ed. C. He. *PLOS Biol* **16**: e2004880. doi: 10.1371/journal.pbio.2004880.

Wang H, Vardy LA, Tan CP, Loo JM, Guo K, Li J, Lim SG, Zhou J, Chng WJ, Ng SB, et al. 2010. PCBP1 Suppresses the Translation of Metastasis-Associated PRL-3 Phosphatase. *Cancer Cell*. doi: 10.1016/j.ccr.2010.04.028.

Wang H, Zuo H, Liu J, Wen F, Gao Y, Zhu X, Liu B, Xiao F, Wang W, Huang G, et al. 2018b. Loss of YTHDF2-mediated m6A-dependent mRNA clearance facilitates hematopoietic stem cell regeneration. *Cell Res* **28**: 1035–1038. doi: 10.1038/s41422-018-0082-y.

Wang J, Xie G, Singh M, Ghanbarian AT, Raskó T, Szvetnik A, Cai H, Besser D, Prigione A, Fuchs N V., et al. 2014a. Primate-specific endogenous retrovirus-driven transcription defines naive-like stem cells. *Nature*. doi: 10.1038/nature13804.

Wang P, Doxtader KA, Nam Y. 2016a. Structural Basis for Cooperative Function of Mettl3 and Mettl14 Methyltransferases. *Mol Cell* **63**: 306–317. doi: 10.1016/j.molcel.2016.05.041.

Wang TH, Lin YS, Chen Y, Yeh CT, Huang Y lin, Hsieh TH, Shieh TM, Hsueh C, Chen TC. 2015a. Long non-coding RNA AOC4P suppresses hepatocellular carcinoma metastasis by enhancing vimentin degradation and inhibiting epithelial-mesenchymal transition. *Oncotarget*. doi: 10.18632/oncotarget.4344.

Wang X, Feng J, Xue Y, Guan Z, Zhang D, Liu Z, Gong Z, Wang Q, Huang J, Tang C, et al. 2016b. Structural basis of N6-adenosine methylation by the METTL3–METTL14 complex. *Nature* **534**: 575–8. doi: 10.1038/nature18298.

Wang X, Lu Z, Gomez A, Hon GC, Yue Y, Han D, Fu Y, Parisien M, Dai Q, Jia G, et al. 2014b. N6-methyladenosine-dependent regulation of messenger RNA stability. *Nature* **505**: 117–20. doi: 10.1038/nature12730.

Wang X, Zhao BS, Roundtree IA, Lu Z, Han D, Ma H, Weng X, Chen K, Shi H, He C. 2015b. N6-methyladenosine Modulates Messenger RNA Translation Efficiency. *Cell* **161**: 1388–1399. doi: 10.1016/j.cell.2015.05.014.

Wang Y, Li Y, Toth JI, Petroski MD, Zhang Z, Zhao JC. 2014c. N6-methyladenosine modification destabilizes developmental regulators in embryonic stem cells. *Nat Cell Biol* **16**: 191–8. doi: 10.1038/ncb2902.

Wang Y, Li Y, Yue M, Wang J, Kumar S, Wechsler-Reya RJ, Zhang Z, Ogawa Y, Kellis M, Duester G, et al. 2018c. N6-methyladenosine RNA modification regulates embryonic neural stem cell self-renewal through histone modifications. *Nat Neurosci*. doi: 10.1038/s41593-017-0057-1.

Wang Y, Melton C, Li YP, Shenoy A, Zhang XX, Subramanyam D, Blelloch R. 2013a. MiR-294/miR-302 Promotes Proliferation, Suppresses G1-S Restriction Point, and Inhibits ESC Differentiation through Separable Mechanisms. *Cell Rep*. doi: 10.1016/j.celrep.2013.05.027.

Wang Y, Xu Z, Jiang J, Xu C, Kang J, Xiao L, Wu M, Xiong J, Guo X, Liu H. 2013b. Endogenous miRNA Sponge lincRNA-RoR Regulates Oct4, Nanog, and Sox2 in Human Embryonic Stem Cell Self-Renewal. *Dev Cell*. doi: 10.1016/j.devcel.2013.03.002.

Warda AS, Kretschmer J, Hackert P, Lenz C, Urlaub H, Höbartner C, Sloan KE, Bohnsack MT. 2017. Human METTL16 is a N6-methyladenosine (m6A) methyltransferase that targets pre-mRNAs and various non-coding RNAs. *EMBO Rep* **18**: 2004–2014. doi: 10.15252/embr.201744940.

Ware CB, Nelson AM, Mecham B, Hesson J, Zhou W, Jonlin EC, Jimenez-Caliani AJ, Deng X, Cavanaugh C, Cook S, et al. 2014. Derivation of naive human embryonic stem cells. *Proc Natl Acad Sci* **111**: 4484–4489. doi: 10.1073/pnas.1319738111.

Warnes GR, Bolker B, Bonebakker L, Gentleman R, Liaw WHA, Lumley T, Maechler M, Magnusson A, Moeller S, Schwartz M, et al. 2016. Package "gplots": Various R programming tools for plotting data. *R Packag version 2170*. doi: 10.1111/j.0022-3646.1997.00569.x.

Webster MW, Stowell JA, Passmore LA. 2019. RNA-binding proteins distinguish between similar sequence motifs to promote targeted deadenylation by Ccr4-Not. *Elife*. doi: 10.7554/eLife.40670.

Wei CM, Gershowitz A, Moss B. 1976. 5'-Terminal and internal methylated nucleotide sequences in HeLa cell mRNA. *Biochemistry* **15**: 397–401.

Wei J, Liu F, Lu Z, Fei Q, Ai Y, He PC, Shi H, Cui X, Su R, Klungland A, et al. 2018. Differential m6A, m6Am, and m1A Demethylation Mediated by FTO in the Cell Nucleus and Cytoplasm. *Mol Cell* **71**: 973-985.e5. doi: 10.1016/J.MOLCEL.2018.08.011.

Weil D, Boutain S, Audibert A, Dautry F. 2000. Mature mRNAs accumulated in the nucleus are neither the molecules in transit to the cytoplasm nor constitute a stockpile for gene expression. *RNA*. doi: 10.1017/S1355838200000479.

Weinberger L, Ayyash M, Novershtern N, Hanna JH. 2016. Dynamic stem cell states: naive to primed pluripotency in rodents and humans. *Nat Rev Mol Cell Biol* **17**: 155–169. doi: 10.1038/nrm.2015.28.

Wen J, Lv R, Ma H, Shen H, He C, Wang J, Jiao F, Liu H, Yang P, Tan L, et al. 2018. Zc3h13 Regulates Nuclear RNA m 6 A Methylation and Mouse Embryonic Stem Cell Self-Renewal. *Mol Cell* **69**: 1028-1038.e6. doi: 10.1016/j.molcel.2018.02.015.

Weng H, Huang H, Wu H, Qin X, Zhao BS, Dong L, Shi H, Skibbe J, Shen C, Hu C, et al. 2018a. METTL14 Inhibits Hematopoietic Stem/Progenitor Differentiation and Promotes Leukemogenesis via mRNA m6A Modification. *Cell Stem Cell* **22**: 191-205.e9. doi: 10.1016/J.STEM.2017.11.016.

Weng Y-L, Wang X, An R, Cassin J, Vissers C, Liu Y, Liu Y, Xu T, Wang X, Wong SZH, et al. 2018b. Epitranscriptomic m 6 A Regulation of Axon Regeneration in the Adult Mammalian Nervous System. *Neuron* **97**: 313-325.e6. doi: 10.1016/j.neuron.2017.12.036.

Wickham H. 2011. The Split-Apply-Combine Strategy for Data Analysis. *J Stat Softw* **40**: 1–29. doi: 10.18637/jss.v040.i01.

Williams KR, McAninch DS, Stefanovic S, Xing L, Allen M, Li W, Feng Y, Mihailescu MR, Bassell GJ. 2016. hnRNP-Q1 represses nascent axon growth in cortical neurons by inhibiting Gap-43 mRNA translation. *Mol Biol Cell* **27**: 518–34. doi: 10.1091/mbc.E15-07-0504.

Wojtas MN, Pandey RR, Mendel M, Homolka D, Sachidanandam R, Pillai RS. 2017. Regulation of m 6 A Transcripts by the 3'→5' RNA Helicase YTHDC2 Is Essential for a Successful Meiotic Program in the Mammalian Germline. *Mol Cell* **68**: 374-387.e12. doi: 10.1016/j.molcel.2017.09.021.

Wolf J, Passmore LA. 2014. mRNA deadenylation by Pan2-Pan3. *Biochem Soc Trans* **42**: 184–187. doi: 10.1042/BST20130211.

Wolf J, Valkov E, Allen MD, Meineke B, Gordiyenko Y, McLaughlin SH, Olsen TM, Robinson C V., Bycroft M, Stewart M, et al. 2014. Structural basis for Pan3 binding to Pan2 and its function in mRNA recruitment and deadenylation. *EMBO J* **33**: 1514–1526. doi: 10.15252/embj.201488373.

Worringer KA, Rand TA, Hayashi Y, Sami S, Takahashi K, Tanabe K, Narita M, Srivastava D, Yamanaka S. 2014. The let-7/LIN-41 pathway regulates reprogramming to human induced pluripotent stem cells by controlling expression of prodifferentiation genes. *Cell Stem Cell*. doi: 10.1016/j.stem.2013.11.001.

Wu B, Su S, Patil DP, Liu H, Gan J, Jaffrey SR, Ma J. 2018a. Molecular basis for the specific and multivariant recognitions of RNA substrates by human hnRNP A2/B1. *Nat Commun* **9**: 420. doi: 10.1038/s41467-017-02770-z.

Wu R, Li A, Sun B, Sun J-G, Zhang J, Zhang T, Chen Y, Xiao Y, Gao Y, Zhang Q, et al. 2019. A novel m6A reader Prrc2a controls oligodendroglial specification and myelination. *Cell Res* **29**: 23–41. doi: 10.1038/s41422-018-0113-8.

Wu R, Liu Y, Yao Y, Zhao Y, Bi Z, Jiang Q, Liu Q, Cai M, Wang F, Wang Y, et al. 2018b. FTO regulates adipogenesis by controlling cell cycle progression via m6A-YTHDF2 dependent mechanism. *Biochim Biophys Acta - Mol Cell Biol Lipids* **1863**: 1323–1330. doi: 10.1016/J.BBALIP.2018.08.008.

Wu Y, Xie L, Wang M, Xiong Q, Guo Y, Liang Y, Li J, Sheng R, Deng P, Wang Y, et al. 2018c. Mettl3-mediated m6A RNA methylation regulates the fate of bone marrow mesenchymal stem cells and osteoporosis. *Nat Commun* **9**: 4772. doi: 10.1038/s41467-018-06898-4.

Wurm JP, Holdermann I, Overbeck JH, Mayer PHO, Sprangers R. 2017. Changes in conformational equilibria regulate the activity of the Dcp2 decapping enzyme. *Proc Natl Acad Sci* **114**: 6034–6039. doi: 10.1073/pnas.1704496114.

Xia P, Wang S, Xiong Z, Ye B, Huang LY, Han ZG, Fan Z. 2015. IRTKS negatively regulates antiviral immunity through PCBP2 sumoylation-mediated MAVS degradation. *Nat Commun*. doi: 10.1038/ncomms9132.

Xiang Y, Laurent B, Hsu C-H, Nachtergaele S, Lu Z, Sheng W, Xu C, Chen H, Ouyang J, Wang S, et al. 2017. RNA m6A methylation regulates the ultraviolet-induced DNA damage response. *Nature* **543**: 573–576. doi: 10.1038/nature21671.

Xiao W, Adhikari S, Dahal U, Chen Y-S, Hao Y-J, Sun B-F, Sun H-Y, Li A, Ping X-L, Lai W-Y, et al. 2016. Nuclear m(6)A Reader YTHDC1 Regulates mRNA Splicing. *Mol Cell* **61**: 507–19. doi: 10.1016/j.molcel.2016.01.012.

Xie W, Schultz MD, Lister R, Hou Z, Rajagopal N, Ray P, Whitaker JW, Tian S, Hawkins RD, Leung D, et al. 2013. Epigenomic analysis of multilineage differentiation of human embryonic stem cells. *Cell*. doi: 10.1016/j.cell.2013.04.022.

Xin Z, Han W, Zhao Z, Xia Q, Yin B, Yuan J, Peng X. 2011. Pcbp2 enhances the antiviral activity of ifn-α against hcv by stabilizing the mrna of stat1 and stat2. *PLoS One*. doi: 10.1371/journal.pone.0025419.

Xu C, Liu K, Ahmed H, Loppnau P, Schapira M, Min J. 2015. Structural Basis for the Discriminative Recognition of N6-Methyladenosine RNA by the Human YT521-B Homology Domain Family of Proteins. *J Biol Chem* **290**: 24902–13. doi: 10.1074/jbc.M115.680389.

Xu C, Liu K, Tempel W, Demetriades M, Aik W, Schofield CJ, Min J. 2014a. Structures of human ALKBH5 demethylase reveal a unique binding mode for specific single-stranded N6-methyladenosine RNA demethylation. *J Biol Chem* **289**: 17299–311. doi: 10.1074/jbc.M114.550350.

Xu C, Wang X, Liu K, Roundtree IA, Tempel W, Li Y, Lu Z, He C, Min J. 2014b. Structural basis for selective binding of m6A RNA by the YTHDC1 YTH domain. *Nat Chem Biol* **10**: 927–929. doi: 10.1038/nchembio.1654.

Xu D, Zhang F, Wang Y, Sun Y, Xu Z. 2014c. Microcephaly-associated protein WDR62 regulates neurogenesis through JNK1 in the developing neocortex. *Cell Rep*. doi: 10.1016/j.celrep.2013.12.016.

Xu K, Yang Y, Feng G-H, Sun B-F, Chen J-Q, Li Y-F, Chen Y-S, Zhang X-X, Wang C-X, Jiang L-Y, et al. 2017. Mettl3-mediated m6A regulates spermatogonial differentiation and meiosis initiation. *Cell Res* **27**: 1100–1114. doi: 10.1038/cr.2017.100.

Xu N, Papagiannakopoulos T, Pan G, Thomson JA, Kosik KS. 2009. MicroRNA-145 regulates OCT4, SOX2, and KLF4 and represses pluripotency in human embryonic stem cells. *Cell* **137**: 647–58. doi: 10.1016/j.cell.2009.02.038.

Yamada T, Akimitsu N. 2019. Contributions of regulated transcription and mRNA decay to the dynamics of gene expression. *Wiley Interdiscip Rev RNA*. doi: 10.1002/wrna.1508.

Yamaji MM, Jishage M, Meyer C, Suryawanshi H, Der E, Yamaji MM, Garzia A, Morozov P, Manickavel S, McFarland HL, et al. 2017. DND1 maintains germline stem cells via recruitment of the CCR4–NOT complex to target mRNAs. *Nature* **543**: 568–572. doi: 10.1038/nature21690.

Yanatori I, Richardson DR, Imada K, Kishi F. 2016. Iron export through the transporter ferroportin 1 is modulated by the iron chaperone PCBP2. *J Biol Chem*. doi: 10.1074/jbc.M116.721936.

Yang Z, Li J, Feng G, Gao S, Wang Y, Zhang S, Liu Y, Ye L, Li Y, Zhang X. 2017. MicroRNA-145 Modulates N6 methyladenosine Levels by Targeting the 3′ Untranslated mRNA Region of the N6-methyladenosine binding YTH Domain Family 2 Protein. *J Biol Chem* jbc.M116.749689. doi: 10.1074/jbc.M116.749689.

Yao QJ, Sang L, Lin M, Yin X, Dong W, Gong Y, Zhou BO. 2018. Mettl3–Mettl14 methyltransferase complex regulates the quiescence of adult hematopoietic stem cells. *Cell Res* **28**: 952–954. doi: 10.1038/s41422-018-0062-2.

Yao Y, Bi Z, Wu R, Zhao Y, Liu Y, Liu Q, Wang Y, Wang X. 2019. METTL3 inhibits BMSC adipogenic differentiation by targeting the JAK1/STAT5/C/EBPβ pathway *via* an m ^{6} A-YTHDF2–dependent manner. *FASEB J*. doi: 10.1096/fj.201802644R.

Ye D, Wang G, Liu Y, Huang W, Wu M, Zhu S, Jia W, Deng ANM, Liu H, Kang J. 2012. MiR-138 promotes induced pluripotent stem cell generation through the regulation of the P53 signaling. *Stem Cells*. doi: 10.1002/stem.1149.

Ye J, Zhou G, Zhang Z, Sun L, He X, Zhou J. 2016. Poly (C)-binding protein 2 (PCBP2) promotes the progression of esophageal squamous cell carcinoma (ESCC) through regulating cellular proliferation and apoptosis. *Pathol Res Pract*. doi: 10.1016/j.prp.2016.05.008.

Ye X, Tam WL, Shibue T, Kaygusuz Y, Reinhardt F, Ng Eaton E, Weinberg RA. 2015. Distinct EMT programs control normal mammary stem cells and tumour-initiating cells. *Nature*. doi: 10.1038/nature14897.

Yeom KH, Mitchell S, Linares AJ, Zheng S, Lin CH, Wang XJ, Hoffmann A, Black DL. 2018. Polypyrimidine tract-binding protein blocks miRNA-124 biogenesis to enforce its neuronal-specific expression in the mouse. *Proc Natl Acad Sci U S A*. doi: 10.1073/pnas.1809609115.

Yi H, Park J, Ha M, Lim J, Chang H, Kim VN. 2018. PABP Cooperates with the CCR4-NOT Complex to Promote mRNA Deadenylation and Block Precocious Decay. *Mol Cell*. doi: 10.1016/j.molcel.2018.05.009.

Yoon JH, Abdelmohsen K, Kim J, Yang X, Martindale JL, Tominaga-Yamanaka K, White EJ, Orjalo A V., Rinn JL, Kreft SG, et al. 2013. Scaffold function of long non-coding RNA HOTAIR in protein ubiquitination. *Nat Commun*. doi: 10.1038/ncomms3939.

Yoon K-J, Ringeling FR, Vissers C, Jacob F, Pokrass M, Jimenez-Cyrus D, Su Y, Kim N-S, Zhu Y, Zheng L, et al. 2017. Temporal Control of Mammalian Cortical Neurogenesis by m6A Methylation. *Cell* **171**: 877-889.e17. doi: 10.1016/J.CELL.2017.09.003.

Yoshihara M, Hayashizaki Y, Murakawa Y. 2017. Genomic Instability of iPSCs: Challenges Towards Their Clinical Applications. *Stem Cell Rev Reports* **13**: 7–16. doi: 10.1007/s12015-016-9680-6.

You F, Sun H, Zhou X, Sun W, Liang S, Zhai Z, Jiang Z. 2009. PCBP2 mediates degradation of the adaptor MAVS via the HECT ubiquitin ligase AIP4. *Nat Immunol*. doi: 10.1038/ni.1815.

Yu J, Li Y, Wang T, Zhong X. 2018. Modification of N6-methyladenosine RNA methylation on heat shock protein expression ed. G. Multhoff. *PLoS One* **13**: e0198604. doi: 10.1371/journal.pone.0198604.

Yue Y, Liu J, Cui X, Cao J, Luo G, Zhang Z, Cheng T, Gao M, Shu X, Ma H, et al. 2018. VIRMA mediates preferential m6A mRNA methylation in 3′UTR and near stop codon and associates with alternative polyadenylation. *Cell Discov* **4**: 10. doi: 10.1038/s41421-018-0019-0.

Zeng Z-LL, Lin X long, Tan L-LL, Liu Y-MM, Qu K, Wang Z. 2018. MicroRNAs: Important Regulators of Induced Pluripotent Stem Cell Generation and Differentiation. *Stem Cell Rev Reports* **14**: 71–81. doi: 10.1007/s12015-017-9785-6.

Zhang B, zur Hausen A, Orlowska-Volk M, Jäger M, Bettendorf H, Stamm S, Hirschfeld M, Yiqin O, Tong X, Gitsch G, et al. 2010a. Alternative Splicing-Related Factor YT521. *Int J Gynecol Cancer* **20**: 492–499. doi: 10.1111/IGC.0b013e3181d66ffe.

Zhang C, Chen Y, Sun B, Wang L, Yang Y, Ma D, Lv J, Heng J, Ding Y, Xue Y, et al. 2017a. m6A modulates haematopoietic stem and progenitor cell specification. *Nature*. doi: 10.1038/nature23883.

Zhang C, Samanta D, Lu H, Bullen JW, Zhang H, Chen I, He X, Semenza GL. 2016a. Hypoxia induces the breast cancer stem cell phenotype by HIF-dependent and ALKBH5-mediated m6A-demethylation of NANOG mRNA. *Proc Natl Acad Sci U S A* **113**: E2047-56. doi: 10.1073/pnas.1602883113.

Zhang F, Kang Y, Wang M, Li Y, Xu T, Yang W, Song H, Wu H, Shu Q, Jin P. 2018a. Fragile X mental retardation protein modulates the stability of its m6A-marked messenger RNA targets. *Hum Mol Genet* **27**: 3936–3950. doi: 10.1093/hmg/ddy292.

Zhang J, Nie D, Rocha JL, Hogan M V, Wang JH-C. 2018b. Characterization of the structure, cells, and cellular mechanobiological response of human plantar fascia. *J Tissue Eng* **9**: 204173141880110. doi: 10.1177/2041731418801103.

Zhang J, Ratanasirintrawoot S, Chandrasekaran S, Wu Z, Ficarro SB, Yu C, Ross CA, Cacchiarelli D, Xia Q, Seligson M, et al. 2016b. LIN28 Regulates Stem Cell Metabolism and Conversion to Primed Pluripotency. *Cell Stem Cell* **19**: 66–80. doi: 10.1016/j.stem.2016.05.009.

Zhang R, Engler A, Taylor V. 2018c. Notch: an interactive player in neurogenesis and disease. *Cell Tissue Res*. doi: 10.1007/s00441-017-2641-9.

Zhang S, Zhao BS, Zhou A, Lin K, Zheng S, Lu Z, Chen Y, Sulman EP, Xie K, Bögler O, et al. 2017b. m 6 A Demethylase ALKBH5 Maintains Tumorigenicity of Glioblastoma Stem-like Cells by Sustaining FOXM1 Expression and Cell Proliferation Program. *Cancer Cell* **31**: 591-606.e6. doi: 10.1016/j.ccell.2017.02.013.

Zhang X, Huang CT, Chen J, Pankratz MT, Xi J, Li J, Yang Y, LaVaute TM, Li XJ, Ayala M, et al. 2010b. Pax6 is a human neuroectoderm cell fate determinant. *Cell Stem Cell*. doi: 10.1016/j.stem.2010.04.017.

Zhang Y, Li T, Preissl S, Amaral ML, Grinstein JD, Farah EN, Destici E, Qiu Y, Hu R, Lee AY, et al. 2019a. Transcriptionally active HERV-H retrotransposons demarcate topologically associating domains in human pluripotent stem cells. *Nat Genet*. doi: 10.1038/s41588-019-

0479-7.

Zhang Y, Si Y, Ma N, Mei J. 2015a. The RNA-binding protein PCBP2 inhibits Ang II-induced hypertrophy of cardiomyocytes though promoting GPR56 mRNA degeneration. *Biochem Biophys Res Commun*. doi: 10.1016/j.bbrc.2015.06.139.

Zhang Y, Wang X, Zhang X, Wang J, Ma Y, Zhang L, Cao X. 2019b. RNA-binding protein YTHDF3 suppresses interferon-dependent antiviral responses by promoting FOXO3 translation. *Proc Natl Acad Sci U S A* **116**: 976–981. doi: 10.1073/pnas.1812536116.

Zhang Z, Chen L-Q, Zhao Y-L, Yang C-G, Roundtree IA, Zhang Z, Ren J, Xie W, He C, Luo G-Z. 2019c. Single-base mapping of m6A by an antibody-independent method. *bioRxiv* 575555. doi: 10.1101/575555.

Zhang Z, Theler D, Kaminska KH, Hiller M, de la Grange P, Pudimat R, Rafalska I, Heinrich B, Bujnicki JM, Allain FH-T, et al. 2010c. The YTH domain is a novel RNA binding domain. *J Biol Chem* **285**: 14701–10. doi: 10.1074/jbc.M110.104711.

Zhang ZZ, Shen ZY, Shen YY, Zhao EH, Wang M, Wang CJ, Cao H, Xu J. 2015b. HOTAIR long noncoding RNA promotes gastric cancer metastasis through suppression of Poly r(C)-binding protein (PCBP) 1. *Mol Cancer Ther*. doi: 10.1158/1535-7163.MCT-14-0695.

Zhao BS, Nachtergaele S, Roundtree IA, He C. 2018. Our views of dynamic N6-methyladenosine RNA methylation. *RNA* **24**: 268–272. doi: 10.1261/rna.064295.117.

Zhao BS, Roundtree IA, He C. 2017a. Post-transcriptional gene regulation by mRNA modifications. *Nat Rev Mol Cell Biol* **18**: 31–42. doi: 10.1038/nrm.2016.132.

Zhao BS, Wang X, Beadell A V., Lu Z, Shi H, Kuuspalu A, Ho RK, He C. 2017b. m6A-dependent maternal mRNA clearance facilitates zebrafish maternal-to-zygotic transition. *Nature* **542**: 475–478. doi: 10.1038/nature21355.

Zhao X, Yang Y, Sun B-F, Shi Y, Yang X, Xiao W, Hao Y-J, Ping X-L, Chen Y-S, Wang W-J, et al. 2014. FTO-dependent demethylation of N6-methyladenosine regulates mRNA splicing and is required for adipogenesis. *Cell Res* **24**: 1403–1419. doi: 10.1038/cr.2014.151.

Zheng G, Dahl JA, Niu Y, Fedorcsak P, Huang C-M, Li CJ, Vågbø CB, Shi Y, Wang W-L, Song S-H, et al. 2013. ALKBH5 Is a Mammalian RNA Demethylase that Impacts RNA Metabolism and Mouse Fertility. *Mol Cell* **49**: 18–29. doi: 10.1016/j.molcel.2012.10.015.

Zheng S, Gray EE, Chawla G, Porse BT, O'Dell TJ, Black DL. 2012. PSD-95 is post-transcriptionally repressed during early neural development by PTBP1 and PTBP2. *Nat Neurosci*. doi: 10.1038/nn.3026.

Zheng Y, Nie P, Peng D, He Z, Liu M, Xie Y, Miao Y, Zuo Z, Ren J. 2018. M6AVar: A database of functional variants involved in m 6 A modification. *Nucleic Acids Res*. doi: 10.1093/nar/gkx895.

Zhong S, Li H, Bodi Z, Button J, Vespa L, Herzog M, Fray RG. 2008. MTA Is an Arabidopsis

Messenger RNA Adenosine Methylase and Interacts with a Homolog of a Sex-Specific Splicing Factor. *PLANT CELL ONLINE* **20**: 1278–1288. doi: 10.1105/tpc.108.058883.

Zhou J, Wan J, Gao X, Zhang X, Jaffrey SR, Qian S-B. 2015a. Dynamic m(6)A mRNA methylation directs translational control of heat shock response. *Nature* **526**: 591–594. doi: doi:10.1016/j.chom.2016.09.015.

Zhou J, Wan J, Shu XE, Mao Y, Liu X-M, Yuan X, Zhang X, Hess ME, Brüning JC, Qian S-B. 2018. N6-Methyladenosine Guides mRNA Alternative Translation during Integrated Stress Response. *Mol Cell* **69**: 636-647.e7. doi: 10.1016/j.molcel.2018.01.019.

Zhou KI, Parisien M, Dai Q, Liu N, Diatchenko L, Sachleben JR, Pan T. 2015b. N6-methyladenosine modification in a long non-coding RNA hairpin predisposes its conformation to protein binding. *J Mol Biol*. doi: 10.1016/j.jmb.2015.08.021.

Zhou X, You F, Chen H, Jiang Z. 2012. Poly(C)-binding protein 1 (PCBP1) mediates housekeeping degradation of mitochondrial antiviral signaling (MAVS). *Cell Res*. doi: 10.1038/cr.2011.184.

Zhu T, Roundtree IA, Wang P, Wang X, Wang L, Sun C, Tian Y, Li J, He C, Xu Y. 2014. Crystal structure of the YTH domain of YTHDF2 reveals mechanism for recognition of N6-methyladenosine. *Cell Res* **24**: 1493–1496. doi: 10.1038/cr.2014.152.

Zhuang M, Li X, Zhu J, Zhang J, Niu F, Liang F, Chen M, Li D, Han P, Ji S-JJ. 2019. The m6A reader YTHDF1 regulates axon guidance through translational control of Robo3.1 expression. *Nucleic Acids Res* **47**: 4765–4777. doi: 10.1093/nar/gkz157.

Zinder JC, Lima CD. 2017. Targeting RNA for processing or destruction by the eukaryotic RNA exosome and its cofactors. *Genes Dev* **31**: 88–100. doi: 10.1101/gad.294769.116.

Zinder JC, Wasmuth E V., Lima CD. 2016. Nuclear RNA Exosome at 3.1 Å Reveals Substrate Specificities, RNA Paths, and Allosteric Inhibition of Rrp44/Dis3. *Mol Cell* **64**: 734–745. doi: 10.1016/j.molcel.2016.09.038.

Zorbas C, Nicolas E, Wacheul L, Huvelle E, Heurgué-Hamard V, Lafontaine DLJ. 2015. The human 18S rRNA base methyltransferases DIMT1L and WBSCR22-TRMT112 but not rRNA modification are required for ribosome biogenesis. *Mol Biol Cell* **26**: 2080–95. doi: 10.1091/mbc.E15-02-0073.

Zou S, Toh JDW, Wong KHQ, Gao Y-G, Hong W, Woon ECY. 2016. N6-Methyladenosine: a conformational marker that regulates the substrate specificity of human demethylases FTO and ALKBH5. *Sci Rep* **6**: 25677. doi: 10.1038/srep25677.

Zviran A, Mor N, Rais Y, Gingold H, Peles S, Chomsky E, Viukov S, Buenrostro JD, Scognamiglio R, Weinberger L, et al. 2018. The Molecular and Functional Foundations of Conducive Somatic Cell Reprogramming to Ground State Pluripotency. *SSRN Electron J*. doi: 10.2139/ssrn.3155731.

Appendices

Appendix 1: miR-145 is highly expressed in HFFs compared to iPSCs

RT-dPCR analysis of miR-145 abundance in HFFs and iPSCs normalized to 5S rRNA. Asterisks indicate significant difference in the relative mean abundance. (**p-value<0.005).

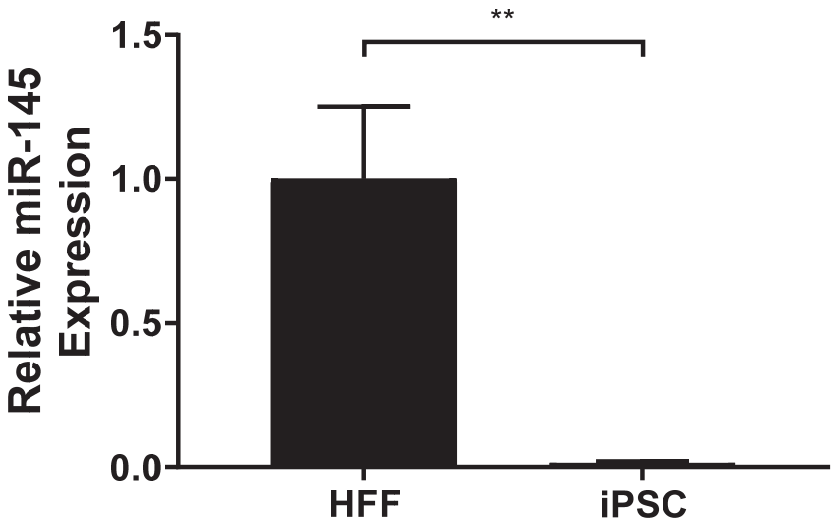

Appendix 2: Depletion of DICER does not impact YTHDF2 expression in HeLa cells

A: Western blot to detect YTHDF2 in control and DICER knockdown HeLa cell lines; three and two independent extracts were assessed, respectively. B: Quantification of (A). No significant decrease in the relative mean protein expression was observed.

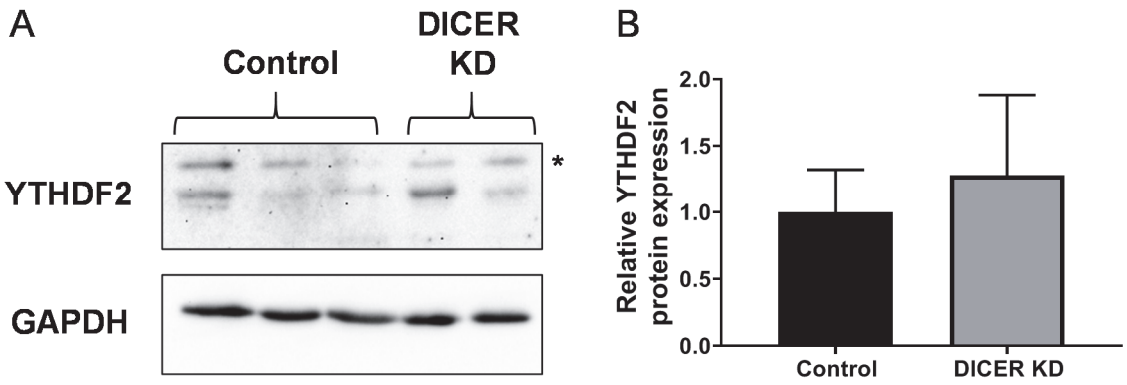

Appendix 3: Depletion of HNRNPQ has a biological effect in iPSCs

RT-dPCR analysis of GAP43 and SYT1, two known HNRNPQ targets, mRNA abundance in siRNA negative control and HNRNPQ depleted iPSC samples normalized to GAPDH mRNA. No statistical analysis was performed because this is preliminary data and n=1.

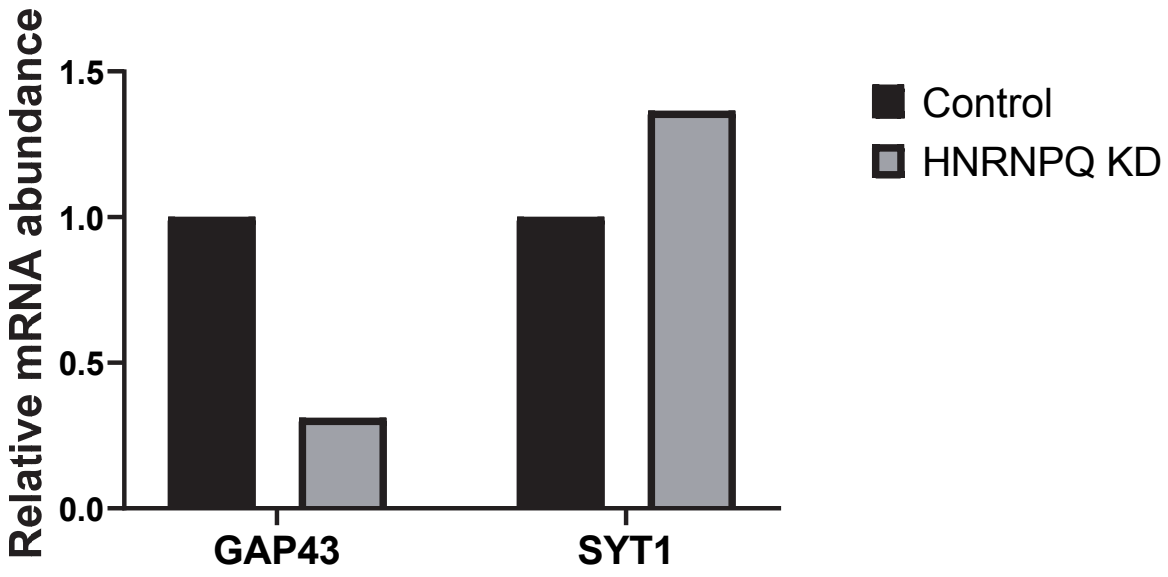

Appendix 4: 414 transcripts were differentially expressed following two days of PCBP2 depletion in iPSCs

A: Distance matrix showing the Euclidean distances between RNA-seq replicates. Replicates with a lower distance (darker blue) are more closely correlated in terms of gene expression. Distances were calculated from log-stabilized normalized read counts of all detected transcripts (>5 read counts per replicate). B: PCA plot of RNA-seq replicates following DESeq2 analysis (Love et al., 2014). Control and PCBP2 depleted samples are labeled in red and blue, respectively. C: Volcano plot generated from sequencing data showing the adjusted p-value (y-axis) plotted against the fold change (x-axis) for individual genes. Differentially expressed genes are shown in green (differential expression: read counts>5, Benjamini-Hochberg adjusted p-value<0.05 and log2-fold change>1.0, represented by grey dotted lines).

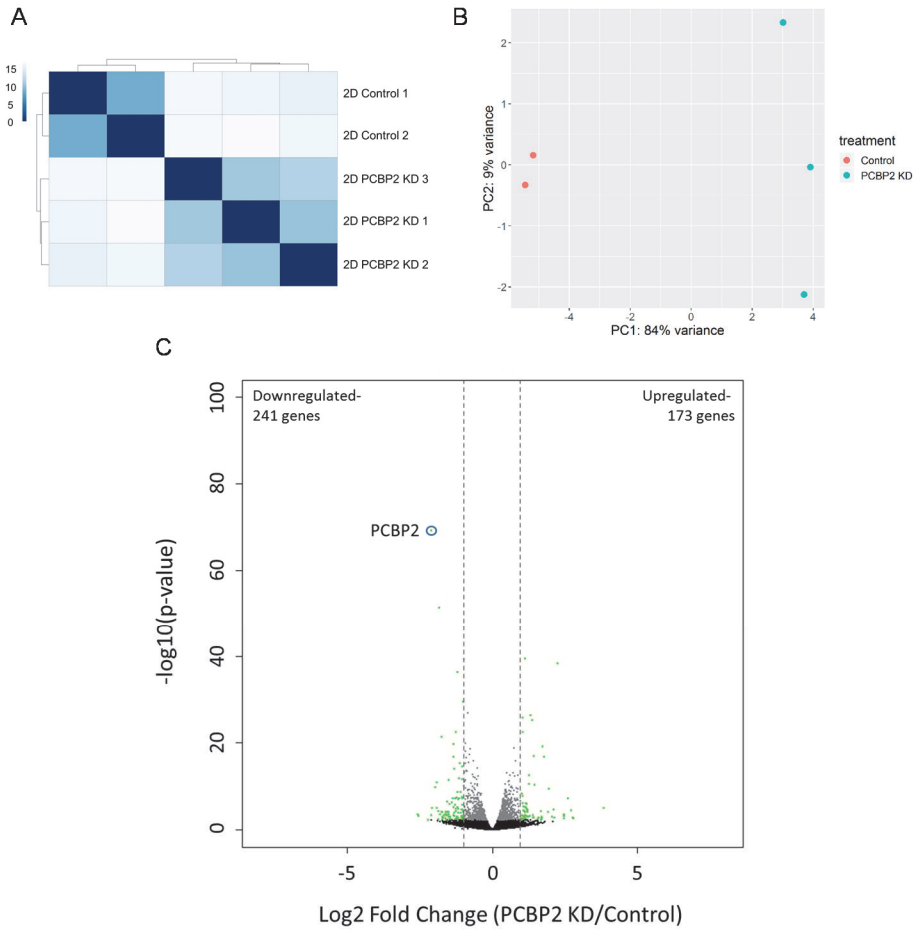

Appendix 5: GO-term analysis and independent validation of results from two day PCBP2 in iPSCs

A and C: Functional annotation clustering of biological process performed by DAVID on genes up- (A) and down- (C) regulated following two days of PCBP2 depletion. Annotation clusters with the highest enrichment according to FDR p-value are listed. The number of genes in each cluster is shown next to the respective bar. Fold enrichment are not listed because these numbers were skewed due to the low number of differentially expressed genes. B and D: RT-dPCR analysis of mRNA abundances in control and PCBP2 depleted samples for transcripts identified as up- (B) and down- (D) regulated in the sequence dataset. mRNA abundance normalized to GAPDH for transcripts. Data is reported as log2 fold change (PCBP2 KD/Control). Asterisks indicate significant difference in mean abundance between control and PCBP2 KD samples (*p-value<0.05, **p-value<0.005).

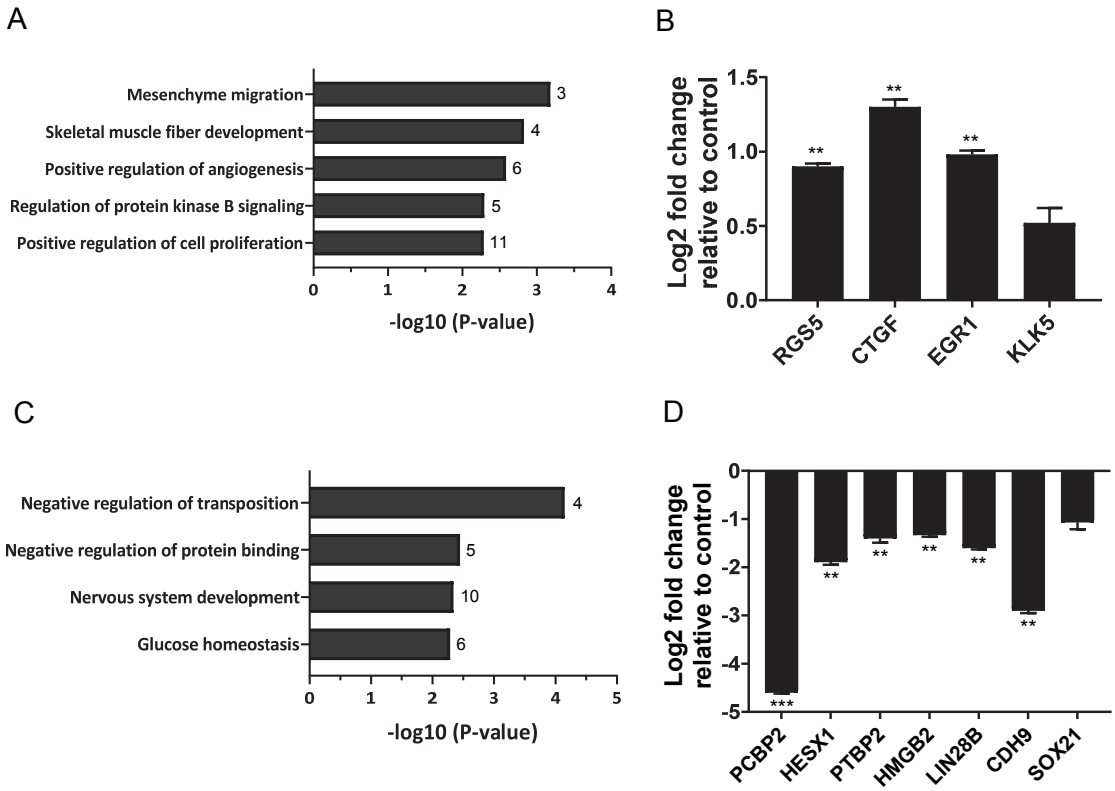

Appendix 6: mRNAs up-regulated following PCBP2 depletion in iPSCs are not bound by PCBP2 protein

RT-dPCR analysis of transcript abundance in IgG and PCBP2 IP samples. Data is represented as fold enrichment over IgG (PCBP2 IP/IgG IP). No statistical analysis was performed because this is preliminary data and n=1.